Structural Evolution of the Northwest Tarim Basin, China

Sebastian Turner

PhD Thesis

Imperial College London

Department of Earth Science & Engineering

October 2006 – December 2009

The mountains that form earth's bones jut starkly out of the high deserts of Central Asia. This antique land has always stimulated the curiosity and imagination of travellers with a strong sense of history. Better known to older civilisations than our own and described for thousands of years as the roof of the world, this is the home of gold-digging ants, of men who know the arts of levitation and self-warming without fire and of peaks on whose slopes grow herbs that cause heads to ache.

Kongur – China's Elusive Summit, 1982

Abstract

The sedimentary and structural record of the NW Tarim Basin, China, provides an insight into the amalgamation of Central Asia and is an ideal area in which to examine the impact of an inherited tectonostratigraphic framework on the evolution of foreland fold-thrust belts. The NW Tarim Basin contains a thick (3-16 km) sedimentary succession which was deposited from the Late Neoproterozoic onwards, and has been exhumed by a foreland fold-thrust belt system associated with the South Tien Shan mountains during the Middle to Late Cenozoic. The research presented in this thesis combines satellite image interpretation and field investigations in order to examine the tectonostratigraphic framework of the NW Tarim Basin and to ascertain the causes of lateral structural variability and partitioning of the foreland fold-thrust belt system.

The Upper Neoproterozoic to Lower Permian sedimentary succession records the progressive evolution of the NW Tarim Basin as a rift, intracratonic and foreland basin. Following a period of subaerial exposure throughout the Mesozoic, tectonic subsidence from the Middle Cenozoic onwards was driven by flexural deflection beneath the Pamirs and Tien Shan orogenic belts. This was coupled with the development of a foreland fold-thrust belt system along the northwest margin of the Tarim Basin. Lateral variations in the structural geometry, architecture and style of the foreland fold-thrust belt system correspond to changes in the thickness of the sedimentary succession and interaction with inherited, basement fault zones. An east-west transition from the wide, arcuate Keping Shan Thrust Belt into the narrow Kashgar Fold Belt is ascribed to thickening of the Cenozoic (syn-tectonic) foreland basin succession. In contrast, internal variations in the structural architecture of the Keping Shan Thrust Belt are governed by lateral changes in the thickness of the Palaeozoic (pre-tectonic) sedimentary succession. These changes occur abruptly across inherited, Early Permian fault zones that have been reactivated as strike-slip faults in order to accommodate these lateral variations in the structure of the fold-thrust belt.

Declaration

Except where explicitly referenced, the work presented in this thesis is my own work. In all instances, including parts of this thesis that have been submitted in modified form for scientific publication, I validate that as first author I wrote the text, prepared all figures and developed the interpretations presented therein.

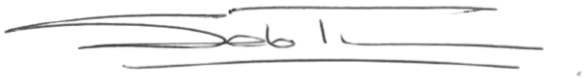

Sebastian Turner
18 December 2009

This thesis was examined by Richard Lisle (University of Cardiff) and Philip Allen (Imperial College London) on 20 May 2010.

Acknowledgements

Foremost, I thank my supervisors, Jian Liu and John Cosgrove, for their guidance, support and encouragement throughout the course of this research. I am indebted to Nick Brook for joining me on fieldwork to the Tarim Basin in the summer of 2008, and for remaining calm in the face of adversity. I am also extremely grateful to Liu, Martin Blunt and Lorraine Craig for negotiating our swift and safe return from China. I would also like to thank Gareth Morgan, Jingfa Zhang and friends at the China Seismology Bureau who helped with field work and logistics during both field seasons in 2007 and 2008.

I would also like to thank Alex Whittaker and Antony Burnham for providing critical feedback on various aspects of this thesis, in addition to Mandefro Belayneh, Kevin Hill and Phil Stone for fruitful discussions on Tarim geology.

I extend my warmest gratitude to all my friends at Imperial College London who have made the last three and a half years so enjoyable. I will never forget the hours spent chatting over coffee, ranting about the state of SCR food and catching up on the latest news over a pint or five in the dark depths of the Holland Bar & Grill.

Contents

PART TWO
FORELAND FOLD-THRUST BELTS OF THE NW TARIM BASIN

PART THREE
DISCUSSION AND CONCLUSIONS

List of Figures

1 Introduction

2 Late Neoproterozoic Rifting

3 Palaeozoic Evolution of the NW Tarim Basin

4 Early Permian Faulting and Volcanism

5 Orogenic Uplift and Flexural Subsidence in the Cenozoic

A Application of Satellite Images for Geological Mapping

B Structural Evolution of the Piqiang Fault Zone

Publications and Abstracts

Parts of this thesis have been submitted for publication in modified form.

TURNER, S. A. 2010. Sedimentary record of Late Neoproterozoic rifting in the NW Tarim Basin, China. *Precambrian Research*, **181** (1-4), 85-96.

TURNER, S. A., COSGROVE, J. W. & LIU, J. G. 2010. Controls on lateral structural variability along the Keping Shan Thrust Belt, SW Tien Shan foreland, China. *In:* GOFFEY, G. P., CRAIG, J., NEEDHAM, T. & SCOTT, R. (eds), *Hydrocarbons in Contractional Belts*, Geological Society, London, Special Publications, **348**, 71-85.

TURNER, S. A., LIU, J. G. & COSGROVE, J. W. 2011. Structural evolution of the Piqiang Fault Zone, NW Tarim Basin, China. *Journal of Asian Earth Sciences*, **40**, 394-402.

Conference Abstracts

TURNER, S., COSGROVE, J. W. & LIU, J. G. 2009. Causes of along-strike structural segmentation in the southwest Tien Shan foreland, NW China. *Geophysical Research Abstracts*, **11**, EGU2009-0, EGU General Assembly, Vienna, Austria.

TURNER, S., BROOK, N. R., COSGROVE, J. W. & LIU, J. G. 2008. Tectonostratigraphic evolution of the NW Tarim Basin and impacts on the structural architecture of fold-thrust belts. *BSRG Annual General Meeting Abstracts*, Liverpool, UK.

TURNER, S., WEEKS, D. H., COSGROVE, J. W. & LIU, J. G. 2008. Fundamental controls on the structural variability of fold-thrust belts in the NW Tarim Basin, China. *Fold-Thrust Belt Exploration Conference Abstracts*, Geological Society, London.

TURNER, S., COSGROVE, J. W. & LIU, J. G. 2007. The role of pre-existing structures in the evolution of the Kepingtagh fold-thrust belt, Tarim Basin, China. *Petroleum Geoscience Collaboration Conference Abstracts*, Geological Society, London.

CHAPTER ONE

Introduction

The remote landscape of Central Asia is characterised by impressively high mountain belts which are separated by vast intracontinental basins. The formation of this remarkable continental landscape is the result of the sequential accretion of numerous cratonic blocks and terranes throughout the Proterozoic and Phanerozoic (Yin & Harrison 2001; Windley *et al.* 2007). The Tarim Basin, in Xinjiang, northwest China, is a major tectonic element of the Central Asian collage. It forms an anomalously flat region that contrasts sharply with the surrounding summits of the Kunlun Shan, Pamirs and Tien Shan mountain belts (Fig. 1.1). The basin represents the surface expression of a rigid, cratonic basement which is overlain by a thick sedimentary cover succession that records the structural, stratigraphic and geodynamic evolution of the region since the Late Neoproterozoic.

1.1 Aims and Objectives

The aim of this thesis is to examine the structural evolution of the NW Tarim Basin from the Late Neoproterozoic to the present. It is based on data gleaned from a spectacular fold-thrust belt system that has developed along the northwest margin of the basin, in the foreland of the South Tien Shan orogenic belt, during the Cenozoic (Fig. 1.1). The fold-thrust belt system has exhumed the thick sedimentary succession of the basin, permitting analysis of the sequence stratigraphy and structures that were

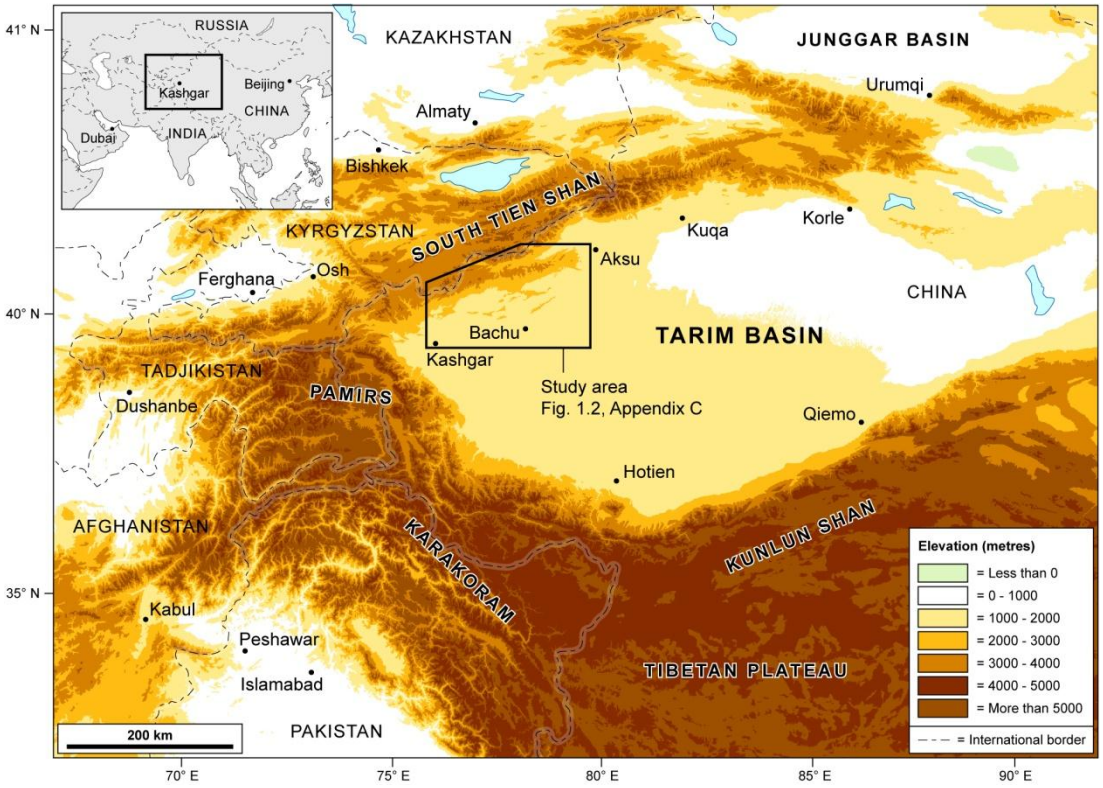

Fig. 1.1. Topographic map of Central Asia showing the location of the study area.

developed during earlier phases of basin evolution. Consecutively, this provides an insight into the causes of lateral variations in structural geometry, architecture and style across the foreland fold-thrust belt system. This research is governed by three primary objectives that are focused in the NW Tarim Basin, and more specifically in the study area defined in Figs. 1.1 and 1.2:

1. The generation of a regional geological map from combined satellite image interpretation (Fig. 1.2) and outcrop investigation;
2. The development of a tectonostratigraphic model to synthesise the structural evolution of the area from the Late Neoproterozoic to the Late Cenozoic;
3. The investigation of the causes of lateral structural variability and seismicity in the Late Cenozoic foreland fold-thrust belts that actively deform the northwest basin margin.

Fig. 1.2. Landsat ETM+ (true colour) satellite image of the study area. Labels with years refer to primary field sites investigated in this study.

1.2 Rationale

The sedimentary record of the Tarim Basin provides a remarkable insight into the tectonic evolution of Central Asia. The basin also contains abundant hydrocarbon reserves, and locally experiences powerful and devastating seismic activity. Despite this, much of the basin history remains cryptic and only in the past two decades have the first reconnaissance-scale studies been published. There is a vast amount of research to be done, and this thesis and the publications that derive from it aim to contribute a wealth of new data and interpretations towards this end.

The tectonostratigraphic framework of the NW Tarim Basin remains poorly constrained. Formation names are vague and span substantial time intervals. Regional studies by Bally *et al.* (1986) and Carroll *et al.* (1995, 2001) cover large areas but are based on limited outcrop data from only a handful of sections. The spatial distribution of individual stratigraphic units across the area has not been discussed and new information concerning the timing of tectonic events associated with the adjacent orogenic belts has not yet been incorporated into regional tectonostratigraphic models. Crucial phases of basin development, including widespread extension and volcanism in the Early Permian (Zhang *et al.* 2008), remain disputed.

The fold-thrust belts that have developed in the NW Tarim Basin during the Middle to Late Cenozoic (Yin *et al.* 1998; Allen *et al.* 1999) provide a spectacular example of contraction in a foreland setting and a prime opportunity to evaluate the relationships between the inherited, tectonostratigraphic framework of the basin and the geometry and structural architecture of the superimposed belts. To date, this aspect has not been examined or commented upon in published literature, plausibly as a result of the poor constraints on the regional tectonostratigraphic framework as outlined above. Active deformation in the region is also the likely cause of powerful seismic activity, which in recent decades alone has caused widespread devastation and casualties. The controls on the spatial and temporal distribution of seismic activity are not known, but a suitable tectonic model of the region would be a crucial step in regional seismic hazard management.

1.3 Thesis Outline

The foundations of this research are based on a regional geological map that was generated during this research and which is presented as Appendix C. Details of how the map was generated and the satellite data used are presented in Appendix A. The map was developed primarily by satellite image interpretation, and progressively modified as data were collected from outcrop sections during two field seasons in the Tarim Basin, in the late summers of 2007 and 2008.

The main body of this thesis consists of six chapters that follow the objectives set out in §1.1, and therefore are presented in two parts: **Part 1** (Chapters 2–5), which investigates the regional tectonostratigraphic framework, and **Part 2** (Chapters 6–7) which analyses the structure of the foreland fold-thrust belts and neotectonic deformation. The chapters are presented in geochronological order and each deals with a particular, discrete aspect of the regional geology. Each chapter is written as a stand-alone document and in a format which can be readily modified for publication. However, for the purpose of this thesis, these chapters form a coherent research strategy that aims to resolve the structural evolution of the NW Tarim Basin and is drawn together in a concluding synthesis and discussion.

In **Chapter 2**, the crystalline basement and overlying Upper Neoproterozoic sedimentary succession is examined, interpreted and correlated across two sections. These represent the oldest lithostratigraphic units in the NW Tarim Basin, and record an early rifting event that may be associated with the separation of the Tarim Craton from NW Australia.

In **Chapter 3**, a comprehensive review of the Palaeozoic stratigraphy is presented using a series of measured outcrop sections at sites across the study area. In addition to sedimentary interpretation and stratigraphic analysis, a series of isopach maps have been generated in order to evaluate the spatial distribution of individual stratigraphic units. These data consecutively yield tectonic subsidence curves, derived from decompaction and backstripping of the sedimentary succession at several sites. The

synthesis of all the data presented in this chapter is considered in the context of the paleogeographic evolution of Central Asia and the adjacent orogenic belts.

Chapter 4 presents a wealth of new data from the Early Permian, a period which is associated with widespread extension and volcanism, the causes of which remain disputed (e.g. Zhang *et al.* 2008). The stratigraphic, structural and magmatic characteristics of the Early Permian are examined at selected sites across the NW Tarim Basin and considered with respect to the regional tectonic setting during this period. Based on these observations, it is proposed that large-scale block rotation within the Tarim Craton occurred as a result of strong transpression in the adjacent South Tien Shan.

In the absence of Mesozoic rocks in the study area, **Chapter 5** progresses to the Cenozoic and examines the evolution of foreland basins at the edges of the Tarim Basin as a result of tectonic loading beneath the growing Pamirs and Tien Shan orogenic belts. Analysis of the stratigraphy and its spatial and temporal distribution is input into a flexural model across the NW Tarim Basin that provides an estimate of the flexural rigidity of the underlying craton and the development of the adjacent orogenic belts through the Miocene and Pliocene.

Chapter 6 presents a structural analysis of the Keping Shan Thrust Belt, one of the primary constituents of the foreland fold-thrust belt system associated with the South Tien Shan mountains. The belt is laterally partitioned by a series of fault zones that are oblique to the general structural trend, and coincide with inherited basement structures. These fault zones control the thickness of the deforming sedimentary succession. This chapter presents a new model for the structural evolution of the belt. This work is in press in a Geological Society, London, Special Publication, *Hydrocarbons in Contractional Belts*, for release in 2010.

Chapter 7 examines the spatial and temporal distribution of seismicity in the NW Tarim Basin. Most recently, in 1997 and 2003, two powerful earthquake swarms caused widespread devastation and casualties in the Jiashi and Bachu areas. It is

proposed that a major, blind strike-slip fault exists within the interior of the Tarim Basin that may relate to similar faults that have surface expression within the foreland fold-thrust belts to the north. It is suggested that a major releasing bend along this blind fault zone is acting as a nucleation site for powerful seismicity.

Finally, in **Chapter 8**, the tectonostratigraphic framework and structural architecture of the foreland fold-thrust belt system are summarised and synthesised, with the aim of presenting a complete, structural model for the NW Tarim Basin. The main conclusions of this thesis are summarised in **Chapter 9**.

PART ONE

Tectonostratigraphic Framework of the NW Tarim Basin

CHAPTER TWO

Late Neoproterozoic Rifting in the NW Tarim Basin

Abstract • Upper Neoproterozoic synrift sediments have been examined in outcrop at two sites in the NW Tarim Basin, China, and provide an insight into an early phase of extension. The synrift succession unconformably overlies high-grade metamorphic basement and consists of the non-marine Sugaitebulake Fm and the marine Qegebulake Fm. The Sugaitebulake Fm is characterised by a basal conglomerate that passes upwards into fluvial and lacustrine facies sandstones and siltstones. The stratigraphic position of the basal unconformity and the thickness of the basal conglomerate is locally variable, relating to the formation of small, isolated depocentres during the initial phase of extension. The Sugaitebulake Fm also contains a series of concordant, extrusive basalts which record episodic volcanism, and together with the fluvial and lacustrine facies indicate the development of the rift system and the growth, interaction and linkage of extensional faults. The conformable Qegebulake Fm is characterised by foreshore to intertidal facies dolomites that contain abundant stromatolites, representing a basin-wide marine transgression and the rift climax stage. This synrift sequence is shown to correlate with a similar succession in NW Australia, and corresponds to at least partial separation of the Tarim Block from East Gondwana during the latest Neoproterozoic to Early Palaeozoic.

Publication Details • Turner, S. A. 2010. Sedimentary record of Late Neoproterozoic rifting in the NW Tarim Basin, China. *Precambrian Research*, **181** (1-4), 85-96.

2.1 Introduction

The formation of continental rift basins and the characteristics of synrift sedimentary successions has been widely discussed (e.g. Leeder & Gawthorpe 1987; Schlische 1991; Gawthorpe *et al.* 1994; Gupta *et al.* 1998, 1999; Davies *et al.* 2000; Gawthorpe & Leeder 2000). The synrift succession provides a useful record of the initiation, growth and linkage of normal faults associated with rift basin development. As initial rift basins grow and coalesce, the transition from isolated to large depocentres is expressed by a progressive change in the sequence stratigraphy, from coarse, alluvial fan and fluvial facies into lacustrine or marine facies (Gawthorpe & Leeder 2000). In addition, if crustal thinning is substantial, decompression melting at the base of the crust (White & McKenzie 1989) results in basaltic magmatism, characterised by the emplacement of mafic dykes and the extrusion of lava flows.

Upper Neoproterozoic sediments in the NW Tarim Basin, China, record an early phase of rifting that is thought to have affected much of the region (Shi *et al.* 1995; Carroll *et al.* 2001), and may have even been associated with the progressive separation of Tarim from East Gondwana (Li *et al.* 1996; Li & Powell 2001). At present, the Tarim Basin is one of the most imposing geographical features of Central Asia, occupying an area of more than 500,000 km^2. In comparison to the surrounding mountain belts, the Tarim Basin acts as a relatively rigid block and is resistant to internal deformation. It represents the surface expression of the Tarim Block, one of the primary tectonic constituents of the Central Asian collage (Fig. 2.1A) (Yin & Harrison 2001; Windley *et al.* 2007). The early development of the NW Tarim Basin remains poorly constrained, chiefly due to a lack of exposed Upper Neoproterozoic sediments in outcrop, as a consequence of the vast quantities (3–6 km) of Palaeozoic–Cenozoic sediment that have been deposited subsequently (Bally *et al.* 1986; Jia 1997). Late Cenozoic contractional deformation along the northwest margin of the basin has exhumed a small number of exceptionally well preserved and complete sections of the Upper Neoproterozoic sequence, in addition to the underlying crystalline basement (Fig. 2.1B). These outcrop sections provide a unique insight into the tectono-stratigraphic evolution of the basin during this period. The aim of this chapter is to

present new sedimentological and sequence stratigraphic data from two 900 m thick sections that were examined in the field, at sites near Aksu and Wushi (Fig. 2.1B). Interpretation and correlation of these sections across the wider area is undertaken with the foresight to developing a model for the tectonostratigraphic evolution of the basin, in the context of the regional paleogeography, during the Late Neoproterozoic to Early Cambrian.

2.2 Geological Setting

The Tarim Block is a major tectonic constituent of the Central Asian collage. It consists of a cratonic, Precambrian basement that is overlain by a thick (3-16 km) sedimentary succession (Bally *et al.* 1986) which records the progressive tectonic and paleogeographic evolution of the basin and the adjacent region since the Late Neoproterozoic (Carroll *et al.* 2001). The origins and timing of separation of the Tarim Block remain disputed and poorly constrained. Recent paleogeographic models (e.g. Li *et al.* 1996; Li & Powell 2001; Metcalfe 2009) have inferred that the Tarim Block was originally connected to the Kimberley region of NW Australia, forming part of East Gondwana. Correlations of the stratigraphy in the two areas reveal that both comprise a crystalline basement that is overlain by remarkably similar Neoproterozoic strata (Brookfield 1994; Corkeron *et al.* 1996; Li *et al.* 1996; Grey & Corkeron 1998) and occupied similar paleo latitudes during the Middle to Late Neoproterozoic (Chen *et al.* 2004; Huang *et al.* 2005; Zhan *et al.* 2007). Furthermore, a series of dykes that intrude the crystalline basement in the Aksu area of the NW Tarim Basin have been shown to correlate in age (800-750 Ma) and geochemistry to dykes in the Kimberley region (Chen *et al.* 2004; Xu *et al.* 2005; Li *et al.* 2006; Zhang *et al.* 2007, 2009).

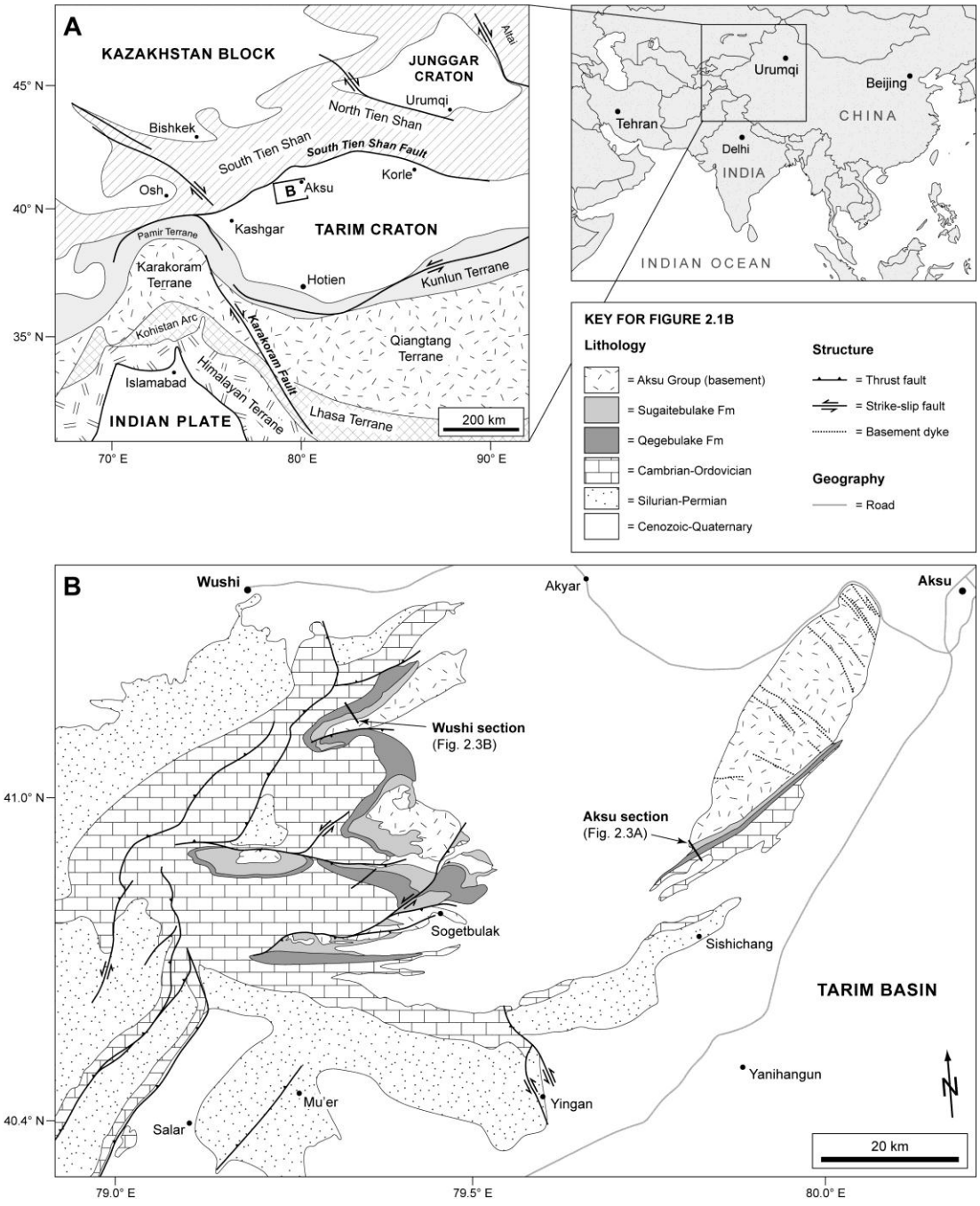

Fig. 2.1. (A) Simplified map of Central Asia showing the main tectonic units and the location of the Tarim Block. (B) Geological map of the Aksu–Wushi area, showing the distribution of the metamorphic basement and the Upper Neoproterozoic succession.

It was proposed that the Tarim Block was separated from NW Australia during a widespread rifting event in the Late Neoproterozoic, that was also responsible for the break-up of eastern and northern Laurentia, and Siberia (Li *et al.* 1996; Li & Powell

2001). The sedimentary and volcanic record of basins in NW Australia indicates that a continental block was rifted away in the latest Neoproterozoic to Early Cambrian (Veevers 1984; Veevers *et al.* 1997; Glass & Phillips 2006), and it has been suggested that this corresponded to the separation of the Tarim Block (Li *et al.* 1996). In contrast, paleontological studies suggest that the Tarim Block remained very close to East Gondwana (i.e. NW Australia) until at least the Ordovician (Fortey & Cocks 2003; Wang *et al.* 2007). Similarly, Huang *et al.* (2005) envisaged that the Tarim Block was partially rifted from NW Australia during the Middle Neoproterozoic break-up of Rodinia but remained relatively close during the Late Neoproterozoic and Early Palaeozoic. Metcalfe (1996, 2009) proposed that the final separation of Tarim did not occur until the Devonian, when a sliver of terranes including North China, South China, Indochina and Tarim were separated from East Gondwana and resulted in the formation of the Paleo-Tethys.

The Tarim Block owes its present position at the core of the Central Asian collage to a series of subsequent accretionary events during the Late Palaeozoic, Mesozoic and Cenozoic. By the Carboniferous, Tarim and its counterpart terranes (including the Kongur-Kunlun terrane) had become proximal to the southern margin of Eurasia (Heubeck 2001; Metcalfe 2009). The ensuing collision resulted in the closure of the intervening Turkestan Ocean and formation of the South Tien Shan orogenic belt by the Early Permian (Burtman 1975; Windley *et al.* 1990). The accretion of numerous terranes to the south of Tarim during the Mesozoic (Hendrix *et al.* 1992; Yin & Harrison 2000) and the collision of India and Eurasia since the Early Cenozoic has resulted in Tarim presently residing in the middle of the Central Asian collage (Fig. 2.1A). Despite the near continuous deformation in the surrounding orogens, Tarim has remained as a rigid block and the flat topography of the present basin surface attests to little internal deformation. During the Late Cenozoic, foreland contraction along the northern periphery of the Tarim Basin has exhumed the thick Late Neoproterozoic–Recent sedimentary succession (Yin *et al.* 1998; Turner *et al.* 2010), permitting investigation of how the basin and thus the underlying cratonic block have evolved through time.

2.3 Stratigraphy and Sedimentary Facies

Across the Tarim Basin, surface outcrops of the cratonic basement and the Upper Neoproterozoic sedimentary succession are very limited. The complete exposure of both in the vicinity of Aksu and Wushi (Fig. 2.1B) thus provides a unique, well preserved and accessible means by which to study the early development of the NW Tarim Basin. The section at Aksu [GR 40° 55' N, 79° 50' E] is characterised by an E-W trending cliff-face which provides a continuous outcrop of the cratonic basement and the Upper Neoproterozoic succession for more than 28 km. The section is accessible at the western end, where it reaches a total thickness of nearly 900 metres. The section at Wushi is c. 40 km to the northwest of the section at Aksu [GR 41° 04' N, 79° 22' E] and provides a section of similar thickness, which is exposed in a cliff-face that is laterally continuous for 20 km. At both sections, the crystalline basement of the Aksu Group is unconformably overlain by the Upper Neoproterozoic Sugaitebulake (or Sugetbrak) Fm and the conformably overlying Qegebulake (or Chigebrak) Fm (Fig. 2.2).

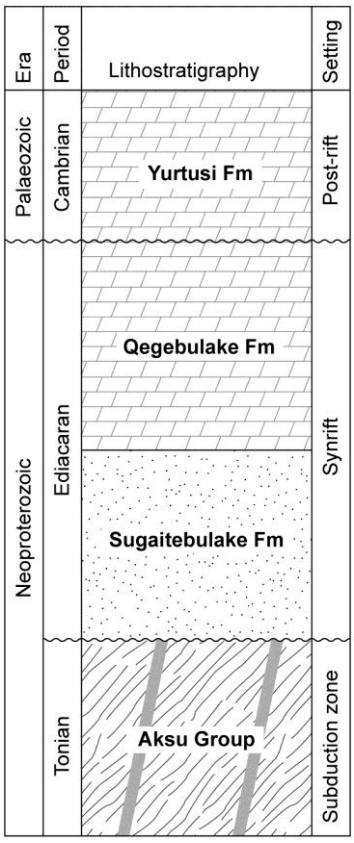

Fig. 2.2. Generalised stratigraphic column for the Neoproterozoic and Lower Cambrian succession in the NW Tarim Basin.

2.3.1 Aksu Group (Basement)

The cratonic basement comprises transitional blueschist to greenschist facies metamorphic rocks of the Aksu Group, which underwent polyphase deformation in a subduction complex (Liou *et al.*, 1989; Nakajima *et al.*, 1990; Chen *et al.*, 2004). The basement was subjected to peak metamorphism at 872–862 Ma (Late Tonian) (Chen *et al.* 2004). At the base of the Aksu section, the Aksu Group is typified by muscovite schists (Figs. 2.3A and 2.4A). The western end of the Aksu section is dominated by blueschists (Fig. 2.4B), which have a high abundance of glaucophane that imparts an intense blue colour to the rock. The presence of blueschist-facies basement attests to the high-pressure low-temperature metamorphism described by Liou *et al.* (1989) and Nakajima *et al.* (1990). At Wushi, evidence of blueschist-facies metamorphism is lacking at outcrop scale and in hand specimen, which likely reflects variations in the respective protoliths at the two sections rather than substantial differences in the conditions of metamorphism. The basement is dominated by chlorite-muscovite schists (Fig. 2.4C) and minor fold axes plunge predominantly to the NW.

A series of consistently NW-trending dykes cross cut the Aksu Group and were observed in abundance at both the Aksu and Wushi sections (Figs. 2.4A and 2.4D). The dykes are up to 30 m wide and have an intermediate to mafic composition. The dykes do not propagate into the unconformably overlying Upper Neoproterozoic succession, indicating they must predate sediment deposition. The timing of dyke emplacement was constrained to the Cryogenian, and although the ages range from 807 Ma (Chen *et al.* 2004) to 760 Ma (Zhang *et al.* 2009) there is general agreement between these authors that they correspond to widespread extension associated with the break-up of Rodinia.

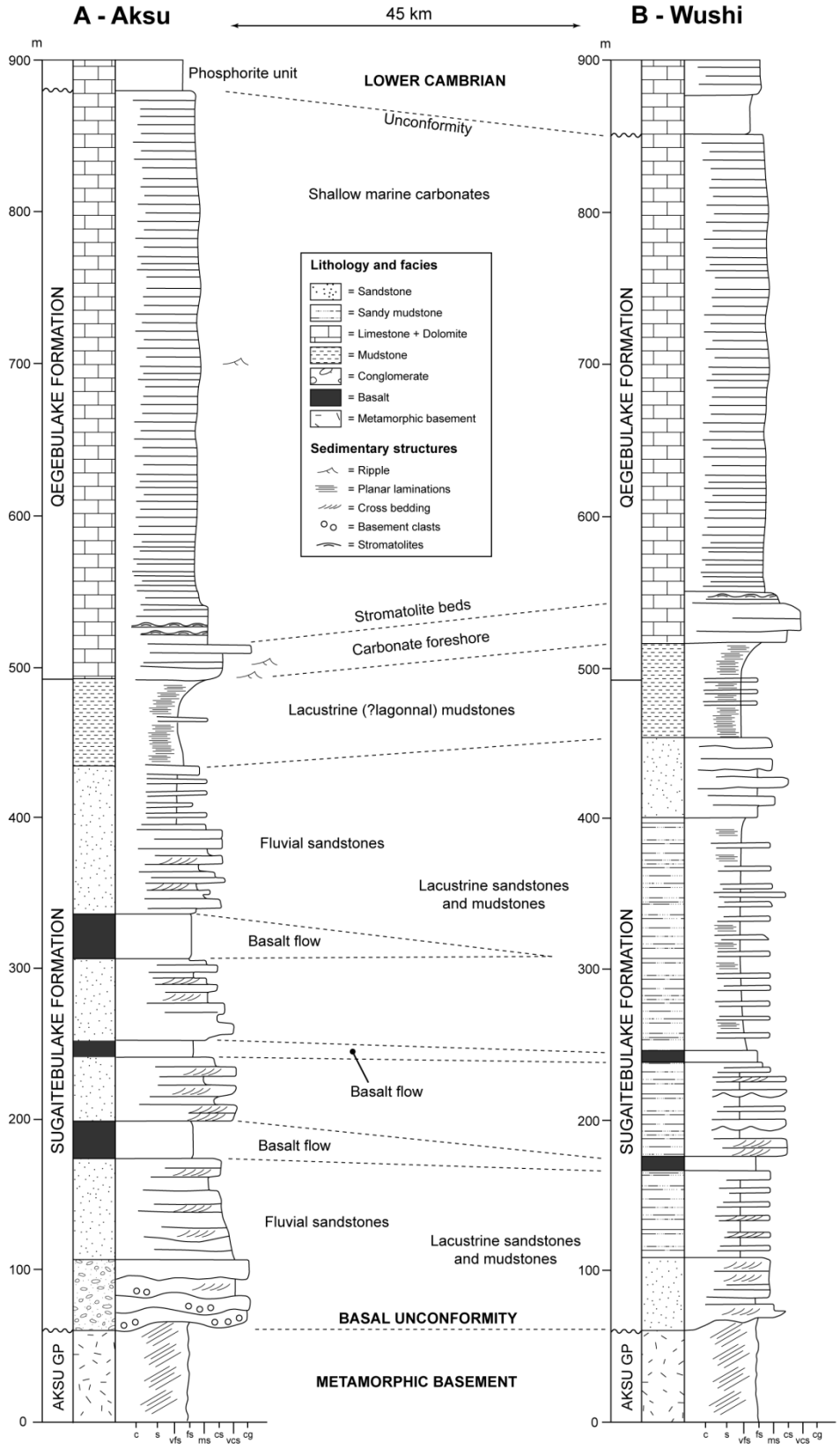

Fig. 2.3. Sedimentary logs from (A) Aksu and (B) Wushi (see Fig. 2.1B for section locations). The Aksu Group (basement) is unconformably overlain by the 400 m thick non-marine Sugaitebulake Fm, which passes upwards into the 400 m thick marine Qegebulake Fm.

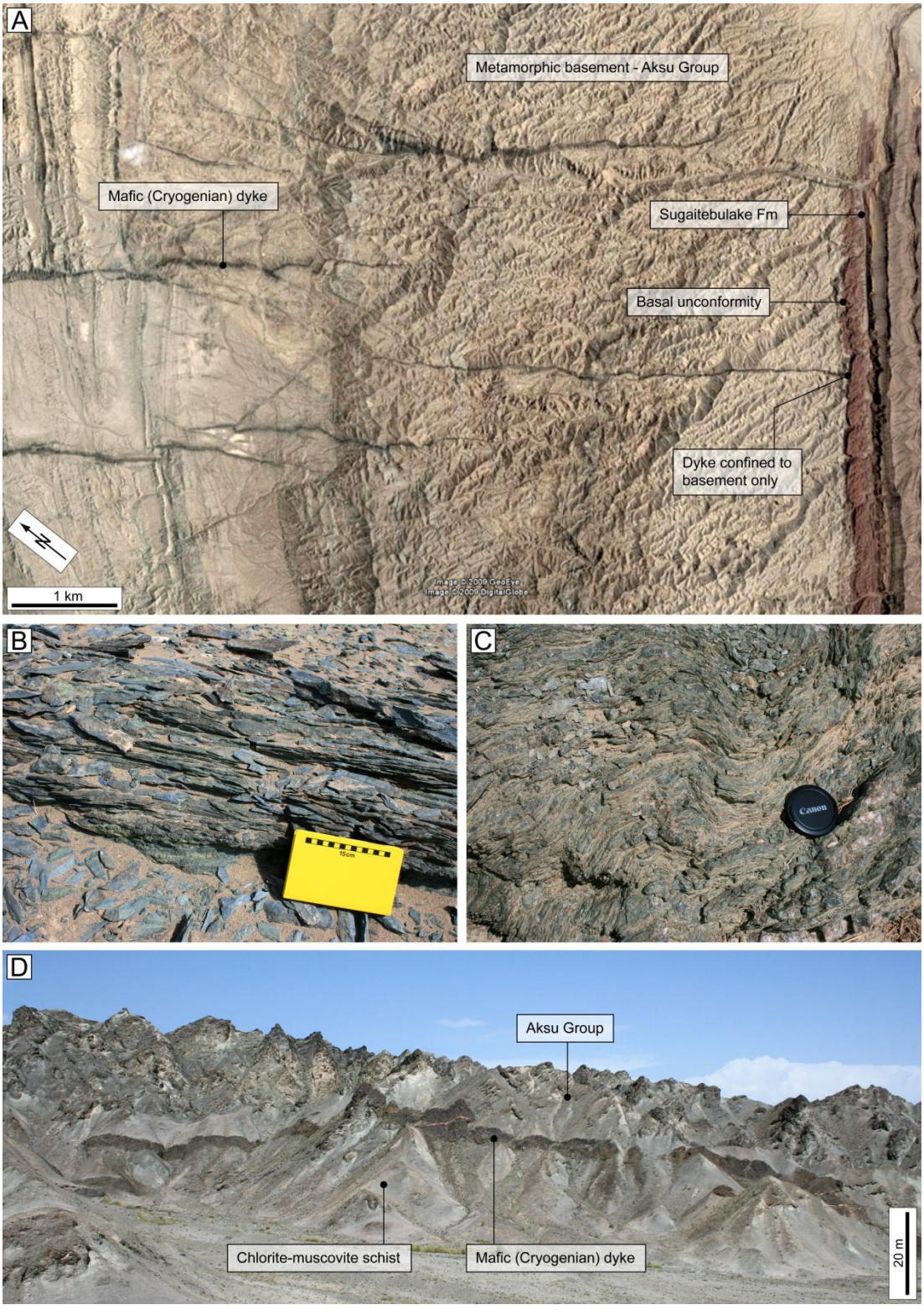

Fig. 2.4. Satellite and field photographs of the Aksu Group (basement). (A) Aerial view of the basement and the basal unconformity at Aksu, showing NW-trending Cryogenian dyke swarm (image from Google™ Earth). (B) Blueschist facies basement near Aksu. (C) Folded chlorite (greenschist facies) schists near Wushi. (D) Mafic dyke cross-cutting the Aksu Group near Wushi.

2.3.2 Sugaitebulake Formation

The Sugaitebulake Fm is 400–450 m thick and comprises an interbedded clastic and volcanic succession that unconformably overlies the crystalline basement (Figs. 2.3A, 2.3B, 2.5A, 2.6A). Although the sections at Aksu and Wushi are broadly similar, there is some variability that indicates localised variations in paleoenvironment.

Aksu section. The base of the Sugaitebulake Fm is characterised by a 10 m red conglomerate in direct contact with metamorphic blueschists of the basement (Fig. 2.3A). The unconformity is sharp and angular. The conglomerate is matrix-supported and comprises 40% sub-rounded clasts of schists, quartzites and mafic rocks which appear to be derived from the underlying basement. The size of clasts decreases up the section, and there is a gradual transition from the red conglomerate into medium- to coarse-grained red sandstones which contain abundant trough- and planar- cross beds (Figs. 2.5A, 2.5B). The red conglomerate is interpreted as a basal conglomerate, representing the stream deposits of an alluvial fan. This grades into a stacked, braided fluvial system in which individual channel bodies are not recognised but in which cross beds indicate fluvial processes and channel migration. Within the red fluvial sandstones there are three 15–20 m thick basalt layers, which are concordant to bedding (Fig. 2.5A). Examination of the internal structure of these layers indicates that they were extruded as lava flows. The lower parts of the flows are dark grey, holocrystalline and columnar jointed, in contrast to the upper parts of the flows that are grey-brown in colour and vesiculated. Flow-top structures were not observed at the top of the lava flow.

Examining the larger-scale exposure at Aksu, the thickness of the Sugaitebulake Fm changes significantly along strike from west (where the succession was described and measured) to east (in the direction of Aksu). At the measured section, the Sugaitebulake Fm is 450 m thick. In contrast, measurement of the succession 20 km along strike yields thicknesses of 200–250 m. Interpretation of high-resolution satellite images (SPOT-5 and Google™ Earth) reveals that individual beds within the Sugaitebulake Fm lap onto the underlying basement, defining a paleo-low in the west

relative to the east. The basalt flows can also be traced laterally along strike for considerable distances. The oldest basalt flow can be traced eastwards of the measured section for more than 18 km, and the younger flow for more than 14 km, before they thin to absence. In both cases, the basalt flows do not change their stratigraphic positions, providing some additional evidence for their emplacement as extrusive flows rather than sills.

Wushi section. The base of the section is characterised by a coarse-grained red subarkosic sandstone lies unconformably above intensely deformed chlorite schists (Figs. 2.3B, 2.6A, 2.6B). The sandstone contains abundant planar- and trough-cross beds and larger cross-sets in beds up to 1 metre thick. This is interpreted to represent a stacked, braided fluvial system and the larger cross-sets may be indicative of fluvial channel migration. Unlike the section at Aksu, there is no basal conglomerate. Upwards, the succession becomes progressively more mud rich, and interbedded sandstones contain abundant evidence of soft-sediment deformation (Fig. 2.6C). The siltstones are green-brown in colour and interpreted to represent deposition in a lacustrine environment. Measured cross-beds indicate that the dominant paleo-current direction was to the NW. Two thin (4-5 m) basalt horizons were observed in the section (Fig. 2.6D) but unlike those observed at Aksu, there is limited evidence to determine whether they were erupted as extrusive lava flows or emplaced as sills: the basalts are holocrystalline throughout, and lack vesiculation.

The basalt horizons may relate to a series of NE-trending mafic dykes that intrude the Sugaitebulake Fm at this site (Fig. 2.6E). Analysis of thin sections from samples of the dykes reveals that they have a mafic composition but are intensely altered. It is unclear whether they relate to the volcanism that occurred in the Late Neoproterozoic or whether they are associated with later (Early Permian) magmatism that affected much of the NW Tarim Basin (e.g. Carroll *et al.*, 1995; Zhang *et al.*, 2008). They must post-date the NW-trending, intermediate dykes that are observed only in the crystalline basement and yield Cryogenian ages (Chen *et al.* 2004). Based on the trends and petrology, the dykes also differ from those of known Early Permian age, which are persistently NW-trending and are not altered in the same manner, such that

the original petrology is well preserved. Consequently, the dykes at Wushi are potential feeder systems relating to the basaltic lava flows that formed in the Late Neoproterozoic. In this case, the structural trends of these dykes are significant and may provide some constraint on the orientation of regional extension. Aside from volcanism in the Late Neoproterozoic and the Early Permian, there are no other magmatic events reported from the sedimentary sequence in the wider region (Sobel 1999; Carroll *et al.* 2001).

2.3.3 Qegebulake Formation

At both sections, the transition from the Sugaitebulake to Qegebulake Fm occurs c. 450 m above the basal unconformity and is characterised by a marked change from the underlying interbedded sandstones and siltstones into a 30-40 m green-grey siltstone unit. This overlain by a 2 m-thick, very coarse and round-grained sand-rich limestone (Fig. 2.5C) which passes somewhat abruptly upwards into a very fine-grained micritic dolomite that contains abundant, well developed stromatolites. The stromatolites are up to 1 m wide and 0.5 m high, and have a well defined internal structure (Fig. 2.5D) but become noticeably smaller further up the succession (Fig. 2.5E), possibly reflecting an increase in water depth or variations in water chemistry. The age of the stromatolites has been constrained to the Late Neoproterozoic (Xinjiang Stratigraphic Table Compiling Group 1981). From this point onwards, the succession is dominated by relatively thickly bedded, pale grey and fine-grained micritic dolomite (Figs. 2.3A, 2.3B).

The Qegebulake Fm is interpreted to represent the development of a wide, aerially extensive lake or a marine transgression, characterised initially by foreshore (beach) to very shallow intertidal facies based on the very coarse-grained limestone and stromatolite sequence. A gradual increase in water depth is inferred from subsequent deposition of the thick, well-bedded micritic dolomite succession.

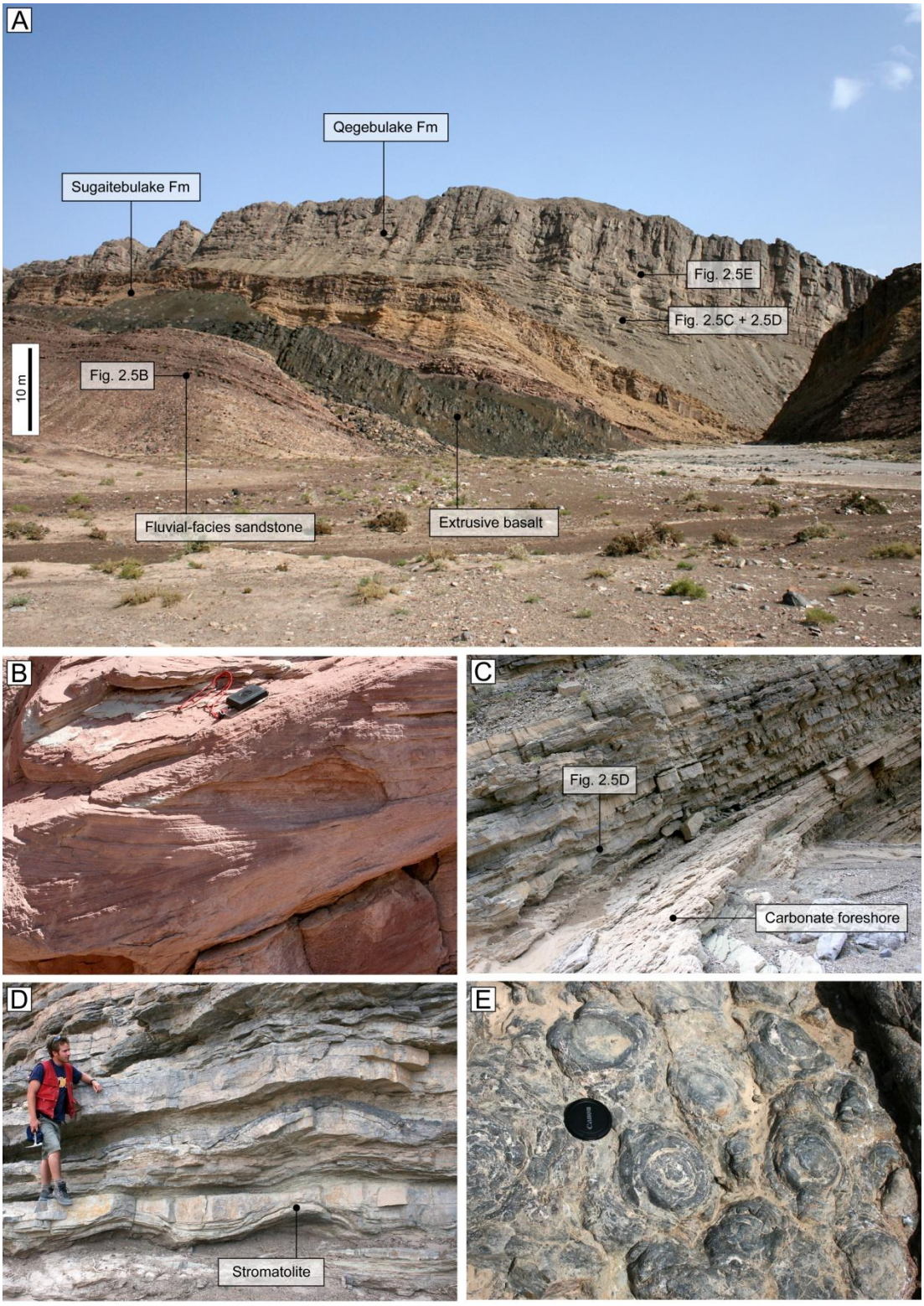

Fig. 2.5. Field photographs of the Upper Neoproterozoic succession at the Aksu section. (A) Fluvial facies sandstones and volcanics passing upwards into dolomites of the Qegebulake Fm. (B) Cross bedding in the fluvial facies red sandstone of the Sugaitebulake Fm. (C) Carbonate foreshore and stromatolite bed at the base of the Qegebulake Fm. (D) Large stromatolites in the lower Qegebulake Fm. (E) Small stromatolites higher in the Qegebulake Fm, possibly indicating an increase in water depth.

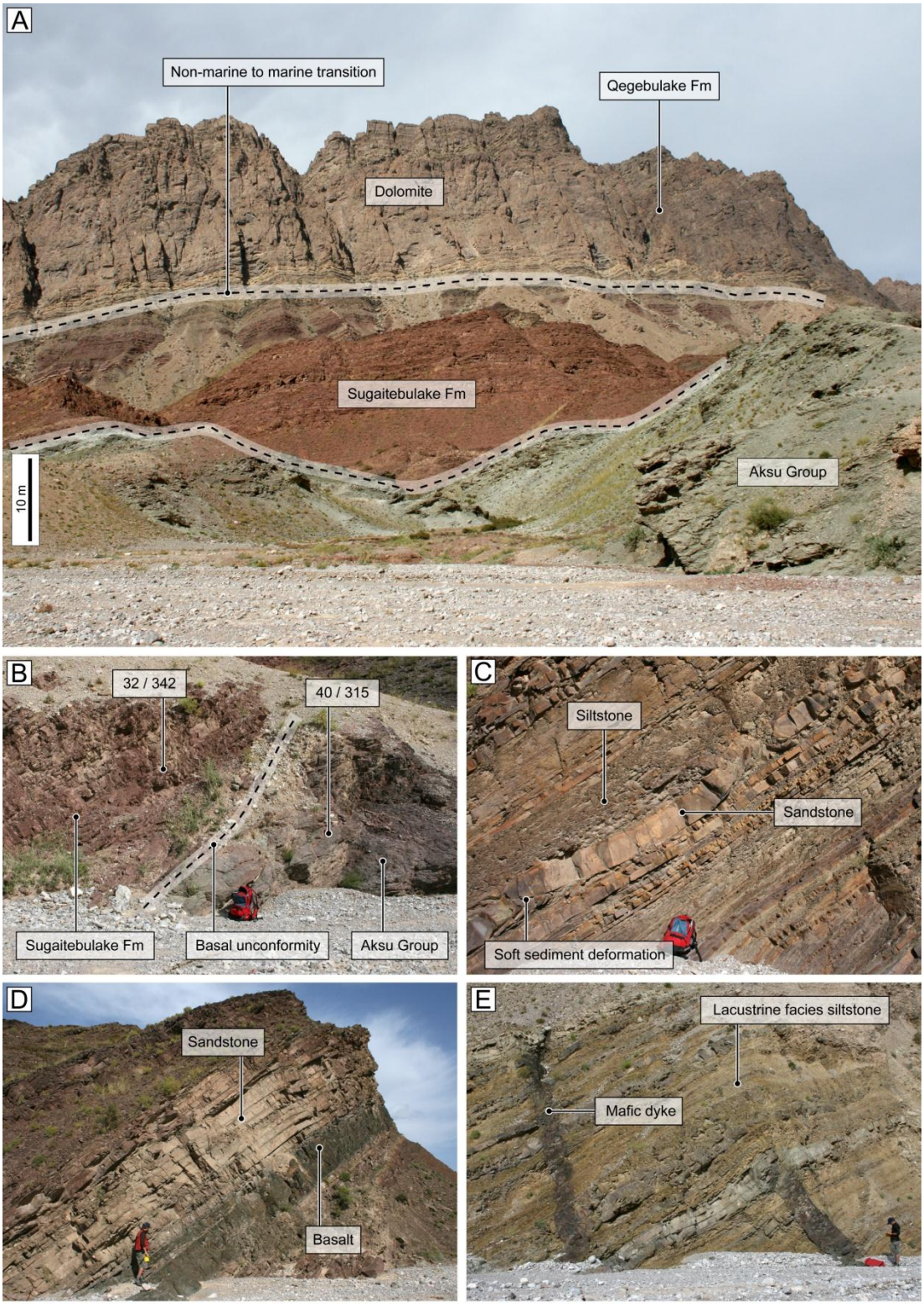

Fig. 2.6. Field photographs of the Upper Neoproterozoic succession at the Wushi section. (A) The Sugaitebulake and Qegebulake formations unconformably overlying chlorite schist basement, showing the measured section (Fig. 2.3B). (B) Angular basal unconformity separating the Aksu Group from the Sugaitebulake Fm. (C) Lacustrine-facies sandstones and siltstones of the Sugaitebulake Fm. Soft sediment deformation is observed in the sandstone beds. (D) Thin basalt layer in the Sugaitebulake Fm. (E) Pair of NE-trending mafic dykes cross-cutting lacustrine-facies siltstones of the Sugaitebulake Fm.

2.3.4 Neoproterozoic to Lower Cambrian transition

An abrupt transition from the Upper Neoproterozoic to the Lower Cambrian is marked by a paraconformity that represents an unknown length of time. The base of the overlying Yurtusi Fm is characterised by an 8-10 m succession of interbedded black shales and organic-rich carbonate beds that correspond to the phosphorite unit described by Carroll *et al.* (2001) and Yu *et al.* (2003) and provide a useful marker horizon. The black shale is interpreted to represent a period of anoxia, and is similar to phosphorite-bearing black shales reported from the Lower Cambrian at sites in Siberia, Australia and India, which were all at low latitudes during the time of deposition (McKerrow *et al.* 1992). The black shale unit passes upwards into thickly bedded, pale grey to pale yellow micritic dolomites that are interpreted to represent carbonate sedimentation in the subtidal to intertidal zone of a warm, shallow marine environment.

2.3.5 Stratigraphic correlation

The sections at Aksu and Wushi (Figs. 2.3A, 2.3B) can be correlated using several stratigraphic markers and the regional geological map (Fig. 2.1B). The stratigraphic markers include the non-marine to marine transition, indicated by the contact between the Sugaitebulake and Qegebulake formations. The base of the Lower Cambrian, characterised by the phosphorite shale unit in the lower part of the Yurtusi Fm, provides a useful marker to determine the upper limit of the Qegebulake Fm. Attempts have also been made to correlate the basalt flows, although they are not considered to be ideal marker horizons as the lateral continuity of individual extrusive basalt flows is difficult to assess with the limited exposure available. The basal unconformity can only be used as a stratigraphic marker to represent the top of the Aksu Group, but does not correlate to the same chronostratigraphic position at the base of the Sugaitebulake Fm as the unconformity does not lie in the same stratigraphic position across the area.

Although the age of the basement has only been constrained at Aksu (c.f. Chen *et al.* 2004), the almost continuous exposure of blueschists and greenschists between the Aksu and Wushi sections (Fig. 2.1B) is considered as adequate evidence that they are part of the same cratonic basement. The overlying sedimentary succession at the two measured sections are broadly similar and their correlation yields new information concerning the local paleogeography during the Late Neoproterozoic. The majority of differences between the sections arise almost solely in the lower, non-marine Sugaitebulake Fm. At Aksu, deposition occurred in a braided, stacked fluvial system and the grain size is coarser throughout. In contrast, the succession at Wushi is interpreted as transitional fluvial to lacustrine facies, resulting in a greater abundance of interbedded siltstones. Overall, the entire succession is finer grained at Wushi and a basal conglomerate is lacking. There are also differences in the thickness and abundance of basalt flows between the two sections. At Aksu, three 10-20 m thick basalt flows are observed, the lower two of which are crudely correlated with the two thinner (< 5 m) flows observed at Wushi. The youngest (uppermost) flow appears to be absent at Wushi. In contrast, the overlying marine Qegebulake Fm shows no substantial differences between either section.

2.4 Late Neoproterozoic Basin Development

Analysis of the Upper Neoproterozoic sedimentary succession that crops out in the Aksu and Wushi area provides an insight into the early stages of basin development in the NW Tarim Basin. The Upper Neoproterozoic succession shares remarkable similarities with synrift sequences described in the models of Gawthorpe & Leeder (2000). It is proposed that the NW Tarim Basin endured a period of rifting during the Late Neoproterozoic, which resulted in extension of the underlying crystalline basement and the eventual establishment of a shallow marine basin by the latest Neoproterozoic. Based on the stratigraphic observations presented in this report, a new model is proposed for an early phase of rifting in the NW Tarim Basin.

2.4.1 Stage 1: Rift Initiation

The initiation of rifting in the Late Neoproterozoic is reflected in the unconformable deposition of conglomeratic and coarse-grained, fluvial facies clastic sediments onto the metamorphic basement of the Aksu Group. The stratigraphic position of the basal unconformity varies laterally, which may have been caused to some extent by a pre-existing topography. Alternatively, this may relate to lateral variations in the accommodation space created adjacent to juvenile normal faults in the earliest stages of rifting (Gawthorpe & Leeder 2000). During the earliest stages of rifting, it is likely that small and isolated depocentres developed that accumulated the coarse, conglomeratic deposits observed immediately above the basal unconformity at Aksu (Fig. 2.7A). Progressive growth of the early extensional faults would have increased the size of the depocentres, resulting in progressive on-lapping of the lower parts of the Sugaitebulake Fm onto the underlying crystalline basement. Although evidence for Late Neoproterozoic normal faulting was not directly observed, the thickness distribution of sediment could be used as an indicator of where the faults may have been. The thicker basal unit at the western end of the Aksu cliff-face section compared to the east implies that, if the effects of paleotopography were negligible, a normal fault may have been actively growing to the west during this period. The structural overprint of subsequent tectonic events (e.g. Early Permian extension, Late Cenozoic contraction) means that it is very difficult to identify fault zones that may have been active in the Late Neoproterozoic. These early, inherited structures may have been subsequently reactivated but in the absence of widespread surface exposure of the Upper Neoproterozoic succession or subsurface data it is difficult to prove this concept.

2.4.2 Stage 2: Rift Development and Volcanism

As extension prevailed, widening and deepening of the rift basin(s) allowed a widespread fluvial-lacustrine system to be established (Fig. 2.7B). The correlation between the two sections implies that the coarser, stacked fluvial facies sediments at

Aksu are the lateral equivalent of finer, lacustrine facies sediments at Wushi. These observations are in agreement with the generalised models of rift basin development by Gawthorpe & Leeder (2000), which suggest that laterally transgressive fluvial-lacustrine facies correspond to the fault growth and linkage stage of rifting. Certainly, the coeval emplacement of mafic dykes and the extrusion of basaltic lava flows during this time is a testament to the development of a significant rift basin system. Although the source and cause of magma generation remains speculative, the basaltic character is broadly indicative of decompression melting of the asthenosphere during crustal thinning (e.g. White & McKenzie 1989). The NE-trending dykes that may be associated with the extrusive volcanism provide a crude NW-SE extension orientation. If this holds true, recently active NE-trending fault zones in the area (e.g. Fig. 2.1B) may correspond to inherited, basement faults associated with the Late Neoproterozoic rifting event.

2.4.3 Stage 3: Rift Climax and Marine Incursion

The transition from non-marine to marine sedimentation (Sugaitebulake to Qegebulake formations respectively) represents an important facies change that is associated with the rift climax stage and possibly a Late Neoproterozoic sea level rise. If the continued development and climax of the rift system was the driving mechanism, the marine facies carbonates of the Qegebulake Fm may correspond to the development of through-going faults which form wide, well established rift basins (Fig. 2.7C). The marine incursion may also imply that rifting was sufficient to connect the intracontinental basins with a larger ocean basin. Continued growth of the through-going normal faults may have resulted in further basin deepening, which is consistent with the gradual change from foreshore facies to deeper, intertidal and subtidal facies. During the rift climax stage, volcanism ceased in the Aksu-Wushi area.

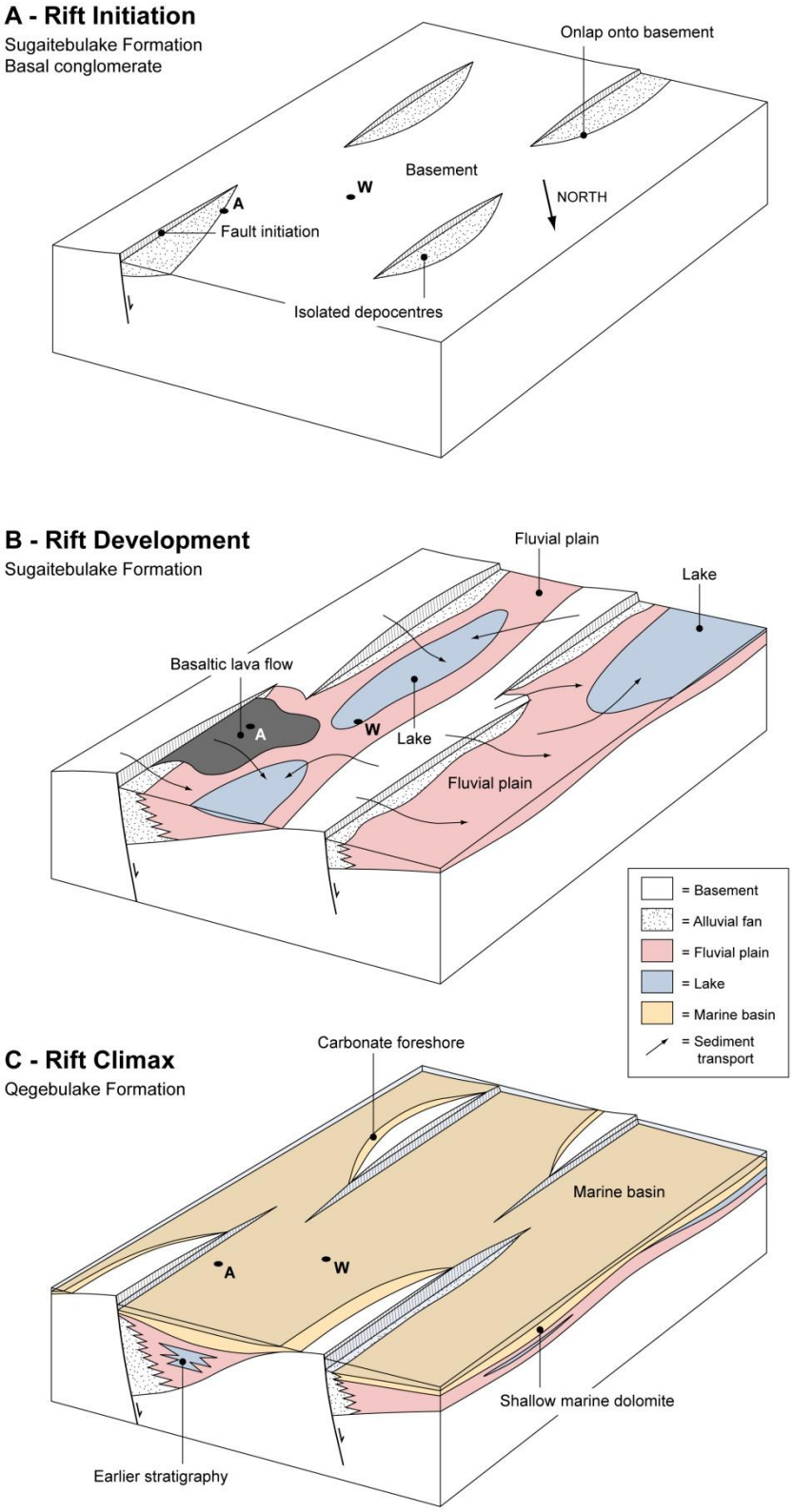

Fig. 2.7. Schematic tectonostratigraphic model for the NW Tarim Basin during the Late Neoproterozoic. (A) Rift initiation stage, characterised by isolated depocentres receiving coarse, conglomeratic sediments. (B) Rift development stage, characterised by fault growth and linkage, resulting in fluvial–lacustrine facies and basaltic lava flows. (C) Rift climax stage, representing the transition to the marine-facies Qegebulake Fm. A = Aksu section, W = Wushi section.

2.4.4 Stage 4: Post-rift Subsidence

The overlying Cambrian succession consists of an upward-shallowing carbonate sequence that eventually becomes supratidal and emergent by the Late Cambrian (Carroll *et al.* 2001). Geochemical analysis of the black phosphorite shale at the base of the Lower Cambrian indicates that mafic volcanism was occurring elsewhere in the basin at this time (Yu *et al.* 2003), suggesting that extension was still active. However, the progressive infilling and shallowing of the basin during the Cambrian, despite a global rise in sea level (Haq & Schutter 2008), is likely to reflect the post-rift phase of subsidence and the fault death stage. There is no evidence of further tectonism from the relatively widespread outcrops of the Cambrian-Ordovician megasequence (Zhang *et al.* 2000; Carroll *et al.* 2001).

2.5 Discussion

Paleogeographic reconstructions, paleomagnetic data and correlation of the Middle to Late Neoproterozoic stratigraphy of the NE Tarim Basin has shown that the Tarim Block once formed part of East Gondwana and was connected to the Kimberley region of NW Australia (Li *et al.* 1996; Chen *et al.* 2004; Huang *et al.* 2005). The timing of the separation of the Tarim Block has been disputed, with different authors proposing ages from the Late Neoproterozoic (e.g. Li *et al.* 1996; Li & Powell 2001) to the Middle Palaeozoic (e.g. Metcalfe 2009).

The sedimentary descriptions and interpretations presented here have been compared with the regional stratigraphy of the Neoproterozoic basins in NW Australia. It is thought that the non-marine, fluvial and lacustrine facies Sugaitebulake Fm in the NW Tarim Basin may correlate with the upper parts of the Louisa Downs and Albert Edward Groups, which are characterised by a thin (up to 120 m), red conglomerate that passes upwards into thick (up to 1,800 m) red fluvial sandstones (Coats & Preiss 1980; Grey & Corkeron 1998; Corkeron & George 2001). The ages of these formations have been constrained to the Ediacaran, and less than 610 Ma (Australian

Stratigraphic Names Database 2009) which is a sufficient match to the Late Neoproterozoic age of strata in the NW Tarim Basin. The Upper Neoproterozoic succession in the Kimberley region is unconformably overlain across a large area by the Antrim Plateau Volcanics. These are characterised by voluminous flood basalts that covered an area of 300,000-400,000 km^2, and were formed during the Early Cambrian (Hanley & Wingate 2000; Glass & Phillips 2006). The Antrim Plateau Volcanics represent the continuation of a widespread extensional event that began at c. 600 Ma (Lindsay *et al.* 1987) and are thought to correspond to the separation of the Tarim Block (Li *et al.* 1996). In contrast, the Early Cambrian in the NW Tarim Basin is characterised by a shallow marine carbonate succession associated with the rift climax or even post-rift phase. Although direct evidence of volcanism is absent, trace element analysis of the black phosphorite shale at the base of the Lower Cambrian in the NW Tarim Basin indicates that there were active sources of mafic material in the basin during deposition (Yu *et al.* 2003).

This suggests that the Tarim Block must have been at least partially separated from East Gondwana during this period in order to have been beyond the extent of the widespread Early Cambrian volcanism in NW Australia. It is not clear whether the rift system evolved into an oceanic basin during the Early Palaeozoic, or whether extension ceased and the absolute separation of the Tarim Block from East Gondwana did not occur until a later stage as proposed by Metcalfe (2009).

It is inferred from the evolution of the orogenic belts that surround the present Tarim Basin to the south and west that the Tarim Block must have been separated from East Gondwana by at least the Middle Ordovician. From this time through until the Middle Devonian, at least three terranes, including the substantially-sized Kunlun-Kongur terrane (Fig. 2.1A), were accreted to the present southern margin of the Tarim Block (Matte *et al.* 1996; Sobel & Arnaud 1999; Yin & Harrison 2000; Xiao *et al.* 2001). If the present northern side of the Tarim Block was still close to East Gondwana beyond the Middle Ordovician, it seems likely that the terrane accretions would have been sufficient enough to drive the block back towards East Gondwana and begin to close the relatively narrow seaway that must have separated them. This

seems unlikely, particularly as by the Devonian the Tarim Block was migrating rapidly northwards (Li 1990; Heubeck 2001) prior to its collision with Eurasia in the Late Palaeozoic. In addition, there is no evidence in the Early or Middle Palaeozoic stratigraphy of the NW Tarim Basin that indicates a rifting event, and instead sedimentation patterns appear to be related almost entirely to the accretionary events that affected the southern margin of the Tarim Block (Carroll *et al.* 2001). Therefore, it seems plausible that the Late Neoproterozoic to Early Cambrian rifting event in the NW Tarim Basin is the most likely cause of the separation of the Tarim Block from East Gondwana, and that the widespread Early Cambrian volcanism reported from NW Australia is compatible with the formation of a new oceanic basin.

An unresolved issue is whether or not the sedimentary succession examined in this report necessarily records the whole of the rifting event, or whether it only reflects extensional activity on the flanks of a much wider rift system, and perhaps even an oceanic basin. Long-term over-thrusting of the orogenic belts that surround the Tarim Basin since the Late Palaeozoic has obscured large parts of the cratonic margins. Consequently, the succession exposed in the present NW Tarim Basin may only provide an insight into events that affected the cratonic interior. In contrast, the sedimentary successions of the Neoproterozoic basins in the comparatively stable Kimberley region of NW Australia provide a much better insight into the magnitude of this rifting event.

2.6 Conclusions

Evidence of an early rifting event in the NW Tarim Basin is recorded in the Upper Neoproterozoic sedimentary succession. The succession unconformably overlies crystalline, blueschist to greenschist facies basement of the Tarim Block. Initially, localised deposition of a basal conglomerate, containing clasts of the underlying basement, corresponds to the initiation of extension and the formation of small, isolated depocentres. The conglomerate passes upwards into fluvial and lacustrine facies sandstones and siltstones, which progressively lapped onto the basement as the

rift system developed and bounding faults began to interact and link. Extrusive basalts and NE-trending dykes attest to rift-related volcanic activity during this stage. The climax of rifting may correspond to the transition to shallow marine facies of the Qegebulake Fm. The overlying, upward-shallowing Lower Cambrian succession corresponds to the post-rift phase and thermally-driven subsidence. The succession can be broadly correlated with Upper Neoproterozoic sediments in the Kimberley region of NW Australia, indicating a widespread rifting event that may have resulted in the separation of the Tarim Block from East Gondwana during the Late Neoproterozoic to Early Palaeozoic.

CHAPTER THREE

Palaeozoic Evolution of the NW Tarim Basin

Abstract • The NW Tarim Basin, China, contains a thick (2-6 km) Palaeozoic succession that records the evolution of the basin and the underlying craton from the Early Cambrian to the Early Permian. Regional geological mapping and outcrop-scale logging of the stratigraphy at a number of sections across the NW Tarim Basin are combined with new, regional-scale isopach maps and tectonic subsidence curves in order to unravel the structural, stratigraphic and geodynamic evolution of the area. In the Cambrian-Ordovician, a thick platform carbonate succession accumulated in an epicontinental sea that covered much of the Tarim Basin. Uplift and subaerial erosion in the Late Ordovician, and the subsequent deposition of a thick, marine to non-marine clastic sequence in the Silurian-Devonian corresponds to a series of arc and terrane collisions at the southern margin of the Tarim Basin. By the Late Palaeozoic, Tarim became proximal to Eurasia and was accreted by the Late Carboniferous. The evolution of the South Tien Shan mountain belt is recorded by a flysch-molasse sequence deposited in a foreland basin that evolved along the northern margin of the Tarim during the Late Carboniferous to Early Permian.

3.1 Introduction

The extraordinary tectonic architecture of Central Asia owes to the amalgamation of numerous cratonic blocks, terranes and island arcs, and the closure of several intervening oceans, throughout the Phanerozoic (Yin & Harrison 2000; Windley *et al.* 2007). This protracted accretionary orogen has led to the formation of a vast continental region. The Tarim Craton, in NW China, is a major tectonic component of the Central Asian collage (Burrett 1974; Yin & Harrison 2001) and is expressed at the surface by the anomalously flat Tarim Basin (Zhang *et al.* 1984). The basin contains a 2-6 km thick succession of Palaeozoic sedimentary rocks that provide an insight into the paleogeographic and geodynamic evolution of the basin during this period.

Across the Tarim Basin, surface outcrops of the Palaeozoic are rare, and data from the limited number of well penetrations within the basin interior are not available in the public domain. Arguably the best surface outcrops of the Palaeozoic succession are exposed within the Keping Shan Thrust Belt, a foreland salient that has deformed the northwest margin of the Tarim Basin during the Late Cenozoic. The Palaeozoic succession is exhumed for considerable distances of more than 250 km in the hanging walls of major E to NE-striking thrust faults (Fig. 3.1), providing an ideal opportunity to study the succession across a relatively large area. In this chapter, a series of outcrop sections across the Keping Shan were examined in the context of the existing structural framework, with the purpose of defining a tectonostratigraphic model for the evolution of the NW Tarim Basin during the Palaeozoic. Analysis of outcrops and sedimentary logging is complimented with information from regional geological maps (Fig. 3.1) in order to develop a stratigraphic framework of the area. Isopach maps for different parts of the succession are generated from measured sections that are distributed across the Keping Shan, and thereby permit analysis of tectonic subsidence. This work follows a similar approach to that of Carroll *et al.* (2001), which focused on examining the Palaeozoic stratigraphy that crops out in the far eastern Keping Shan, with the intention of synthesising new geological interpretations with data derived from the wider area in recently published literature.

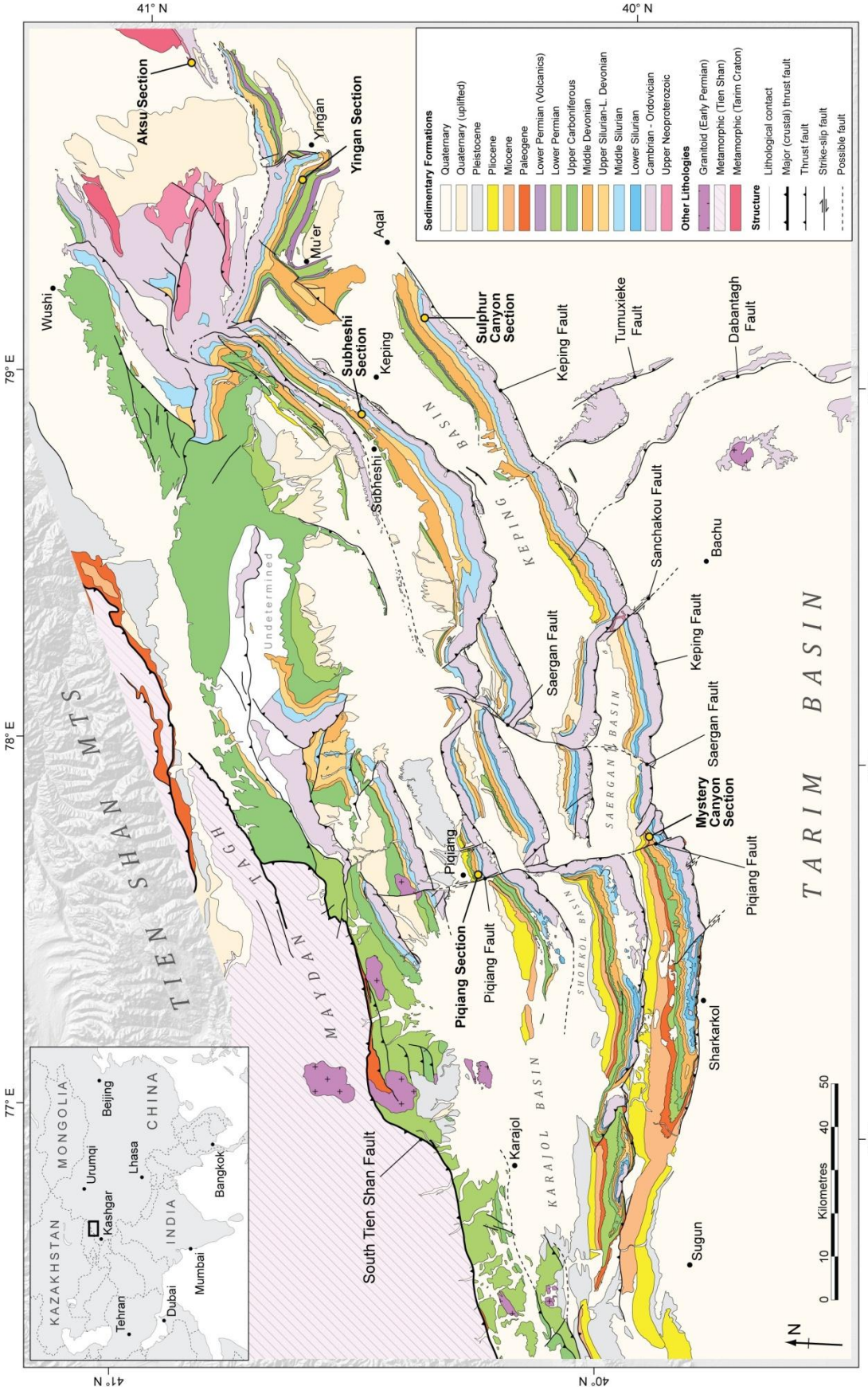

Fig. 3.1. Geological map of the Keping Shan Thrust Belt showing key stratigraphic sections.

3.2 Geodynamic Evolution of the Tarim Basin

In essence, the evolution of the Tarim Basin can be divided into three principal phases: (1) Rifting and separation from East Gondwana in the Late Neoproterozoic to Early Palaeozoic, (2) Isolation and continental drift from the Early to Mid Palaeozoic, (3) Collision with 'stable' Eurasia in the Late Palaeozoic (Chapter 2; Li *et al.* 1996; Heubeck 2001; Metcalfe 2009). An insight into these events is provided by the thick sedimentary succession that was accumulated in the NW Tarim Basin during the Palaeozoic, which locally exceeds thicknesses of 6 km (Fig. 3.2).

The sedimentary cover succession of the NW Tarim Basin is underlain by a crystalline basement that reached peak metamorphism at 872-862 Ma (Chen *et al.* 2004). Based on correlations of the basement characteristics, it has been suggested that Tarim was attached to NW Australia prior to the break-up of Gondwana (Li & Powell 2001). In the NW Tarim Basin, the basement is unconformably overlain by Upper Neoproterozoic sediments that record an early rifting event (Chapter 2). Initially, sedimentation and volcanism occurred in a non-marine, alluvial setting that passes conformably upwards into a shallow marine, carbonate succession as extension progressed. It has been speculated that this sequence could record the separation of Tarim from the young Gondwana, and that by Early Cambrian, Tarim was an isolated entity (Li & Powell 2001; Chapter 2). However, contrasting evidence from paleontological reconstructions indicates that Tarim may have remained close to Gondwana until at least the Ordovician (Fortey & Cocks 2003). In either case, a thick (1.5-6 km), predominantly carbonate succession was accumulated during this period (Bally *et al.* 1986; Zhang *et al.* 2000; Carroll *et al.* 2001) (Fig. 3.2A).

By the Ordovician, it is suspected that an ocean basin, representing a branch of the proto-Tethys, lay beyond an Andean-type margin along the southern edge of the Tarim Craton (Pan 1996; Xiao *et al.* 2002). From the Ordovician to the Devonian, a series of terranes were sequentially accreted to this margin leading to the development of a complex orogenic belt that is preserved in the modern Kunlun Shan and Pamir. Initially, the Yixieke arc collided during the Middle Ordovician following a period of

north-dipping subduction from 490-460 Ma (Xiao *et al.* 2002). Subsequently, the collision of the Kudi terrane from 452-428 Ma (Zhou 1999) is preserved by the Lapeiquan suture in the Kunlun Shan (Sobel & Arnaud 1999), which is the lateral equivalent of the Kudi suture in the Pamirs (Xiao *et al.* 2002). Sobel & Arnaud (1999) suggested that the suture represented the closing of an ocean basin that occurred between the Early Silurian and Middle Devonian. This was in turn succeeded by the collision of the much larger Kunlun-Kongur terrane in the Mid Devonian to Carboniferous (Yin & Harrison 2000; Heubeck 2001; Xiao *et al.* 2002), and which is the prime constituent of the Kunlun Shan and Pamir mountain belts (Robinson *et al.* 2004).

From the Devonian to Carboniferous, Tarim drifted rapidly northwards by 18° of latitude, largely driven by slab-pull associated with the subduction of the Turkestan Ocean, that lay to the north of Tarim, beneath Kazakhstan (Li 1990). This rapid northward migration ceased abruptly in the Mid Carboniferous, as the Turkestan Ocean entered the final stages of closure and Tarim became proximal to the southern margin of 'stable' Eurasia (Li 1990; Heubeck 2001). The ensuing collision of Tarim and its counterpart terranes (Yixieke, Kudi and Kunlun-Kongur) with Eurasia during the Late Carboniferous to Permian generated the South Tien Shan orogenic belt (Burtman 1975; Windley *et al.* 1990; Heubeck 2001). The collision was diachronous, and a 26° clockwise rotation of Tarim between the Late Carboniferous to Early Permian implies that it began earlier in the east than in the west (Li *et al.* 1988).

The present position of Tarim at the core of Central Asia owes to a series of subsequent terrane collisions to the south throughout the Mesozoic, amalgamating to form the Tibetan Plateau (Yin & Harrison 2001; Robinson *et al.* 2004). The most recent collision of India into the southern margin of Eurasia has led to rejuvenation of many of the ancestral belts across Central Asia (Tapponnier & Molnar 1979), including the Tien Shan (Windley *et al.* 1990). This has resulted in contraction along the marginal zones of the Tarim Basin, resulting in Mid-Late Cenozoic deformation of the thick sedimentary cover succession and thus permitting analysis of the earlier tectonostratigraphic evolution of the basin.

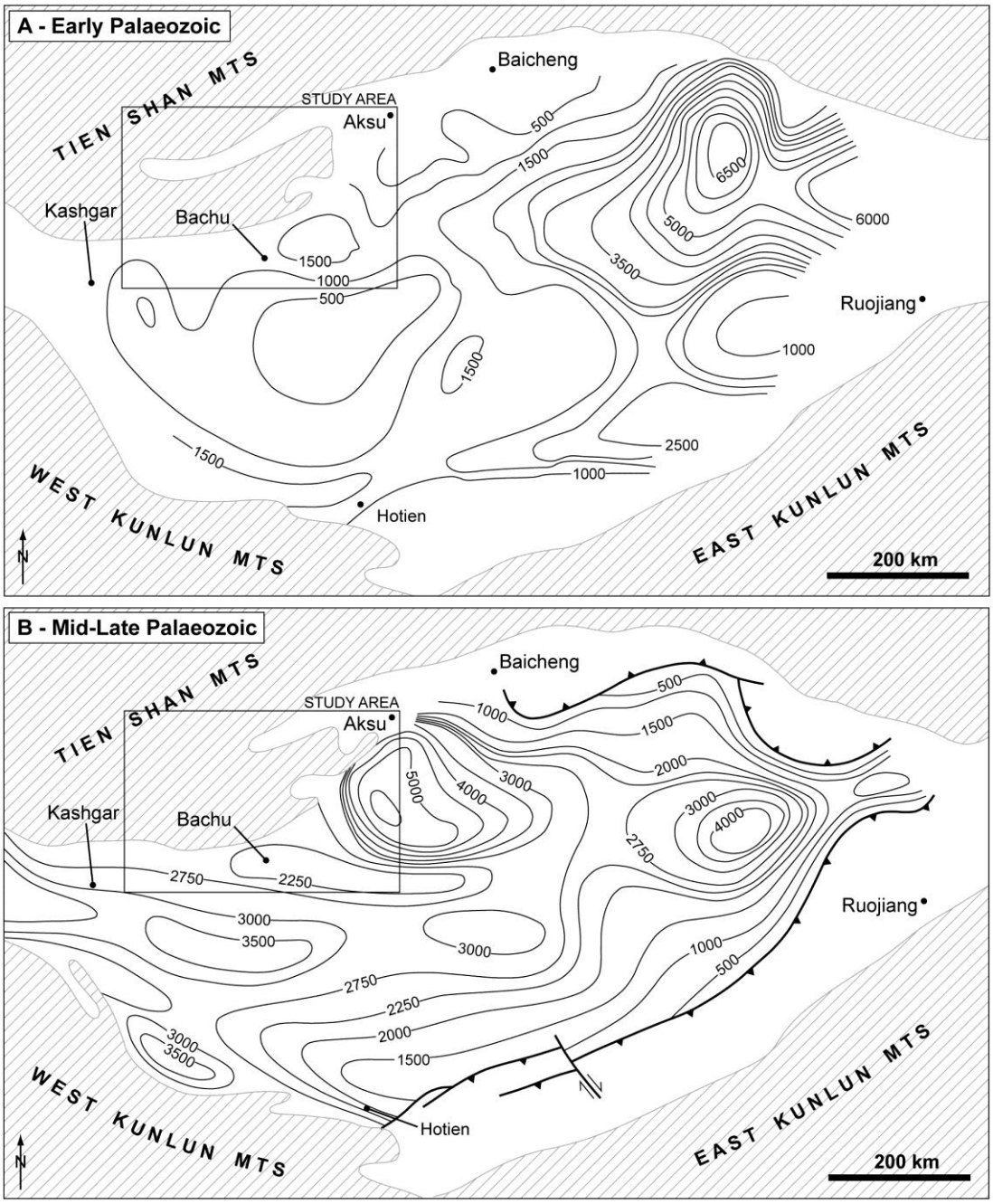

Fig. 3.2. Isopach maps of the Tarim Basin, redrawn from Bally *et al.* (1986). (A) The Early Palaeozoic (Cambrian–Ordovician), showing a relatively even distribution of 500–1500 m of sediment in the western Tarim Basin and a substantial thickening to more than 6500 m in the east. (B) The Middle to Late Palaeozoic (Silurian–Permian), showing a more complex distribution of sediment including substantial accumulations exceeding 5500 m in the Aksu area. Comments made by Bally *et al.* (1986) question the accuracy of these isopach maps, and therefore they are used only to provide a general overview of the sediment distribution patterns in the Tarim Basin during the Palaeozoic.

3.3 Palaeozoic Stratigraphy

The Palaeozoic consists of three stratigraphic groups, each recording a different phase of basin evolution: the Cambrian–Ordovician, Silurian–Devonian and Carboniferous–Permian. The age of the Palaeozoic formations was constrained by fauna and floral assemblages (Xinjiang Stratigraphic Table Compiling Group 1981; Carroll *et al.* 2001 and references therein) and by fission track sampling (Dumitru *et al.* 2001). Across the whole of the Tarim Basin, the total thickness of the Palaeozoic varies from 3–8 km (Fig. 3.2), while in the Keping Shan area the total thickness varies from less than 3 km in the central parts of the area to more than 6 km at Mu'er, in the east.

At outcrop scale, the sedimentology and stratigraphy are derived from sedimentary logging of 5–40 m sections. The spatial distribution of the Palaeozoic succession is analysed by generating isopach maps using the thicknesses of stratigraphic formations or units measured at sites distributed across the Keping Shan. Regional-scale isopach maps of the Tarim Basin (Fig. 3.2) do not cover the Keping Shan area, nor do they provide sufficient information concerning localised variations in stratigraphic thickness that could prove crucial to understanding the paleogeography and be of use in future structural studies of the NW Tarim Basin (Chapters 6–8). Stratigraphic thicknesses were estimated at over 50 sites across the area, and were measured directly in the field or indirectly using satellite images and the geological map. In order to obtain an estimate the stratigraphic thickness at a particular site, several values are required: (1) the apparent width, w, of the formation of sequence in plan view, derived from ground-based GPS or measurement from the geological map; (2) the average structural dip, θ, of the beds, derived from field measurement (for field sites, see Fig. 1.2) or published geological maps; (3) the change in elevation, Δh, across the formation or sequence. Using these values, the true thickness can be calculated using Equation 3.1:

$$t = \left(w + \frac{\Delta h}{\tan\theta}\right) \sin\theta \tag{3.1}$$

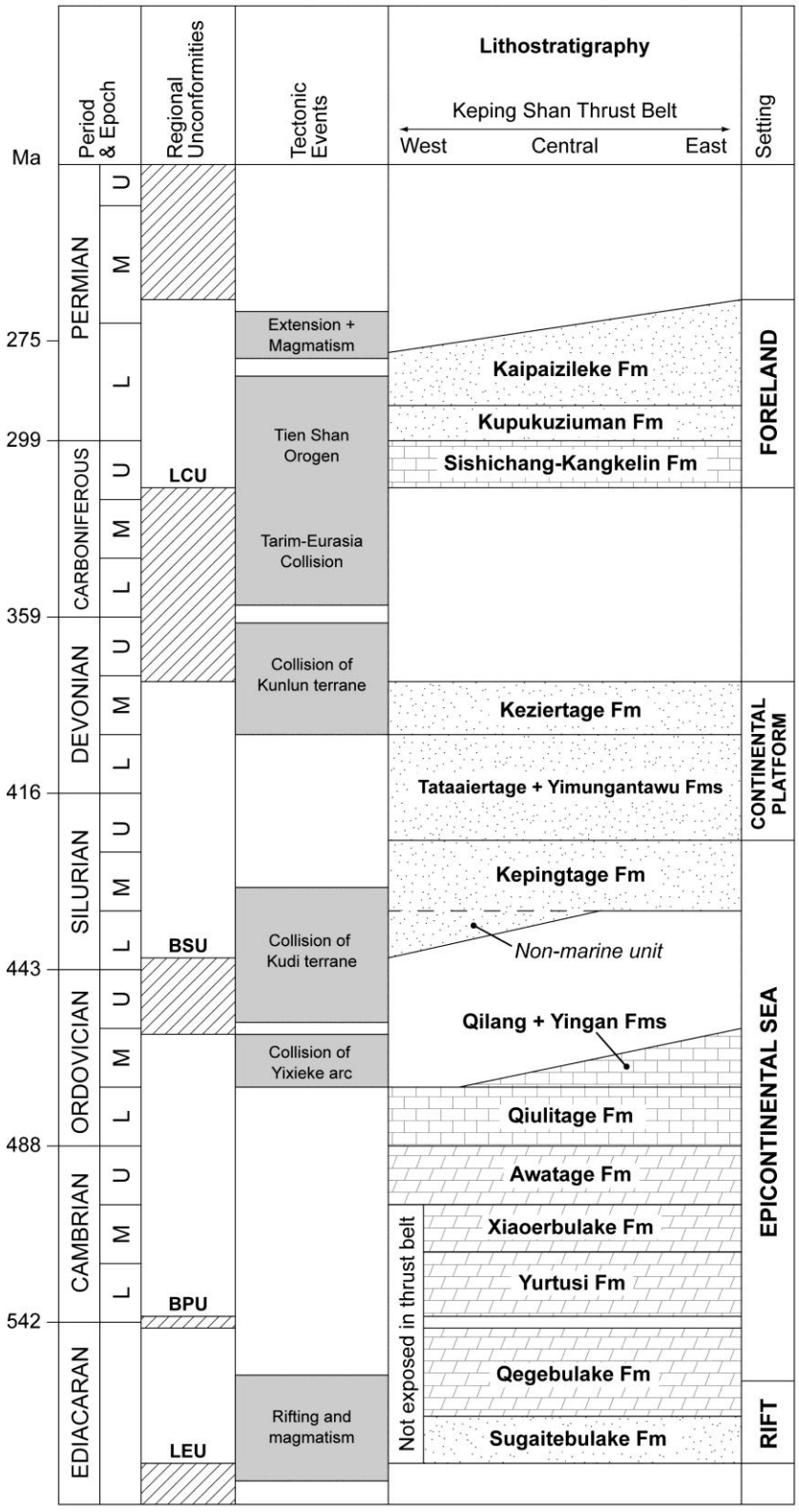

Fig. 3.3. Generalised stratigraphic column for the Keping Shan Thrust Belt, NW Tarim Basin, showing regional unconformities, significant tectonic events and the regional setting. LEU = Late-Ediacaran unconformity; BPU = Base-Palaeozoic unconformity; BSU = Base-Silurian unconformity; LCU = Late-Carboniferous unconformity. Age constraints on formation ages are derived from Carroll *et al.* (2001 and references therein).

3.3.1 The Cambrian-Ordovician Group

The Cambrian-Ordovician Group comprises a 1.6-1.8 km thick succession of carbonates that unconformably overlie Upper Neoproterozoic strata (Fig. 3.3). The base of the Lower Cambrian is defined by an 8-10 m succession of interbedded black shales and organic-rich carbonate beds that correspond to the phosphorite unit described by Carroll *et al.* (2001) and Yu *et al.* (2003). This is overlain by a c. 100 m thick, fine-grained dark grey dolomite which, along with the underlying shale unit, characterise the Yurtusi Fm. This formation is interpreted as a shallow, intertidal marine environment. The black shale at the base of the formation is thought to represent a brief period of anoxia. Similar phosphorite-bearing black shales are reported from the Lower Cambrian at sites in Siberia, Australia and India, which were all at low latitudes during the time of deposition (McKerrow *et al.* 1992).

The Yurtusi Fm passes abruptly upwards into the 500-600 m thick, pale grey and well bedded dolomite of the Xiaoerbulake Fm (Fig. 3.4, A and B). At the Aksu section (Fig. 3.1), individual beds are 1-2 m thick and coarsen upwards from fine-grained and planar laminated in their lower parts to coarse-grained units containing abundant, rounded carbonate pebbles in the upper parts (Fig. 3.4A). Nodular, very dark grey chert horizons constitute up to 5% of the succession. The Xiaoerbulake Fm is likely to reflect deposition in slightly shallower water depths (1-10 m) of the intertidal zone. The coarsening-upward and conglomeratic beds is thought to represent foreshore deposits, while the dark grey chert horizons may be the diagenetically altered remains of organic rich units. Both the Yurtusi and Xiaoerbulake formations crop out only in the eastern Keping Shan.

In contrast, the Upper Cambrian Awatage Fm crops out across the Keping Shan and is characterised by a 100-200 m thick succession of dolomites, consisting of alternating pale yellow, fine to medium-grained sand rich intervals (Fig. 3.5A) and grey, very fine to fine-grained mud-rich intervals. The sand-rich intervals contain thin (10-20 cm), nodular dark grey chert horizons (Fig. 3.4C) similar to those in the Xiaoerbulake Fm. Based on borehole data, Zhang *et al.* (2000) report a series of evaporite horizons in the

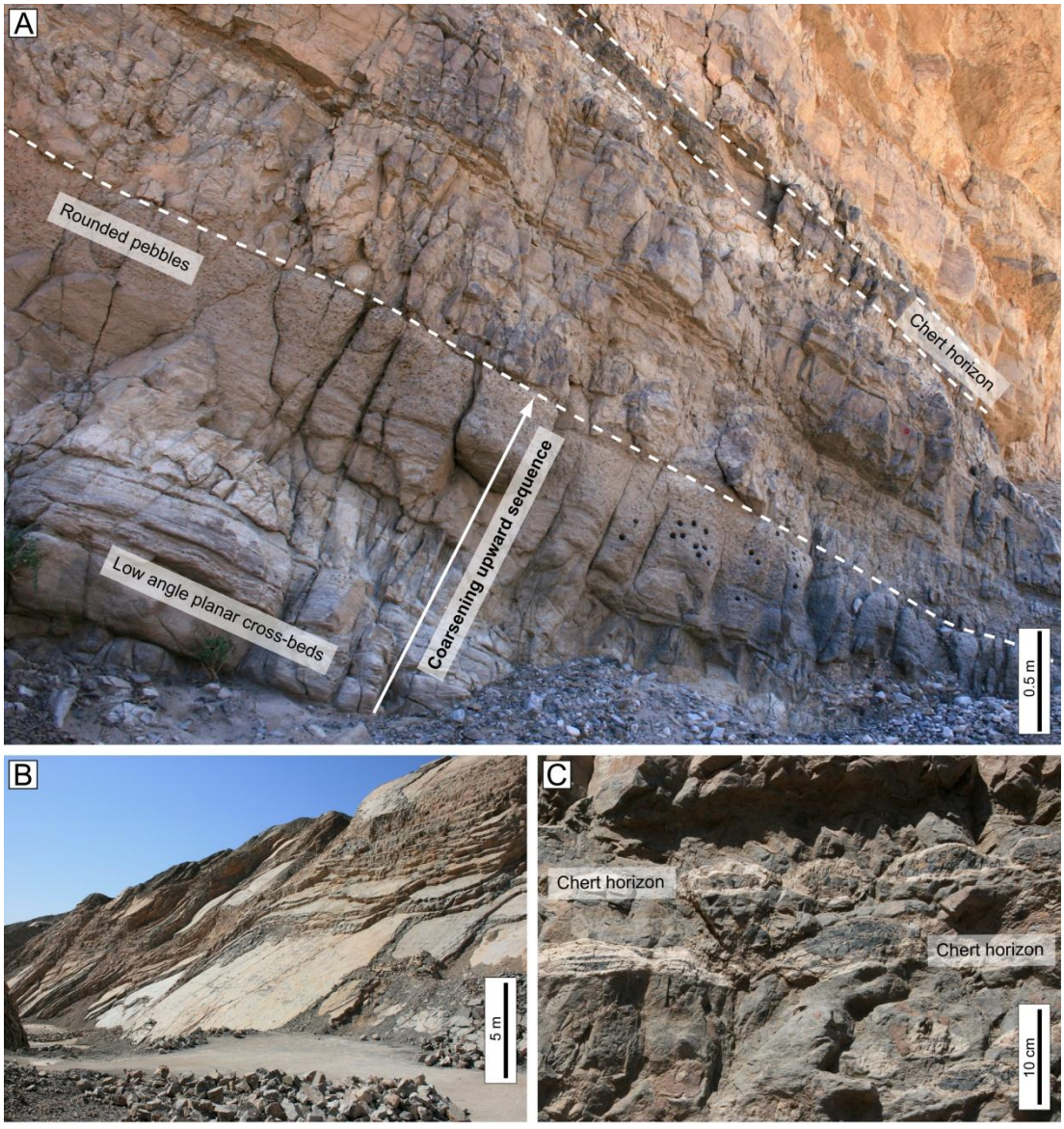

Fig. 3.4. Outcrop photographs of the Cambrian stratigraphy. (A) Intertidal, foreshore facies dolomites of the Xiaoerbulake Fm near Yingan, showing upward coarsening beds and chert horizons. (B) Well-bedded, pale grey dolomites of the Xiaoerbulake Fm at a quarry near Yingan. (C) Nodular dark-grey chert horizons in Awatage Fm dolomites near Subheshi.

in the lower part of the Awatage Fm, but these were not observed in outcrop. The Awatage Fm is interpreted to represent alternating shallow, intertidal facies (dolomites and cherts) and emergent, supratidal facies (evaporites). Zhang *et al.* (2000) interpreted the grey, mud-rich intervals as lagoonal facies although considered in the broader context of the depositional environment, these intervals may simply represent deeper, intertidal facies.

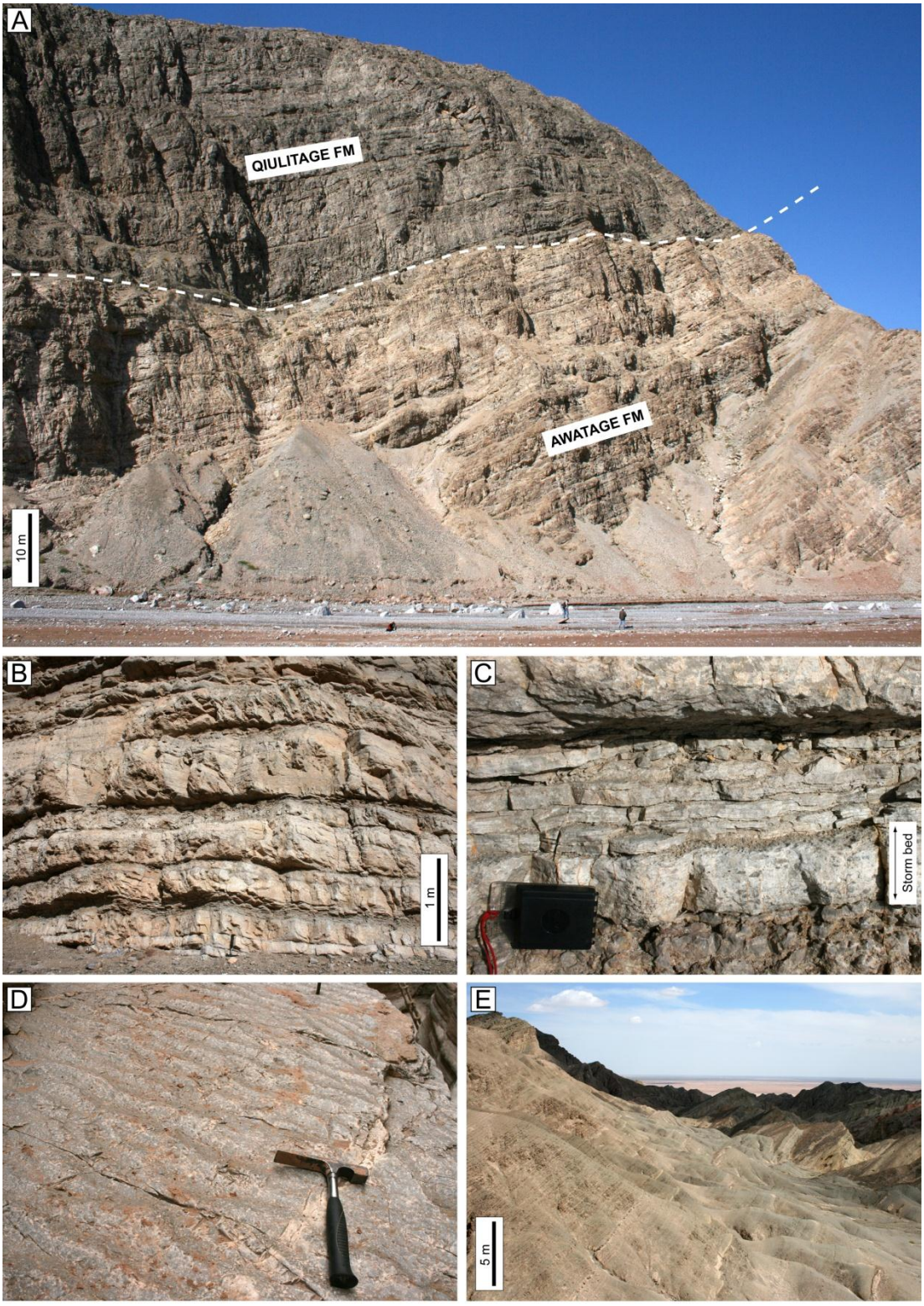

Fig. 3.5. Outcrop photographs of the Cambrian and Ordovician stratigraphy. (A) Conformable contact between the Cambrian Awatage Fm (dolomite) and the Ordovician Qiulitage Fm (limestone), at Subheshi. (B) Well-bedded limestones of the Qiulitage Fm, at Sanchakou, as presented in log section (Fig. 3.5). (C) Close-up photograph of *(b)*, showing a storm bed and laminated limestone. (D) Asymmetric, straight-crested (striking 100-120º) ripples on a bedding surface of Qiulitage Fm limestone, in the Mystery Canyon. (E) Interbedded green siltstones and pale brown limestones of the Yingan Fm, above the Sulphur Canyon. The Tarim Basin can be seen in the background.

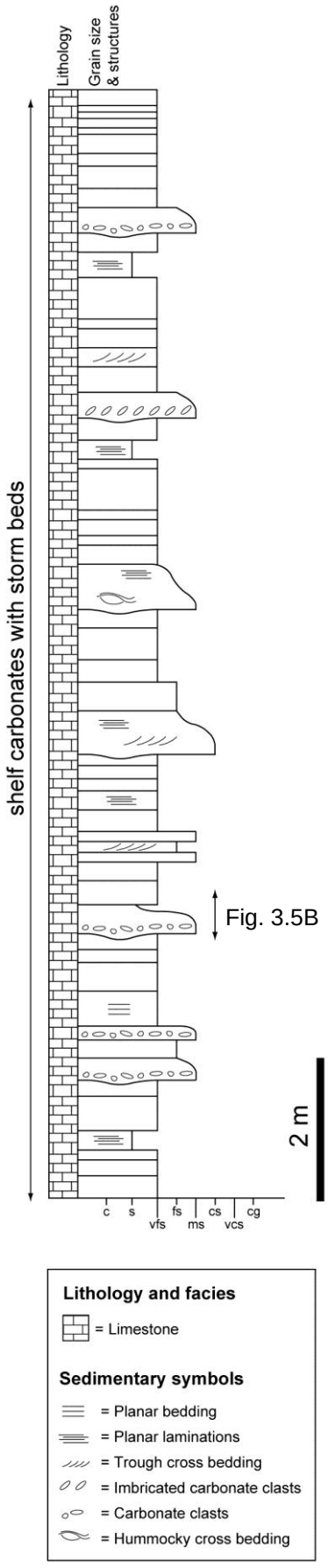

The pale yellow dolomites of the Awatage Fm pass conformably and abruptly upwards into the pale grey, cliff-forming micritic limestones of the 600–700 m thick Lower Ordovician Qiulitage Fm (Fig. 3.5A). A measured interval of the formation at Sanchakou (Fig. 3.5B and 3.6) exhibits cyclic 2–5 m sequences that commence with thin (0.5 m) beds containing abundant rounded clasts of carbonate (Fig. 3.5C), which are occasionally imbricated. These beds grade crudely upwards into fine to very-fine grained micritic limestone that contains hummocky and planar cross bedding. This repeating sequence is interpreted to represent storm deposits (*tempestites*) and intermittent periods of quiescence, implying deposition occurred in shallow to moderate water depths (15–20 m) within the subtidal zone. Towards the upper parts of the formation, bedding surfaces exhibit asymmetric, straight-crested wave ripples (Fig. 3.5D), which may imply shallower, intertidal water depths.

A thin black shale, representing the Saergan Fm, is reported to conformably overlie the Qiulitage Fm (Carroll *et al.* 2001) but was not observed in the sections examined during this investigation. The overlying Qilang Fm is c. 120 m thick and is characterised by nodular, thinly bedded (0.2–0.5) fine to medium-grained pale grey limestone.

Fig. 3.6. Sedimentary log of the Lower Ordovician Qiulitage Fm at Sanchakou. The formation comprises thin, coarse-grained conglomeratic storm beds that are interbedded with very fine-grained, micritic limestones.

Much like the Qiulitage Fm, it contains thin (0.3–0.5 m), conglomeratic beds that are interpreted as storm deposits. The younger Yingan Fm comprises a 200 m green siltstone succession that contains thin (0.5–1 m), bioturbated dark-yellow limestone (Fig. 3.5E), speculated to represent deep (30–40 m), subtidal conditions in the offshore transition zone.

The Cambrian–Ordovician Group reflects a prolonged period of carbonate sedimentation that occurred in relatively shallow depositional environments throughout. A gradually shallowing sequence through the Cambrian resulted in the accumulation of an 800–900 m succession, characterised by a progressive change from an intertidal to a supratidal setting. The conformable Lower–Middle Ordovician succession locally reaches similar thicknesses of up to 800 m and marks an abrupt regression to deposition in a deeper, subtidal setting that was periodically affected by storm activity. Water depths appear to have increased further into the Middle Ordovician.

3.3.2 The Silurian-Devonian Group

The base of the Silurian–Devonian Group is defined by a regional unconformity that spans the Middle Ordovician to Early Silurian. In contrast to the preceding Cambrian–Ordovician succession, the Lower Silurian to Middle Devonian was characterised by the deposition of a 2–3 km thick clastic sequence in a variety of paleoenvironments. The base-Silurian unconformity crops out in the Mystery Canyon (Fig. 3.1), where the Lower Silurian Kepingtage Fm unconformably overlies the Lower Ordovician Qiulitage Fm. The unconformity is surface is characterised by a thin (1–1.5 m) green-yellow clay that overlies a karstic surface at the top of thickly-bedded, micritic limestones (Fig. 3.7A, 3.8A). The clay is interpreted as a paleosol, which infills shallow (10–15 cm) paleogrykes on the weathered, karst surface (Fig. 3.7A). Across the Keping Shan, the unconformity removes different amounts of the underlying succession, accounting for the absence of the Middle Ordovician Qilang and Yingan formations across much of the Keping Shan.

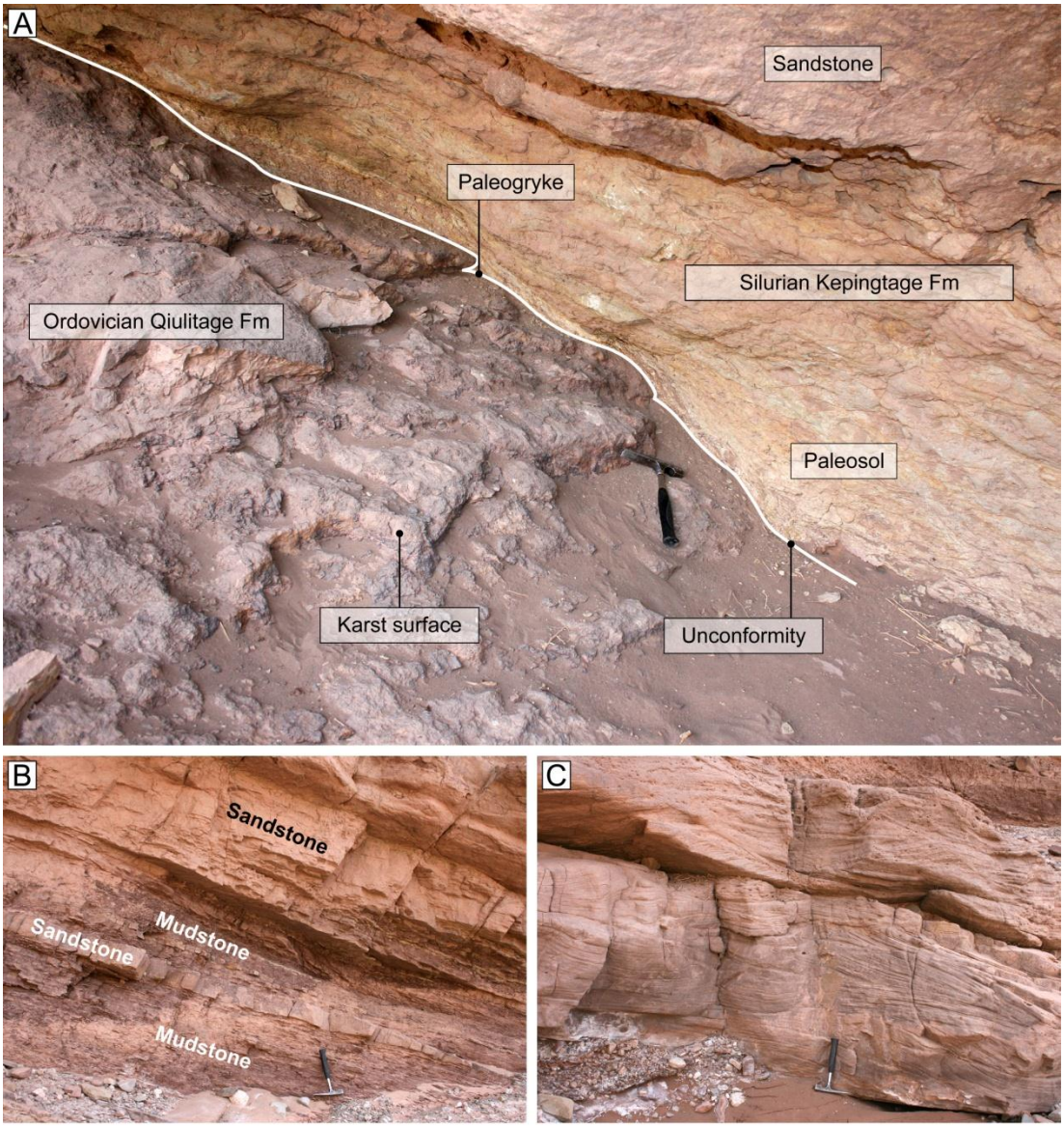

Fig. 3.7. Outcrop photographs of the lower part of the Silurian Kepingtage Formation: (A) The base-Silurian unconformity and the underlying karstic surface at the top of the Qiulitage Fm; (B) Interbedded sandstones and siltstones, showing a sandstone bed that thins (from left to right); (C) Channel sandstone showing well defined trough cross bedding.

Fan & Ma (1991) suggested that this unconformity represented an erosional relief of tens to hundreds of metres. However, our field measurements imply that this is likely to have been an underestimate. At Aqal, the Middle Ordovician Qilang and Yingan formations are c. 320 m thick, but are completely absent in the Mystery Canyon, 100 km to the west. As there appears to have been little structural control on the distribution of Middle Ordovician sediments, these observations suggest that the paleo-relief of the unconformity surface was at least 300 m.

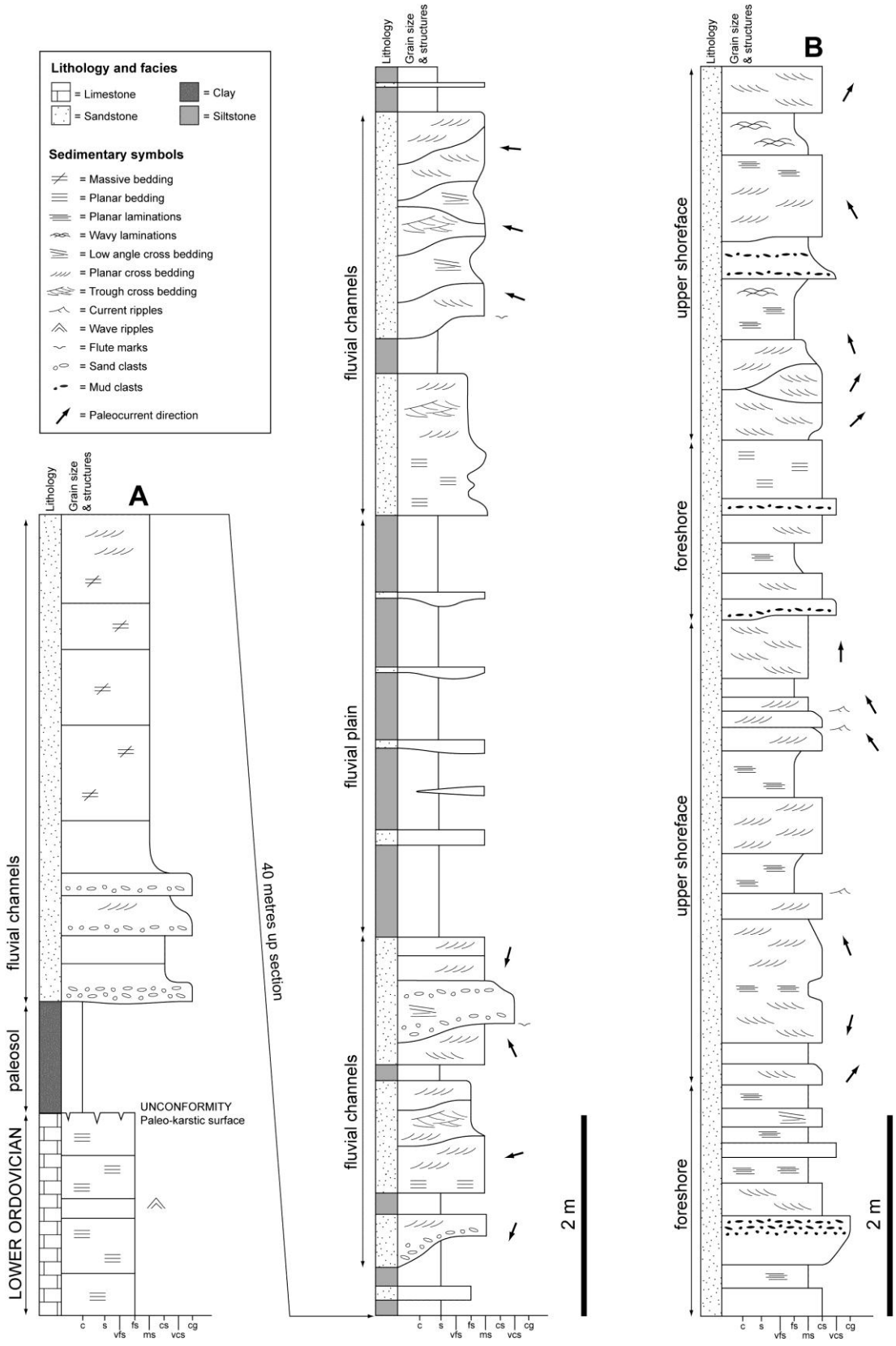

Fig. 3.8. Sedimentary logs of the Lower to Middle Silurian Kepingtage Fm. (A) The base-Silurian unconformity and the non-marine, alluvial plain facies of the lower Kepingtage Fm. (B) Upper shoreface to foreshore facies sandstones of the upper Kepingtage Fm.

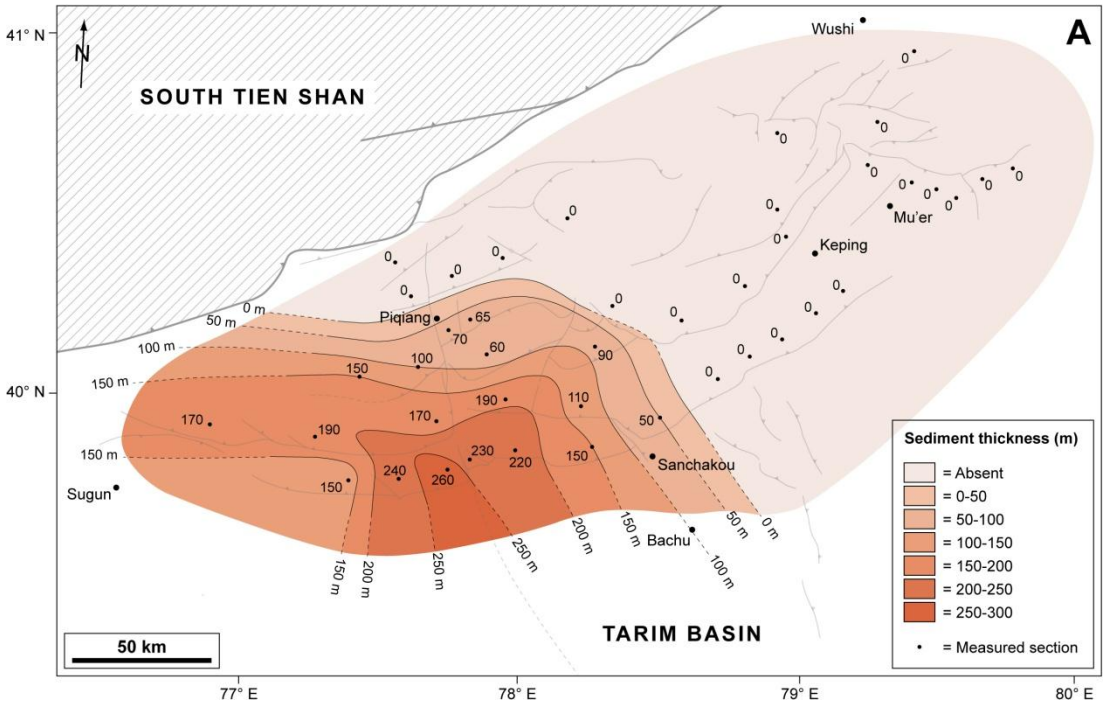

Fig. 3.9. Isopach map of the Lower Silurian non-marine, fluvial facies unit.

The Lower to Middle Silurian – fluvial facies unit. Immediately above the clay horizon, the lower part of the Kepingtage Fm comprises a unit of interbedded brown-red siltstones and sandstones that is up to 250 m thick. The sandstone intervals are medium to coarse-grained and contain planar and trough cross bedding. The bases of individual beds are often erosive and undulatory, above which there is occasionally a conglomeratic lag. The interbedded siltstones contain thin (less than 0.5 m), laterally discontinuous sandstone beds. This lower unit is interpreted to represent deposition on an alluvial floodplain. The isolated sand bodies within the siltstone intervals are thought to represent short-lived fluvial channels with limited lateral accretion, while the thicker sandstone intervals represent longer-lived, multi-storey meandering channel systems. Across the region, the thickness of the fluvial facies unit varies considerably (Fig. 3.9). The unit exceeds 250 m thickness in the central parts of the Keping Shan, but thins to absence to the north and west. It is for this reason that description of the fluvial facies unit is omitted from much of the published literature (e.g. Carroll *et al.* 2001). Limited paleocurrent data collected at the Mystery Canyon section (Fig. 3.8A) shows a dominantly westward flow direction, suggesting that the fluvial facies unit may relate to a paleo-valley in the southwest Keping Shan (Fig. 3.9)

The Lower to Middle Silurian – marine facies unit. In the central parts of the Keping Shan, the fluvial-facies unit passes rapidly upwards into a unit characterised by dark green siltstones (60%) interbedded with fine-grained sandstones (40%) (Fig. 3.10A). The sand-rich intervals contain hummocky cross bedding and are bioturbated (Fig. 3.10B). The dark green siltstone-sandstone succession passes gradationally upwards into medium to coarse-grained, pale green sandstones (Figs. 3.8B, 3.10A and C) that characterise the upper part of the Kepingtage Fm. The sandstones contain an abundance of planar laminations and bi-directional, planar cross bedding (Fig. 3.10D) associated with tidal water motion. Asymmetric, straight-crested ripples are preserved on a number of bedding surfaces. The middle to upper part of the Kepingtage Fm is interpreted to represent a gradually shallowing marine succession, in which deposition initially occurred in the offshore transition zone to distal lower shoreface, around the storm-wave base. Progressive shallowing is recorded by upward coarsening and the change in colour from dark to pale green. The upper part of the Kepingtage Fm is interpreted as an upper shoreface to foreshore environment, in which the sediment was continually reworked in alternating N-S current directions by tides (Fig. 3.8B).

An isopach map reveals that the thickness of the Silurian marine-facies unit (Fig. 3.11) varies across the region, from 200-300 m in the west to 500-600 m in the east and southeast. In comparison, the underlying fluvial-facies unit (Fig. 3.9) is absent in the east but thickest in the west. It seems plausible that the lower parts of the marine facies unit in the east are the lateral, offshore equivalent of the fluvial facies unit in the east. However, this is inconsistent with the paleocurrent directions from the Mystery Canyon area that suggest southward flow into a paleo-valley system. In the absence of better age constraints of these units and paleocurrent data from a wider area, this cannot be evaluated further.

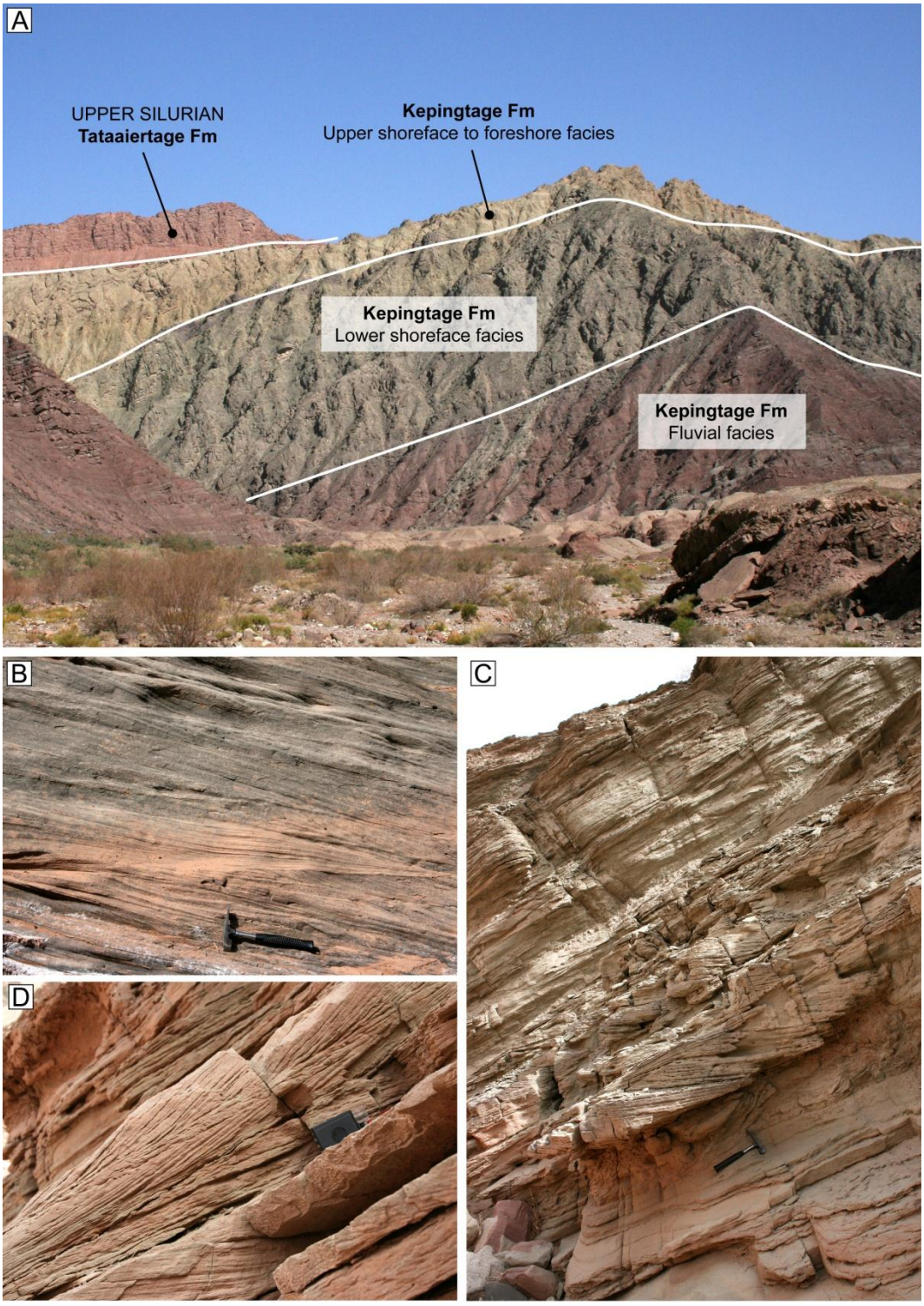

Fig. 3.10. Field photographs illustrating the sedimentological characteristics of the middle and upper parts of the Kepingtage Fm. (A) Cliff section in the Mystery Canyon, showing the colour changes through the Silurian, including the abrupt change non-marine to marine facies. Within the latter, there is a variation from dark to pale green, reflecting the transition from lower shoreface to upper shoreface and foreshore facies. (B) Hummocky cross bedding as an indicator of lower shoreface facies in the lower part of the Upper Kepingtage Fm. (C) Coarse-grained, sand-rich succession in the upper part of the Kepingtage Fm, shown as a sedimentary log in Fig. 3.8B. (D) Bi-directional cross bedding in the upper part of the Kepingtage Fm, indicating sediment reworking in the upper shoreface to foreshore.

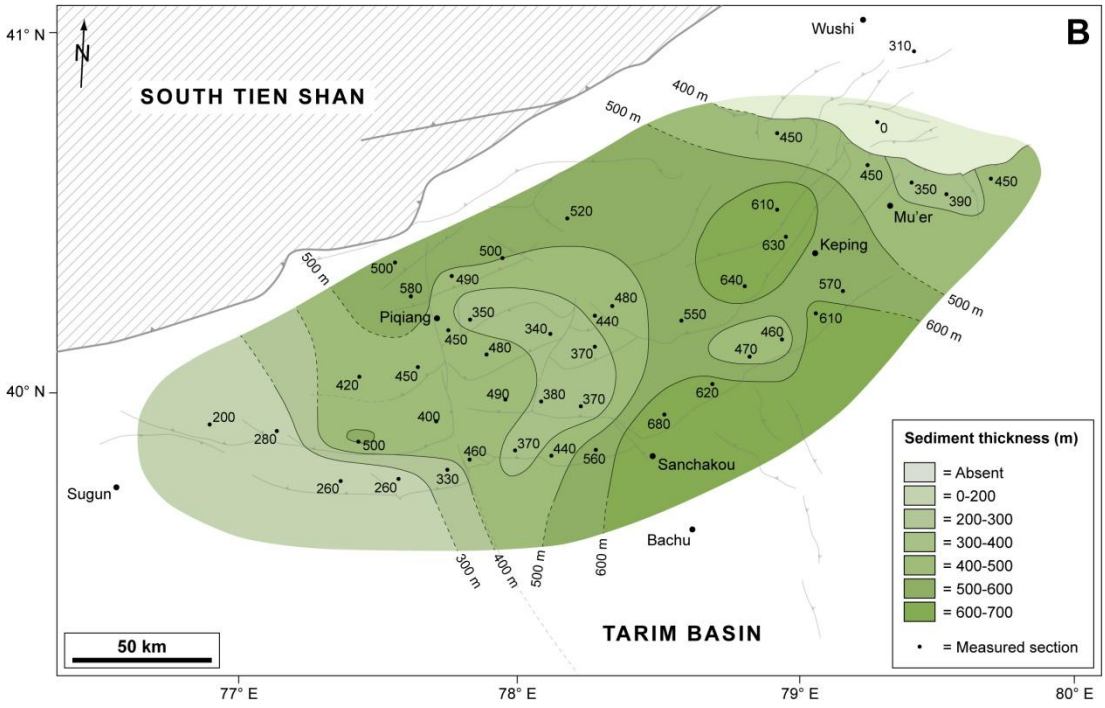

Fig. 3.11. Isopach map of the Middle Silurian marine, shoreface facies unit.

The Upper Silurian to Middle Devonian. The Upper Silurian Tataaiertage Fm is characterised by medium to coarse-grained red sandstones (80%) and interbedded siltstones (20%) that conformably overlie the preceding Middle Silurian, marine-facies unit (Figs. 3.12A, 3.13A and B). The sandstone beds have erosive bases and contain planar and trough cross bedding. Occasionally, broken shell fragments and conglomeratic lags are present at the bases of individual beds (Fig. 3.12A). The Tataaiertage Fm is interpreted to represent deposition in a sand-rich, meander belt system resulting in the development of multi-storey sand bodies. Consequently, the transition from the Kepingtage to the Tataaiertage Fm reflects a basin-wide marine regression. This transition is not abrupt, and thin red sandstone intervals within the uppermost, shoreface to foreshore facies of the Kepingtage Fm (Fig. 3.12A) imply periodic fluvial incursions and a gradual drop in relative base level.

The Lower Devonian Yimungantawu Fm has similar sedimentary characteristics to the Tataaiertage Fm but is dominated by finer red sands and red-brown siltstones (80%), while sand bodies are thin (<1 m) and isolated. It is speculated that there was

either a reduction in the amount of sand-rich sediment delivered to the basin during this period, or that subsidence rates increased. The Yimungantawu Fm is conformably overlain by the topographically prominent, cliff-forming Lower-Middle Devonian Keziertage Fm (Figs. 3.13A and D). The erosional character reflects an abrupt increase in sand content and grain size. The beds are medium to coarse-grained red sandstones comprising less than 10% interbedded red siltstones, and contain planar and low-angle cross bedding throughout. Paleocurrent data indicates a consistently WNW flow direction, which is similar to data collected by Carroll *et al.* (2001) at Aksu. The Keziertage Fm is interpreted as a stacked, fluvial system that formed in a wide meander belt. The abrupt transition from the Yimungantawu Fm to the Keziertage Fm implies either a sudden increase in the delivery of sand-rich sediment into the basin, or a decrease in subsidence rates.

The thickness of the Upper Silurian to Middle Devonian red beds varies substantially across the region (Fig. 3.14), reaching thicknesses of 1,500-2,000 m around Keping and Mu'er. This continues a trend set in the Middle Silurian (Fig. 3.11), when the same area accumulated a thicker stratigraphic succession than other parts of the region. In contrast, across the central and northern parts of the Keping Shan thicknesses are reduced to less than 400 m. In some cases, changes in thickness occur abruptly across fault zones that have been active during the Late Cenozoic. The gradual thinning of sediment to the north appears to be mostly attributed to the progressive loss of the Middle Devonian Keziertage Fm (c.f. Fig. 3.1). Carroll *et al.* (1995) proposed that this loss occurs as a result of erosion by the late-Carboniferous unconformity during the development of a Late Palaeozoic foreland basin.

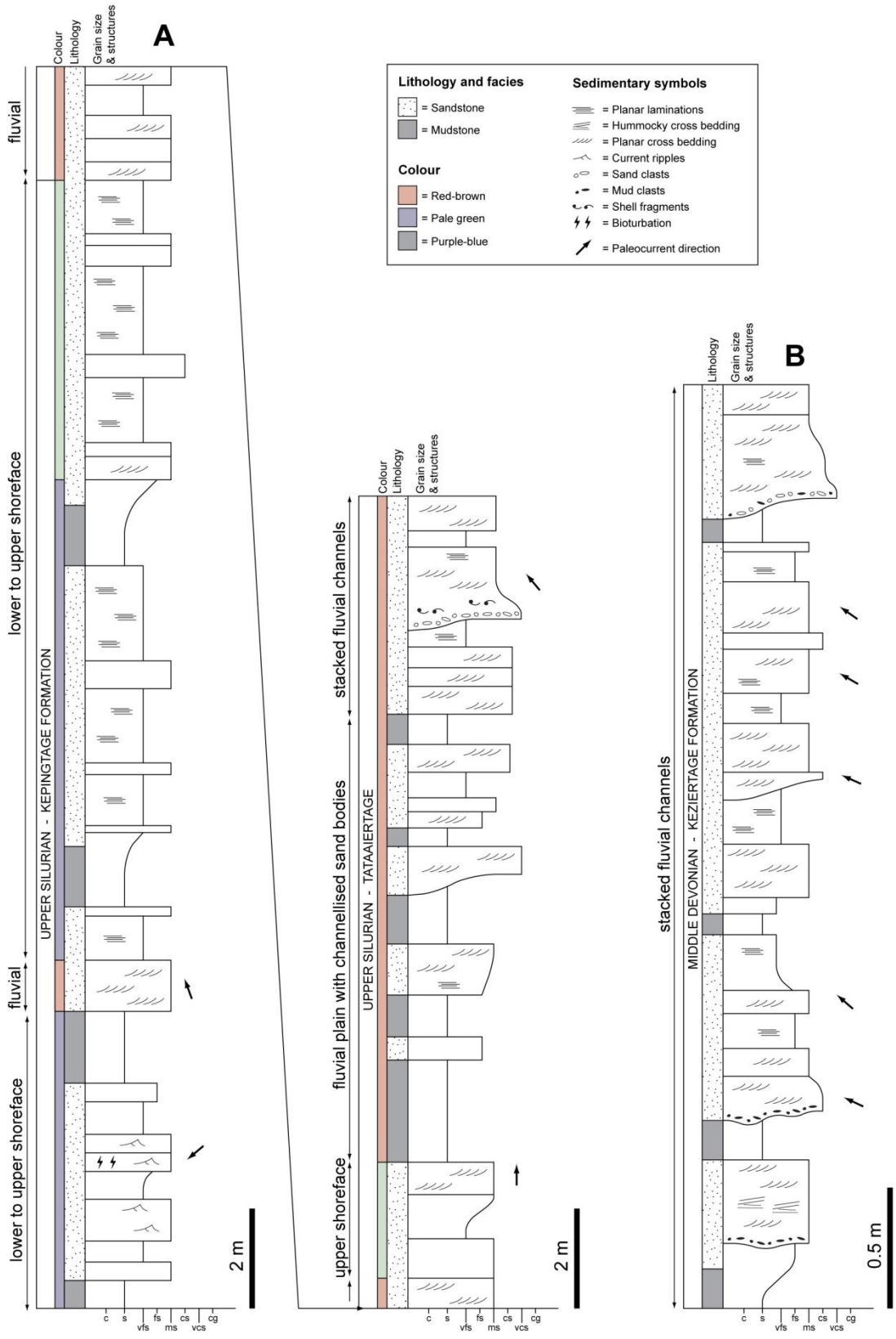

Fig. 3.12. Sedimentary logs of the Upper Silurian to Middle Devonian succession measured near Subheshi. (A) The conformable, gradual transition from Middle Silurian shoreface facies to Upper Silurian fluvial facies. (B) Type section through the Middle Devonian Keziertage Fm.

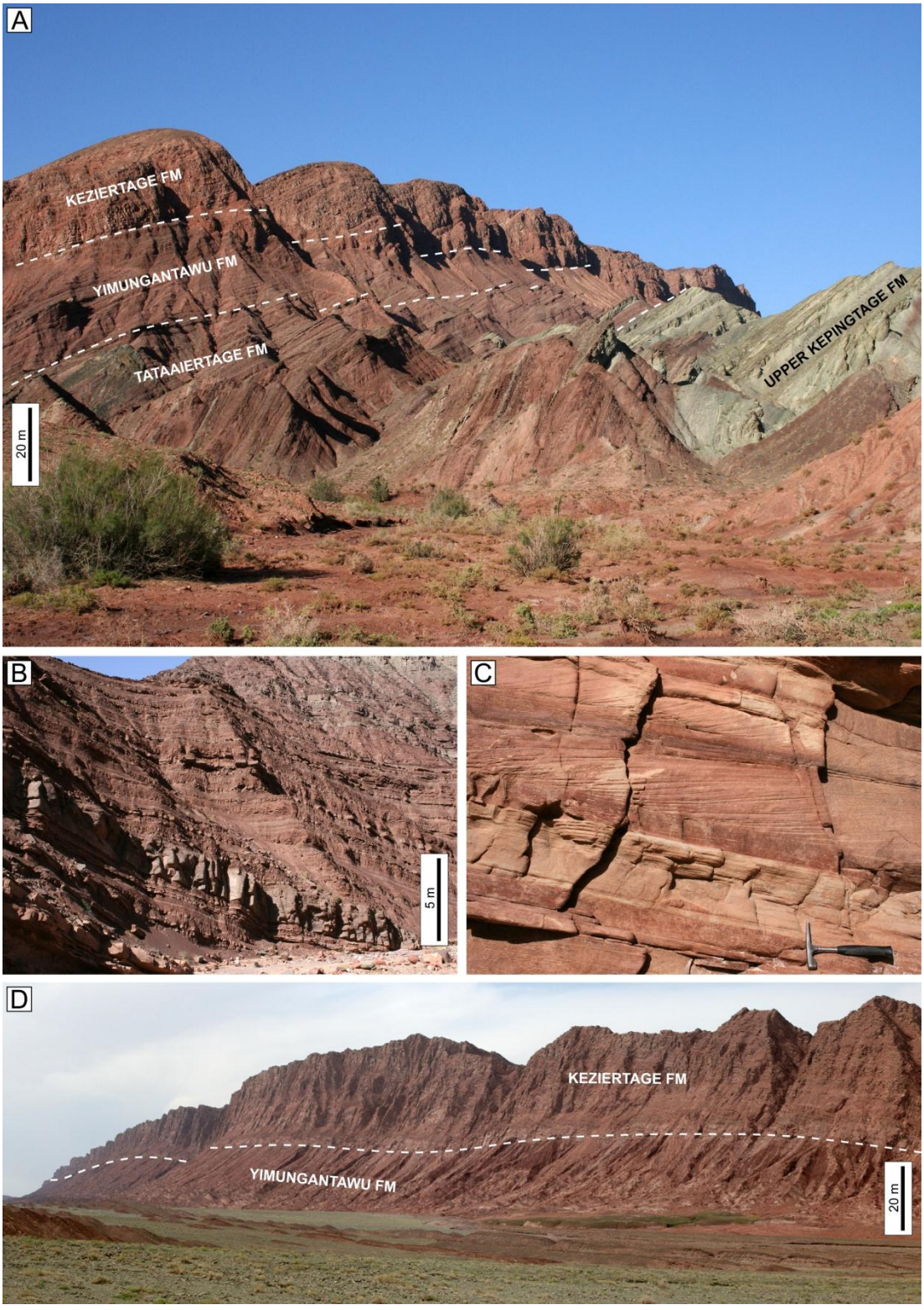

Fig. 3.13. Field photographs illustrating the character of Upper Silurian to Lower Devonian stratigraphy: (A) The succession exposed at Piqiang, showing the transition from marine (Upper Kepingtage Fm) to fluvial (Tataaiertage through Keziertage Fm) deposition and the associated colour change. (B) Interbedded sandstones and siltstones of the Tataaiertage Fm, in the Mystery Canyon, younging into the progressively mud-rich Yimungantawu Fm. (C) Trough cross bedding in the Keziertage Fm, in the Mystery Canyon. (D) Panoramic view of cliff-forming, sand-rich Keziertage Fm overlying the mud-rich, slope-forming Yimungantawu Fm, in the Subheshi Canyon.

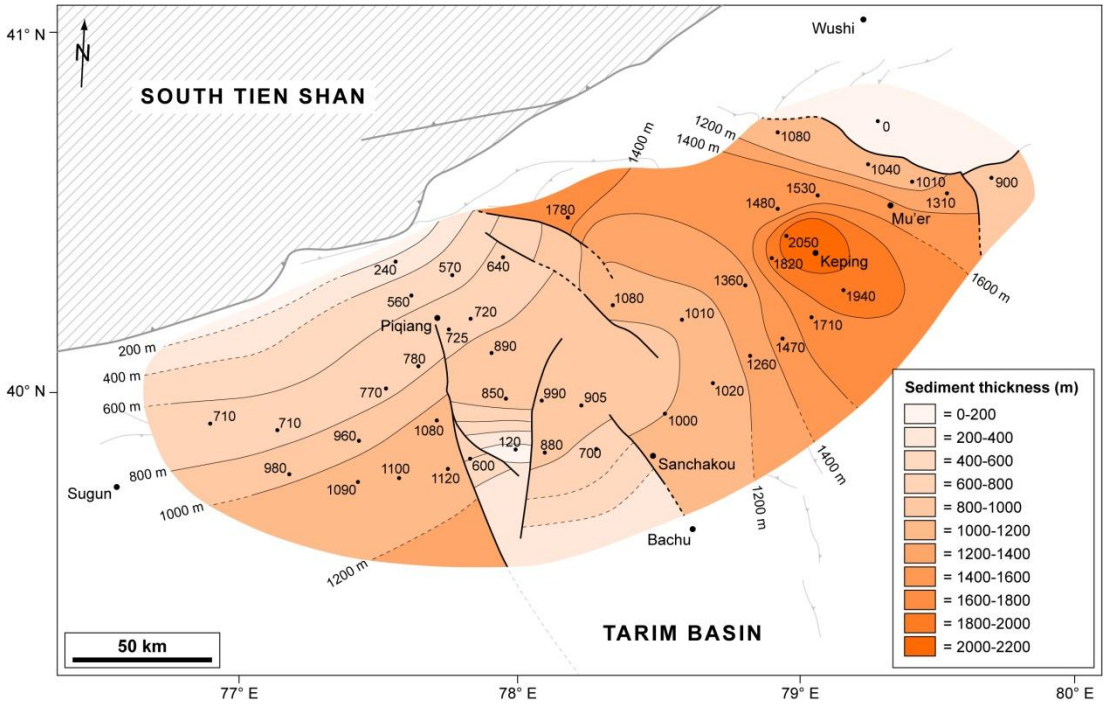

Fig. 3.14. Isopach map of the Upper Silurian to Middle Devonian red sandstone succession.

3.3.3 The Carboniferous-Permian Group

Upper Carboniferous sandstones, limestones and siltstones lie above an angular unconformity which locally removes a substantial part of the underlying Middle Devonian Keziertage Fm. The unconformity and the overlying Sishichang and Kangkelin formations were examined and measured at a section near Subheshi (Fig. 3.15A and 3.16A). At measured field sections across the southern Keping Shan, the thickness of the Upper Carboniferous succession is 120–200 m and forms a characteristic pale-grey cap above cliff-forming Devonian red beds (Fig. 3.16A). The succession is absent across the central part of the Keping Shan, in the same area that the Lower Permian succession is missing (c.f. Fig. 3.18). In contrast, it becomes rapidly thicker (>800 m) in the northern parts of the Keping Shan (Fig. 3.16B), thereby dominating the regional geological map (Fig. 3.1). Because the succession is relatively thin across much of the area, and the topographic variations across it are significant, it was not possible to obtain measurements from additional sections

without inducing substantial degrees of error, and therefore an accurate isopach map could not be generated.

Upper Carboniferous Sishichang and Kangkelin formations. At Subheshi, the Sishichang Fm is 50-60 m thick and comprises a series of upward-shallowing (regressing) parasequences that are bounded at their tops by abrupt marine transgressions (Fig. 3.15A). The lowest parasequence is characterised by a very coarse-grained, 4-6 m thick dark yellow sandstone bed immediately above the late-Carboniferous unconformity, which contains planar cross beds and planar laminations. This fines upwards into an 8-10 m thick brown-coloured siltstone bed, which in the upper part becomes progressively more green-yellow in colour and contains abundant 1-2 cm thick gypsum veins that are concordant to bedding, and lenticular sandstone nodules. The siltstone is overlain by a 20-25 m succession of interbedded medium-grained sandstones (70%) and siltstones (30%). The sandstone beds are finely laminated and have a pale yellow colour, while the interbedded siltstones are green-yellow. This lower parasequence is interpreted as foreshore to supratidal (sabkha) facies, with periodic foreshore incursions (minor marine transgressions) in the upper part of the unit. The second and third parasequences (Fig. 3.15A) consist of massively bedded interbedded limestones and sandstones in their lower sections which are overlain by interbedded red-brown siltstones and pale yellow sandstones and are relatively devoid of sedimentary structures throughout. Speculatively, these parasequences are interpreted as subtidal facies limestones that shallow upwards into inter- to supra-tidal mud flat facies.

The overlying Kangkelin Fm is 60-80 m thick (at Subheshi) and is characterised by planar bedded grey to dark grey limestones (grainstones) (Fig. 3.16B) that contain an abundance of marine fauna, predominantly bryozoans and brachiopods (Fig. 3.16C). The limestones are interpreted as shallow marine, subtidal facies and indicate a deepening marine basin. In addition, this appears to represent the end of the fluctuations in relative sea level that caused the facies variability in the preceding Sishichang Fm.

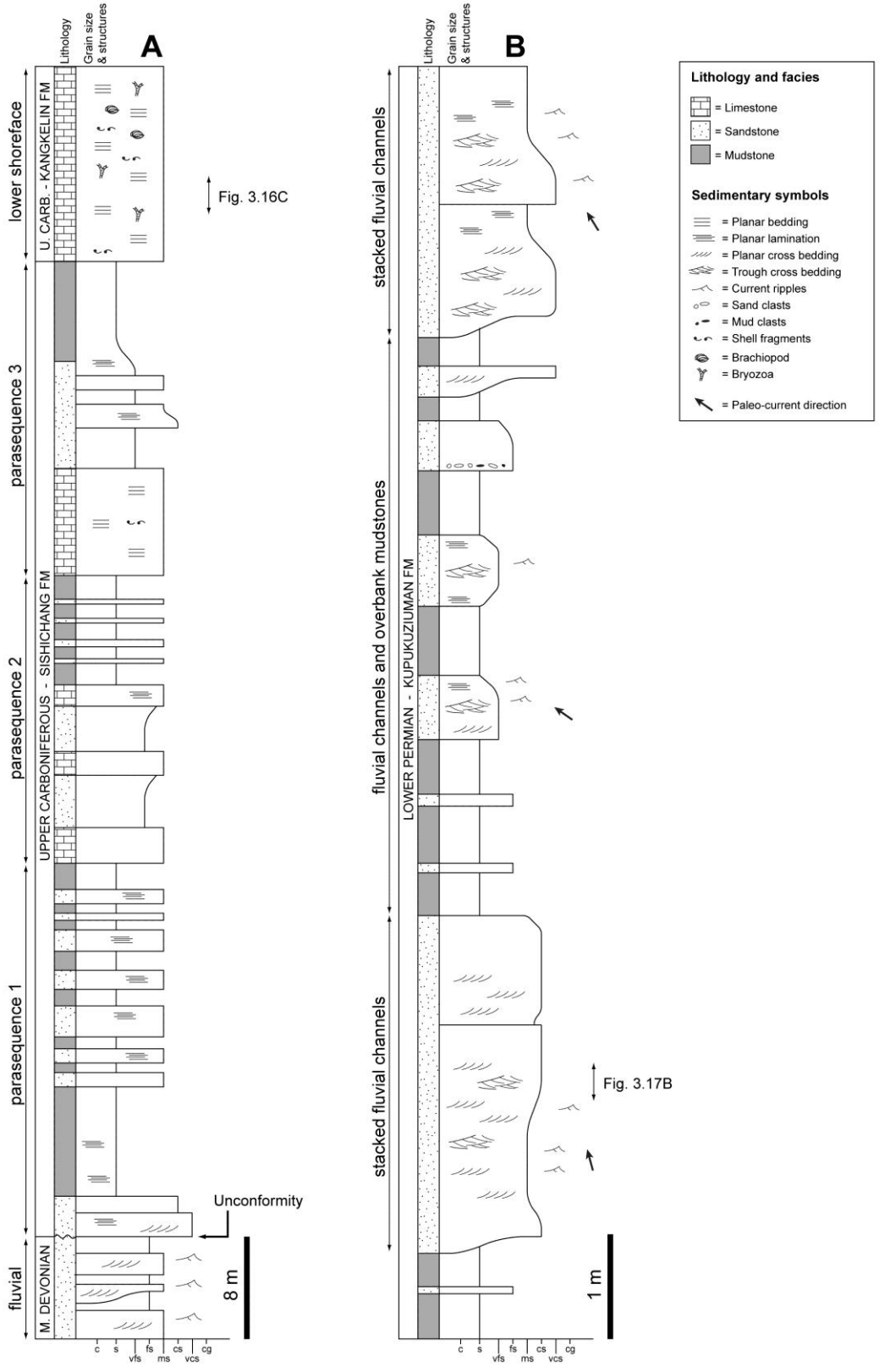

Fig. 3.15. Sedimentary logs of the Carboniferous-Permian megasequence near Subheshi. (A) The transition into and basal section of the Upper Carboniferous Sishichang-Kangkelin Fm, unconformably overlying the Middle Devonian Keziertage Fm. (B) Type section through fluvial facies of the Lower Permian Kupukuziuman Fm.

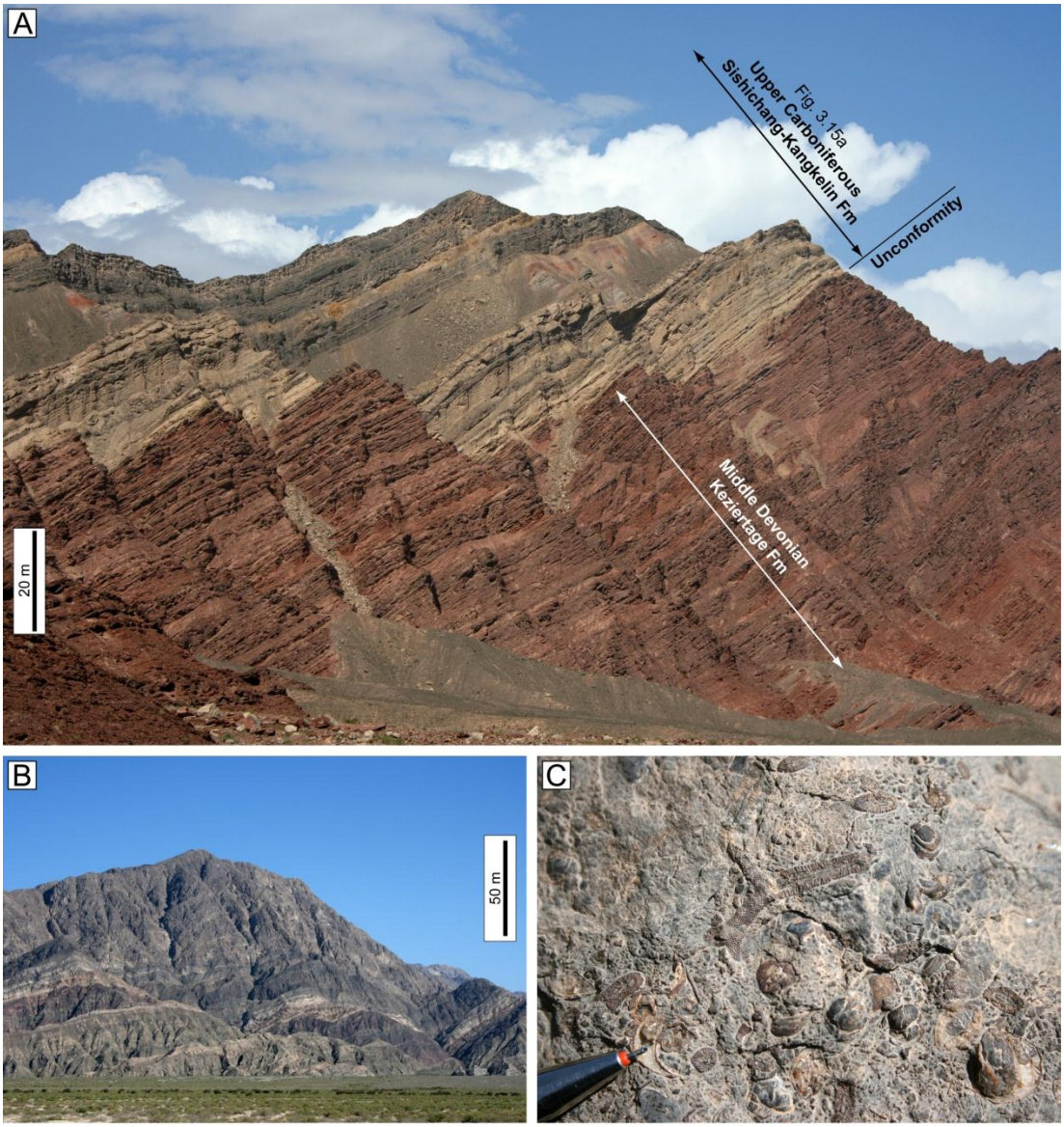

Fig. 3.16. Field photographs of the Upper Carboniferous succession: (A) The late-Carboniferous angular unconformity at Subheshi, defined by an abrupt transition from red sandstones of the Middle Devonian Keziertage Fm to the foreshore and shoreface facies of the Upper Carboniferous Sishichang Fm. (B) Thick limestone succession of the Upper Carboniferous Kangkelin Fm cropping out in a thrust sheet north of Piqiang. (C) Typical fossil assemblage in the Kangkelin Fm, including bryozoans, brachiopods and other broken shell fragments.

The Lower Permian. The Kupukuziuman and Kaipaizileke formations (Fig. 3.3) consist of interbedded sandstones, siltstones and volcanics that conformably overlie the marine-facies limestones of the Kangkelin Fm. The clastic intervals consist of pale yellow to pale pink interbedded sandstones and siltstones (Figs. 3.15B, 3.17A). The sandstone beds contain planar and trough cross beds (Fig. 3.17B), and climbing ripples (Fig. 3.17C). The bases of individual beds are commonly erosive and undulatory,

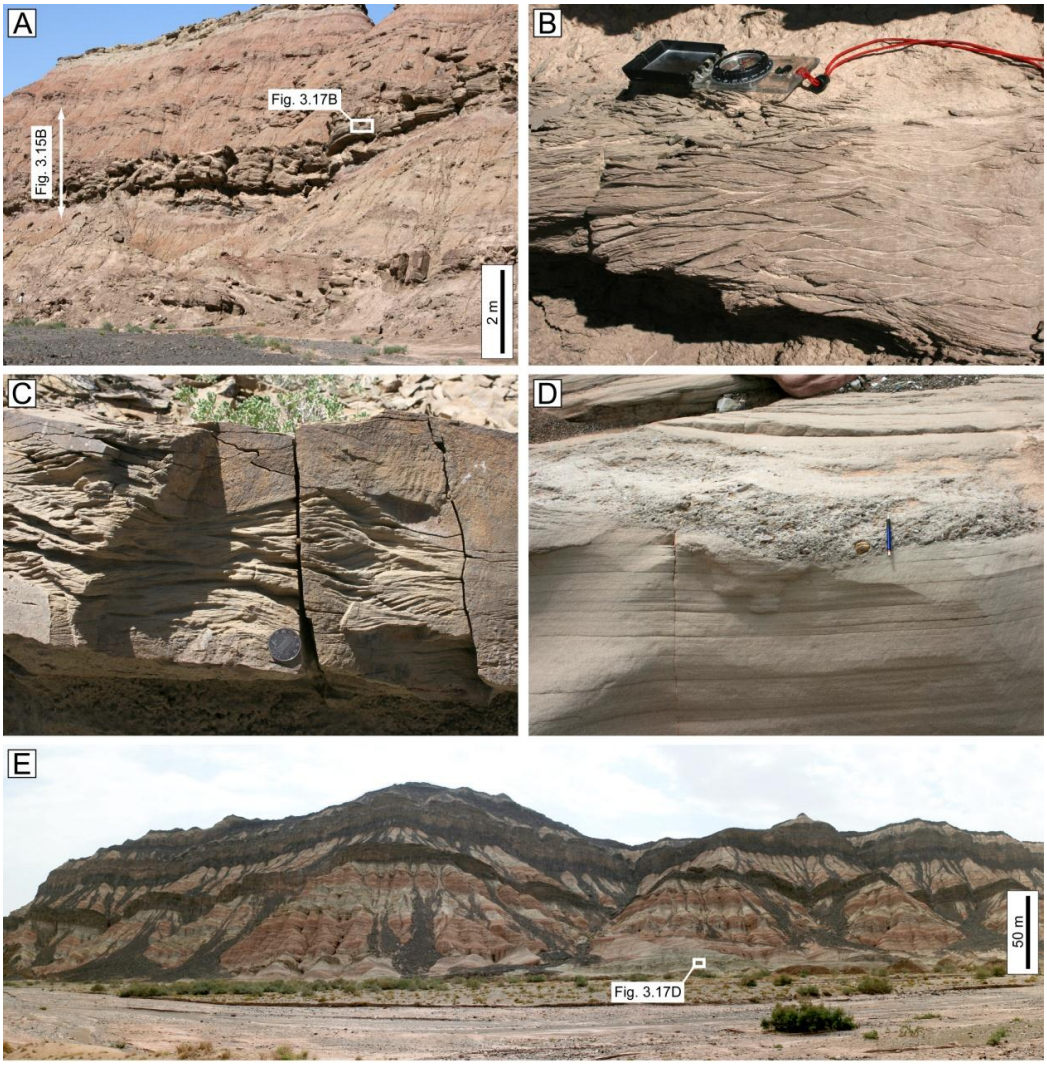

Fig. 3.17. Field photographs illustrating the Lower Permian succession: (A) Interbedded semi-arid fluvial sandstones and siltstones of the Kupukuziuman Fm at Subheshi, and shown in log section in Fig. 3.12b. (B) Trough cross-bedding in a fluvial channel sandstone in the Kupukuziuman Fm at Subheshi. (C) Climbing ripples in profile view in a fluvial channel sandstone in the Kupukuziuman Fm at Piqiang. (D) Erosive scour and conglomeratic lag in a fluvial channel sandstone in the Kaipaizileke Fm at Yingan. (E) Series of extrusive basalts within the fluvial sandstones and siltstones of the Kaipaizileke Fm at Yingan.

above which there is a thin conglomeratic lag (Fig. 3.17D). These sand bodies are inferred to represent meandering, fluvial channels, while the interbedded siltstones are interpreted as overbank deposits of an alluvial plain. The volcanic intervals consist of basalts (Fig. 3.17E), which based on their internal structure are likely to have been extruded as a series of pahoehoe lava flows. Individual basaltic lava flows are characterised by a dark grey, crystalline and columnar-jointed core section and a brown, vesiculated upper crust section. Flow-top lobe structures are observed on the upper surface of individual lava flows.

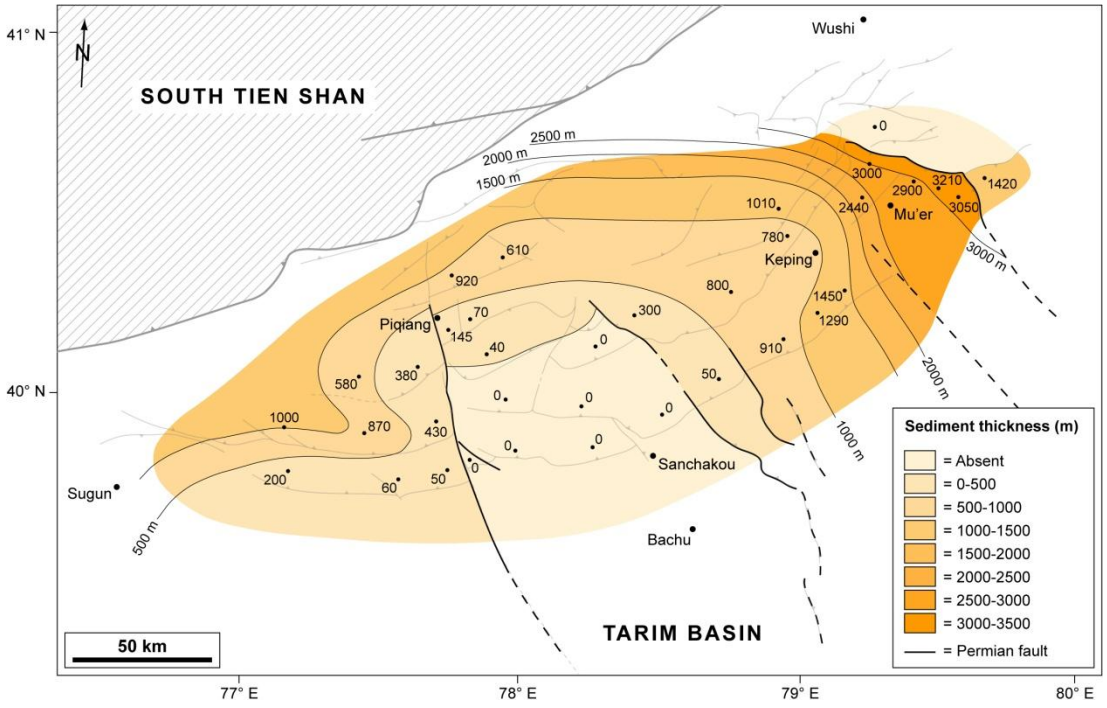

Fig. 3.18. Isopach map of the Lower Permian.

The thickness of the Lower Permian succession varies more significantly across the Keping Shan than any other formation. An isopach map (Fig. 3.18) shows that the Lower Permian is completely absent across the central parts of the region. In contrast, the succession exceeds thicknesses of more than 3,000 m at Mu'er. In a similar manner to the Middle Devonian and Upper Carboniferous successions, the changes in thickness occur abruptly across fault zones that have been active during the Late Cenozoic, the implications of which are examined in Chapter 4.

3.4 Subsidence History

Using the data presented in this report, it is possible to backstrip the sedimentary succession in order to derive the rate of tectonic subsidence through time. The tectonic subsidence of the basin provides a quantitative estimate of the depth that the basement would have been during a particular time period, by accounting for the effects of sediment and water loading, and provides critical information for unravelling the tectonic evolution of the basin.

3.4.1 Methodology

The subsidence plots presented in this report are derived using the methods described by Bond & Kominz (1984), Watts (2001) and Allen & Allen (2005). The subsidence history has been estimated for three of the sections: Mu'er, Subheshi and the central Keping Shan. These sections provide the most complete stratigraphic sections and the most accurately measured stratigraphic thicknesses.

Firstly, the stratigraphic succession must be decompacted in order to derive the thickness of each unit prior to burial. This is achieved by estimating the porosity of the unit at the present depth, and the porosity prior to burial. These values are not directly available for the measured stratigraphic sections and are therefore obtained from the porosity-depth curves by Bond & Kominz (1984) (Table 3.1). The decompacted thickness of a particular unit is given by:

$$S_i^* = \frac{S_i\,(1-\phi_i)}{(1-\phi_i^*)} \tag{3.2}$$

where S_i and ϕ_i are the measured thickness and porosity at burial depth, and S_i^* and ϕ_i^* are the decompacted thicknesses and porosity respectively. With this information, the process of calculating the tectonic subsidence initially requires the bulk sediment density, $\overline{\rho_s}$, of the succession to be calculated for each known time horizon. For any given horizon, the bulk sediment density is the sum of the density of each preceding unit divided by the total, decompacted thickness of the succession, S^*:

$$\overline{\rho_s} = \sum_{i=1}^{n} \frac{\left[\rho_w\,\phi_i^* + \rho_{gi}\,(1-\phi_i^*)\right]S_i^*}{S^*} \tag{3.3}$$

where n is the total number of stratigraphic units in the succession at a particular time and ρ_{gi} is the density of the sediment grains, obtained from Sclater & Christie (1980).

Table 3.1. Parameters used to decompact the sedimentary succession.

Stratigraphic Unit	Lithology	ϕ_i	ϕ_i^*	ρ_{gi} (kg m^{-3})
Lower Permian	Sandstone, siltstone	0.3	0.35	2680
Upper Carboniferous	Limestone, sandstone	0.3	0.6	2700
Middle Devonian	Sandstone	0.2	0.3	2650
Upper Silurian – Early Devonian	Sandstone, siltstone	0.2	0.25	2680
Early – Middle Silurian	Sandstone	0.15	0.3	2650
Lower – Middle Ordovician	Limestone (micrite)	0.1	0.5	2700
Lower – Upper Cambrian	Limestone (micrite)	0.1	0.4	2700

The tectonic subsidence or uplift, Y, is then calculated by taking into account Airy isostasy and the effects of paleobathymetry, eustatic sea-level change and the sediment load for each particular time horizon:

$$Y = W_d + S^* \left[\frac{(\rho_m - \bar{\rho_s})}{(\rho_m - \rho_m)}\right] - \Delta_{sl} \frac{\rho_m}{(\rho_m - \rho_w)} \tag{3.4}$$

where W_d is the water depth and Δ_{sl} is the sea-level height at a particular time (Table 3.2). Values for water depth are derived from the facies analyses presented in this report. Throughout the Palaeozoic, water depths remained relatively shallow (20-60 m) and for prolonged periods, deposition occurred in non-marine (e.g. alluvial plain) environments at elevations that are difficult to constrain. The sea-level heights for different time horizons were derived from Miller *et al.* (2005), Haq & Schutter (2008), and references therein. The mantle density, ρ_m, is assumed to be 3300 kg m^{-3} and water density, ρ_w, is assumed to be 1000 kg m^{-3}.

Errors are likely to be induced in the subsidence calculations and therefore this method provides only an estimate of tectonic subsidence rates through time. The parameters most likely to affect the calculations are the estimated porosities (obtained from Bond & Kominz (1984)) and the accuracy of the formation ages.

Table 3.2. Parameters used to calculate tectonic subsidence.

Horizon (Ma)	**Description**	W_d (m)	Δ_{sl} (m)
265	Top Lower Permian	-50	100
299	Top Upper Carboniferous	40	100
305	Base Upper Carboniferous (unconformity)	0	90
390	Top Middle Devonian	-20	130
400	Top Lower Devonian	-20	120
425	Top Middle Silurian	60	210
440	Base Silurian (unconformity)	30	180
470	Top Middle Ordovician	30	170
490	Top Upper Cambrian	30	200
540	Base Lower Cambrian	N/A	N/A

3.4.2 Results

Subsidence curves were calculated for three sites across the Keping Shan (Fig. 3.19), from which sedimentation and subsidence rates were calculated (Fig. 3.20). The data shows that there were three periods of subsidence, separated by two periods of non-deposition and erosion that generated the regional unconformity surfaces. At all three sites, the patterns of total and tectonic subsidence are broadly similar, and correlate well with a similar exercise undertaken on the Palaeozoic succession near Aksu (Carroll *et al.* 2001). Local variations in subsidence rate between the three sites arise in part by the action of subsequent unconformities, and therefore must be treated with some caution.

During the Cambrian-Ordovician, tectonic subsidence reached depths of 1.5-2 km. Rates of tectonic subsidence increased from 0.01 to 0.02-0.06 mm yr^{-1} between the Cambrian and Ordovician (Fig. 3.19). At Subheshi, a comparatively small increase in subsidence rates (Fig. 3.20) reflects a relatively thin Lower Ordovician succession that is probably attributed to erosion prior to the Early Silurian. This is likely to apply to all of the measured sections, such that values for Ordovician sedimentation and subsidence rates only provide a minimum estimate.

Following a depositional hiatus during the Late Ordovician to earliest Silurian, 1-2 km of tectonic subsidence is estimated to have occurred between the Early Silurian and Middle Devonian (Fig. 3.19). Sedimentation and subsidence rates were higher than the preceding Cambrian-Ordovician interval (Fig. 3.20). During the Early to Middle Silurian, subsidence rates of 0.02-0.03 mm yr^{-1} correspond to deposition of the clastic non-marine to marine succession of the Kepingtage Fm. The transition to non-marine, mud-rich fluvial facies in the Late Silurian to Early Devonian coincides with a noticeable decrease in tectonic subsidence rates to 0.01-0.02 mm yr^{-1} across the region, but the abrupt transition into the sand-rich fluvial facies of the overlying Keziertage Fm at the start of the Middle Devonian corresponds to an increase in subsidence rates. At Subheshi and Mu'er, the Middle Devonian qualifies as the fastest period of tectonic subsidence in the Palaeozoic, reaching 0.07-0.08 mm yr^{-1}. A much lower rate of 0.03-0.04 mm yr^{-1} in the Central Keping Shan is attributed to the removal of part of the Keziertage Fm by the late-Carboniferous unconformity, resulting in an anomalously low (under-estimated) subsidence rate.

The Late Carboniferous to Early Permian interval is the third pulse of subsidence in the NW Tarim Basin and follows a protracted period of non-deposition and erosion. Subsidence rates for the Late Carboniferous are 0.03-0.05 mm yr^{-1} across the region, but unusually, the models predict that tectonic subsidence rate during this period marginally exceeded sedimentation rate. This appears to occur because the measured sediment thicknesses are relatively thin (120-170 m), and therefore the effects of eustasy and bathymetry are much more pronounced. Subsequent subsidence and sedimentation rates in the Early Permian vary across the region. At Mu'er, tectonic subsidence rates of c. 0.05 mm yr^{-1} are attributed to the localised accumulation of a thick sedimentary succession exceeding 3,000 m. In contrast, where the Lower Permian succession is absent in the central parts of the Keping Shan (c.f. Fig. 3.18), the rate is effectively zero (Fig. 3.19). Consequently, the total amount of tectonic subsidence during the Carboniferous-Permian interval varies significantly, from 0.3-1.9 km across the region.

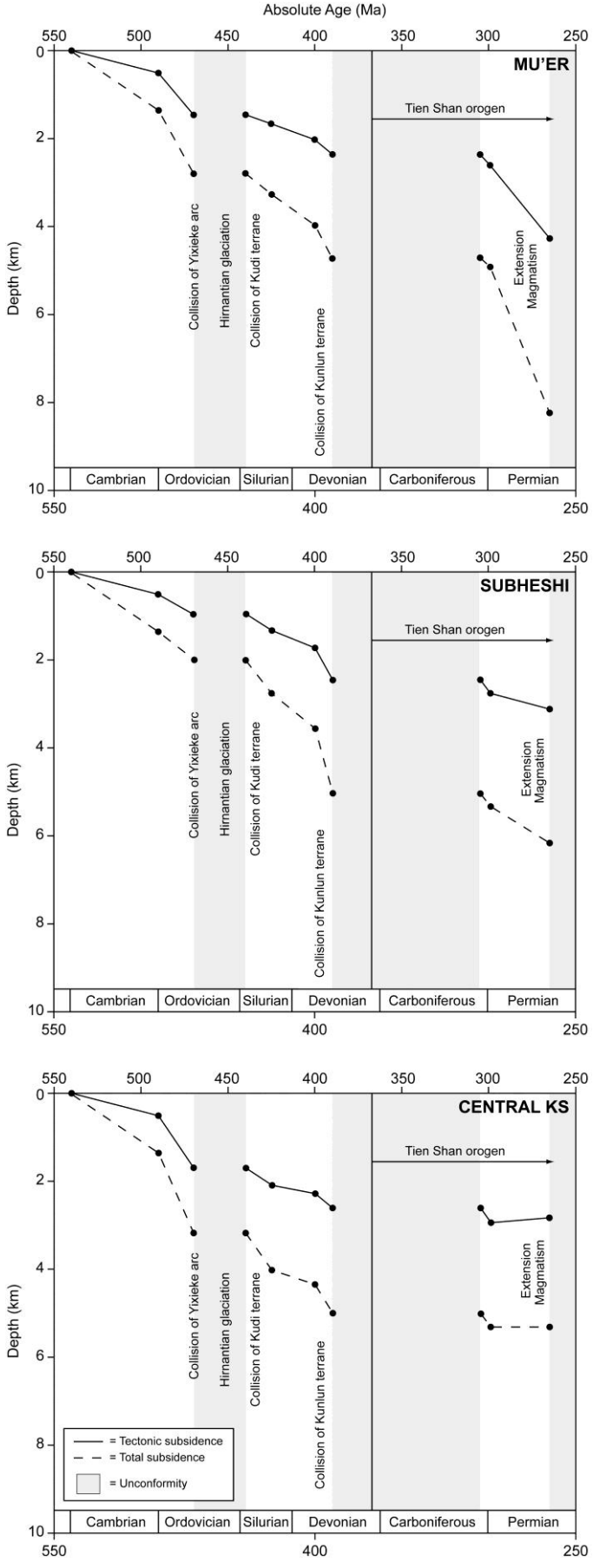

Fig. 3.19. Decompacted and back-stripped subsidence plots for a series of measured stratigraphic sections across the study area, at Mu'er, Subheshi, and the Central Keping Shan (KS). The tectonic subsidence plots use an Airy isostatic model and are corrected for relative sea level and paleobathymetry at each measured time point. Major unconformities and tectonic events have been added for reference.

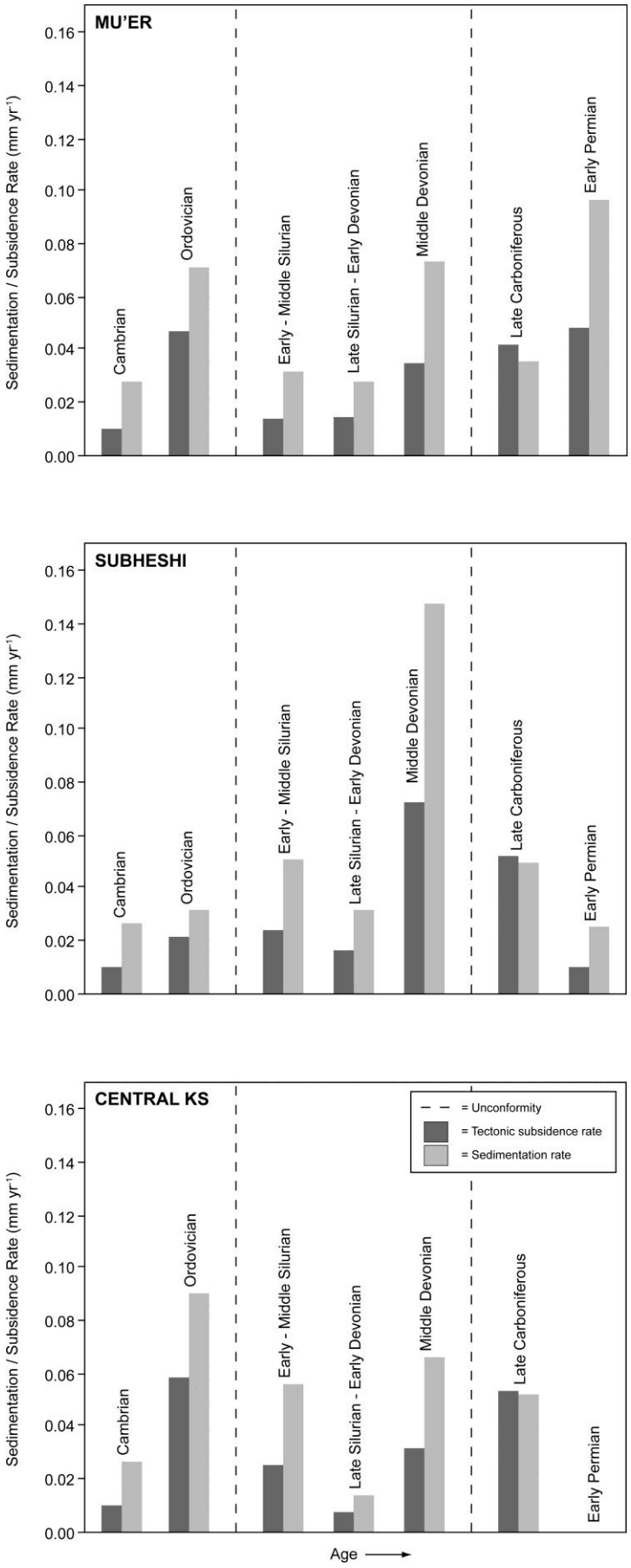

Fig. 3.20. Sedimentation and tectonic subsidence rates derived from the subsidence plots in Fig. 3.19.

3.5 Model for the Evolution of the NW Tarim Basin

Analysis of the sedimentary characteristics, facies architecture and tectonic subsidence derived from the Palaeozoic succession provides insights into the paleogeographic and geodynamic evolution of the Tarim Basin. Considering the information presented in this report with respect to the plate-scale events that affected the Tarim Craton during the Palaeozoic, a model is developed for the progressive evolution of the Tarim Basin from the Cambrian to the Middle Permian.

3.5.1 Stage 1: Epicontinental Carbonate Sea (c. 550-350 Ma)

From the Lower Cambrian to Middle Ordovician, a prolonged period of carbonate sedimentation occurred in a relatively shallow marine setting, plausibly in an epicontinental sea that covered much of the Tarim Craton (Fig. 3.21A). This follows from the paleoenvironment of the Late Neoproterozoic, which was characterised by shallow marine carbonates deposited in recently formed rift basins (Chapter 2).

During the Cambrian, relatively low tectonic subsidence rates are coupled with a gradual decrease in water depths and the progressive change from intertidal to supratidal facies. Zhang *et al.* (2000 and references therein) report that by the Late Cambrian, isolated basins became anoxic, while in the NW Tarim Basin, intervals of intertidal dolomite and chert are interbedded with supratidal evaporite horizons. It is likely that by this time, the extensional rift basins which developed during the Late Neoproterozoic (Chapter 2) had failed to develop further and became gradually filled up with sediment, explaining the decrease in water depth through the succession and the low rates of tectonic subsidence during a post-rift phase of thermally-driven subsidence. Sea levels are reported to have risen gradually by c. 150 m throughout the Cambrian (Haq & Schutter 2008; Miller *et al.* 2005), thereby counteracting the upward-shallowing succession and implying that the stratigraphic changes must be almost entirely related to tectonic subsidence. However, short-lived periods of

emergence and evaporite deposition during the Late Cambrian may be related to short term (<1 Myr) sea-level changes on the order of ±50 m (Haq & Schutter 2008).

The start of the Ordovician coincides with an abrupt increase in tectonic subsidence in the NW Tarim Basin and an abrupt rise in water depths, resulting in the deposition of a thick micritic limestone succession in the subtidal zone. Water depth appears to have increased further by the Middle Ordovician, indicated by green siltstones and limestones deposited in the distal lower shoreface to offshore transition zone. The transition and increase in tectonic subsidence rates may relate to the approach and collision of the Yixieke oceanic arc and the formation of the Akaz suture at the end of the Middle Ordovician (Fig. 3.21A–B).

The abundance of lime mud and dolomite that appears to have formed in situ implies that the carbonates were deposited in warm, tropical conditions and it follows that the Tarim Basin is likely to have occupied relatively low latitudes throughout this period. Paleogeographic reconstructions by Li & Powell (2001 and references therein) suggest that Tarim drifted from 30–40° N in the Early Cambrian to 30° S by the Late Ordovician, passing across the equator at c. 505 Ma.

An abrupt termination in carbonate sedimentation occurs in the Middle–Late Ordovician, and subsequent erosion of up to several hundred metres of the preceding strata shows that the region was subaerially exposed for 15–20 Myr. Subsurface data confirms that this unconformity is present across the whole of the Tarim Basin (Li *et al.* 1996), but the exact cause of it remains unstudied. A global decline in sea level of up to 100 m occurred during the Late Ordovician, and corresponds to the Hirnantian glaciation (Brenchley *et al.* 1994; Miller *et al.* 2005). Prior to this event, large parts of the continental regions had been covered by epicontinental seas of similar nature to the Tarim Basin (Sheehan 2001). While this decline in sea level would have been sufficient to subaerially expose the preceding Middle Ordovician succession, it alone does not account for the significant topographic relief of at least 300 m or more. Matte *et al.* (1996) and Xiao *et al.* (2002) suggested that north-dipping subduction beneath the southern margin of the Tarim Craton occurred from 490–460 Ma, and

was terminated by the collision of the Kudi terrane during the Early Silurian to Middle Devonian. It is not certain how this forthcoming collision could relate to widespread uplift across the Tarim Craton in the Late Ordovician. One possible mechanism is that the subducting oceanic slab beneath the southern Tarim Craton resulted in dynamic uplift of the cratonic interior to the north (Fig. 3.21B). This mechanism has been shown to affect the continental interior over large wavelengths of up to 5×10^3 km (Burgess *et al.* 1997), and occurs as a response to mantle flow generated by the subduction and eventual detachment of the cold slab.

3.5.2 Stage 2: Clastic Sea to Continental Platform (c. 440–390 Ma)

The Early Silurian marks a new period of subsidence in the NW Tarim Basin and a transition from carbonate to clastic sedimentation. This is likely to reflect a change in sediment source, rather than a change in latitude. Based on magnetostratigraphic analysis, Li (1990) reports that by the Devonian, Tarim was situated at latitudes of 15° N. If the model of Li & Powell (2001, and references therein) is correct, this implies that Tarim migrated from a latitude of 30° S in the Late Ordovician, and must have drifted across the equator during the Silurian to Early Devonian. Continued subsidence resulted in a rapid transgression which flooded the basin and resulted in the deposition of marine lower shoreface facies.

This renewed phase of subsidence in the NW Tarim Basin may have been caused by further tectonism at the southern margin of the Tarim Craton. Sobel & Arnaud (1999) identified a major suture within the Kunlun Shan that corresponds to the closure of an ocean basin between the Early Silurian and Middle Devonian. The lateral equivalent of this suture was later identified by Xiao *et al.* (2002) in the Pamirs, and is thought to be related to the collision of the Kudi terrane (Fig. 3.21B–C). The collision continued for around 20 Myr (452–428 Ma) (Zhou 1999) and is contemporaneous to the development of a long-lived foreland basin along the southern margin of the Tarim Basin (Wei *et al.* 2002).

The thick succession of non-marine, fluvial facies sandstones and siltstones that characterise the Upper Silurian to Middle Devonian are conformable to the marine succession that preceded it. This regression coincides with a decrease in tectonic subsidence rates during the Late Silurian to Early Devonian, which suggests that the basin reached an overfilled state. Additionally, a global decline in sea level of up to 50 m in the Early Devonian may have been sufficient to reduce base level and establish a non-marine, coastal floodplain in the NW Tarim Basin. The mud-rich alluvial facies of the Tataaiertage and Yimungantawu formations imply a period of relative stability in the basin, and may reflect the weakening effect of the Kudi orogen to the south.

An abrupt transition to much coarser, sand-rich fluvial facies sediments denotes the base of the Keziertage Fm and is linked to an increase in tectonic subsidence to the highest rates recorded for the Palaeozoic. This occurs contemporaneous to another, major terrane collision at the southern margin of Tarim. The Kunlun-Kongur terrane, which is the primary constituent of the Kunlun Shan and Pamir mountain belts, collided during the Mid Devonian to Carboniferous (Yin & Harrison 2000; Xiao *et al.* 2002) (Fig. 3.21D). This orogenic event is likely to have promoted subsidence and provided a rejuvenated source of large quantities of coarse-grained sediment. Sandstone provenance studies by Carroll *et al.* (2001) confirm that the source of the Devonian sediment is likely to be an orogenic belt to the east of the study area, and paleocurrent data is consistently WNW across the area, which is compatible with the presence of a long-lived orogenic belt along the southern margin of Tarim (Fig. 3.21D).

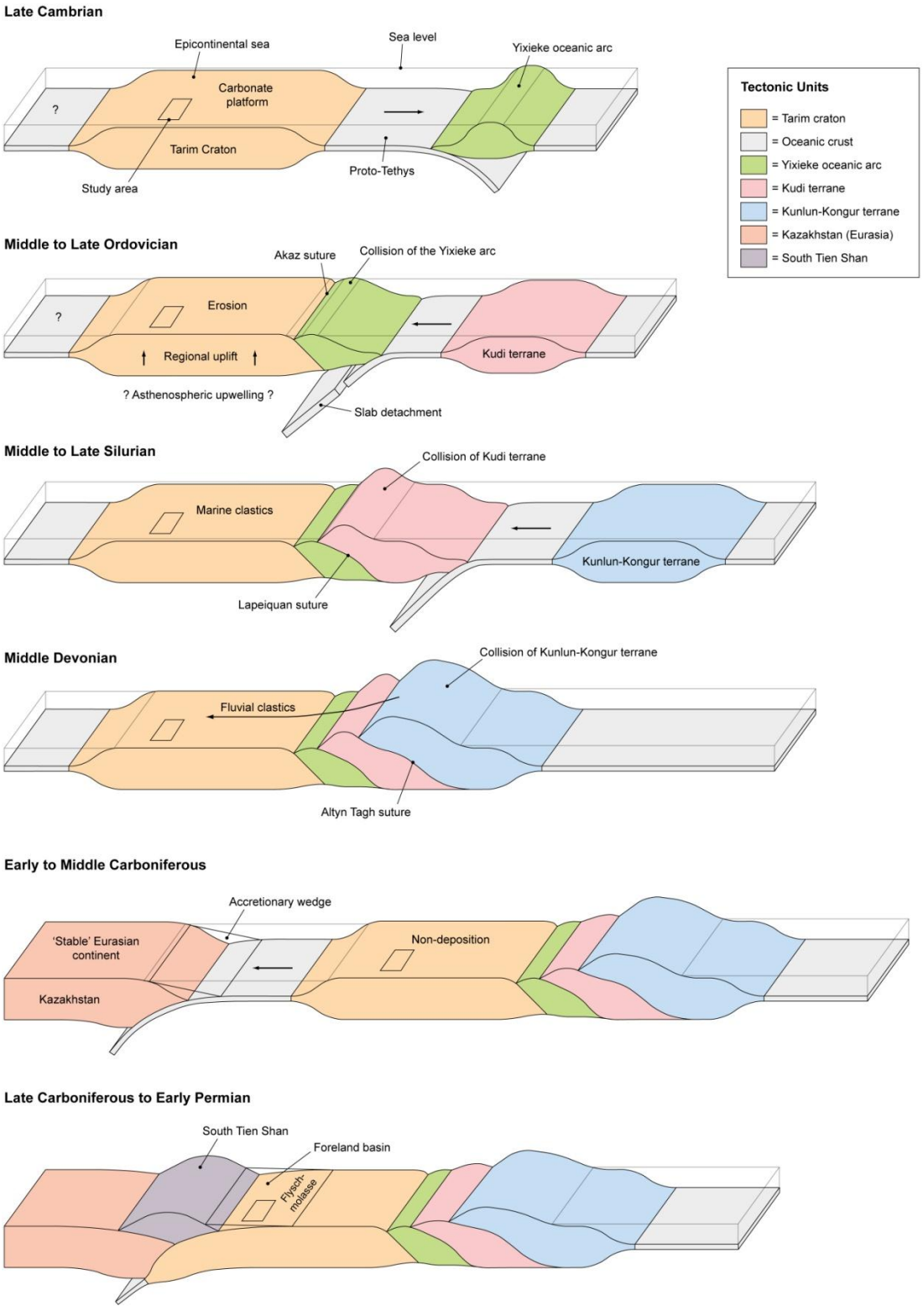

Fig. 3.21. Schematic model showing the paleogeographic evolution of the Tarim Craton and adjacent tectonic units during the Palaeozoic. Early stage models are adapted from Xiao *et al.* (2002) and integrated with new results presented in this report.

3.5.3 Stage 3: Compressional Foreland Basin (c. 310-260 Ma)

A new phase of basin development is defined by the collision of Tarim and its counterpart terranes with the Eurasian margin, during the Late Palaeozoic (Burrett 1974; Li *et al.* 1989; Heubeck 2001). During the Late Carboniferous to Early Permian, Tarim occupied latitudes of 30-35° N, ending the rapid northward migration during the Devonian (Li 1990). The collision resulted in the formation of the South Tien Shan mountain belt (Fig. 3.21E-F) (Burtman 1975; Windley *et al.* 1990), resulting in flexural subsidence along the northern margin of the Tarim Basin (Carroll *et al.* 1995, 2001; Allen *et al.* 1999) (Fig. 3.21F). The spatial and temporal pattern of sedimentation during the Late Carboniferous to Early Permian is analogous to both ancient and modern foreland basins (c.f. DeCelles & Giles 1996). As flexural subsidence began to affect the Keping Shan area, the shallow shoreface facies that define a series of parasequences in the Upper Carboniferous Sishichang Fm pass conformably into deeper marine facies of the Kangkelin Fm. The parasequences in the Sishichang Fm may correspond to pulses of subsidence, creating accommodation space that is quickly filled with sediment derived from the evolving South Tien Shan. The thickening of the Upper Carboniferous formations to the north reflects the deepening of the foreland basin towards the orogenic belt. Carroll *et al.* (1995) report that a series of older (Middle to Upper Carboniferous) formations crop out in the northeast Keping Shan and consist of a succession of interbedded sandstones and siltstones. The absence of these formations in the study area to the south maintains the characteristic features of a foreland basin, in which subsidence progressively affected a wider area during the continued uplift of the mountain belt.

A rapid transition from deposition in a shallow marine environment to a terrestrial, semi-arid fluvial environment occurs around the Carboniferous-Permian boundary. Such a transition is akin to other foreland basins and is likely to represent the change from the underfilled (molasse) to overfilled (flysch) stage (DeCelles & Giles 1996). However, Early Permian sedimentation patterns are complicated by a phase of extension and volcanism that affected the NW Tarim Basin for a relatively brief period at c. 270-275 Ma (Chen *et al.* 2006; Zhang *et al.* 2008). It is maintained here that the region remained under a general state of contraction throughout this period.

Consequently, various models have been proposed to explain the cause of extension, including post-orogenic collapse (Zhou *et al.* 2006), extension associated with an oblique collision (Carroll *et al.* 2001), back-arc extension (Yang *et al.* 2007), or a short-lived mantle plume (Zhou *et al.* 2004; Zhang *et al.* 2008). This subject forms the basis of Chapter 4, in which the Early Permian evolution of the NW Tarim Basin is examined in detail.

3.6 Conclusions

A thick (2-6 km) succession of sediments were accumulated in the NW Tarim Basin during the Palaeozoic, which record a series of transient depositional environments and three distinct periods of tectonic subsidence. Initially, carbonate sedimentation occurred during the Cambrian in a shallowing, epicontinental sea that covered much of the basin, and corresponds to the post-rift stage of an extensional event that affected the region during the Late Neoproterozoic. Possible rejuvenation of the extensional structures and further separation of Tarim from Gondwana resulted in renewed subsidence in the Ordovician, which was also characterised by a thick carbonate succession, deposited in a deeper epicontinental setting. An abrupt end to the carbonate sedimentation and subaerial uplift of the region appears to be related to the collision of the Yixieke arc at the southern margin of Tarim during the Middle Ordovician. The subaerial exposure may have been further enhanced by a global decline in sea level during the Late Ordovician.

A new phase of basin development is associated with tectonic subsidence in the Early Silurian to Middle Devonian, corresponding to the collision of the Kudi terrane in the Silurian and the Kunlun-Kongur terrane in the Middle Devonian. This evolving orogenic belt is the likely source of the large quantities of sediment that were supplied to the Tarim Basin during this time, which in the northwest part of the basin were deposited as marine and non-marine facies on a progressively shallowing continental platform.

The final phase of basin development in the Palaeozoic occurred in the Late Carboniferous to Early Permian, and was associated with the collision of Tarim and its counterpart terranes with 'stable' Eurasia. The closure of the intervening Turkestan Ocean led to the formation of the South Tien Shan, which tectonically loaded the northern margin of the Tarim Basin resulting in flexural subsidence. This period was characterised initially by marine facies and later by non-marine fluvial facies, synonymous to the flysch and molasse stages of foreland evolution. The Early Permian was further complicated by widespread volcanism and extension, which occurred in an otherwise contractional setting. The characteristics of this latter event, and a new model for its cause, is discussed in Chapter 4.

CHAPTER FOUR

Early Permian Faulting and Volcanism

Abstract • The tectonostratigraphic record of the NW Tarim Basin, China, reveals an important phase of tectonism in the Early Permian that is inconsistent with the regional contractional setting at this time. The development of a northwest-striking, right-lateral strike-slip fault population had a marked impacted on the thickness of the Lower Permian sedimentary succession and controlled the emplacement of a northwest-trending mafic dyke swarm. These dykes fed voluminous extrusive basalts that covered a large part of the Tarim Basin. New outcrop, satellite-derived observations and measurements from the Keping Shan Thrust Belt, in the NW Tarim Basin, are combined with data gleaned from published literature in order to reanalyse the tectonostratigraphic evolution and regional kinematics of the NW Tarim Basin during the Early Permian. A new model is proposed that suggests these structures and volcanic activity were a consequence of large-scale anticlockwise block rotation within the interior of the Tarim Craton as a response to crustal-scale, left-lateral shear in the Tien Shan mountain belt immediately to the north.

4.1 Introduction

The Tarim Basin, NW China, contains a thick (3–16 km) sedimentary succession that provides an almost complete evolutionary record of the basin and the adjacent South Tien Shan mountain belt during the Phanerozoic. The basin presently occupies a surface area of more than 500,000 km^2, and contrasts sharply with the surrounding Tien Shan, Pamir and Kunlun Shan mountain belts (Fig. 4.1). The Tien Shan mountain belt, which lies immediately north of the Tarim Basin, initially formed during the Late Palaeozoic as a result of the collision between the Tarim Craton and Kazakhstan (Windley *et al.* 1990, 2007) (Fig. 4.1). By the Late Carboniferous to Early Permian, the NW Tarim Basin was acting as the foreland to the South Tien Shan and accumulated a thick sedimentary succession (Carroll *et al.* 1995). However, recent work (e.g. Jiang *et al.* 2004; Chen *et al.* 2006; Zhang *et al.* 2008; Tian *et al.* 2009; Chapter 6) yields evidence for an important phase of extension and magmatism during this period, that was characterised by the emplacement of a mafic dyke swarm, the eruption of voluminous basalts and the development of fault zones that strongly impacted on the thickness of the sedimentary sequence. This presents an interesting paradox of apparently widespread extension in what was otherwise a contractional foreland setting.

The aim of this chapter is to present a new model for the Early Permian evolution of the NW Tarim Basin by examining the surface exposure of Late Palaeozoic lithostratigraphy in the Keping Shan Thrust Belt (KSTB) (Fig. 4.2). Sedimentary logs, structural measurements and samples of the volcanic suite were collected during fieldwork in the KSTB, and combined with regional-scale geological maps derived from the interpretation of satellite images. These data were interpreted in the context of published observations, which have focused particularly on geochemical analysis of the volcanic suite.

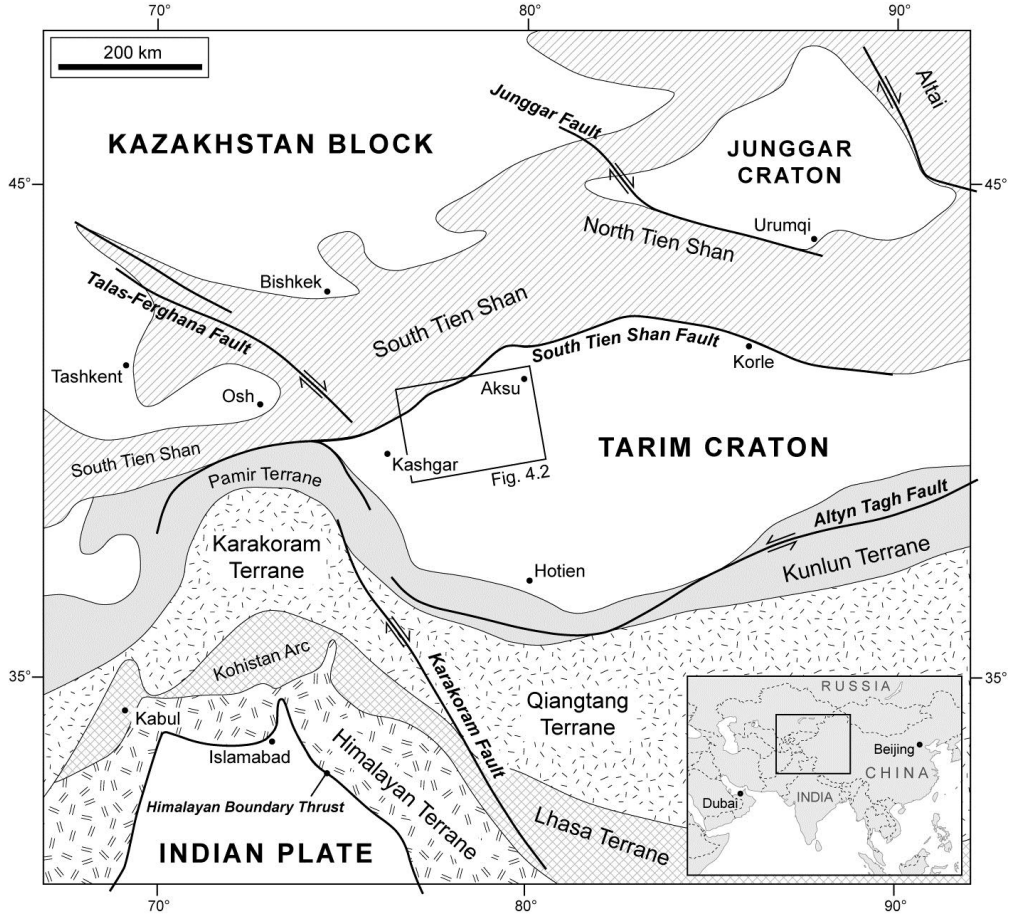

Fig. 4.1. Simplified map showing the major tectonic units of Central Asia (based on Tapponier & Molnar 1979, Robinson *et al.* 2004 and references therein). The Tarim Craton collided with the Kazakhstan Block in the Late Palaeozoic, leading to the closure of the intervening Turkestan Ocean and the formation of the South Tien Shan orogenic belt.

4.2 Regional Setting

The Tarim Basin represents the surface expression of the Tarim Craton (Fig. 4.1), a microcontinent which was separated from northern Australia during a widespread rifting event in the Late Neoproterozoic (Li & Powell 2001). During the Early Palaeozoic, the Tarim Craton remained isolated and drifted gradually northwards, accumulating a thick shelf sequence of carbonates and clastics. In the Carboniferous–Permian, Tarim collided with Kazakhstan (Burrett 1974; Burtman 1975; Li 1990), and closure of the intervening Turkestan Ocean led to the formation of the South Tien Shan orogenic belt (Windley *et al.* 1990, 2007) (Fig. 4.1). This led to the

formation of a foreland basin along the northern margin of the Tarim Basin that accumulated a thick marine to non-marine sequence (Carroll *et al.* 1995). The collision was diachronous, initiating earlier in the east than in the west. This resulted in a 26° clockwise rotation of the Tarim Craton between the Late Carboniferous and Early Permian (Li *et al.* 1988). Subsequent to the collision, at c. 290-270 Ma, it is reported that the South Tien Shan mountain belt evolved into a transpressional orogen, and deformed by left-lateral shear across a series of trans-crustal, E-W trending strike-slip fault zones (Biske 1995; Konopelko *et al.* 2007; Biske & Seltmann, in press). Contemporaneously, the NW Tarim Basin to the south experienced widespread magmatism and intracontinental extension, the cause of which has been widely discussed but remains disputed. Various models have been proposed, including post-orogenic collapse (Zhou *et al.* 2006), extension associated with an oblique collision (Carroll *et al.* 2001), back-arc extension (Yang *et al.* 2007), or a short-lived mantle plume (Zhou *et al.* 2004; Zhang *et al.* 2008).

During the Mesozoic, a series of terranes were accreted to the southern margin of the Tarim Craton. These include the present-day Kunlun Shan and Pamir mountain belts, and the Tibetan Plateau (Yin & Harrison 2001; Robinson *et al.* 2004) (Fig. 4.1). These events led to periodic rejuvenation of the South Tien Shan, resulting in pulses of sedimentation in a series of depocentres at the margins of the Tarim Basin (Hendrix *et al.* 1992; Hendrix 2000). Most recently, contraction during the Cenozoic as a result of the Himalayan Orogen (Tapponier & Molnar 1979; Yin & Harrison 2001) has rejuvenated the South Tien Shan into its present form (Windley *et al.* 1990). As a result, deformation along the northern margin of the Tarim Basin has generated a foreland fold-thrust belt system which exhumes the sedimentary succession of the basin (Yin *et al.* 1998; Turner *et al.* 2010), permitting detailed analysis of the earlier phases of basin evolution in outcrop. This study focuses on the Keping Shan Thrust Belt (KSTB) (Fig. 4.2), a 300 km-wide arcuate salient that is characterised by imbricate thrusts. The belt provides the most complete, regional-scale exposure of the Lower Permian sedimentary and volcanic sequence in the Tarim Basin, and is particularly valuable because of the absence of publically-available subsurface data from the basin interior.

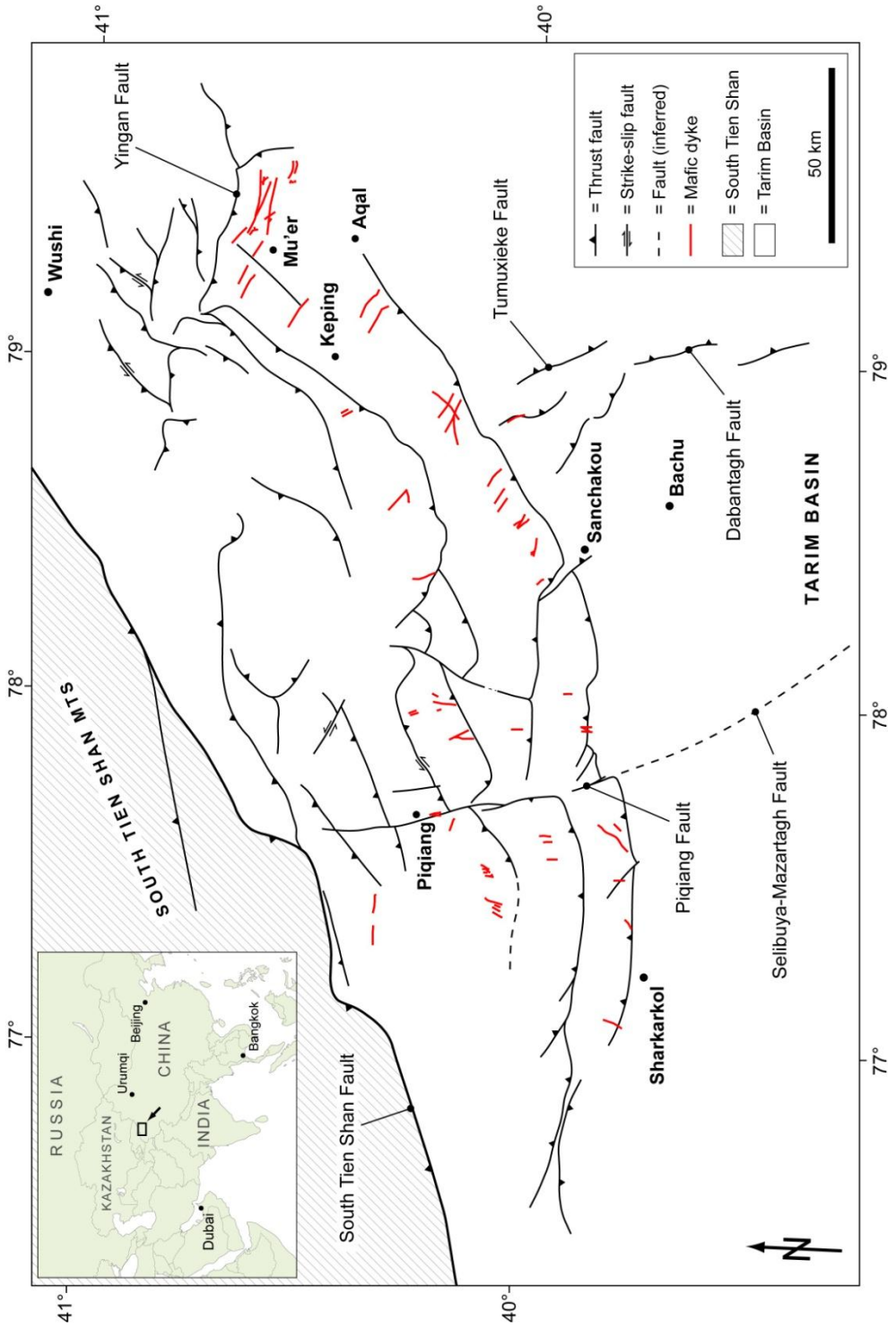

Fig. 4.2. Structural map of the Keping Shan Thrust Belt, NW Tarim Basin, showing major fault zones and mafic dykes. The map was generated by a combination of satellite image interpretation and field-based mapping.

4.3 Early Permian Stratigraphy

4.3.1 Description

Lower Permian sediments which crop out in the KSTB are characterised by a clastic sequence that contains several basalt horizons and locally exceeds thicknesses of 3,200 m. The Lower Permian comprises the Kupukuziuman and Kaipaizileke Fms (Fig. 4.3), which were examined and interpreted at four sites (Mu'er, Aqal, Subheshi and Piqiang, see Fig. 4.2). The Kupukuziuman Fm conformably overlies shallow marine limestones of the Upper Carboniferous Kangkelin Fm (Fig. 4.3). The lower part of the Kupukuziuman Fm is characterised by a 30-40 m thick sequence of interbedded sandstones, mudstones and siltstones (Figs. 4.3, 4.4A). The sandstones have erosive, undulating bases and contain abundant planar and trough cross beds (Fig. 4.4B and C). The upper part of the formation is dominated by extrusive basalt horizons which are ~150 metres thick at Mu'er. The Kupukuziuman Fm is conformably overlain by the Kaipaizileke Fm which in the lower part also comprises an interbedded succession of sandstones, mudstones and siltstones (Fig. 4.4A) which contain abundant planar and trough cross beds. The colour of the clastic sequence varies between pale greys, yellows and pinks (Fig. 4.4A). The sandstone contains regular conglomeratic lags that pick out erosive channel scours (Fig. 4.4D). In the upper part, the Kaipaizileke Fm is dominated by extrusive basalt horizons that are interbedded with the clastic sequence (Fig. 4.4E). The characteristics of these basalts are described later in this report.

4.3.2 Interpretation

The above description of the stratigraphy is in agreement with the interpretation by Carroll *et al.* (1995) that the Early Permian was characterised by deposition on a semi-arid, fluvial plain upon which there were episodic basalt eruptions. Within the clastic intervals, the sandstone units are interpreted as migrating fluvial channels, based on the abundance of unidirectional flow structures (Figs. 4.4B and C), erosive scours and

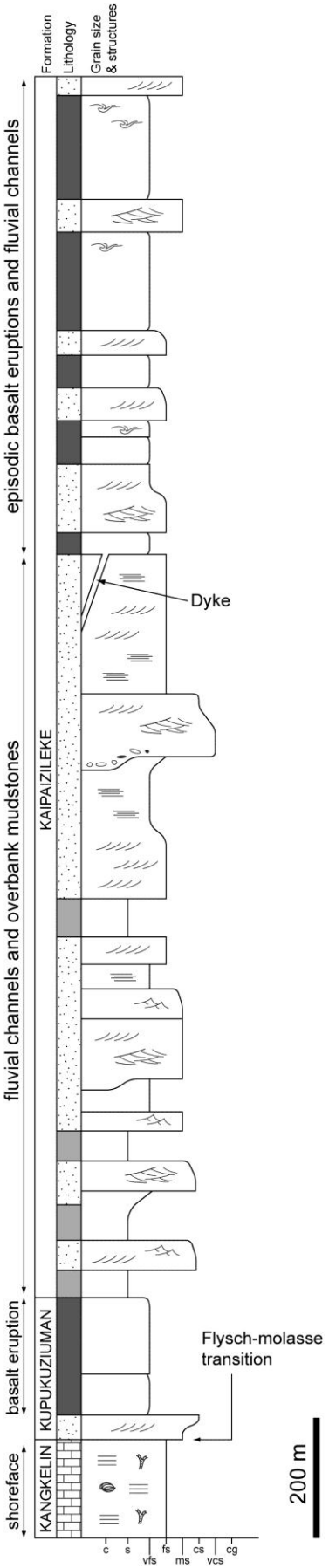

conglomeratic lags (Fig. 4.4D). The interbedded mud and siltstone units are interpreted as overbank (floodplain) deposits of the broader fluvial plain system. Given that deposition is reported to have occurred in a foreland setting adjacent to the South Tien Shan mountain belt, the Kupukuziuman and Kaipaizileke Fms are characteristic of the overfilled (molasse) stage of foreland basin evolution (c.f. DeCelles & Giles 1996). The base of the Kupukuziuman Fm therefore represents not only the transition from marine to non-marine sedimentation and the start of the Lower Permian succession, but also the progressive evolution of the foreland from the underfilled (flysch) to the overfilled stage.

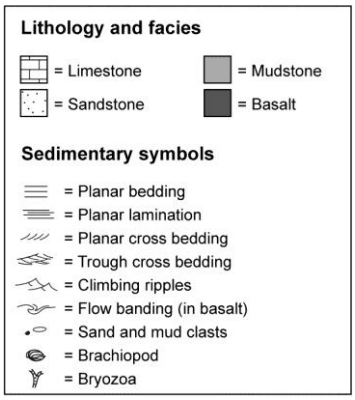

Fig. 4.3. Sedimentary log of the Upper Carboniferous Kangkelin Fm and the Lower Permian Kupukuziuman and Kaipaizileke Fms, measured at Mu'er. The Lower Permian sequence is dominated by semi-arid, fluvial sandstones and mudstones, with episodic basalt eruptions. These conformably overlie shallow marine, shoreface facies carbonates, representing a transition from the underfilled (flysch) to overfilled (molasse) stage of foreland evolution.

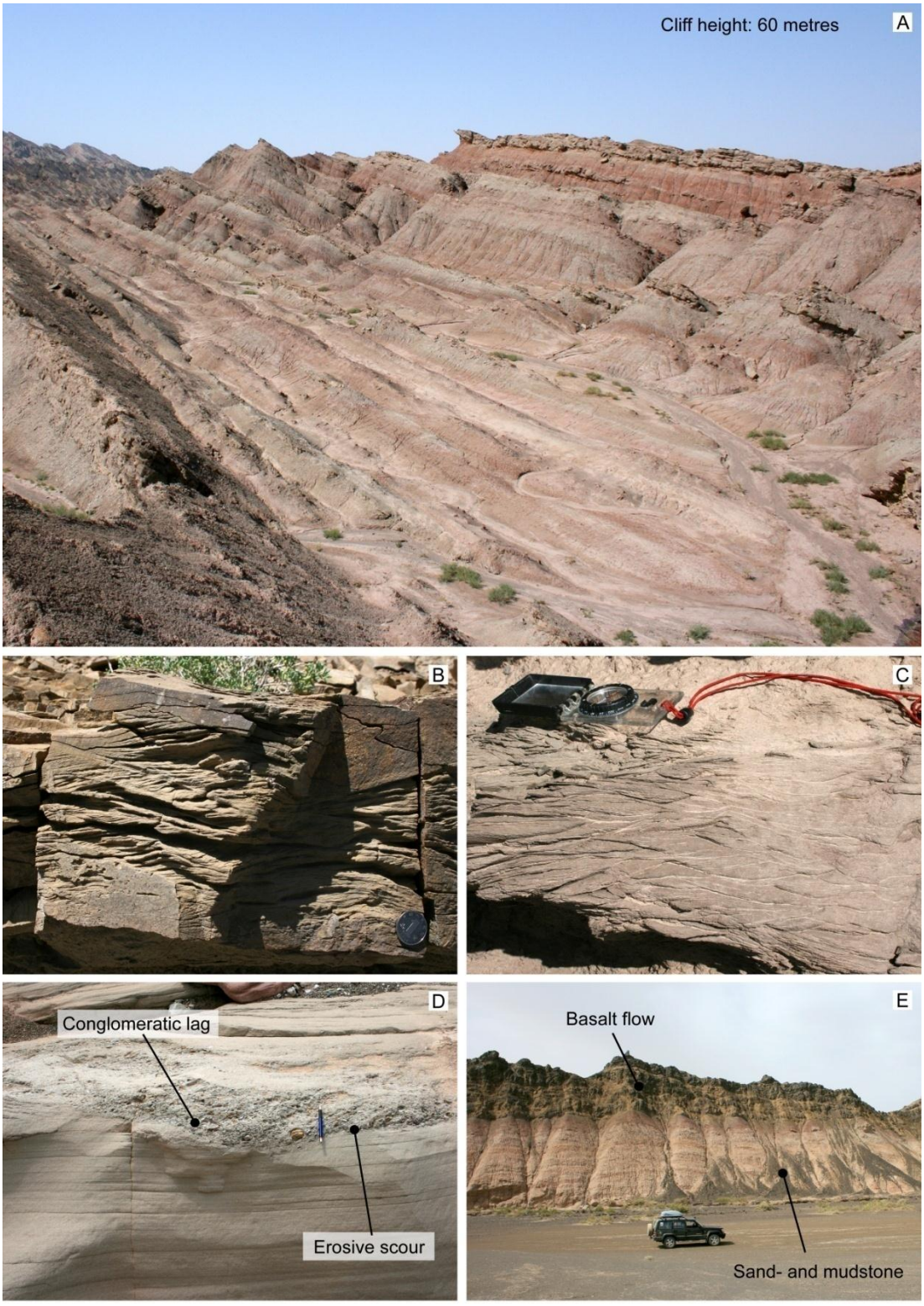

Fig. 4.4. Outcrop photographs of the Lower Permian succession: (A) Interbedded sandstones, mudstones and siltstones of the lower Kaipaizileke Fm near Aqal; (B) Climbing ripples in a fluvial sandstone unit, upper Kupukuziuman Fm at Piqiang; (C) Trough cross bedding in a fluvial sandstone unit, upper Kupukuziuman Fm at Subheshi; (D) Erosive channel scour and conglomeratic lag, lower Kaipaizileke Fm at Mu'er; (E) Interbedded sandstones and mudstones conformably overlain by an extrusive basalt flow, upper Kaipaizileke Fm at Mu'er.

4.3.3 Sediment Thickness Distribution

In order to evaluate the spatial distribution of Lower Permian sediments, a series of 36 ground and satellite-measured sections from across the KSTB were used to generate an isopach map (Fig. 4.5A). The isopach map reveals that the thickness of the Lower Permian succession varies substantially across the region. Across the central part of the KSTB, the Lower Permian is completely absent. To the west, north and east, the thickness of the succession increases rapidly, exceeding more than 3,200 m at Mu'er (Fig. 4.5B). Abrupt changes in the sediment thickness also occur across several northwest-striking fault zones, the implications of which are considered later in this chapter.

The pattern of sediment distribution broadly defines a radial geometry, with sediment thickening in all directions from a dome-shaped high which is centred around the Bachu-Sanchakou area. The isopach maps were derived from measurements taken in the hanging walls of major thrusts, and therefore they do not take into account the effects of Late Cenozoic shortening across the thrust belt. Balanced cross sections across the central part of the KSTB yield shortening estimates of 33% (Turner *et al.* 2010), and by stretching the isopach map parallel to the north-south shortening direction the radial pattern of sediment distribution becomes even more apparent. It remains unclear whether this pattern represents the geometry of the depositional setting during the Early Permian, or whether subsequent uplift and erosion across the central KSTB has removed the sediment at a later stage. Based on borehole data from the interior of the Tarim Basin, Chen *et al.* (2006) suggested that the radial pattern of sediment thickness was a syndepositional feature that primarily affected the Late Cisuralian to the Guadalupian part of the succession, ~275-270 Ma, and was related to a regional-scale doming event centred on the Bachu area.

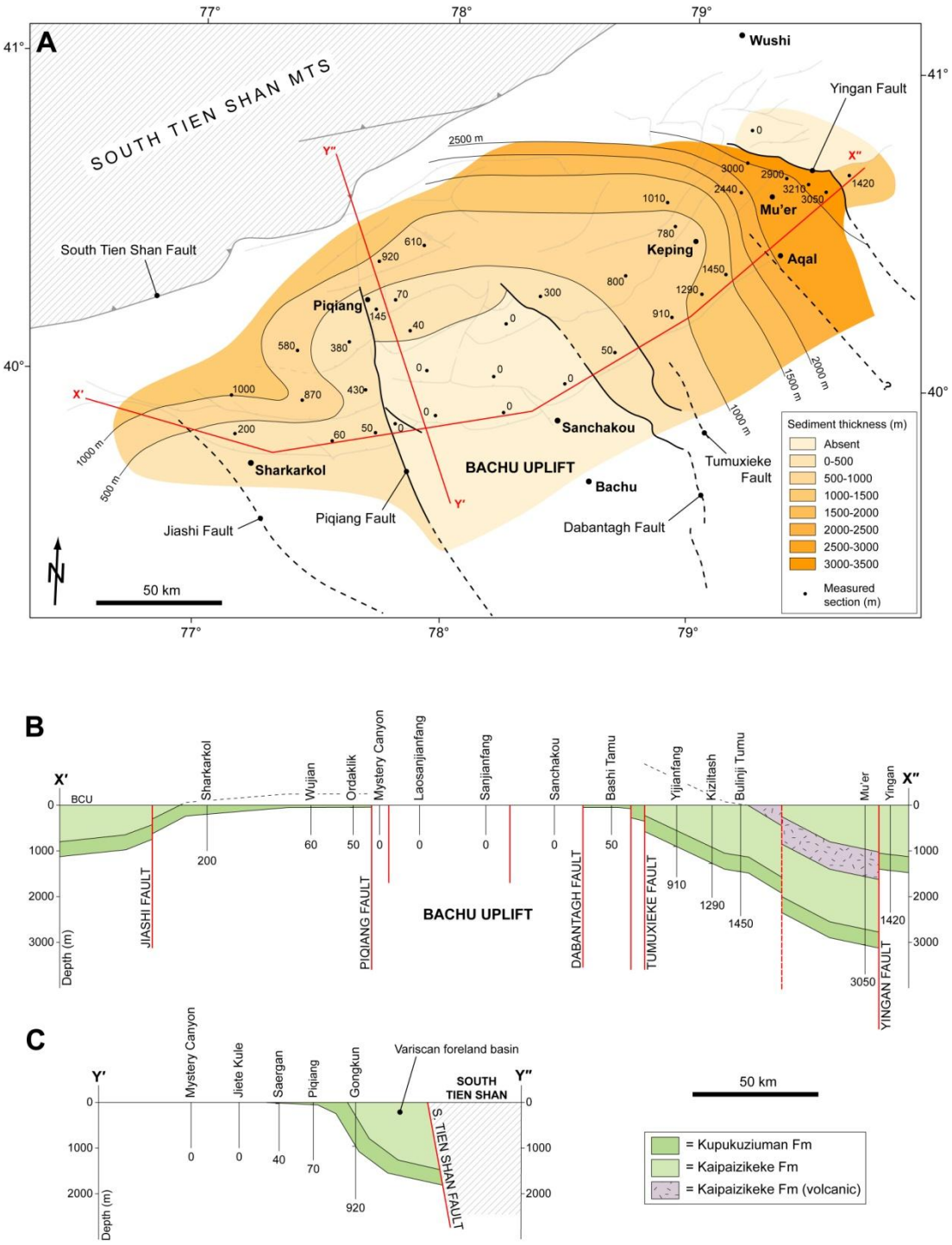

Fig. 4.5. Lower Permian sediment distribution in the NW Tarim Basin. (A) Isopach map showing sediment thickness derived from measurements at 35 sites across the Keping Shan Thrust Belt. (B) East-west oriented correlation panel across transect X′-X″, hung from the BCU (base-Cenozoic unconformity). (C) North-south oriented correlation panel across transect Y′-Y″, showing thickening of the Lower Permian into the Variscan foreland basin. The thickness of the Lower Permian sequence varies substantially when traced from west to east. Sediment is completely absent across the Bachu Uplift but exceeds thicknesses of 3,000 m to the east of Keping. The thickness changes abruptly across north-west striking fault zones.

4.4 Early Permian Volcanism and Dyke Emplacement

4.4.1 Basaltic Lava Flows

A series of basalt horizons crop out within the Lower Permian sequence (Fig. 4.3). Field evidence from Mu'er suggests that these basalts were formed as extrusive lava flows. The basalts are concordant to bedding and occur in two stratigraphic intervals: an older, thinner (100–200 m) series of at least two flow fields in the upper part of the Kupukuziuman Fm, and a thicker (400–600 m) series of at least 5–6 flow fields within the mid to upper part of the overlying Kaipaizileke Fm (Fig. 4.6). Each flow field comprises a series of discrete flows, that can be distinguished according to the characteristic colours, structures and crystal textures that exist within a single flow (Self *et al.* 1998). At their bases, the flows are characterised by a thin (0.2–0.4 m), very dark grey to black, hypocrystalline (glassy) and vesiculated layer (Fig. 4.7A) that corresponds to the lower crust of the flow. The cores of the basalt flows comprise a fine-grained, dark grey-black crystalline layer that is up to 5–10 m thick and contains little jointing or vesiculation. In contrast, the upper parts of the flows are characterised by an abrupt change to a pale brown colour (Fig. 4.6), with an abundance of spherical vesicles (Fig. 4.7B), and are interpreted as the upper crust section of the flow. The change in colour is thought to relate to weathering (oxidation) of the upper part of the flow. Meteoric water was able to percolate through the jointed, vesiculated part of the flow but was unable to penetrate the flow core. In addition, some flows contain very large amygdales up to 0.4–0.5 m diameter that have been filled with spectacular megacrysts of calcite and muscovite mica. In the uppermost parts of the flows, there are abundant flow structures and uneven, internal banding that is interpreted as preserved ropes and rope fold trains that characterise the upper, exposed surface of basalt flows (Fig. 4.7C) (c.f. Fink & Fletcher, 1978).

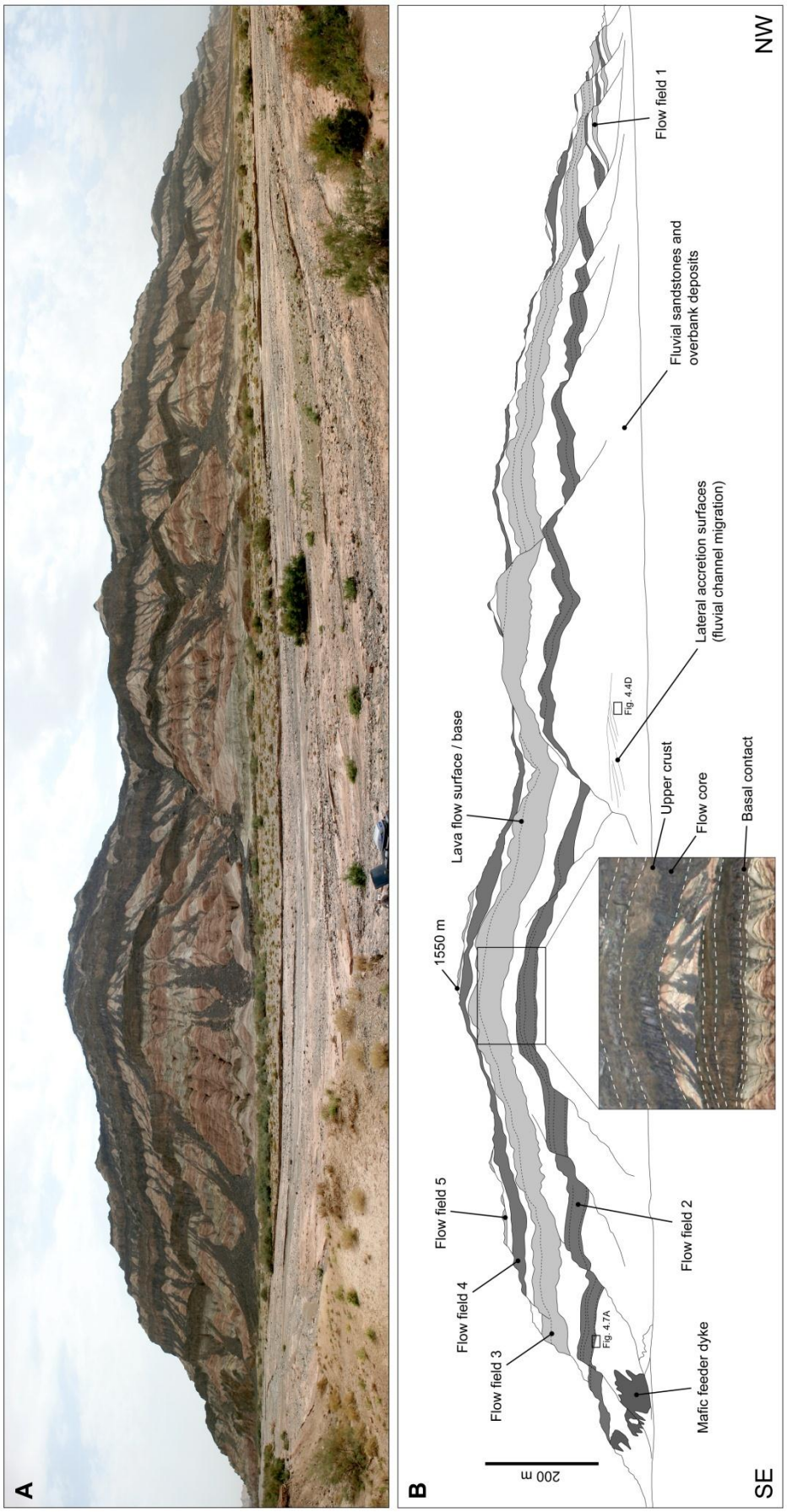

Fig. 4.6. Large-scale characteristics of the Lower Permian basalt flows within the Kaipaizileke Fm at Mu'er. (A) Stitched panoramic photograph of the cliff section covering a distance of 2-3 km. (B) Interpreted section showing 5 flow fields, each comprising a series of discrete lava flows (see inset). A mafic dyke is visible in the lower southeast (left) corner, which is discordant to bedding and is thought to have fed the overlying lava flows.

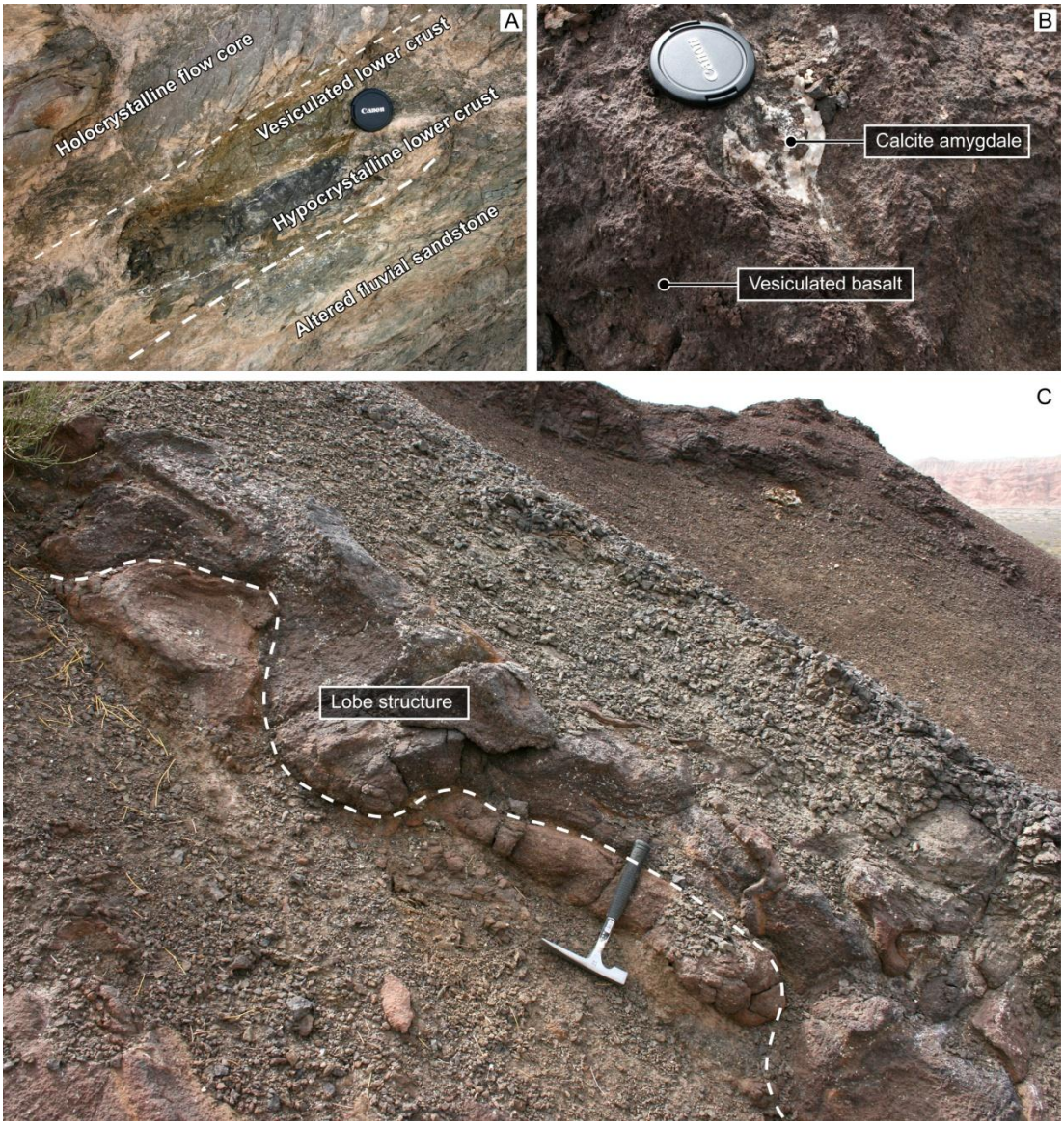

Fig. 4.7. Outcrop photographs of basaltic lava flows at Mu'er. (A) Basal section of a lava flow showing the underlying, altered fluvial sandstones of Early Permian age and a thin, hypocrystalline (glassy) and vesiculated lower crust. (B) Vesiculated zone in the upper crust of a lava flow, with a large calcite-filled amygdate. (C) Flow-top lobe structures on the upper surface of a pahoehoe lava flow.

Borehole data from the interior of the Tarim Basin reveals that the thicker series of Lower Permian basalts within the Kaipaizileke Fm are not confined to the KSTB (Fig. 4.8). They can be correlated across a vast area of more than 250,000 km^2 (Jia 1997; Chen *et al.* 2006) and assuming an average thickness of 300 m, constitute an estimated volume of 75,000 km^3 (Zhang *et al.* 2008). Geochemical studies reveal that the Tarim basalts have high Nb/La ratios (0.9–1.3), which implies that they were derived from a long-term enriched lithospheric mantle source (Jiang *et al.* 2004; Tian *et al.* 2009). Geochronological constraints indicate that the basalts were erupted from 280–270 Ma (Jia 2004; Jiang *et al.* 2004; Zhou *et al.* 2006), which is synonymous to the approximate stratigraphic age based on the measured sections in the KSTB (Fig. 4.3).

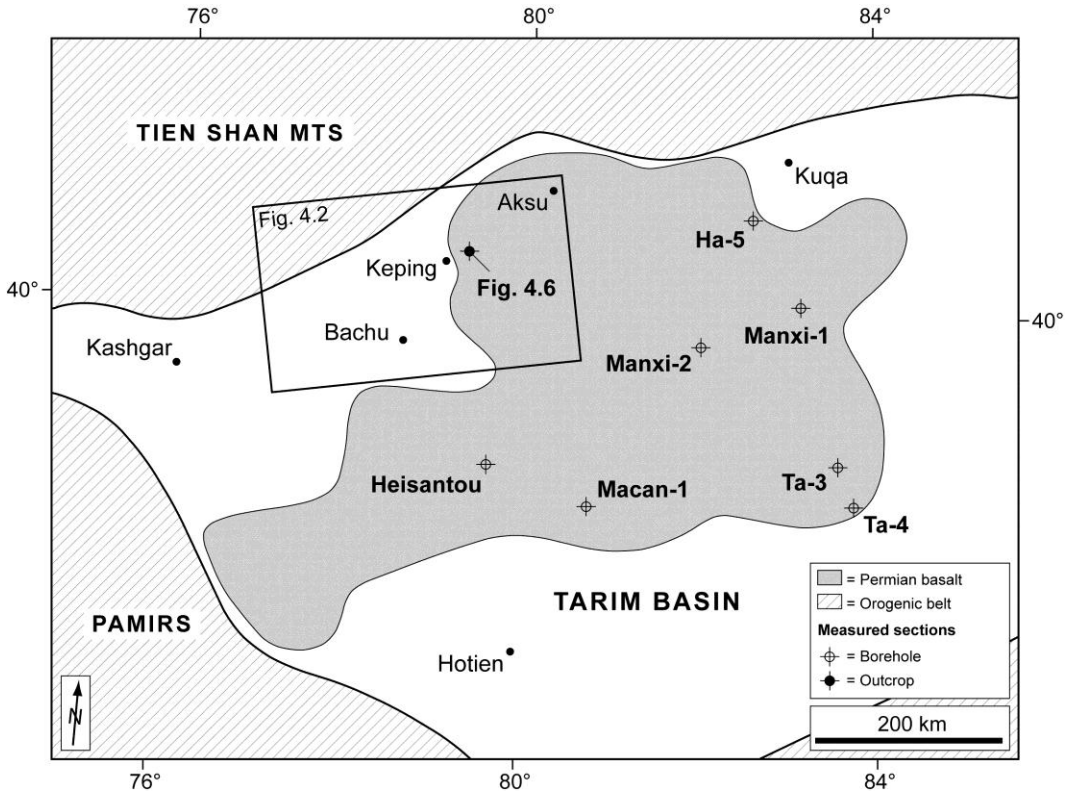

Fig. 4.8. The distribution of Lower Permian basalts in the Tarim Basin, modified from Zhang *et al.* (2008) and based on correlated borehole data from Jia *et al.* 2004. Although the basalts only crop out at the subsurface in the Keping Shan Thrust Belt, their regional distribution covers an area of more than 250,000 km^2 and have an estimated volume of 75,000 km^3.

4.4.2 Dyke Structure and Petrology

During this investigation, more than 80 dykes were mapped in the KSTB, the majority of which had not previously been recorded. The dykes intrude sediments up to Early Permian in age (Fig. 4.9A) but are absent in the stratigraphic succession beyond the extrusive basalt horizons in the upper part of the Kaipaizileke Fm. The dykes have a consistent northwest trend (average 300°) (Fig. 4.2), which is confirmed by stereographic restoration on 15 of the mapped dykes, to remove the effects of tilting associated with Late Cenozoic thrusting. The largest dykes have widths of up to 20–25 m and can be traced laterally for up to several kilometres (Fig. 4.9A and B). Many dykes have an en-echelon organisation that is persistently left-stepping (Fig. 4.9B). Rarely, sub-horizontal slickensides are observed at the dyke-country rock contact. It is thought that the dykes were permissive, and exploited recently opened fractures (Fig. 4.9C) across which there had been small amounts of right-lateral, strike-slip displacement. The northwest-trending dykes appear to be particularly abundant in the vicinity of major northwest-striking fault zones (Fig. 4.2) indicating a direct genetic link between them.

Petrologically, the dykes have mafic mineral assemblages and are highly magnetic. Grain size varies substantially between individual dykes, suggesting local variations in emplacement depth and country rock water content. Dykes emplaced within Lower Permian sediments are persistently fine-grained, with well developed chilled-margins (Fig. 4.9D) and hexagonal cooling fractures (Fig. 4.9E). Those dykes that intrude into older (e.g. Devonian, Silurian) sediments are medium to coarse-grained and have poorly developed chilled margins. This suggests that the Lower Permian sediments were close to the surface at the time of dyke emplacement. At Mu'er, dykes directly feed the thick sequence of extrusive basalts within the upper Kaipaizileke Fm (Fig. 4.6), providing a further constraint on the Early Permian age of emplacement.

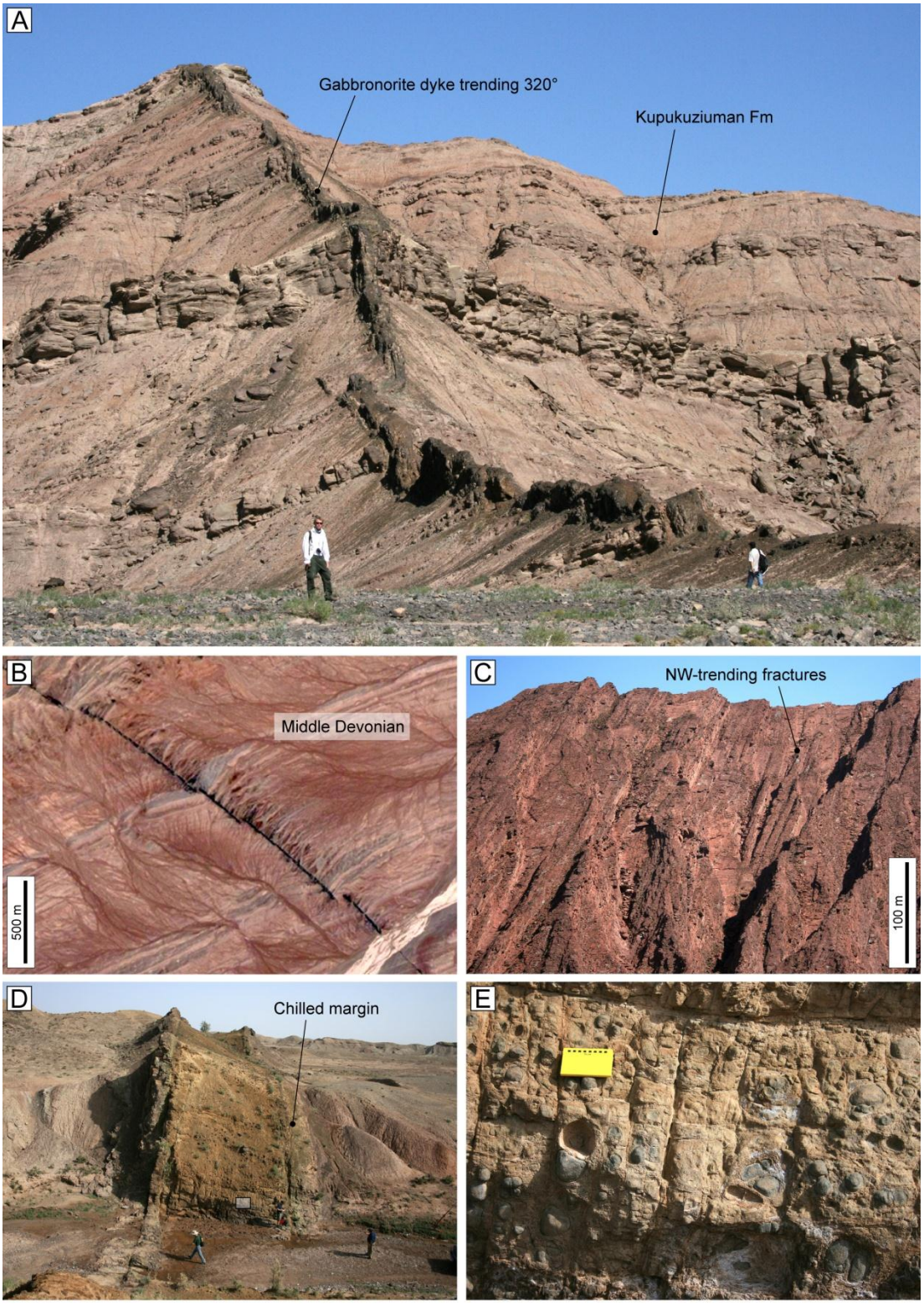

Fig. 4.9. Outcrop photographs and satellite image of Early Permian dykes and fractures. (A) NW-trending gabbronorite dyke cross-cutting the Lower Permian Kaipaizileke Fm near Subheshi. (B) En-echelon, left-stepping dyke cross-cutting Middle Devonian strata near Aqal (from Google™ Earth). (C) NW-striking, steep-dipping fracture set in Middle Devonian red beds near Subheshi, adjacent to a series of NW-trending dykes. (D) 15 m-wide gabbronorite dyke with 1 m chilled margin cross-cutting Lower Permian siltstones near Mu'er. (E) Close-up photograph of *(D)* showing nodular weathering of cooling fractures in the dyke core, which form both perpendicular and parallel to the dyke margin.

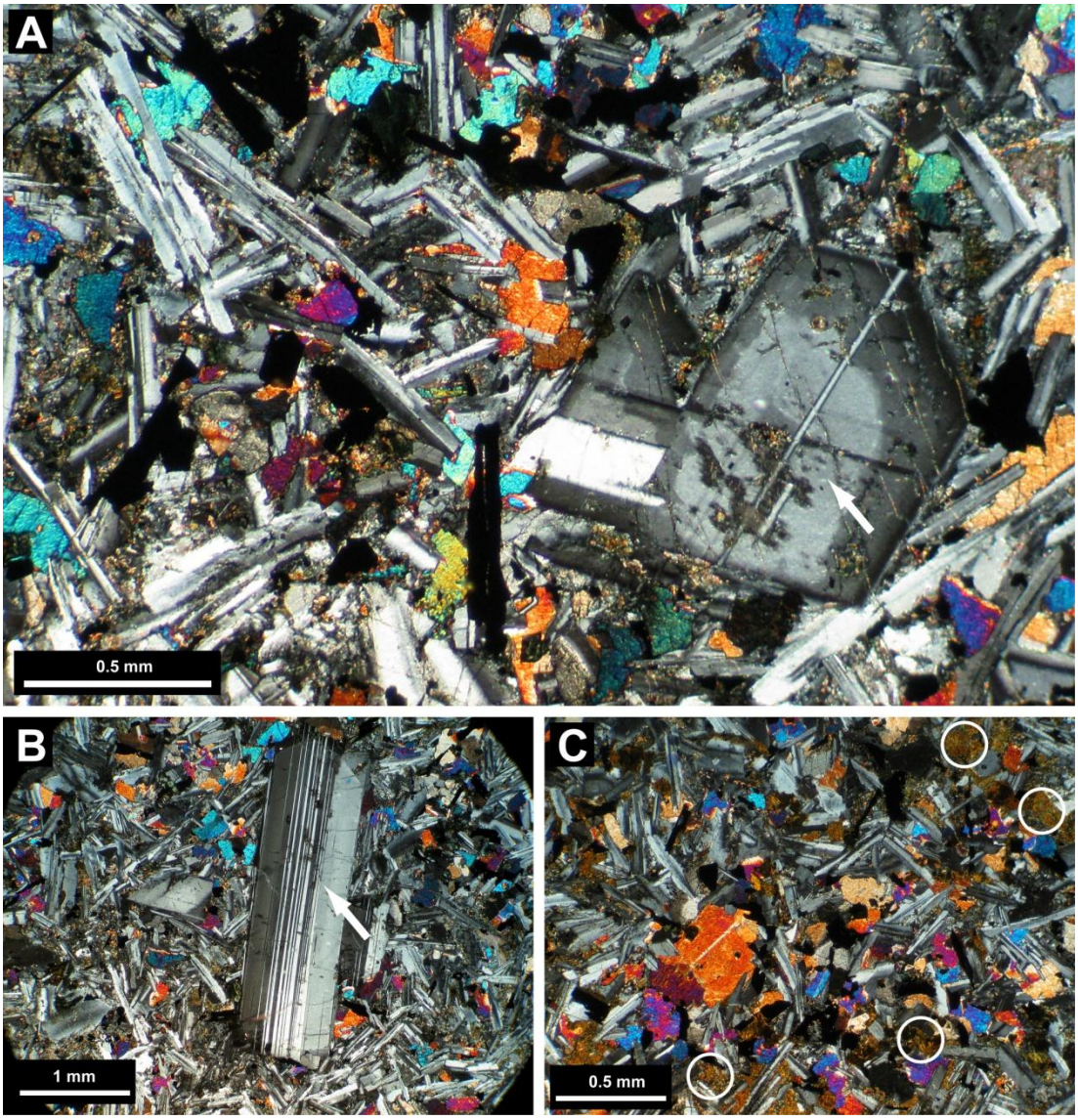

Fig. 4.10. Cross-polarised thin section photographs of Lower Permian dykes from the Keping Shan Thrust Belt. (A) Typical mineral assemblage from dyke at Keping, with a large zoned plagioclase phenocryst (see arrow). (B) Twinned phenocryst of plagioclase in a dominantly plagioclase and clinopyroxene groundmass. (C) Approximately equivalent volume of plagioclase and pyroxenes from a dyke at Mu'er, with heavily altered orthopyroxenes (ringed).

In thin section (Figs. 4.10A-C), the dominant mineral constituent is plagioclase feldspar (50-60% volume) and it is present as both randomly orientated groundmass and larger phenocrysts up to 1-3 mm in size. Clinopyroxene (augite) (20-30%), altered orthopyroxenes (=/<20%) and magnetite (10%) are also present, the latter accounting for the strong magnetism of the hand specimens. Trace apatite, commonly associated with the mafic minerals, is observed in clusters of small (<0.5mm), high

relief crystals. In some cases, the dykes have been affected by later hydrothermal fluid migration, which is expressed by small amounts of calcite in some of the samples and which may account for the alteration of the orthopyroxenes. This may be related to the formation of the calcite and muscovite megacrysts in the uppermost basalt horizons of the Kaipaizileke Fm. According to the classification scheme of Le Maître (2002), this mineral assemblage classifies the dykes as gabbronorite. In all cases, olivine is completely absent in samples from the KSTB. Geochemical analysis by Zhang *et al.* (2008) of similar dykes from the Bachu area suggest that they originate from an ocean island basalt (OIB) source and that there was little crustal contamination prior to emplacement.

4.5 Early Permian Fault Zones

Fault zones that have been active during the Late Cenozoic in the KSTB can be classified according to their structural trend. Belt-parallel fault zones are consistently thrust faults which are east to northeast-striking and are subparallel to the trend of the adjacent South Tien Shan mountain belt. There are also a series of belt-oblique structures, comprising strike-slip and oblique-slip fault zones that strike dominantly to the northwest and in some cases have acted to laterally partition deformation in the KSTB (Fig. 4.2) (Turner *et al.* 2010).

Stratigraphic correlations across the northwest-striking belt-oblique fault population reveals that they coincide with abrupt lateral variations in the thickness of the Late Palaeozoic sequence, while the overlying Cenozoic sequence is unaffected. This implies that the fault zones had an earlier history of activity that predates the Late Cenozoic evolution of the KSTB. The most prominent inherited fault zone is the Piqiang Fault, a major NNW–SSE trending fault zone that has a surface expression for more than 70 km across the centre of the KSTB (Fig. 4.2). During the Late Cenozoic, the fault has acted as a strike-slip (tear) fault with lateral separations of up to 3.8 km. Measurement of stratigraphic thicknesses across the southern part of the fault reveals a net loss of Late Palaeozoic sediment from west to east (Fig. 4.11). On the

eastern side of the fault, more than 800 metres of sediment is absent compared to the west, and includes the Lower Permian, Upper Carboniferous and a substantial part of the Middle Devonian sequence (Fig. 4.11). This difference occurs abruptly across the fault zone. The Piqiang Fault is not unique: abrupt changes in the thickness of Late Palaeozoic sediment also occur across the Sanchakou, Dabantagh and Tumuxieke Fault Zones (Figs. 4.2 and 4.5; Turner *et al.* 2010). The timing of the initiation of this northwest-striking fault population remains disputed. Evidence from the western Tarim Basin suggests that northwest-striking, right-lateral strike-slip faults were prevalent during the Jurassic, leading to the formation of narrow transtensional basins (Sobel 1999; Pers. comm., J. Suppe). Throughout this time, the Tarim Basin was divided into two isolated depocentres in the east and west by the Bachu Uplift (Li *et al.* 1996), an intrabasinal high that trends northwest-southeast and intercepts the KSTB. The western margin of the Bachu Uplift was bounded by the Selibuya-Mazartagh Fault Zone, which is the lateral equivalent of the Piqiang Fault to the southeast (Fig. 4.2).

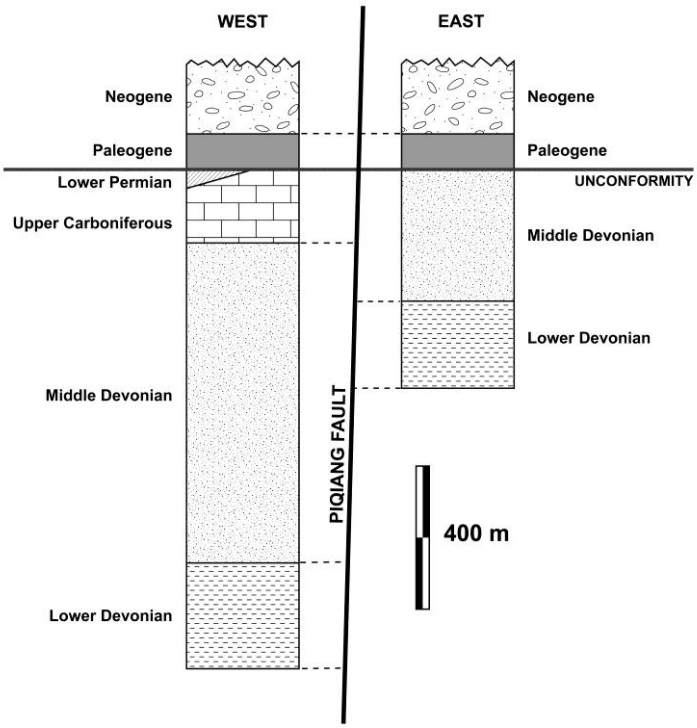

Fig. 4.11. Correlation of the stratigraphy across the Piqiang Fault, showing an 800 m net loss of stratigraphy from east to west prior to deposition of the overlying Cenozoic formations. This implies that the fault zone was active during or shortly after the Late Palaeozoic, and is likely to correspond to regional deformation in the Early Permian.

In contrast to the observations from the western Tarim Basin, the evidence presented here suggests that the northwest-striking fault zones in the KSTB area were likely to have been initiated or reactivated during the Early Permian, and that an associated northwest-striking fracture set controlled the emplacement of the mafic dykes. The fault zones controlled the distribution of Lower Permian sediment, accounting for the dramatic thickness variations across the region. Based on the thickness variations, the fault zones had a considerable dip-slip component. However, the en-echelon geometry of the northwest-trending dykes indicates an element of right-lateral shear and overall indicates a transtensional fracture set. In this case, the Bachu Uplift is an Early Permian feature that remained an intrabasinal high throughout the Mesozoic. Consequently, differential erosion across the uplifted and tilted fault blocks may have further reduced the sediment thickness across the central portion of the KSTB prior to the Cenozoic, thus accounting for the localised absence of pre-Permian (Middle Devonian and Upper Carboniferous) sediments (e.g. Fig. 4.11, Piqiang Fault).

4.6 Discussion

The substantial variation in sediment thickness, the initiation of large-scale, strike-slip fault zones and coeval volcanism implies that an important phase of tectonism occurred in the NW Tarim Basin during the Early Permian. These tectonostratigraphic features are unusual given that the region was thought to have been under a north-south contractional stress state throughout the Late Palaeozoic. In this report, new observations have been combined with data gleaned from published literature in order to review the Early Permian evolution of the Tarim Basin. Combining these observations and interpretations has enabled a model for the tectonostratigraphic evolution and regional kinematics of the Tarim Basin during this period to be developed.

4.6.1 Sediment Thickness and Structure

The radial pattern of sediment distribution across the KSTB, thickening in all directions from a paleo-high in the Bachu area, and the abrupt change in sediment thickness across northwest-striking fault zones, convincingly indicates that there was a structural control on sediment distribution in the Early Permian. Chen *et al.* (2006) proposed that the radial distribution of sediment occurred as a result of crustal doming that affected the region between 270-275 Ma, and Zhang *et al.* (2008) suggested this was the result of a short-lived mantle plume that resided beneath the NW Tarim Basin at ~275 Ma. However, regional-scale isopach maps (Bally *et al.* 1986) indicate that sediment thins onto the Bachu Uplift, an intrabasinal high which remained a significant feature throughout the Mesozoic (Li *et al.* 1996; Sobel 1999). Therefore, the radial pattern of sediment distribution is not reflected to the south of the KSTB, within the basin interior.

Therefore, it is proposed that the variations in sediment thickness arise because of interference between Late Carboniferous-Early Permian crustal flexure and the development of an Early Permian fault population. Gradual thickening of Lower Permian sediment to the north probably reflects the geometry of the Late Palaeozoic foreland basin (Carroll *et al.* 1995; Allen *et al.* 1999) that evolved to the south of the Tien Shan. Simultaneously, a series of sub-basins that were oblique to the trend of the orogen were superimposed onto the foreland as a result of activity on the northwest-striking fault zones, causing substantial variations of sediment thickness in an east-west orientation. These variations occur abruptly across major fault zones (e.g. Piqiang, Sanchakou and Tumuxieke Faults). On a regional scale, the cumulative effect of the northwest-striking faults on the stratigraphic succession is expressed in thickness variations of more than 3,200 m. Further work is required to determine the extent to which sediment thickness was controlled by syntectonic deposition or by differential erosion across raised fault blocks, although it is suggested by the present authors that elements of both are responsible for the thickness variations in the region.

It is likely that the northwest-trending mafic dyke swarm was permissive, exploiting a shear fracture set that developed coeval to the northwest-striking fault zones. In this case, the 275 Ma age of dyke emplacement derived by Zhang *et al.* (2008) provides a good constraint on the timing of fault activity and fracture development in the NW Tarim Basin. The consistent left-stepping en-echelon geometry of many of the dykes and the sub-horizontal slickensides along the dyke margins suggests that the pre-existing fractures had accommodated a component of right-lateral shear. It is therefore likely that the northwest-striking fault zones were also characterised by similar displacements, forming a strike-slip fault system under a regional principal stress that was oriented approximately north-south. Local variations in the trend of these faults would therefore enhance the extensional or compressional component of displacement. The Piqiang Fault, with a trend of NNW-SSE, may have been a predominantly extensional structure, thus accounting for the more substantial change in sediment thickness across it in comparison to other northwest-striking fault zones (c.f. Turner *et al.* 2010). It is unusual that the conjugate (northeast-striking) fault zones or dykes are lacking, and this has important implications that lead towards the regional model described later in the chapter.

4.6.2 Magma Source and Emplacement

While there is general agreement regarding the age of volcanism in the published literature on the region, the source and cause of the magma emplacement remains disputed. Zhang *et al.* (2008) argued that continental rifting could not account for the large-scale partial melting of the asthenospheric mantle required to produce the estimated quantities of basalt that are observed and following Zhou *et al.* (2004) proposed that magmatism occurred as the result of a short-lived mantle plume at c. 275 Ma. However, the estimated volume of basalt that was erupted is relatively low compared to other flood-basalt provinces associated with mantle plumes (pers. comm., A. Jay). Another suggestion by Zhang *et al.* (2008) was that the magmatism may have been associated with post-orogenic collapse is thought to be unlikely given that the Tarim Basin remained as a relatively low foreland region throughout the Late Palaeozoic. Yang *et al.* (2007) proposed that subduction to the north of the Qiangtang

Terrane (Fig. 4.1) shortly after the Tarim Block had accreted to Eurasia was the cause, although trace element distribution patterns (Zhang *et al.* 2008) show that the basalts share similarities with alkali rocks from extensional (rift) settings rather than subduction zone settings. Given the regional tectonic setting in the Late Palaeozoic, there are very limited means by which to generate such large-scale melting of the asthenospheric mantle. Roddaz *et al.* (2002) suggested that in a pro-foreland setting, only decompression melting associated with a significant amount of extension could be responsible for magmatic activity because neither volatiles or heat sources are usually expected beneath the down-going plate.

Early Permian A-type granites are reported from the South Tien Shan (Konopelko *et al.* 2007) and were also observed within the northernmost Tarim Basin during field investigations in the KSTB. It was suggested that granite emplacement was aided by the development of a left-lateral, trans-crustal strike-slip shear zone (Biske 1995; Konopelko *et al.* 2007; Biske & Seltmann, in press), which provided a conduit for the rapid ascent of asthenospheric mantle. This also permitted Kazakhstan to move westward with respect to Tarim, and consequently the South Tien Shan became strongly transpressional. Geochronological investigations constrain the ages of granite emplacement to 279-296 Ma, although most yield ages towards the younger end of this interval (c. 280 Ma) (Konopelko *et al.* 2007). The granites have depleted mantle ages of 1.05-1.43 Ga, and therefore has been suggested that asthenospheric mantle mixed with Precambrian crustal components that are likely to have been derived from the Mesoproterozoic Tarim Craton (Solomovich & Trifonov 2002; Konopelko *et al.* 2007), which was underthrust beneath the South Tien Shan following the Late Palaeozoic collision with Kazakhstan. The authors also suggested that the ascending asthenospheric material in the crustal-scale shear zone exploited a number of crustal detachment zones deep within the Tarim Craton, providing a means for relatively uncontaminated mafic material to erupt within the Tarim Basin.

4.6.3 Model for Early Permian Basin Evolution

From the Devonian to the Carboniferous, the Tarim Craton migrated rapidly northward by 18º of latitude (Li 1990). This is likely to have been driven by slab-pull, caused by the subduction of the oceanic crust of the Turkestan Ocean (which lay to the north of the Tarim Craton) beneath Kazakhstan (Li 1990; Zhu *et al.* 2009). The closure of the Turkestan Ocean and the formation of the South Tien Shan occurred in the Late Carboniferous to Early Permian (Windley *et al.* 2007), during which time the Tarim Craton experienced a clockwise rotation of 26º but did not move any further northwards (Li *et al.* 1988). This has been attributed to an oblique collision, in which eastern Tarim collided first. As a flexural foreland basin developed parallel and adjacent to the Tien Shan along the northwest margin of the Tarim Craton, it was filled initially with marine sediments during the underfilled (flysch) stage in the Late Carboniferous, and non-marine sediments during the overfilled (molasse) stage in the Early Permian.

Shortly subsequent to the collision of Tarim and Kazakhstan, at 280-270 Ma, the Tien Shan mountain belt became strongly transpressional. Trans-crustal, left-lateral strike-slip movement was accommodated across the belt (Biske 1995; Konopelko *et al.* 2007; Biske & Seltmann, in press) such that Tarim moved eastwards with respect to Eurasia. Although the Tarim Craton had previously and has subsequently acted as rigid, undeformed block, the development of major, strike-slip fault zones, the emplacement of mafic dykes and the eruption of a thick sequence of extrusive basalts implies that regional stress during a short period in the Early Permian was sufficient to deform the cratonic interior. It is proposed that the west-trending, transpressional left-lateral shear in the Tien Shan induced northwest-striking, right-lateral strike-slip faulting and fracturing in the Tarim Craton, and thereby permitted large-scale counter-clockwise block rotation. This not only created intrabasinal highs and lows, which strongly impacted on the distribution of Lower Permian sediments, but also provided a fracture network that could be exploited by the mafic dyke swarm. Major fault zones, including the Selibuya-Mazartagh and Tumuxieke Faults, may have reached sufficient depths to become ideal conduits for the rapid ascent and subsequent eruption of large quantities of uncontaminated magma. The cause of magma

generation still remains speculative; whether partial melting was induced immediately beneath the Tarim Craton as a result of large-scale block rotation and associated extension, or was aided by a trans-crustal shear zone in the South Tien Shan (c.f. Konopelko *et al.* 2007) will require further, detailed study of the dyke and basalt geochemistry.

Such large-scale, anticlockwise block rotation can be efficiently accommodated by a northwest-striking, right-lateral strike-slip faulting, which may explain the absence of a conjugate northeast-striking set of faults and fractures. In addition, it is likely that the orientations of the faults changed progressively during block rotation, towards the northwest trends that have been preserved and which have been reactivated during Late Cenozoic N-S oriented shortening (Turner *et al.* 2010). As this occurred, the faults and fractures would have rotated into an increasingly higher angle to the regional NE-SW oriented maximum principal stress direction, becoming transpressional or even compressional. This increase in normal stress across the fractures may have caused an abrupt end to volcanic activity, accounting for the sudden absence of basalt in the upper part of the Kaipaizileke Fm.

There is evidence from paleomagnetic data that the Tarim Craton experienced an anticlockwise rotation (Gilder *et al.* 1996) that would be compatible with the model proposed here. From the Carboniferous to Early Permian, the Tarim Craton rotated clockwise by 26º, which has been attributed to an oblique collision with Kazakhstan that began earlier in the east than in the west (Li *et al.* 1988). However, since the Permian, the craton has experienced a 30º anticlockwise rotation with respect to Siberia (Gilder *et al.* 1996). It is suggested by the authors that this could, in part, be accounted for by internal counter-clockwise block rotation, rather than rotation of the entire Tarim Craton (Fig. 4.12).

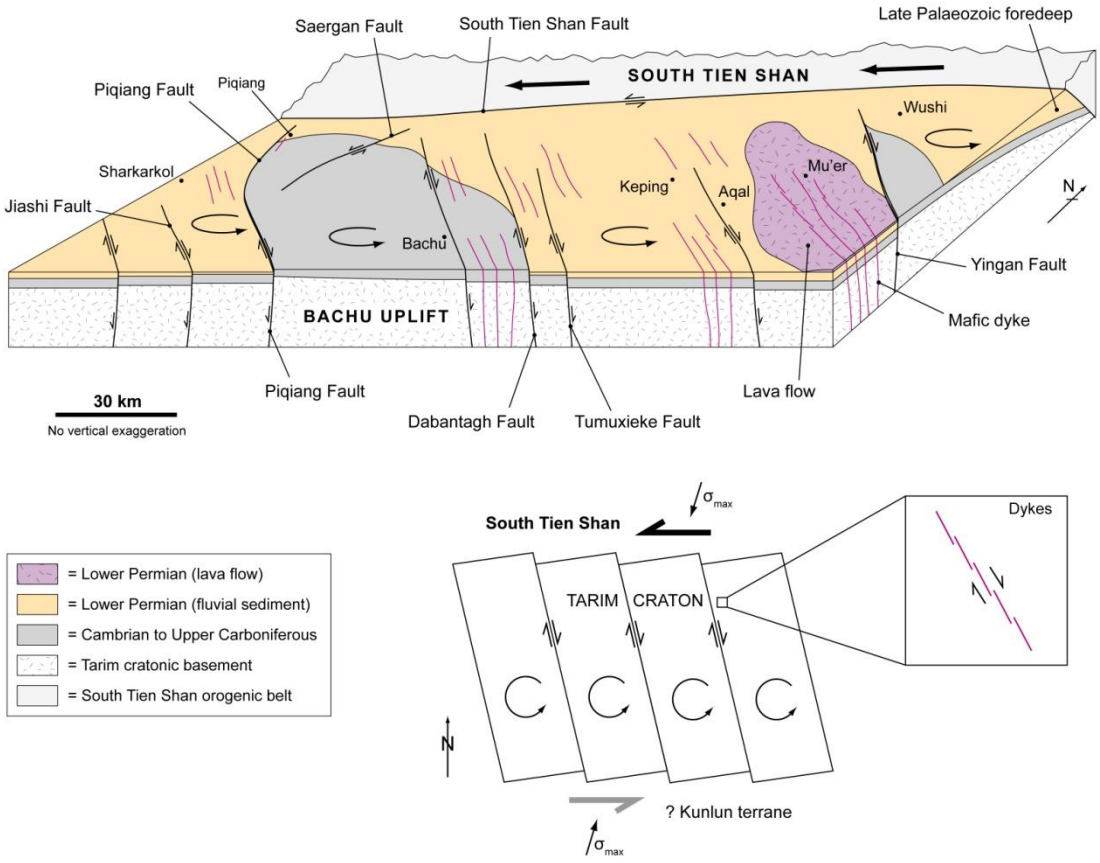

Fig. 4.12. Schematic model of the NW Tarim Basin (Keping Shan Thrust Belt region) during the Early Permian. Trans-crustal, left-lateral shear in the South Tien Shan mountains invokes large-scale block rotation in the rigid Tarim Craton to the south. This is accommodated by the formation of northwest-striking right-lateral fault zones and fractures, some of which are exploited by the mafic dyke swarm and result in the extrusion of lava flows.

Why the Tarim Craton should deform, having acted as a rigid block prior to the Early Permian even during the earlier stress imposed during the earlier stages of the South Tien Shan orogen, remains unclear. It is possible that a previously weakened cratonic basement may have aided the development of northwest-striking fractures during large-scale block rotation in the Early Permian. Fieldwork in a small exposure of crystalline, cratonic basement near Aksu, shows that a dense network of northwest-striking intermediate dykes were intruded into the basement (Chapter 2), the ages of which have been constrained to the Early Cryogenian (c. 807 Ma) (Chen *et al.* 2004). The dykes are indicative of an extensional fracture set that predates the Early Permian by a considerable time, and appears to be the dominant inherited weakness within the crystalline basement of the Tarim Craton. Alternatively, small-scale extensional

fracturing may have been induced during the earlier stages (Middle to Late Carboniferous) of the South Tien Shan orogen, creating belt-oblique extensional structures by the mechanisms proposed by Sengör (1976) and Hancock & Bevan (1987), which could be subsequently reactivated during large-scale block rotation during the latest stages of the orogen.

The mechanism proposed for Early Permian strike-slip faulting and magmatism in the NW Tarim Basin is similar to the model proposed for active deformation in eastern Tibet by England & Molnar (1990). In this example, north-trending, right-lateral shear across the region is thought to be responsible for block rotation between a series of east to southeast-striking, left-lateral strike-slip faults that permit the clockwise rotation of large-scale blocks. This represents an identical situation to the NW Tarim Basin during the Early Permian, but with the opposite sense of regional shear. Allen *et al.* (1995) suggested that large-scale block rotation was the cause of isolated depocentres, transtensional faulting and widespread magmatism during the Late Permian evolution of the Junggar Basin, which lies to the north of the Tien Shan. This model is similar to the mechanisms proposed for deformation in the Aegean (McKenzie & Jackson 1986; Jackson 1994) whereby large-scale block rotation was induced by right-lateral shear on a series of major fault zones to the north of the region.

4.7 Conclusions

Examination of Lower Permian sedimentary and volcanic rocks in the Keping Shan Thrust Belt, NW Tarim Basin, reveal an important phase of tectonism that is apparently incompatible with the regional contractional stress regime during the latest stages of the South Tien Shan orogen. The initiation and development of a northwest-striking, right-lateral strike-slip fault population that was coeval to the emplacement of a northwest-trending, mafic dyke swarm strongly impacted on the distribution of Lower Permian sediments. The northwest-trending mafic dykes fed voluminous basalt eruptions, which covered large parts of the Tarim Basin and which

are preserved within two distinct intervals within the Lower Permian sedimentary succession. A new model has been proposed that differs from previous interpretations of these sedimentary, igneous and tectonic features. Trans-crustal, left-lateral ~E-W trending shear accommodated across the South Tien Shan mountain belt during the latest stages of the orogen resulted in large-scale block rotation within the Tarim Craton to the south. The northwest-striking fault zones accommodated counter-clockwise rotation of these blocks, creating a series of intrabasinal highs and lows, including the Bachu Uplift, which has been periodically reactivated during the Mesozoic and Cenozoic.

CHAPTER FIVE

Orogenic Uplift and Flexural Subsidence in the Cenozoic

Abstract • Subsidence in the NW Tarim Basin, China, during the Cenozoic has been largely driven by flexural deflection of the underlying Tarim Craton beneath the Pamirs and Tien Shan orogenic belts. This has generated a series of deep, elongate foreland basins that have filled with an upward-coarsening sequence of lacustrine and fluvial-facies clastic sediment that locally exceeds thicknesses of 10 km. The sedimentology, combined with the spatial and temporal distribution of the sequence, records the progressive development of the adjacent belts. Numerical models constrain the flexural rigidity of the Tarim Craton to be 4×10^{23} Nm, which corresponds to an effective elastic thickness of c. 37 km. The models also show that the Pamirs began to uplift during the Early Miocene, at least 5-6 Myr before the Tien Shan became a topographically prominent feature. An abrupt increase in the mean elevations of both orogenic belts occurs in the Middle to Late Miocene, and is attributed to a regional change in geodynamics and rapid uplift in the Tibetan Plateau to the south. By the Pliocene, it is likely that both the Pamirs and Tien Shan had attained mean elevations that are comparable to their present, observed topographic profiles.

5.1 Introduction

Flexural deformation of the continental lithosphere has been recognised as an important mechanism for the development of foreland basins associated with orogenic belts (DeCelles & Giles 1996; Allen & Allen 2005). The uplift of an orogenic belt creates a source of sedimentary detritus, whilst simultaneously loading and deflecting the continental lithosphere in the foreland region and thus creating an important site for sediment accumulation. As a consequence, the spatial and temporal distribution of the foreland basin sediment is dynamically linked to the growth of the orogenic belt, and provides a useful record for examining the progressive flexural deflection of the underlying plate or craton.

During the Cenozoic, subsidence in the NW Tarim Basin, China, has been driven primarily by flexural deformation of the underlying Tarim Craton (Yang & Liu 2003). The Tarim Basin is surrounded by a series of mountain ranges, including the Tien Shan, Pamirs and Kunlun Shan (Fig. 5.1) that have been rejuvenated during the Middle to Late Cenozoic as a response to far-field stresses associated with the India-Asia collision (Tapponnier & Molnar 1979; Windley *et al.* 1990). The progressive uplift of these belts has generated a series of exceptionally deep foreland basins at the peripheries of the craton, which have been filled with a sedimentary sequence that locally exceeds thicknesses of 10,000 m (Bally *et al.* 1986; Jia 1997). The purpose of this chapter is to analyse the progressive uplift of the Pamirs and Tien Shan orogenic belts and to examine the resultant flexural deflection of the NW Tarim Craton during the Cenozoic. This is achieved by examining the sedimentary facies and thickness distribution of the foreland stratigraphy using isopach maps and outcrop sections. This data provides the basis for 2-dimensional numerical modelling of the flexural deflection, which follows a similar approach taken by Cardozo & Jordan (2001) in the Andes, Argentina, and Yong *et al.* (2003) in the Longmen Shan, China.

5.2 Lithospheric Flexure and Foreland Basin Systems

Flexural subsidence is caused by long wavelength deflection of the lithosphere beneath an applied load (Allen & Allen 2005). This chapter is concerned with foreland basins, which are caused by lithospheric deflection beneath an applied tectonic load (an orogenic belt). Foreland basins form parallel to orogenic belts and are asymmetric in cross section, becoming progressively deeper towards the thrust front. As the orogenic belt is uplifted and eroded, it delivers large quantities of sediment to the foreland which provide a record of the progressive deflection of the lithosphere and development of the belt.

The depth and width of the foreland basin is controlled by a series of variable boundary conditions. The flexural rigidity, D, defines the strength of the tectonically-loaded lithosphere and its resistance to flexure, and scales with the effective elastic thickness, T_e. If a load is applied to a strong lithosphere ($D = 10^{23}$-10^{24} Nm), a wide but shallow foreland basin is generated, while a weak lithosphere ($D = 10^{21}$-10^{22} Nm) will generate a narrower but deeper foreland basin. In addition, the weight and area distribution of the tectonic load, and the sedimentary load that it delivers to the foreland, play an critical role in determining the flexural response of the lithosphere.

The foreland basin consists of different depozones that reflect different positions in the foreland with respect to the orogenic belt (DeCelles & Giles 1996). The foredeep depozone forms immediately adjacent to the thrust front, and is the area in which the flexural subsidence is most pronounced. The depozone thins away from the orogenic belt until the forebulge, an area across which the flexural deflection is expressed positively and commonly results in subaerial exposure and erosion. Beyond the forebulge, the backbulge depozone is characterised by a thin accumulation of sediment and represents the most distal depozone of the foreland basin system. Continued growth of the orogenic belt commonly results in deformation of the foreland succession in the vicinity of the belt, creating a wedge-top depozone which is characterised by piggy-back basins within a foreland fold-thrust belt.

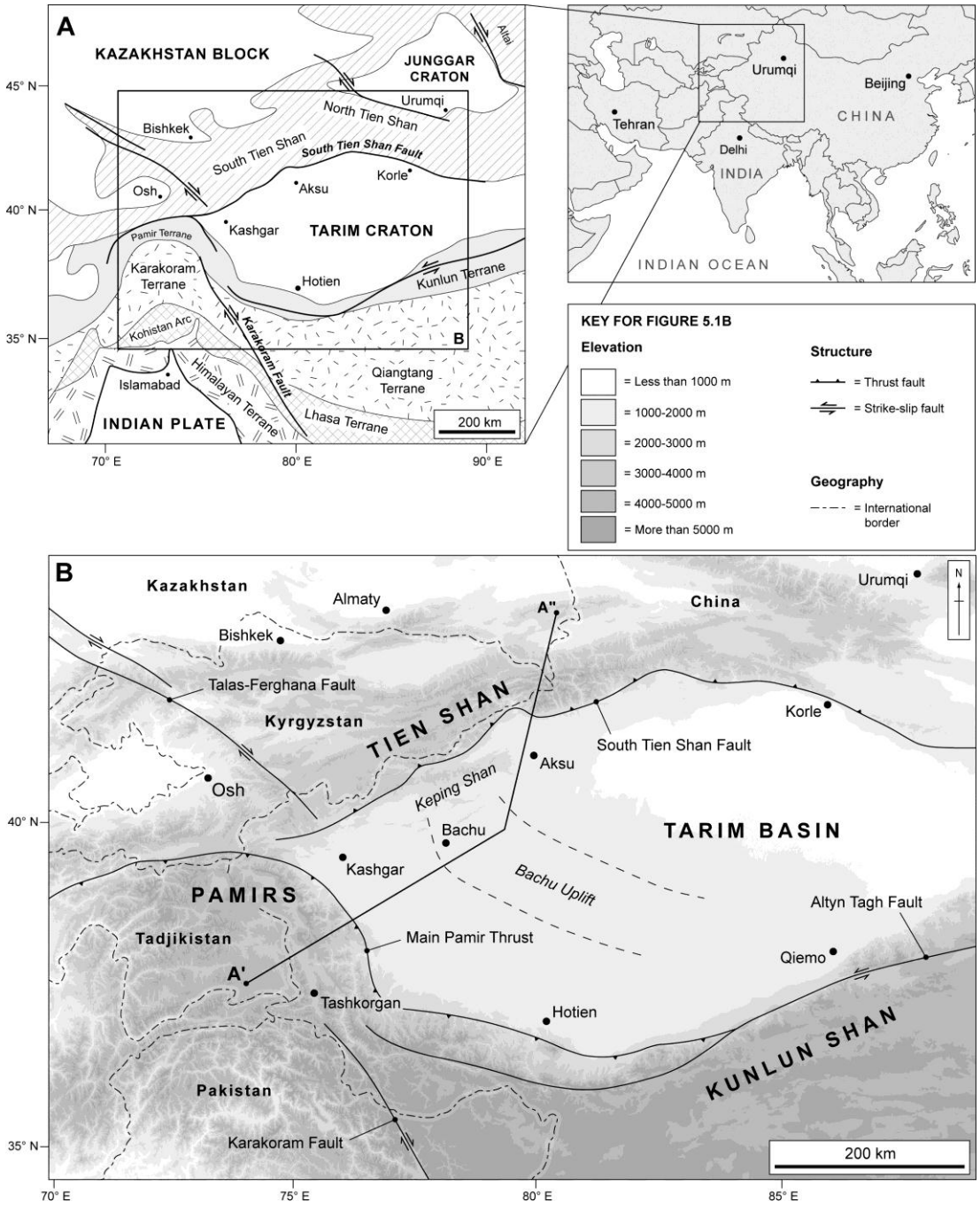

Fig. 5.1. (A) Simplified tectonic map of Central Asia, showing the major terranes and cratonic blocks that have been accreted to the continent during the Phanerozoic. (B) Topographic and simplified structural map of the Tarim Basin, Pamirs and Tien Shan mountain belts. The line of section (A'-A") examined in this study is shown, following an approximate NE-trend.

5.3 Regional Setting

5.3.1 The Tarim Basin

The Tarim Basin covers an area of c. 500,000 km^2 and overlies the crystalline basement of the Tarim Craton, a microcontinent that was accreted to Central Asia in the Late Palaeozoic (Burtman 1975; Li 1990; Windley *et al.* 1990; Chapter 3). The NW Tarim Basin contains a thick (3-16 km) sedimentary cover succession which spans the Late Neoproterozoic to Recent. Variations in the thickness of the pre-Cenozoic succession yield information about earlier phases of tectonism and basin evolution (Chapters 3 and 4). One of the most prominent structural elements is the Bachu Uplift, a NW-trending, 150 km-wide intrabasinal high that intersects the Keping Shan at its northern end. The Bachu Uplift is bounded on both sides by major, NW-striking fault zones which are thought to have been initiated during the Early Permian (Chapter 4). It remained an important feature throughout the Mesozoic, partitioning the Tarim Basin into two isolated depocentres in the west and east (Sobel 1999). During the Cenozoic, subsidence in the NW Tarim Basin was driven predominantly by flexural deflection associated with the growth of the surrounding mountain belts (Yang & Liu 2002). This resulted in the accumulation of up to 10 km of sediment (Bally *et al.* 1986; Jia 1997) in a series of elongate foreland basins along the margins of the NW Tarim Basin, adjacent to the Pamirs and Tien Shan orogenic belts (Figs. 5.1 and 5.2).

5.3.2 The Tien Shan

The Tien Shan form a 2,500 km-long mountain belt that extends from NW China into Kyrgyzstan, acting as a natural border between the two countries. To the north of the Tarim Basin, the Tien Shan is 200-300 km wide with an average elevation of 3-4 km (Figs. 5.1 and 5.2) and a small number of summits are in excess of 7 km. The Tien Shan belt comprises intensely deformed metamorphic rocks that are largely the remnants of a thick Palaeozoic marine succession that once filled the ocean which

separated Tarim from Kazakhstan, prior to their collision in the Late Palaeozoic (Windley *et al.* 1990). The Tien Shan remained a prominent topographic feature during the Mesozoic, maintained by a series of collisions to the south of Tarim (Hendrix *et al.* 1992, 2000). During the Cenozoic, widespread contraction across Central Asia has been associated with the collision of India and Eurasia (Tapponnier & Molnar 1979), and has resulted in rejuvenation of the Tien Shan since c. 20 Ma (Windley *et al.* 1990; Abdrakhmatov *et al.* 1996; Sun *et al.* 2004). The Tien Shan is separated from the Tarim Basin by the South Tien Shan Fault, a steep (50–60°), north-dipping reverse fault that is thought to continue to depths of at least 20–30 km (Chapter 6). The fault zone juxtaposes metamorphic rocks of the orogenic belt against the sedimentary rocks of the basin. To the south of this fault zone, the sedimentary succession has been deformed by thin-skinned tectonics during the Middle to Late Cenozoic, creating a series of foreland fold-thrust belts (Yin *et al.* 1998; Allen *et al.* 1999; Chapter 6).

5.3.3 The Pamirs

The Pamirs form an arcuate orogenic belt that lies to the west of the Tarim Basin. It is composed of a series of terranes that were accreted to the Tarim Craton during the Palaeozoic and Mesozoic (Burtman & Molnar 1993; Xiao *et al.* 2002; Robinson *et al.* 2004). It also represents the lateral equivalent of the Kunlun Shan orogenic belt, which lies to the south of the Tarim Basin, but which has been offset by a series of major right-lateral fault zones, including the Karakoram Fault (Fig. 5.1) (Yin & Harrison 2000). The Pamirs are topographically higher than the Tien Shan, with average elevations of 4–5 km and many summits in excess of 7 km. The rapid growth of the Pamirs during the Cenozoic has led to large-scale orogenic collapse (Robinson *et al.* 2004). The Pamirs are separated from the Tarim Craton by the Pamirs Main Thrust (PMT), which is a crustal-scale fault zone with an estimated displacement of 300 km, having translated the metamorphic rocks of the Pamirs over the sedimentary succession of the Tarim Basin since the Mid Palaeozoic (Burtman & Molnar 1993; Matte *et* al. 1996; Sobel & Dumitru 1997).

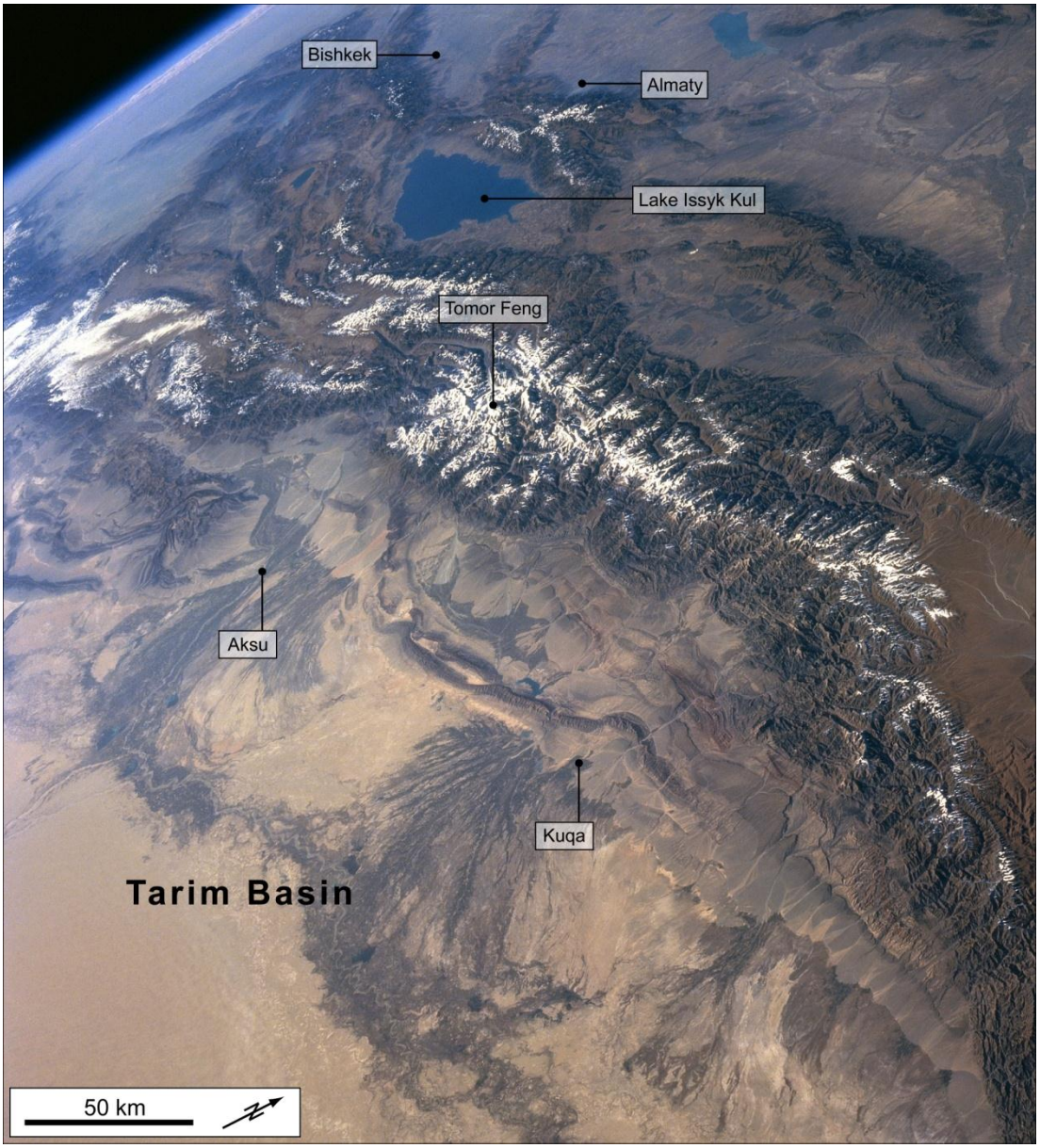

Fig. 5.2. The Tien Shan mountains and the Tarim Basin as seen from space on 18 October 1997. The Tien Shan forms a 2,500 km long mountain belt that extends through NW China and into Kyrgyzstan and has an average elevation of 3,000–4,000 m. To the south, the Tarim Basin is anomalously flat, with an average elevation of 1,000–1,200 m. Image courtesy of Earth Sciences and Image Analysis Laboratory, NASA Johnson Space Center, reference NASA06-701-38.

5.4 Foreland Basin Stratigraphy

Sediment supplied to the NW Tarim Basin during the Cenozoic is likely to have been sourced almost solely from the Pamirs and Tien Shan orogenic belts as they were progressively rejuvenated during the Himalayan orogen. These belts generated tectonic loads sufficient to deflect the Tarim Craton and create accommodation space in which these sediments were accumulated. Consequently, the thickness of the Cenozoic succession varies from 1–10 km across the NW Tarim Basin (Bally *et al.* 1986; Jia 1997). It comprises an upward-coarsening sequence of Neogene-Pleistocene formations (Fig. 5.3) (Scharer *et al.* 2004; Heermance *et al.* 2007, 2008), which are locally exhumed in a series of E-W trending anticlines to the north of Kashgar (Fig. 5.4). Recent studies have focused on resolving the precise ages of the formations using magneto-stratigraphic techniques (e.g. Chen *et al.* 2002; Heermance *et al.* 2007), providing invaluable data that can be used to refine the age intervals of sediment isopach maps derived from borehole data (e.g. Jia 1997).

The Neogene–Pleistocene sequence unconformably overlies an underlying bedrock of Neoproterozoic, Palaeozoic and Mesozoic sediments, which in turn overlie a crystalline basement allegedly representing the Tarim Craton. Deposition in the Kashgar area began at 17.5 Ma (Heermance *et al.* 2007) and continued until at least 1 Ma, prior to contractional uplift. Consequently, the maximum average sedimentation rate in the deepest part of the Pamirs foreland is high (c. 0.6 mm yr^{-1}), but decreases substantially (c. 0.04 mm yr^{-1}) where the Cenozoic sequence is very thin. This is in strong contrast to deposition in the Palaeozoic, when sedimentation rates rarely exceeded c. 0.08 mm yr^{-1} (Chapter 3).

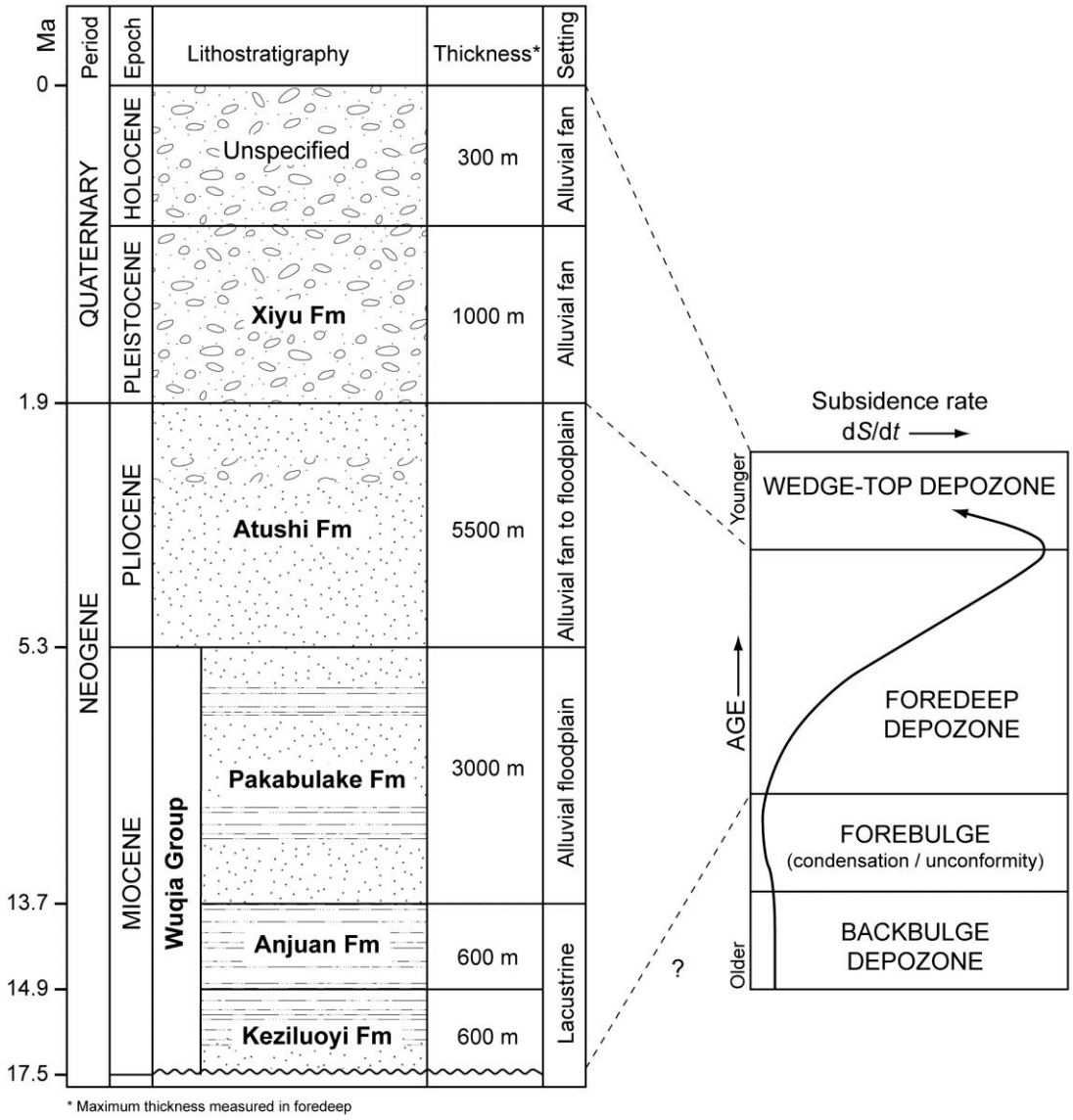

Fig. 5.3. Cenozoic stratigraphy of the NW Tarim Basin modified from Scharer *et al.* (2004) and Heermance *et al.* (2007) and combined with observations presented in this report. Age constraints were obtained by Chen *et al.* (2002) and Heermance *et al.* (2007). Maximum stratigraphic thickness were obtained from isopach maps, presented later in this chapter, from Jia (1997). The stratigraphic framework is correlated with a summary of the depozones in the foreland basin system with respect to the change in subsidence rate over time, modified from DeCelles *et al.* (1998).

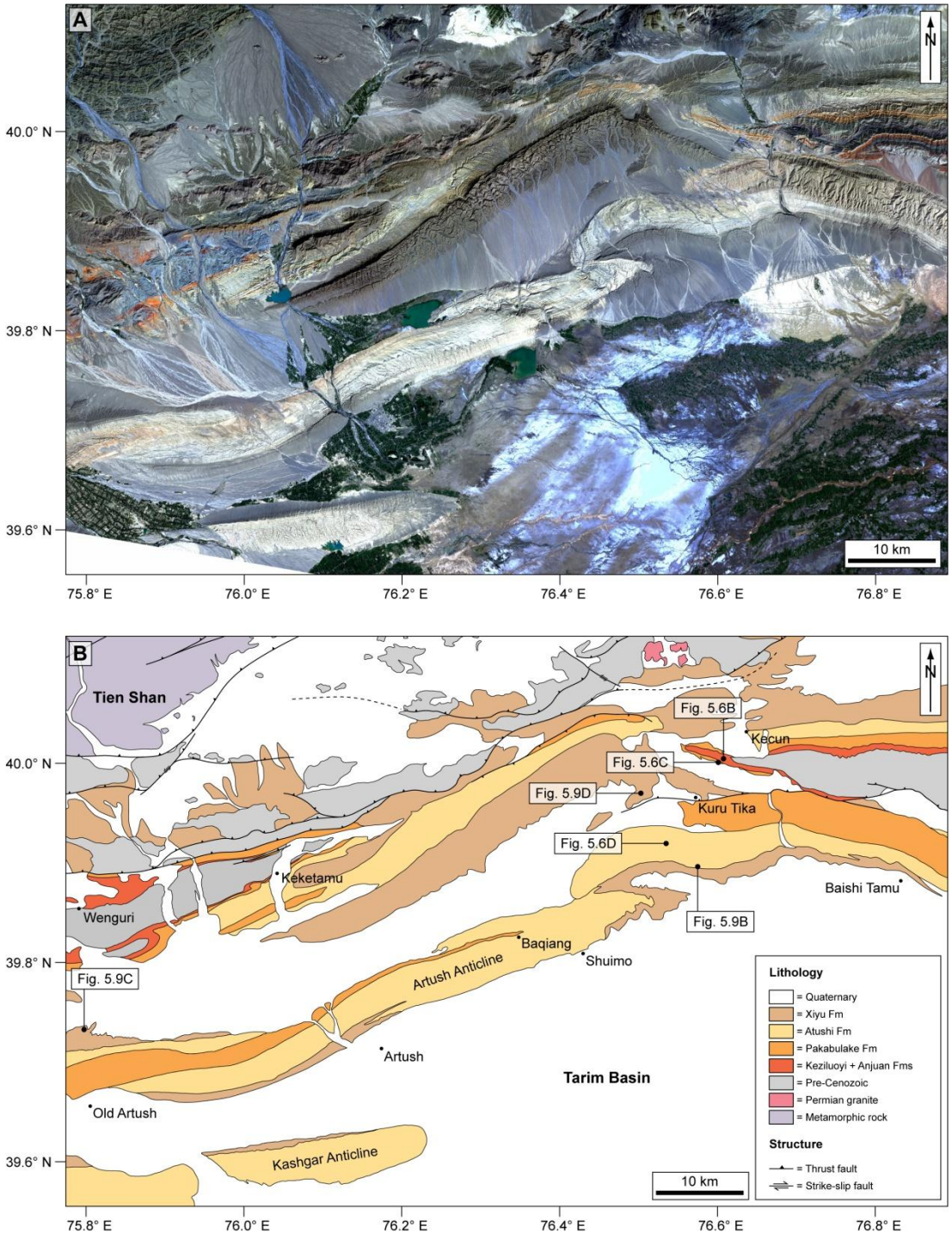

Fig. 5.4. Outcrop exposures of the Cenozoic stratigraphy. (A) Enhanced Landsat ETM true colour composite image of the Kashgar Fold Belt on the northwest margin of the Tarim Basin. (B) Interpreted geological map of *A* showing the distribution of Cenozoic formations and the structural style of the area. The Cenozoic formations crop out in a series of E–W trending anticlines.

5.4.1 Wuqia Group

The Wuqia Group is the collective name for three formations that were deposited during the Miocene: the Keziluoyi Fm (Early Miocene), Anjuan Fm (late Early Miocene) and Pakabulake Fm (Late Miocene) (Figs. 5.3 and 5.4). The total thickness of the Wuqia Group locally exceeds 4,500 m in the foredeep adjacent to the Pamirs, yielding a maximum sedimentation rate of 0.5 mm yr^{-1}, but thins to less than 300 m across the Bachu Uplift.

Keziluoyi and Anjuan Formations. Together, the Early Miocene Keziluoyi and Anjuan formations reach a combined thickness in excess of 1,800 m in the foredeep adjacent to the Pamirs, thinning to less than 100 m across the Bachu Uplift (Fig. 5.5). The 500–550 m thick Keziluoyi Fm consists of two units. The lower unit is characterised by interbedded, pale yellow-brown sandstones and siltstones. These sandstone bodies have erosive bases and channel-body geometries (Fig. 5.6A), and internally contain trough cross bedding, mud rip-up clasts and discrete horizons of rounded pebbles. The upper surfaces of individual beds have asymmetric ripples, which yield S to SW paleocurrent directions in the Kecun area (see Fig. 5.4B). The sandstones and siltstones are interpreted as meandering fluvial channels and the overbank deposits of an alluvial floodplain. These facies pass gradually upwards into a second unit consisting of red-brown shales and siltstones, with thin (1–2 cm) gypsum horizons (Fig. 5.6B). Some of the siltstone beds have symmetric ripples on their upper surfaces. In areas of tight folding (e.g. Kecun, Fig. 5.4B), the gypsum horizons have been exploited as detachments that have accommodated displacement between individual beds. The second, upper unit is interpreted as lacustrine deposits of an arid, perennial saline lake. Using magnetostratigraphic techniques, Heermance *et al.* (2007) constrained the age of the Keziluoyi Fm to 17.5–14.9 Ma. It was also proposed that the upper parts of the lower, fluvial-facies unit grade laterally into the lower parts of the lacustrine-facies unit across the area.

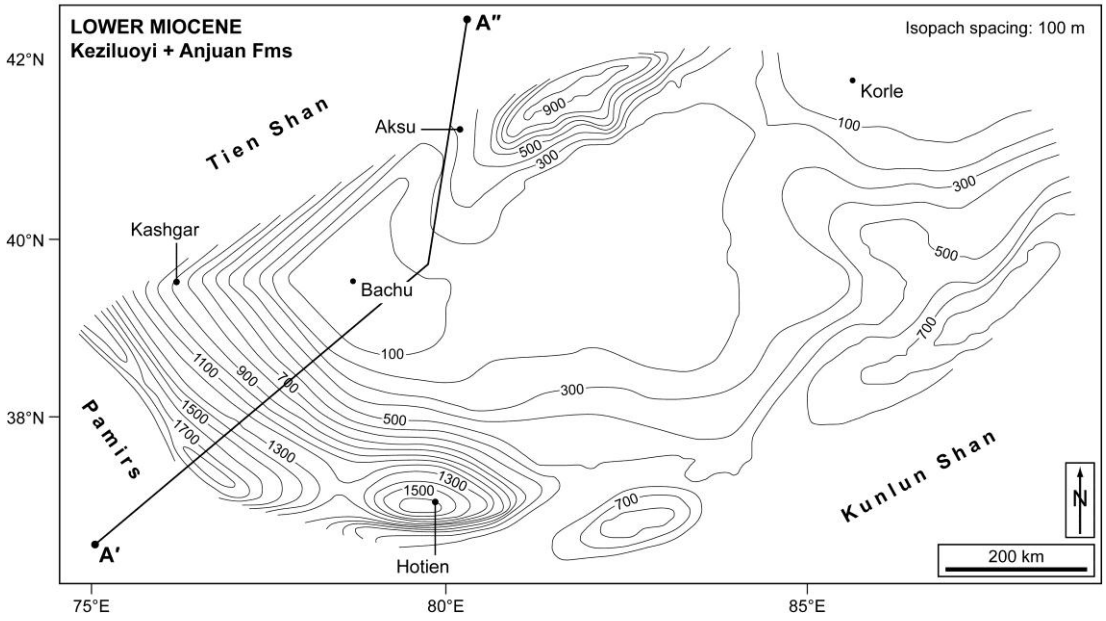

Fig. 5.5. Isopach map of the Lower Miocene Keziluoyi and Anjuan Fms (modified from Jia 1997).

The base of the Anjuan Fm is characterised by a 50-100 m thick pale green-grey fissile shale unit (Fig. 5.6C), which is overlain by a 100 m succession of red-brown shales, siltstones and thin gypsum horizons of similar nature to the underlying Keziluoyi Fm. Heermance *et al.* (2007) constrained the depositional age of the formation to 14.9-13.7 Ma. It is interpreted as a continuation of the arid, lacustrine facies that preceded it. The basal shale unit provides a useful marker bed for identifying the Anjuan Fm, and may represent deeper lacustrine conditions.

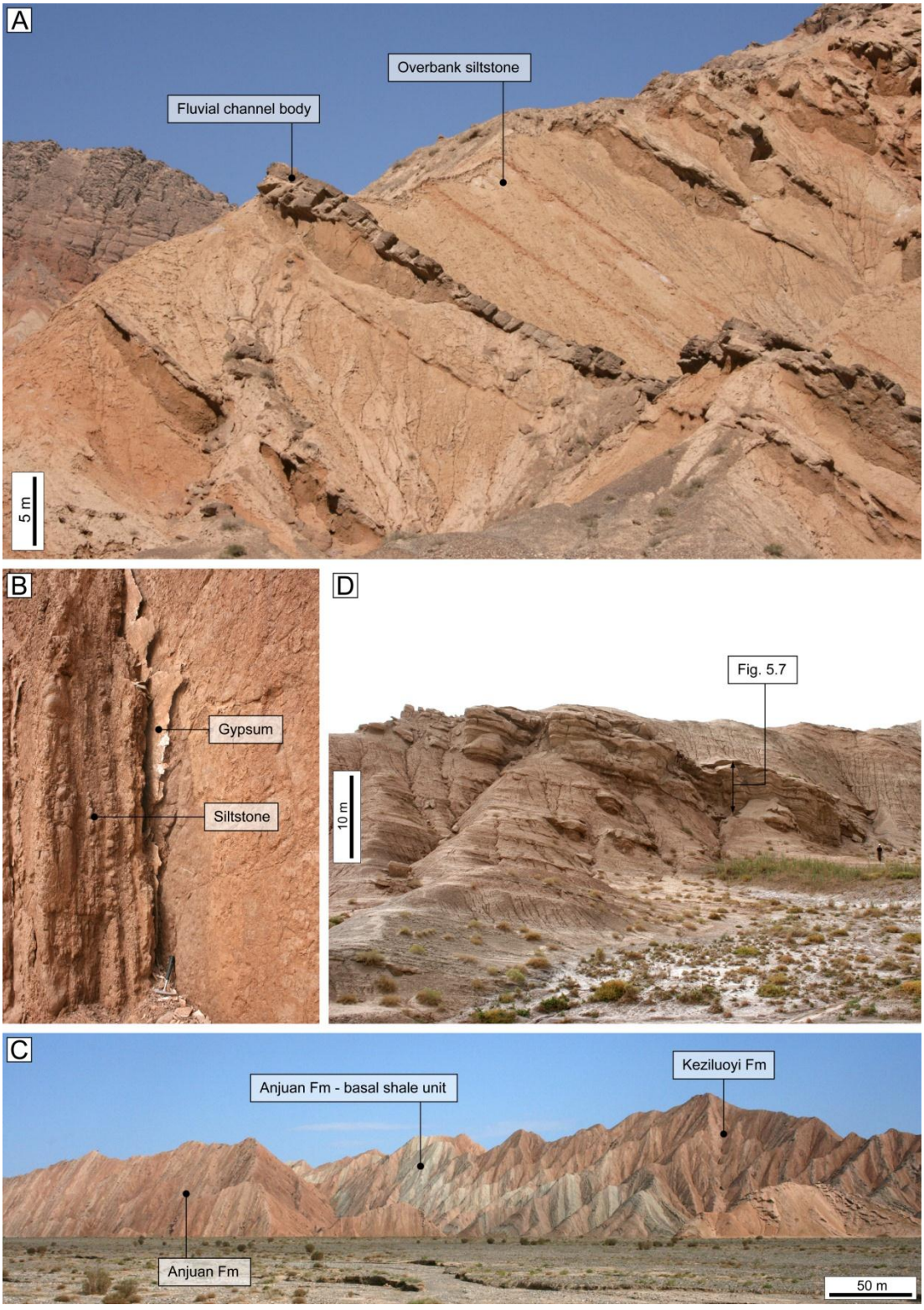

Fig. 5.6. Outcrop photographs of the Wuqia Group. (A) Fluvial and overbank facies sandstones and siltstones of the lower part of the Keziluoyi Fm near Bachu. (B) Thin gypsum horizon and red-brown siltstone of the upper part of the Keziluoyi Fm near Kecun. (C) Profile view of the Keziluoyi Fm passing conformably upwards into the Anjuan Fm, marked by the pale grey basal shale unit near Kecun. (D) Interbedded siltstones and sandstones of the Pakabulake Fm near Kuru Tika. A log section of the sandstone unit is shown in Fig. 5.7.

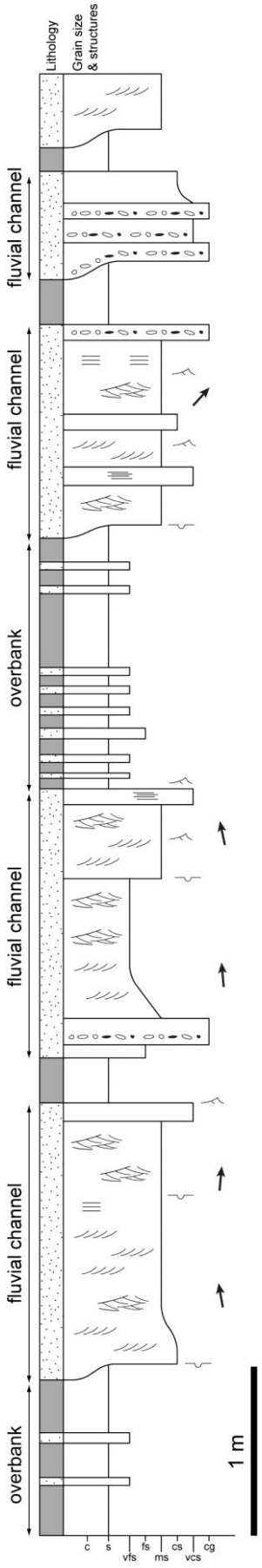

Pakabulake Formation. The Pakabulake Fm comprises a succession of interbedded pale yellow-grey siltstones (60%) and sandstones (40%) (Figs. 5.6D, 5.7) that locally reaches thicknesses of 2,000 m in the Kashgar area (Fig. 5.8). The sandstone intervals are medium to coarse-grained and commonly have erosive, undulatory bases with groove casts that are overlain by thin conglomeratic lags. Internally, they contain planar and trough cross bedding, planar and wavy laminations and thin pebble horizons. Bedding surfaces commonly show asymmetric current ripples. Paleocurrent data from the Sugun–Karajol area indicate a predominantly northerly flow direction (Fig. 5.7). The Pakabulake Fm is interpreted as a return to alluvial floodplain facies.

Fig. 5.7. Sedimentary log from the lower to middle Pakabulake Fm at Kuru Tika, which is characterised by interbedded fluvial channel sandstones and overbank siltstones, corresponding to an alluvial floodplain succession.

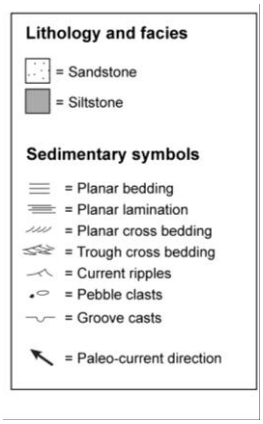

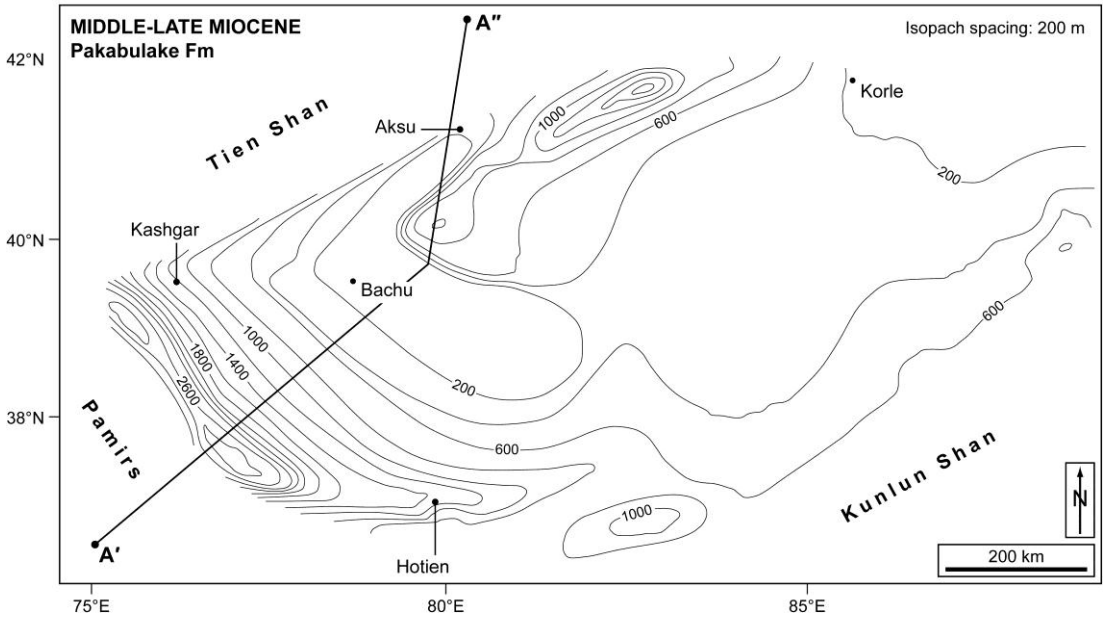

Fig. 5.8. Isopach map of the Middle–Upper Miocene Pakabulake Fm (modified from Jia 1997).

5.4.2 Atushi Formation

The Pakabulake Fm passes conformably upwards into the Atushi Fm, which is characterised by pale yellow-brown sandstones, siltstones and pebbles of lighter colour than the preceding Pakabulake Fm (Fig. 5.9A), but otherwise containing similar sedimentary characteristics. The Atushi Fm is also interpreted as meandering, alluvial floodplain facies although the coarser nature of some fluvial beds implies an increase in energy. Deposition of the Atushi Fm began at 5.3 Ma, coinciding with the start of the Pliocene (Heermance *et al.* 2007). The thickness of the Atushi Fm locally exceeds 5,000 m, both within the deep foreland basin that runs parallel to the Pamirs and a second, newly developed depression to the south of Aksu and the Tien Shan (Fig. 5.10). The age and thickness constraints yield a maximum, average sedimentation rate of 1.6 mm yr^{-1}. In the uppermost part of the formation, conglomeratic beds begin to dominate (Fig. 5.9B), characterising a gradual transition into the overlying Xiyu Fm.

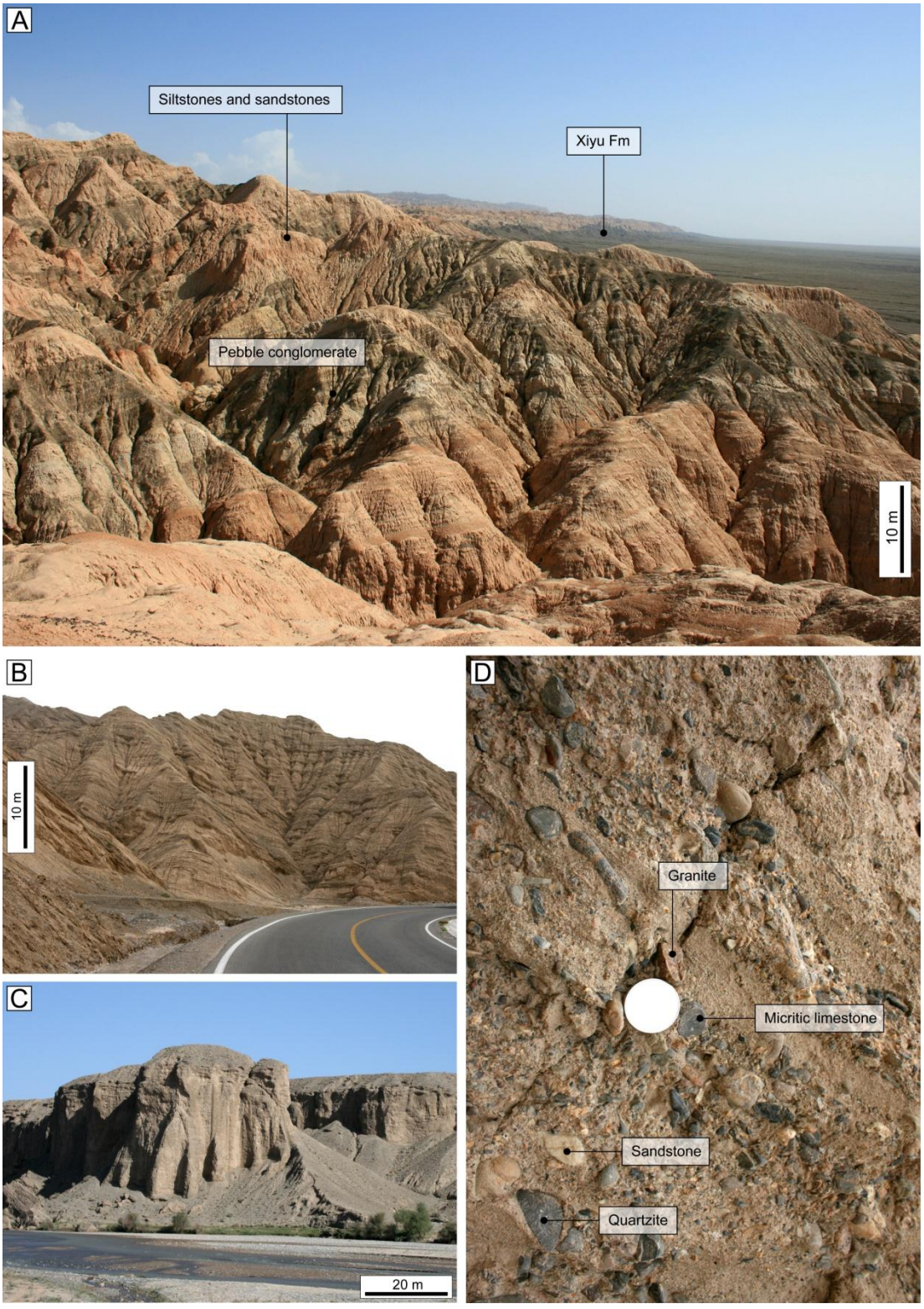

Fig. 5.9. Outcrop photographs of the Pliocene and Pleistocene. (A) Interbedded siltstones, sandstones and pebble conglomerates of the Atushi Fm, exposed in the core of an anticline near Aksu. (B) Gradual transition from the Atushi Fm into the Xiyu Fm near Kuru Tika, shown by progressive increase in interbedded dark grey conglomerates. (C) Thickly bedded conglomerate of the Xiyu Fm near Wuqia, to the west of Old Atushi. (D) Moderately sorted igneous, metamorphic and sedimentary pebbles in the Xiyu Fm near Kuru Tika (1 Yuan coin for scale, 2 cm diameter).

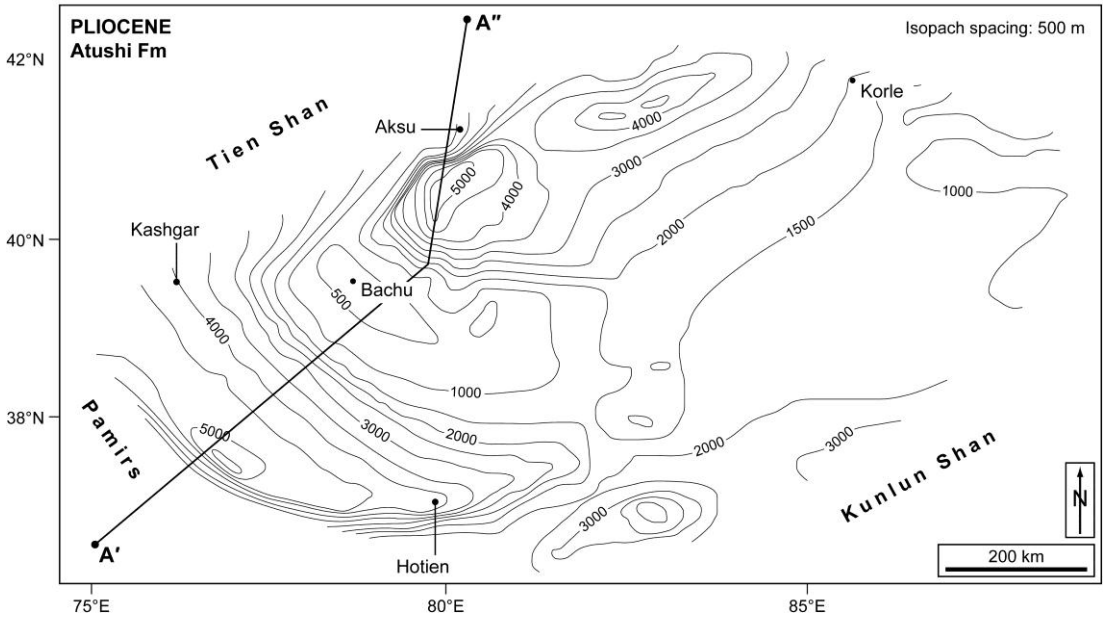

Fig. 5.10. Isopach map of the Pliocene Atushi Fm (modified from Jia 1997).

5.4.3 Xiyu Formation

The Xiyu Fm is characterised by a dark grey, clast-supported conglomerate (Figs. 5.9C, 5.9D) that locally exceeds thicknesses of 800 m (Chen *et al.* 2002). An isopach map is not available for the Xiyu Fm. At Kuru Tika (Fig. 5.4), the conglomerate contains moderately sorted, rounded metamorphic, igneous and sedimentary pebbles and boulders (Fig. 5.9D). The metamorphic and igneous clasts (quartzites, schists, granites) are consistent with the lithologies observed within the Tien Shan to the north, which indicates a change in the general paleoflow direction since deposition of the Pakabulake Fm in the same area (Fig. 5.7). The sedimentary clasts include limestones and sandstones that are derived from the preceding Palaeozoic sequence (Chapter 3), and were eroded from the hanging walls of imbricate thrusts that developed during Late Cenozoic contractional deformation of the foreland. The Xiyu Fm is interpreted as a prograding, time-transgressive gravel wedge that was deposited predominantly in the Pleistocene (Scharer *et al.* 2004; Heermance *et al.* 2007). In the Atushi area (Fig. 5.4), the base of the Xiyu Fm yields an age of 1.9 Ma (Chen *et al.* 2002), whilst to the north of Keketamu it yields an age of 15.5 Ma (Heermance *et al.* 2007).

5.5 Flexural Modelling

The temporal and spatial distribution of the Cenozoic sedimentary sequence within the NW Tarim Basin is dynamically linked to the growth of the Pamirs and Tien Shan orogenic belts, and the concurrent deflection of the Tarim Craton. Numerical modelling provides a useful tool for analysing these processes and can be used to derive estimates of boundary conditions that are otherwise difficult to obtain, including the flexural rigidity of the craton and the height of the orogenic belts.

5.5.1 Model Setup

A model is developed that assumes the Tarim Craton to be an elastic plate with a uniform flexural rigidity, D, that rests on a viscous substrate. The plate is deformed beneath a spatially and temporally distributed load. The distributed load consists of a series of load blocks that each have a given width, height and density, and includes tectonic loads (orogenic belts) and sedimentary loads (foreland basin fill). At a given distance, x, each load block causes a certain amount of deflection, w_i. Therefore, the total deflection, w, at distance x, is equal to the sum of the deflections produced by individual blocks (Fig. 5.11).

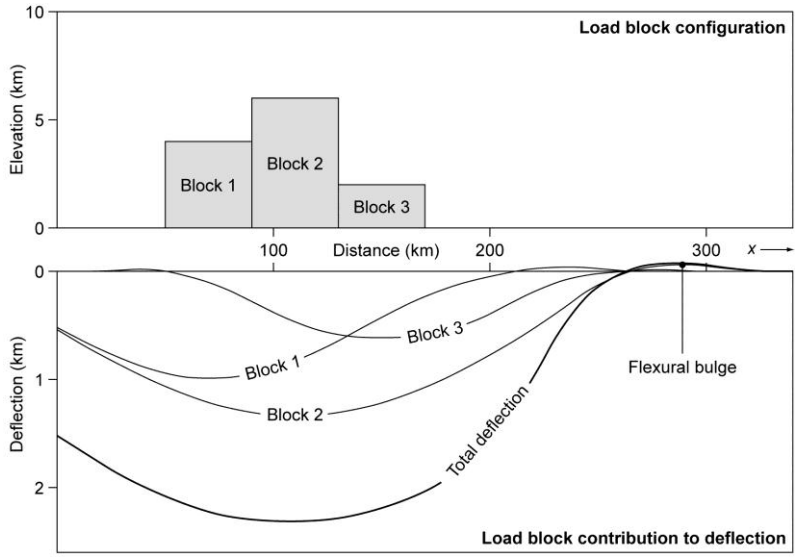

Fig. 5.11. Schematic explanation of the model used in this report. A configuration of load blocks are used to model a distributed tectonic or sedimentary load. The deflection caused by each individual load block contributes to the total deflection of the plate. Modified from Allen & Allen (2005).

A series of equations modified from Hetényi (1979), Jordan (1981) and Allen & Allen (2005) are used in order to calculate the deflection produced by a particular load block, w_i, for different values of x. The equation that is used for a given distance, x, is dependent on the relative position of the load block.

If x is situated under the load block, then:

$$w_i = -\frac{h}{2}\frac{\rho_c}{\rho_m}\left\{\begin{matrix} 2 - \exp[-\lambda(x - s + z)]\cos[\lambda(x - s + z)] \\ -\exp[-\lambda(-x + s + z)]\cos[\lambda(-x + s + z)] \end{matrix}\right\} \tag{5.1}$$

where h is the height of the load, s is the position of the centre of the load, z is the half-width of the load, and λ is the inverse of the flexural parameter ($1/\alpha$), which in turn is defined by:

$$\alpha = \left\{\frac{4D}{\Delta\rho_m g}\right\} \tag{5.2}$$

where D is the flexural rigidity of the deflecting craton. A list of additional parameters that are applied in these models (including ρ_c and ρ_m) are presented in Table 4.1.

Table 5.1. Parameters used in the flexural model.

Parameter	Notation	Value
Young's modulus	E	70 GPa
Poisson's ratio	υ	0.25
Mantle density	ρ_m	3300 kg m^{-3}
Crustal density	ρ_c	2800 kg m^{-3}
Gravitational acceleration	g	9.8 ms^{-2}

If x is situated basinward (i.e. into the foreland) from the load block, then:

$$w_i = -\frac{h}{2}\frac{\rho_c}{\rho_m}\begin{Bmatrix}\exp[-\lambda(x-s+z)]\cos[\lambda(x-s+z)] \\ -\exp[-\lambda(x-s-z)]\cos[\lambda(x-s-z)]\end{Bmatrix} \tag{5.3}$$

If x is situated behind (i.e. to the left in Fig. 5.11) of the load block, then:

$$w_i = -\frac{h}{2}\frac{\rho_c}{\rho_m}\begin{Bmatrix}\exp[-\lambda(-x+s-z)]\cos[\lambda(-x+s-z)] \\ -\exp[-\lambda(-x+s+z)]\cos[\lambda(-x+s+z)]\end{Bmatrix} \tag{5.4}$$

Therefore, the total deflection at a given distance, w_x, is a sum of the individual deflections, w_i, associated with n load blocks:

$$w_x = \sum_{i=1}^{n} w_i \tag{5.5}$$

Information about the height of the sedimentary loads blocks is derived directly from the isopach maps. Likewise, the height of the tectonic load blocks for the latest deflection can be partly constrained by the observed topographic profile. Therefore, unknown parameters such as the flexural rigidity of the Tarim Craton are varied until the modelled deflection and topographic profile most closely matches the observed data.

There are a number of assumptions within this model that may induce errors which should be taken into account when analysing the results. Yong *et al.* (2003) summarised these errors to include spatial and temporal variations in the tectonic loads, lateral changes in the strength (flexural rigidity) of the deforming plate, and the interaction of surface processes.

5.5.2 Model Results

Model 1: Deriving flexural rigidity using instantaneous flexure. Initially, a model is run in order to obtain an estimate of the flexural rigidity (and effective elastic thickness) of the Tarim Craton. The model attempts to achieve the observed deflection of the craton, as determined by the spatial distribution and thickness of the complete Miocene–Pliocene succession. As isopach data is not available for the Xiyu Fm, the most recent stage of foreland evolution cannot be numerically modelled.

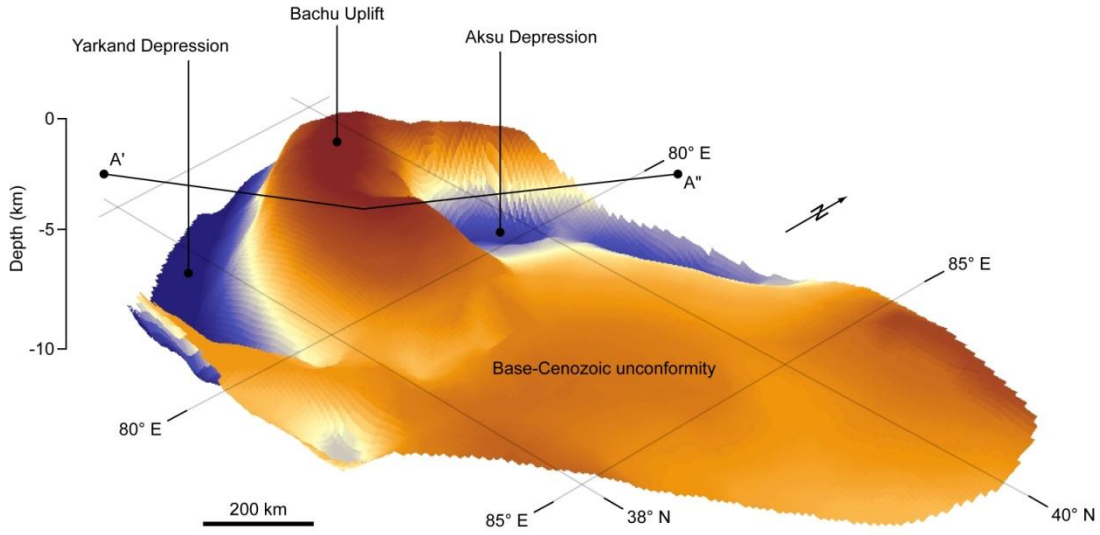

Fig. 5.12. 3D representation of the base-Cenozoic unconformity with the Cenozoic sediment removed. The image was generated by summing the isopach maps for individual stratigraphic intervals using ArcGIS Spatial Analyst. Blue indicates a deep depression, while brown indicates subsurface highs.

By the end of the Pliocene, the foredeep adjacent to the Pamirs (the Yarkand depression) had accumulated 10 km of sediment, while the foredeep adjacent to the Tien Shan (the Aksu depression) had accumulated 8 km of sediment (Fig. 5.12). The sedimentary sequence thins to less than 1 km across the Bachu Uplift. The heights and widths of the sedimentary load blocks were set using these observations. The bulk densities of individual sedimentary load blocks were scaled according to their height.

Where the sediment is thin (< 2 km), the bulk density was estimated to be 2,200 kg m^{-3}. In contrast, where the sediment is thick (> 8 km), bulk densities were increased to 2,600 kg m^{-3}. These values correspond to those used in similar models by Cardozo & Jordan (2001) and Yong *et al.* (2003). The elevation of the orogenic belts and the basin surface is constrained using the present, observed topographic profile, and assumes that this was approximately the same at the end of the Pliocene (c. 1 Ma). The Pamirs and Tien Shan are estimated to have overthrust the Tarim Craton by 200 km and 180 km respectively.

The model was run for a range of flexural rigidity values, from 10^{22}–10^{24} Nm (equivalent to 11–50 km effective elastic thickness), in order to derive the most suitable value that satisfies both the observed sediment thickness and the actual topographic profile (Fig. 5.13). If the Tarim Craton is modelled as a very weak plate (e.g. 10^{22} Nm, line D on Fig. 5.13), the foredeeps attain sufficient depths of 9–10 km adjacent to the Pamirs, and 7–8 km adjacent to the Tien Shan. However, the foredeep depozones are too narrow and the forebulge is too wide, creating a modelled topography that is 0.5–1 km above the observed elevation of the basin surface. In addition, the mountain belts become too low, deviating by up to 2 km below the observed topographic profile. Increasing the height of the tectonic loads only generates foredeeps that are too deep.

In contrast, if the Tarim Craton is modelled as a very strong plate with a high flexural rigidity (e.g. 10^{24} Nm, line A on Fig. 5.13), the foredeeps widen whilst retaining similar depths to those of the weaker plate, creating a narrower and marginally less pronounced forebulge. The modelled topography in the basin is satisfactory, and averages out to a flat surface that approximates to the observed elevation of the Tarim Basin. However, the modelled topography of the orogenic belts exceeds the observed topography by 0.5–1 km. Reducing the height of the tectonic loads only acts to cause a shallowing of the foredeeps, deviating from the observed sediment thicknesses and increasing the elevation of the basin surface.

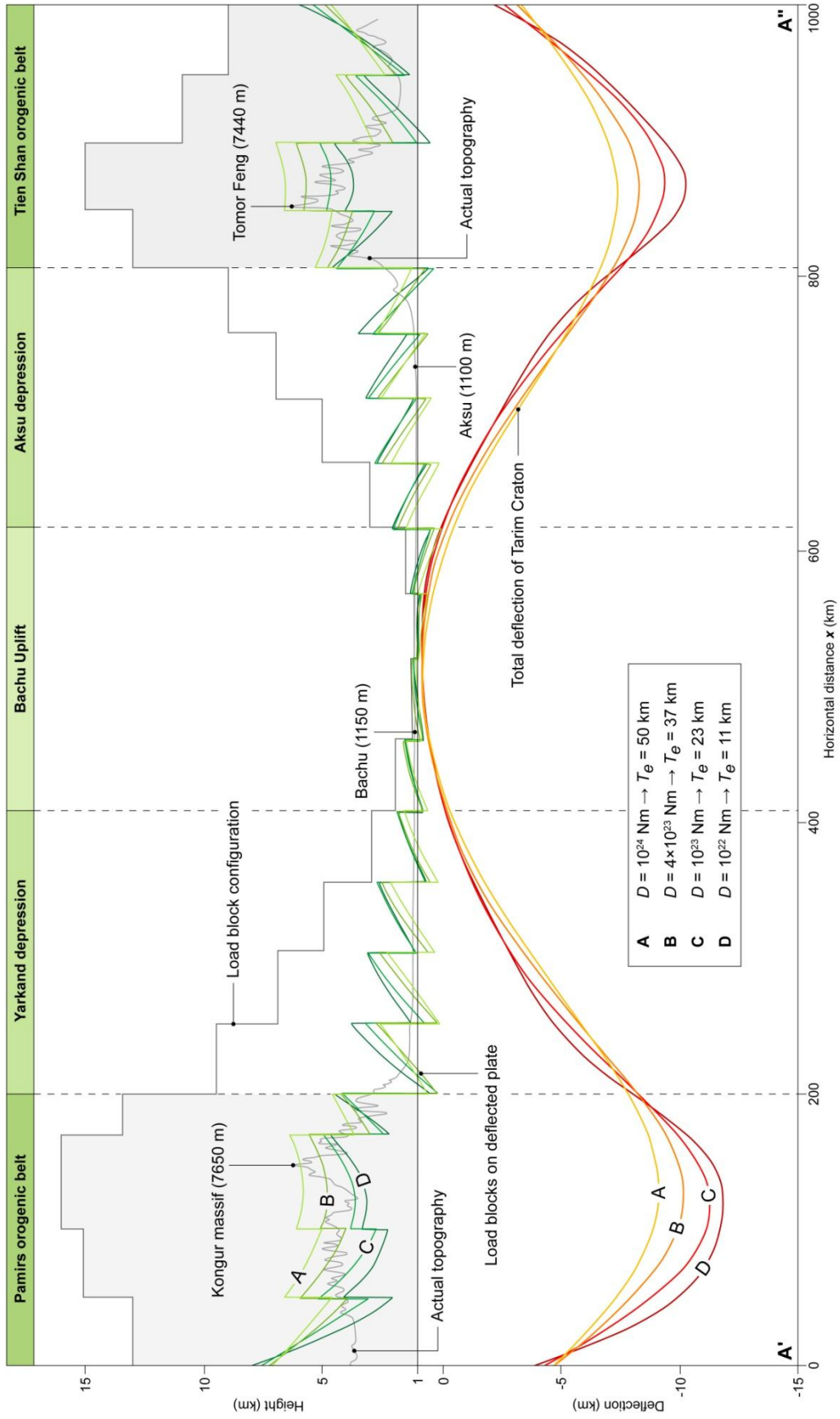

Fig. 5.13. Modelled deflection of the Tarim Craton during the Cenozoic to account for the cumulative Miocene–Pliocene sedimentary succession.

The best-fitting model was obtained using a flexural rigidity of 4×10^{23} Nm, which corresponds to an effective elastic thickness of 37 km. This produces foredeeps adjacent to the Pamirs and Tien Shan that are of similar depths to those generated by weaker and stronger plate models, and a close match to the observed sediment thicknesses. The foredeeps are sufficiently wide that the modelled topography across the basin averages to a flat surface that deviates by <100 m from the observed topographic profile. Similarly, the orogenic belts attain average elevations that are in accordance with the observed topographic profiles across them at present. This value of flexural rigidity corresponds well with previous estimates (e.g. Watts 2001), which predicted the elastic thickness of the Tarim Craton to be c. 40 km, equivalent to a flexural rigidity of $4\text{–}5 \times 10^{23}$ Nm.

Model 2: Progressive orogenic uplift and foreland development. The estimate of flexural rigidity derived in Model 1 can be used to run a further series of models in order to analyse the progressive deflection of the Tarim Craton during the Early Miocene and Middle–Late Miocene intervals. This series of models will also yield information concerning the uplift and growth of the Pamirs and Tien Shan orogenic belts during the earlier phases of foreland evolution.

In this model it is assumed that during the Early Miocene, both the Pamirs and Tien Shan overthrust the Tarim Craton by 100 km, primarily reflecting the pre-Cenozoic setup of the region. According to the isopach maps, subsidence during this period was driven largely by flexure associated with tectonic loading of the Pamirs, producing a foredeep in the western Tarim Basin that reached a depth of 1,800 m and had a width of 250–300 km. The model results (Fig. 5.14A) show that in order to achieve this, the Pamirs should have attained an average elevation of no more than 2,000–3,000 m. In this model, the forebulge was poorly developed, and had minimal subaerial relief. During this period, the Tien Shan produced very little flexural subsidence and had a relief of no more than a few hundred metres. It has been proposed (Abdrakhmatov *et al.* 1996) that the earliest rejuvenation of the Tien Shan occurred at c. 20 Ma, but was only a weakly developed topographic entity until c. 10 Ma, when uplift accelerated substantially. It therefore follows that the Pamirs must have begun to uplift at least 4–5

Myr earlier than the Tien Shan, and that the Keziluoyi and Anjuan formations predominantly comprise sediment that was sourced from the Pamirs.

Both deformation and subsidence increased rapidly in the Middle to Late Miocene. The model assumes that the Pamirs was overthrust c. 50 km further across the Tarim Craton during this time, while the Tien Shan remained in the same position. In order to account for the observed flexural deflection, the Pamirs must have attained a topographic relief of 3–4 km (Fig. 5.14B), while the Tien Shan was uplifted to at least 2 km. The foredeep adjacent to the Pamirs reached maximum depths of 4 km. Contemporaneously, the initiation of a foredeep adjacent to the Tien Shan (the Aksu depression) produced a new site of sediment accumulation, reaching depths of up to 3 km. This suggests that the Middle to Upper Miocene Pakabulake Fm was derived from sediment eroded from both the Pamirs and Tien Shan orogenic belts. The model also demonstrates that the Tien Shan became a prominent topographic feature during this period, which correlates well with the study by Abdrakhmatov *et al.* (1996) that indicated an abrupt acceleration in uplift at c. 10 Ma.

The final stage of foreland evolution (Fig. 5.14C) corresponds to the results derived from Model 1, and shows that both the Pamirs and Tien Shan continued to uplift subsequent to the Late Miocene, attaining elevations that were probably similar to those observed at present. Critically, the Tien Shan appears to have continued to uplift more rapidly than the Pamirs during this period.

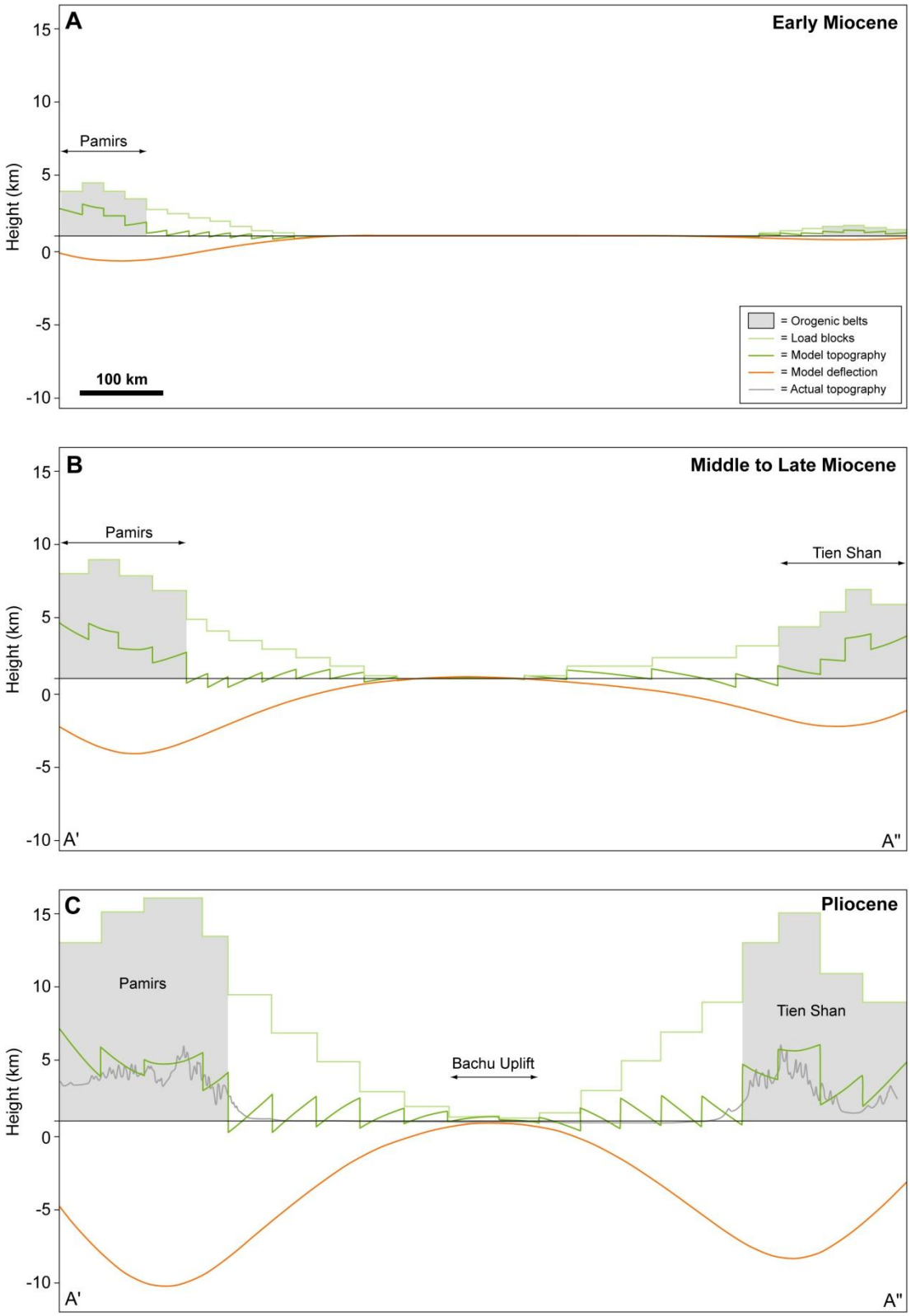

Fig. 5.14. Flexural models showing the progressive deflection of the Tarim Craton beneath the Pamirs and Tien Shan for: (A) Early Miocene, (B) Middle to Late Miocene, and (C) Pliocene. All the models assume a flexural rigidity for the craton of $D = 4 \times 10^{23}$ Nm.

5.6 Bending Stress

Deflection beneath an applied load generates extensional and compressional stresses in the bending plate. These stresses are potentially large enough to create new fractures in the plate or to reactivate ancestral fractures which are suitably orientated. The stress varies through and across the plate depending on how it bends. If a plate is being flexed beneath a tectonic load, the outer arc of the flexed plate will experience a negative (tensile) bending stress (Fig. 5.15), while the lower part of the plate will experience a positive (compressional) bending stress. Half way through the plate, along the neutral surface (at *h/2*), the bending stress will be zero. A model has been developed that allows the bending stress to be estimated across the same transect used for flexural modelling (§5.5). The normal (fibre) stress, σ_{xx} at the **top** of the plate (modified from Watts 2001) is given by:

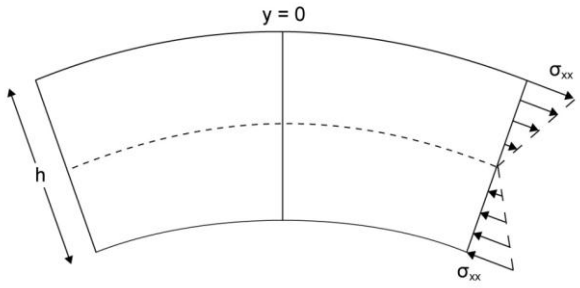

Fig. 5.15. Schematic illustration to show the stresses induced in a bending plate with an effective elastic thickness *h* (modified from Allen & Allen 2005).

$$\sigma_{xx} = -\frac{E}{(1-\upsilon^2)}\frac{2V_0 h}{(\rho_m - \rho_i)g\alpha^3} exp(-x/\alpha)\, sin(x/\alpha) \tag{5.6}$$

where h is the effective elastic thickness of the plate, α is the flexural parameter (see equation 5.2), ρ_i is the density of the sedimentary basin fill, and V_0 is defined by:

$$V_0 = w_0\left(\frac{4D}{\alpha^3}\right) \tag{5.7}$$

where w_0 is the deflection at $x = 0$, i.e. adjacent to the thrust front.

5.6.1 Model Results

Initially this model was used to investigate the effects of varying the flexural rigidity of the craton on the magnitude and distribution of the induced bending stress, using the total sediment accumulation recorded for the Miocene–Pliocene by isopach maps. In this case, the maximum deflection (w_0) at the Main Pamir Thrust (MPT) is 10,000 m and at the South Tien Shan Fault (STSF) is 8,000 m. The results from the model (Fig. 5.16A) show that different flexural rigidities yield not only different amounts of bending stress, but also determine whether or not the bending stress across the surface of the craton is entirely tensional.

If the Tarim Craton is modelled as a very rigid plate (i.e. $D = 10^{24}$ Nm), tensional stresses reach a maximum of -1.3 and -1.0 GPa in the Yarkand and Aksu depressions respectively (Fig. 5.16A). Across the Bachu Uplift, these stresses are reduced to -0.7 to -0.8 GPa. In contrast, if the craton is modelled as a very weak plate (i.e. $D = 10^{22}$ Nm), the tensional stresses increase to a maximum of -2.9 and -2.3 GPa in the Yarkand foredeep and Aksu depression, but the stress adjacent to this, in the forebulge region, becomes compressional (0.1-0.2 GPa). A 50 km-wide zone across the central part of the craton is unaffected by bending stresses. Modelling of the flexural deflection (Fig. 5.13) concluded that the most suitable value of flexural rigidity for the Tarim Craton was c. 4×10^{23} Nm. As can be seen from Fig. 5.15, in this case the bending stresses reach a maximum of -1.5 and -1.3 GPa in the Yarkand foredeep and Aksu depression respectively, and are -0.3 to -0.4 GPa across the region that corresponds to the Bachu Uplift. Compressional stresses are not induced at any point.

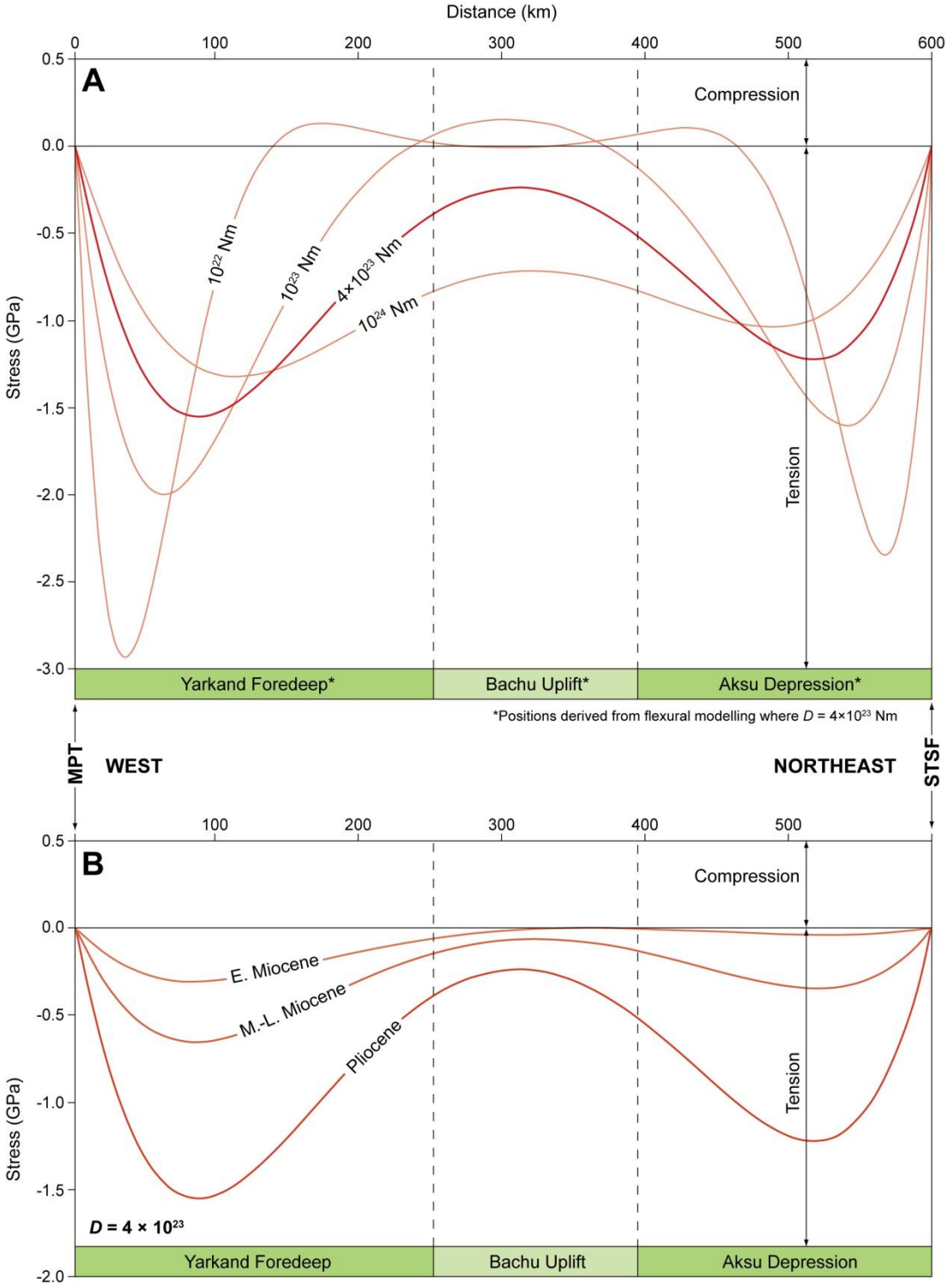

Fig. 5.16. Bending stress across the NW Tarim Basin (transect A'-A" on Fig. 5.1B, excluding orogenic belts) during the Cenozoic. (A) Modelled result for the Pliocene (total Cenozoic sediment accumulation) to evaluate the effect of changes in flexural rigidity. (B) Modelled results for the Early Miocene, Middle to Late Miocene, and Pliocene, showing the progressive change in bending stress during deflection assuming the flexural rigidity is 4×10^{23} Nm. MPT = Main Pamir Thrust, STSF = South Tien Shan Fault.

A second model was run to examine the progressive change in bending stress during the three tectonostratigraphic intervals (Fig. 5.16B). For the purpose of this model, it was assumed that the flexural rigidity of the Tarim Craton was 4×10^{23} Nm, corresponding to the most suitable value derived from the modelling of flexural deflection (Fig. 5.13). For each interval, the values of w_0 were modified according to the isopach maps and values of ρ_i were estimated (2000 kg m^{-3} in the Early Miocene, 2200 kg m^{-3} in the Middle–Late Miocene, and 2400 kg m^{-3} in the Pliocene) in order to reflect the progressive increase in bulk density of the sedimentary load due to compaction. The model predicts that during the Early Miocene, a weak tensional stress (< -0.3 GPa) was induced across the surface of the Tarim Craton that becomes negligible at a distance of c. 300 km from the Main Pamirs Thrust and c. 200 km from the South Tien Shan Fault (Fig. 5.1B). By the Middle–Late Miocene interval, tensional stresses increase in the foredeep areas (-0.4 to -0.6 GPa), but remained relatively low (< -0.1 GPa) across the forebulge region at c. 300 km. During the Pliocene interval, the tensional stress increased substantially, exceeding -1.5 GPa and -1.2 GPa in the Yarkand and Aksu depressions respectively. Across the area that corresponds to the Bachu Uplift, tensional stresses approach -0.5 GPa.

5.7 Discussion

Analysis of the Cenozoic stratigraphy and the flexural deflection of the Tarim Craton yields information concerning the regional tectonic evolution during the Himalayan Orogen. Numerical modelling demonstrates that tectonic subsidence in the NW Tarim Basin during this period was largely driven by flexural deflection beneath the growing tectonic loads of the Pamirs and Tien Shan orogenic belts, as they were rejuvenated from the Early Miocene onwards. The Tarim Craton acted as an elastic plate, which has an estimated flexural rigidity of 4×10^{23} Nm, corresponding to an effective elastic thickness of c. 37 km. The flexural deflection generated a series of elongate foreland basins that became sites of sediment accumulation, resulting in stratigraphic thicknesses locally exceeding 10 km.

The distribution of the Early Miocene Keziluoyi and Anjuan formations (Fig. 5.17) suggests that the Pamirs must have begun to uplift earlier than the Tien Shan. By the end of the Early Miocene, the flexural model suggests that the Pamirs had a mean elevation of 2–3 km. This yields uplift rates of 0.5–0.8 mm yr^{-1} during the Early Miocene, which may relate to rapid uplift that occurred in the Tibetan Plateau at the same time (Copeland *et al.* 1987). The uplift of the Pamirs was sufficient to cause the Tarim Craton to deflect by 1.5–2 km adjacent to the thrust front. The basin was predominantly characterised by arid, shallow lacustrine facies that plausibly represent the underfilled (flysch) stage of foreland basin evolution. Although it is suggested that the Tien Shan began to uplift from c. 20 Ma (Abdrakhmatov *et al.* 1996), the flexural model suggests that it could not have attained a mean elevation of more than a few hundred metres and is unlikely to have become a prominent topographic feature until at least the Middle Miocene. It is therefore unlikely that the Tien Shan was a major source of detritus to the NW Tarim Basin at this time, and that the Lower Miocene sediments were derived almost solely from the Pamirs.

An abrupt and significant increase in the mean elevation of both the Tien Shan and Pamirs occurred during the Middle to Late Miocene, resulting in the onset of significant flexural subsidence in the northern Tarim Basin, and continued flexural subsidence in the western Tarim Basin (Fig. 5.17). This period is characterised by deposition of the floodplain-facies Pakabulake Fm, and possibly represents a transition to the overfilled (molasse) stage of foreland basin evolution. During this period, the Pamirs and Tien Shan attained mean elevations of 3-4 and 2-3 km respectively. A particularly abrupt increase in uplift rates has been constrained to 10-8 Ma (Abdrakhmatov *et al.* 1996; Sun *et al.* 2004). This is reflected in the Pamirs by the onset of orogenic collapse (extension) at 7-8 Ma (Robinson *et al.* 2004) and the formation of NW-striking normal faults that bound a series of exceptionally high summits, including the Kongur Shan (presently 7,649 m) and Muztagh (presently 7,546 m) massifs.

The abrupt uplift of the Pamirs and Tien Shan and the subsequent increase in flexural subsidence in the NW Tarim Basin coincides with a rapid and substantial (> 1 km)

increase in the mean elevation of the Tibetan Plateau at 8 Ma (Molnar *et al.* 1993). This timing was constrained by the onset of extension across the plateau (Harrison *et al.* 1992; Pan & Kidd 1992), which implies that the mean elevations were too high to be supported by the compressive stresses at the plateau margins.

Evidence for this sudden increase in elevation across Central Asia is also provided by an abrupt change in the climate of the northern Indian Ocean at 6-9 Ma, indicated by an increase in the strength of the monsoon (Kroon *et al.* 1991; Prell & Kutzbach 1992). It was also suggested that raising the Tibetan Plateau by more than 1 km during this period was sufficient enough to cause an increase in the horizontal compressive stress and induce folding as far away as the Indo-Australian plate to the south of India (England & Houseman 1992; Molnar *et al.* 1993). If this is the case, it is possible that the transfer of horizontal stress across the rigid Tarim Craton was adequate to result in accelerated uplift of the Tien Shan.

By the Pliocene, the Tien Shan had reached a mean elevation of 3–4 km, causing a total of 8 km of flexural subsidence adjacent to the thrust front. The Pamirs maintained a marginally higher mean elevation of 4–5 km, and had generated a foreland basin more than 10 km deep adjacent to the thrust front. By this time, shortening was being accommodated largely by the development of fold-thrust belts in the foreland to the south of the Tien Shan (Yin *et al.* 1998; Scharer *et al.* 2004; Heermance *et al.* 2008; Chapter 6). Published geodetic measurements taken across the NW Tarim Basin and the Tien Shan mountains indicate that current shortening rates across the foreland fold-thrust belts are up to 8 ($\pm$ 3) mm yr^{-1} (Reigber *et al.* 2001), and represent a substantial component (c. 50%) of the total shortening rate across the entire Tien Shan orogenic belt. Whether the Pamirs and Tien Shan will retain the rapid rates of uplift observed in the Late Cenozoic is uncertain, particularly given that both belts have achieved significantly high mean elevations and that the Pamirs has already been deforming by extensional, topographic collapse for a considerable time (Robinson *et al.* 2004).

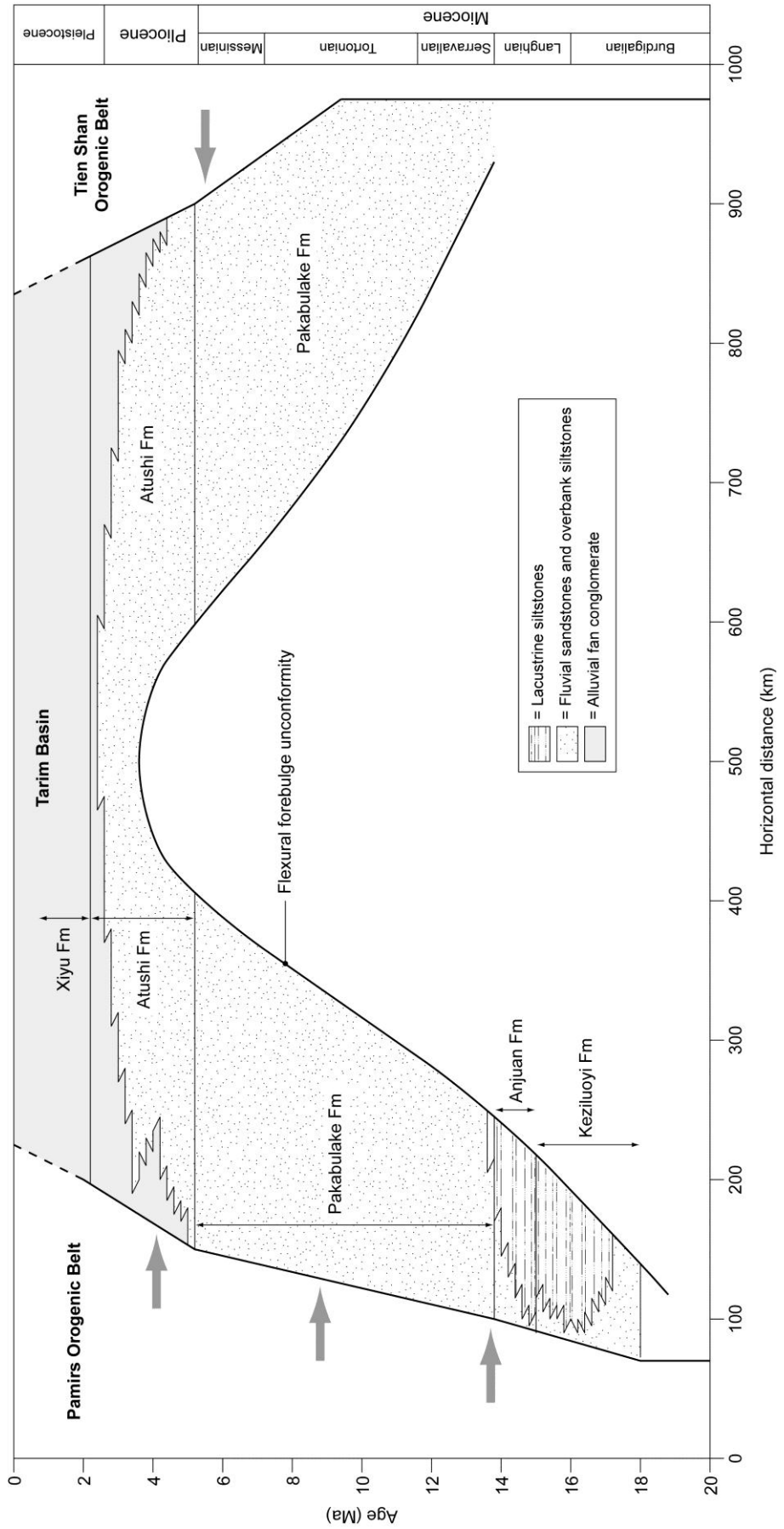

Fig. 5.17. Chronostratigraphy of the NW Tarim Basin during the Middle to Late Cenozoic, based on the results of sedimentary facies analysis and flexural modelling. The framework of this figure is based on a similar representation of foreland basin evolution by Yong *et al.* (2003) for the Longmen Shan.

5.7.1 Inherited Fractures and Forebulge Positioning

The development of extensional faults and fractures in the upper crust of deflected, foredeep regions has been recognised for some time (e.g. Bradley & Kidd 1991). A model of the bending stress imposed on the surface of the Tarim Craton during flexural deflection implies that tensile stresses may have become sufficient enough to generate or reactivate basement fractures across large parts of the basin. During the Middle Miocene to Pliocene, a forebulge associated with flexural deflection on both the western and northern margin of the Tarim Basin was located in a region that corresponds to the Bachu Uplift, a long-lived intrabasinal high that has controlled the distribution of sediment since at least the Early Permian. The Bachu Uplift is bounded on both sides by NW-striking faults, which are subparallel to the Pamirs orogenic belt and the elongate foredeep that has developed adjacent to it. Numerical modelling suggests that the tensional stresses induced on the upper surface of the Tarim Craton by flexural deflection were adequate (i.e. -0.3 GPa) to reactivate the NW-striking fault zones in the forebulge area. Furthermore, it is possible that the presence of inherited, basement fractures may have acted to locally reduce the effective strength of the cratonic surface and could have controlled the position of the forebulge.

5.8 Conclusions

The Cenozoic stratigraphy of the NW Tarim Basin is characterised by a thick, upward-coarsening sequence that records the progressive uplift of the adjacent Pamirs and Tien Shan orogenic belts. Flexural subsidence began in the western Tarim Basin during the Early Miocene, as a response to tectonic loading of the Pamirs. The foreland basin was predominantly filled with lacustrine-facies siltstones and shales that were largely sourced from the Pamirs and are indicative of the underfilled (molasse) stage of foreland evolution. By the Middle to Late Miocene, accelerated deformation across the region resulted in continued uplift of the Pamirs and the initiation of uplift in the Tien Shan. This produced a series of converging foreland basin systems that

shared a common forebulge in the region corresponding to the Bachu Uplift. The foreland basins were filled with coarser, fluvial-facies sandstones and siltstones that indicate the overfilled (molasse) stage of basin evolution. The rapid increase in mean elevations of both the Pamirs and Tien Shan, and the corresponding increase in flexural subsidence in the NW Tarim Basin, is likely to correspond to a regional change in geodynamics that was also responsible for widespread uplift in the Tibetan Plateau. Both the Pamirs and Tien Shan continued to grow significantly into the Pliocene, attaining mean elevations that were probably similar to the present, observed topographic profiles, and continued to deliver sediments to the Tarim Basin that produced an upward-coarsening succession of fluvial-facies siltstones, sandstones and conglomerates. It is estimated that throughout the Cenozoic, the Tarim Craton had a flexural rigidity of 4×10^{23} Nm, which corresponds to an effective elastic thickness of 37 km.

PART TWO

Foreland Fold-Thrust Belts of the NW Tarim Basin

CHAPTER SIX

Late Cenozoic Evolution of the Keping Shan Thrust Belt

Abstract • Lateral structural variability and partitioning of fold-thrust belts often reflects lateral variations in the stratigraphy of the deforming foreland and interaction with inherited structures. The Keping Shan Thrust Belt, NW China, was initiated during the Late Cenozoic and is a spectacular example of contractional deformation in a foreland setting. The belt is characterised by a series of imbricate thrusts which form a broadly arcuate salient and deform the thick (3-6 km) Phanerozoic sedimentary succession of the NW Tarim Basin (SW Tien Shan foreland). Abrupt lateral changes in the thickness of the sedimentary succession are associated with a series of major pre-existing basement faults which cross-cut the belt and which were probably initiated during the Early Permian. These lateral variations in the basin template have impacted strongly on the structural architecture of the superimposed thrust belt. Variations in the thickness of the sediment pile affect the spatial distribution of thrusts, which increase in abundance where the sediment is thinnest. The inherited cross-cutting basement faults and the associated abrupt changes in sediment thickness combine to generate partitioning of the thrust belt.

Publication Details • Turner, S. A., Cosgrove, J. W. & Liu, J. G. 2010. Controls on lateral structural variability along the Keping Shan Thrust Belt, SW Tien Shan Foreland, China. *In:* Goffey, G. P., Craig, J., Needham, T. & Scott, R. (eds) *Hydrocarbons in Contractional Belts*. Geological Society, London, Special Publications, **348**, 71-85.

6.1 Introduction

Lateral structural variability and partitioning within foreland fold-thrust belts is commonly associated with lateral variations in the deforming basin. An increasing number of studies into the evolution of foreland fold-thrust belts have examined the interplay between pre-existing structures, variations in the thickness and rheology of the sediment pile, and lateral differences in the type and thickness of the detachment horizon (e.g. Liu *et al.* 1992; Marshak *et al.* 1992; Lawton *et al.* 1994; Macedo & Marshak 1999; Sepehr & Cosgrove 2004, 2007; Butler *et al.* 2006). Such variations have important consequences on the structural architecture of the fold-thrust belt, causing lateral variations in horizontal shortening, deformation style and the spatial organisation of structures. Furthermore, such lateral variations are often accommodated by the formation of lateral ramps and strike-slip (transfer) faults which are oblique or perpendicular to the general structural trend of the fold-thrust belt. The interplay between the pre-existing basin template and a later fold-thrust belt therefore has important implications for hydrocarbon exploration in compressional belts, causing lateral compartmentalisation of reservoirs and structural complexity.

The Keping Shan Thrust Belt is one of several fold-thrust belt salients which have evolved in the foreland of the SW Tien Shan, NW China, during the Late Cenozoic. The Keping Shan is characterised by a spectacular series of imbricate thrusts which deform a predominantly Palaeozoic sedimentary pile (Fig. 6.1). The thrusts have trends varying from E-W to NE-SW across the belt and broadly form an arcuate salient (Figs. 6.1 & 6.2). The internal structural architecture of the Keping Shan is complex. A series of major strike-slip faults which are oblique or perpendicular to the general trend of the thrusts partition the belt into a series of structural domains, characterised by lateral variations in horizontal shortening and the spatial organisation of structures.

The aim of this chapter is to examine the structural architecture of the Keping Shan Thrust Belt and to identify the underlying causes of lateral (along-strike) structural variability. By examining the pre-existing structure and stratigraphy within the NW

Tarim Basin, relationships between the architecture of the Late Cenozoic thrust belt and the inherited basin template can be examined and assessed in order to provide a new model for the long-term structural evolution of the region. The data used in this study was obtained through satellite image interpretation and field-based mapping. A regional scale geological interpretation map (Fig. 6.1) was developed using Landsat ETM and high-resolution (5×5 metre) SPOT satellite images. These maps were enhanced with structural measurements and observations made at outcrop scale during two field seasons to the Keping Shan. These methods combined provide the basis for analysing the large- and small-scale structure and investigating the stratigraphic framework of the region. The latter yields information concerning inherited structures and lateral variations in the rheology and thickness of the sediment pile, which could prove crucial in unravelling the causes of structural variability in the Keping Shan.

6.2 Geological Setting

The Keping Shan Thrust Belt actively deforms the 3-6 km thick Neoproterozoic-Recent sedimentary succession of the NW Tarim Basin, an area that equates to the foreland of the SW Tien Shan (Fig. 6.1). The sedimentary succession records the complex and protracted history of the Tarim Basin, which began in the Neoproterozoic. At this time, the underlying Tarim Craton rifted from Australia during a widespread rifting event (Li & Powell 2001; Chen *et al.* 2004). Subsequently, the Tarim Craton accumulated a thick passive margin succession prior to collision with the developing Eurasian margin during the Late Devonian to Early Carboniferous (Carroll *et al.* 1995, 2001). The collision resulted in the formation of the Tien Shan orogenic belt (Burrett 1974; Burtman 1975; Coleman 1989; Jun *et al.* 1998) and sedimentation within the NW Tarim Basin occurred in a foreland setting (Carroll *et al.* 1995). A short but important phase of extension occurred in the Early Permian (~275 Ma, Zhang *et al.* 2008) which was associated with magmatic activity and the generation of major normal faults, which impacted on the thickness of the sedimentary succession across the region. As a result, the NW Tarim Basin remained an intrabasinal high throughout the Mesozoic and did not receive any sediment

during this period (Li *et al.* 1996). Thick Mesozoic successions are recorded in two isolated depocentres in the western and eastern Tarim Basin, recording a series of smaller collisions at the southern margins of the growing Eurasian continent during the formation of the Tibetan collage (Watson *et al.* 1987; Hendrix *et al.* 1992; Sobel 1999). The collision of India and Eurasia in the Early Cenozoic marked the onset of renewed contraction across Central Asia. Ancestral mountain belts including the Tien Shan were reactivated and rejuvenated, shedding large quantities of sediment into the Tarim Basin. Flexure at the margins of the basin resulted in accumulations of Paleogene–Neogene sediments which locally exceed 10,000 metres (Bally *et al.* 1986; Yang & Liu 2002). Reactivation of the Tien Shan did not begin until ~20 Ma, and has accelerated since ~10 Ma (Abdrakhmatov *et al.* 1996; Sun *et al.* 2004). During this time the belt has accommodated around ~200 (± 50) km of crustal shortening (Avouac *et al.* 1993; Abdrakhmatov *et al.* 1996). The initiation of folding and thrusting within the SW Tien Shan foreland (NW Tarim Basin) probably began during or shortly after this time (?10–5 Ma). Seismicity along the boundary zone between the Tarim Basin and the Tien Shan indicates that folding and thrusting is presently active (USGS 2009), while geodetic (GPS) measurements suggest shortening rates of 8 (± 3) mm yr^{-1} across the Keping Shan and adjacent Kashgar Fold Belt. This corresponds to approximately 40% of the total shortening rate across the whole Tien Shan belt (Reigber *et al.* 2001) and serves to demonstrate the importance of foreland fold–thrust belts in accommodating crustal shortening across orogenic belts.

Fig. 6.1. *(next page)* Geological map of the Keping Shan Thrust Belt showing the master structural elements described in this chapter. Belt-parallel faults are characterised by E–W to NE–SW trending thrust faults that define a broad, arcuate thrust belt. The belt is partitioned by a series of belt-oblique (strike-slip and oblique-slip) faults that predominantly trend NW–SE. The northern margin of the Keping Shan Thrust Belt is defined by the South Tien Shan Fault, which separates the metamorphic rocks of the Tien Shan from the sedimentary rocks of the Tarim Basin.

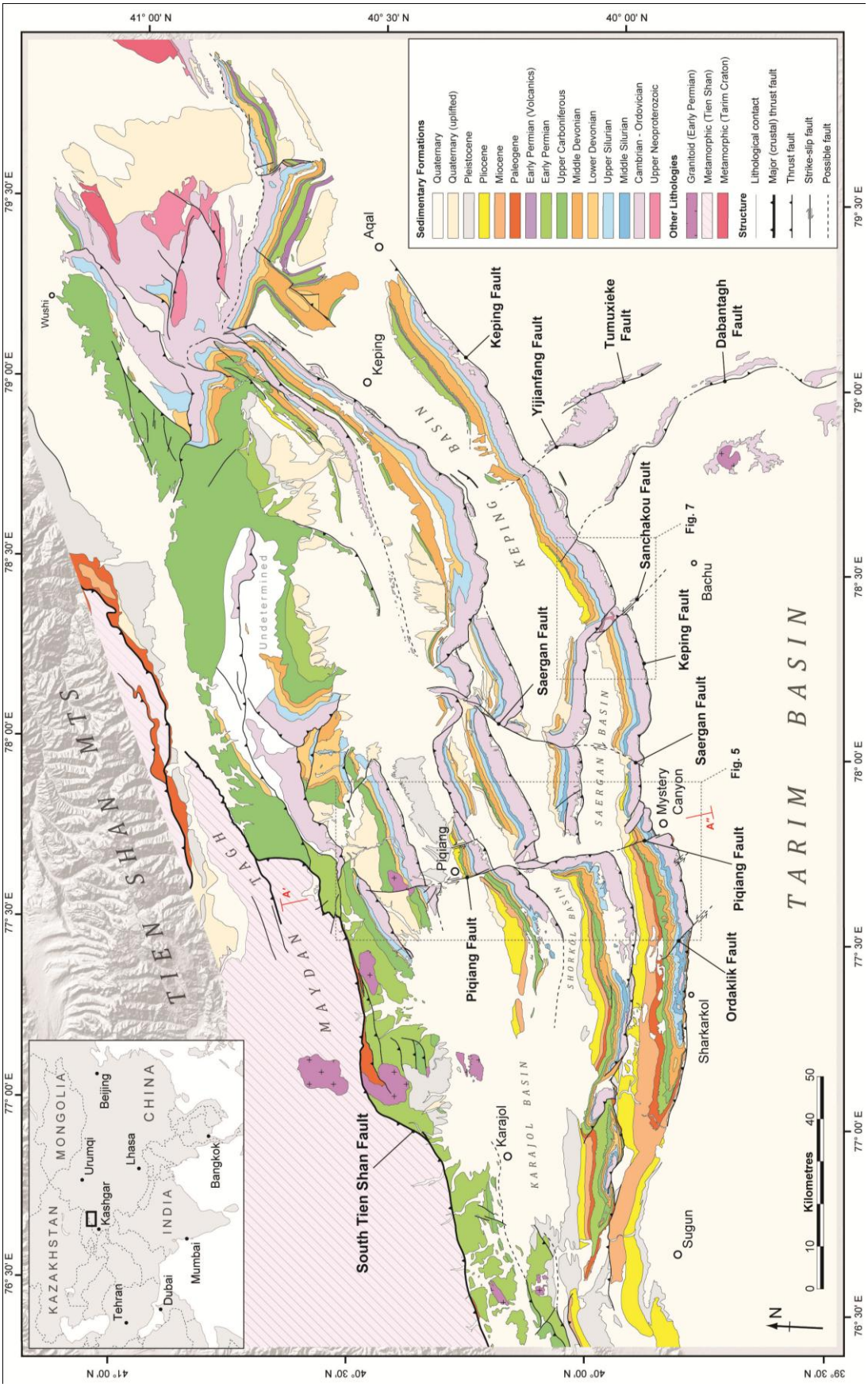

Fig. 6.1 – *Figure caption on previous page.*

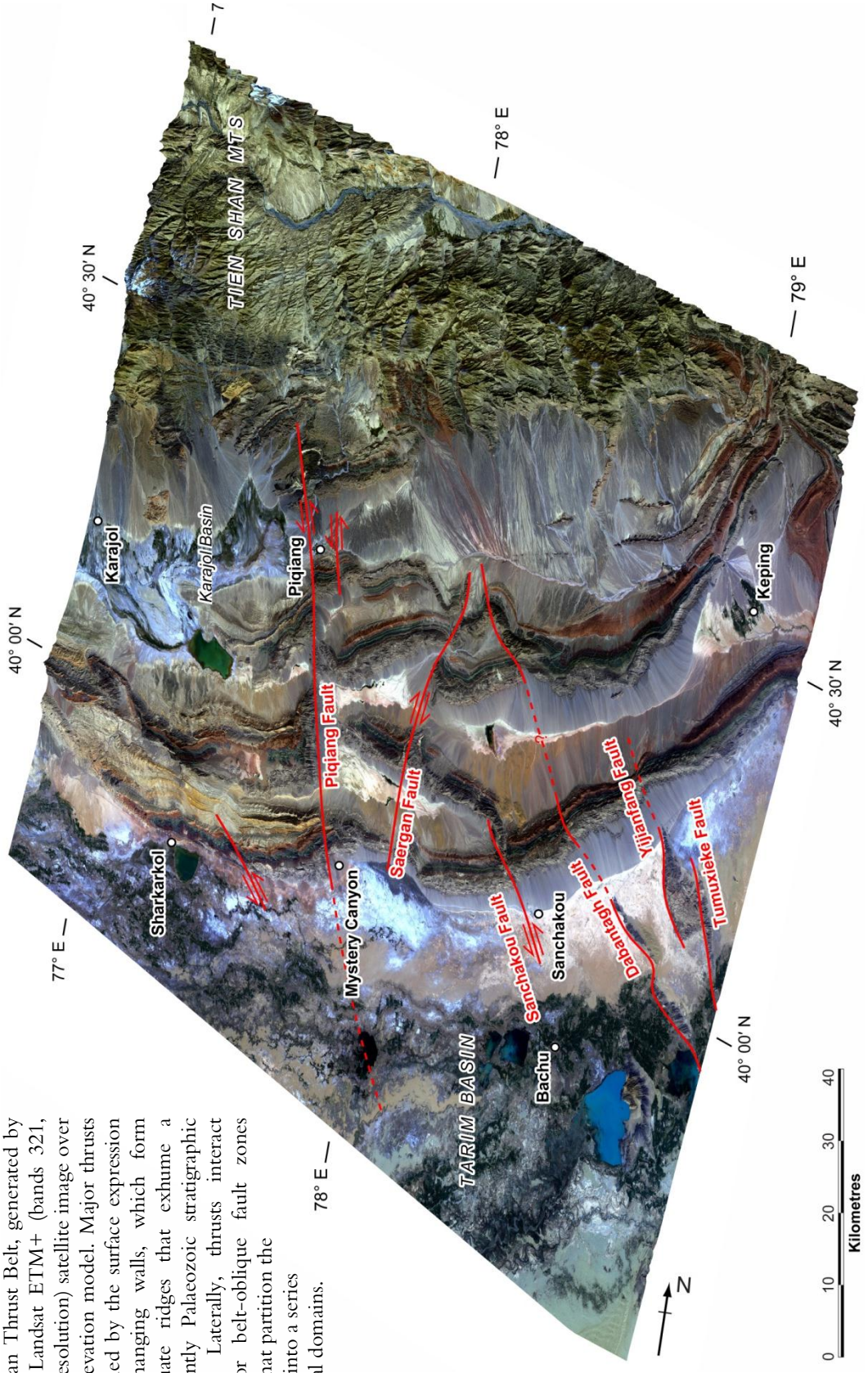

Fig. 6.2. 3D perspective view of the Keping Shan Thrust Belt, generated by draping a Landsat ETM+ (bands 321, 30 metre resolution) satellite image over a digital elevation model. Major thrusts are identified by the surface expression of their hanging walls, which form long, arcuate ridges that exhume a predominantly Palaeozoic stratigraphic succession. Laterally, thrusts interact with major belt-oblique fault zones (marked) that partition the thrust belt into a series of structural domains.

6.3 Structure of the Keping Shan Thrust Belt

The morphology of the Keping Shan is characterised by major fault zones which were generated (or reactivated) during contraction in the Late Cenozoic (Yin *et al.* 1998; Allen *et al.* 1999). Following the format of Sepehr & Cosgrove (2007), these fault zones are categorised for the purpose of this study according to structural trends. Major fault zones within the Keping Shan can be broadly divided into two categories: (1) belt-parallel fault zones; (2) belt-oblique fault zones (Fig. 6.2).

6.3.1 Belt-Parallel Fault Zones

Belt-parallel fault zones comprise NE-SW to E-W trending faults which are parallel to the trend of the Tien Shan orogenic belt (Figs. 6.1–6.3). Without exception, all the fault zones in this category are thrusts, which predominantly verge to the south towards the interior of the Tarim Basin. Allen *et al.* (1999) proposed that the thrusts detach onto a thin Upper Cambrian salt horizon. Palaeozoic and Cenozoic strata of the basin are exhumed in the hanging walls of the thrusts, forming topographically prominent ridges which rise up to 1,200 metres high relative to the piggy-back basins which have developed between thrusts. These basins are narrow (6 - 15 km in width), internally draining, and filled with Quaternary sediments.

The general strike of the thrusts varies across the Keping Shan, giving the belt an overall arcuate salient geometry (Figs. 6.1 & 6.2). Thrust trends vary from NE-SW in the east to E-W in the west. The eastern end of the Keping Shan tapers into a 50 km-wide recess which we have termed the Aksu Re-entrant. To the west, there is a gradual transition from the Keping Shan Thrust Belt into the Kashgar Fold Belt (Fig. 6.1). In contrast to the Keping Shan, the Kashgar Fold Belt is dominated by simple detachment folds which only affect Cenozoic strata and there is little surface expression of thrusts (Scharer *et al.* 2004).

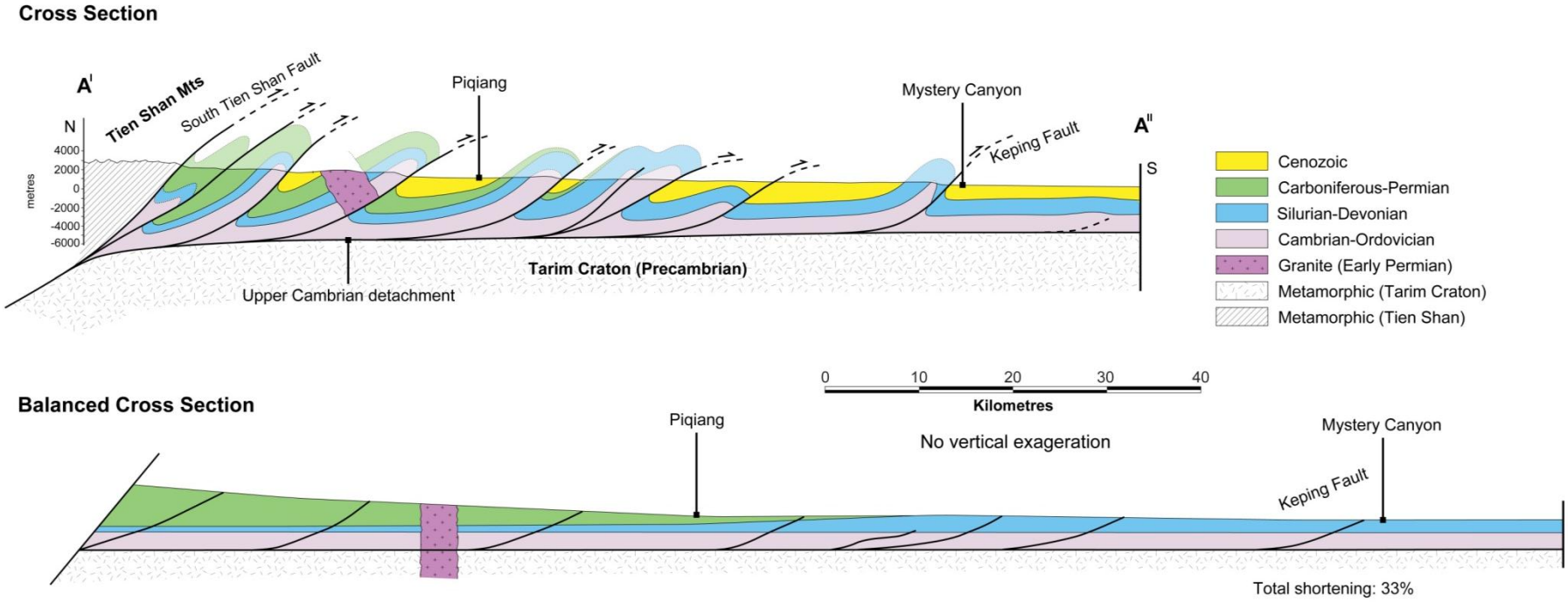

Fig. 6.3. Balanced cross section across the Keping Shan (A′ – A″, see Fig. 6.1 for line of section). Major thrusts detach onto a Middle Cambrian evaporite surface (sensu Allen et al., 1999), predominantly dipping to the north and verging to the south. Once balanced, the horizontal shortening across the section is 33%. This section assumes that deformation is completely thin-skinned but in the absence of sub-surface data we cannot determine whether basement faults are involved.

South Tien Shan Fault. This fault acts as the major bounding fault which separates metamorphic rocks of the Tien Shan from the sedimentary cover succession of the Tarim Basin to the south (Fig. 6.1). Cenozoic activity on the fault and related exhumation of the Tien Shan mountains began around 24 Ma, at the Oligocene-Miocene boundary (Sobel & Dumitru 1997). The fault is a steep (40-50º) north-dipping thrust that trends ENE-WSW. Within the metamorphic mica-schists immediately north of the fault, there is an abundance of shear structures and minor folds, which have E-W trending fold axes and axial planes that dip 50-60° to the north (Fig. 6.4a). These features are attributed to intense ductile deformation associated with the fault zone. The fault juxtaposes the metamorphic rocks against the Phanerozoic sedimentary cover succession of the Tarim Basin. It is therefore assumed that the South Tien Shan fault zone continues to substantial depth (c. 20-30 km), acting to allow the Tarim Block to be underthrust beneath the Tien Shan.

Keping (Frontal) Fault. This fault separates the present alluvial Tarim Basin from the Keping Shan. It is the most southerly of the belt-parallel thrusts and has the most topographically prominent hanging wall (Figs. 6.1, 6.2). In addition, it is the most seismically active of all the belt-parallel faults, with focal mechanism solutions indicating relatively pure thrust displacement (USGS 2009). These seismogenic and geomorphic attributes suggest that the Keping Fault is the youngest belt-parallel fault and that each respective thrust to the north is progressively older, and that the thrust belt has largely evolved as a simple foreland-directed (piggy-back) series (Dahlstrom 1970; Butler 1982). Along much of its length, cliff-forming Cambrian-Ordovician limestones which dip gently to the north define the base of the thrust hanging wall. Only in a few localities are the remnants of fault-related folding preserved, but it is postulated that folds of similar form were once continuous along the mountain front (Fig. 6.3). The southern limbs of these folds are steeply dipping and often overturned, while the northern limbs dip between 20-40º. Where present, the cores of fault-related folds are characterised by internal deformation, and minor thrusts and folds are abundant (Figs. 6.4c-e). Minor folds have axes which are subparallel to the local trend of the Keping Fault.

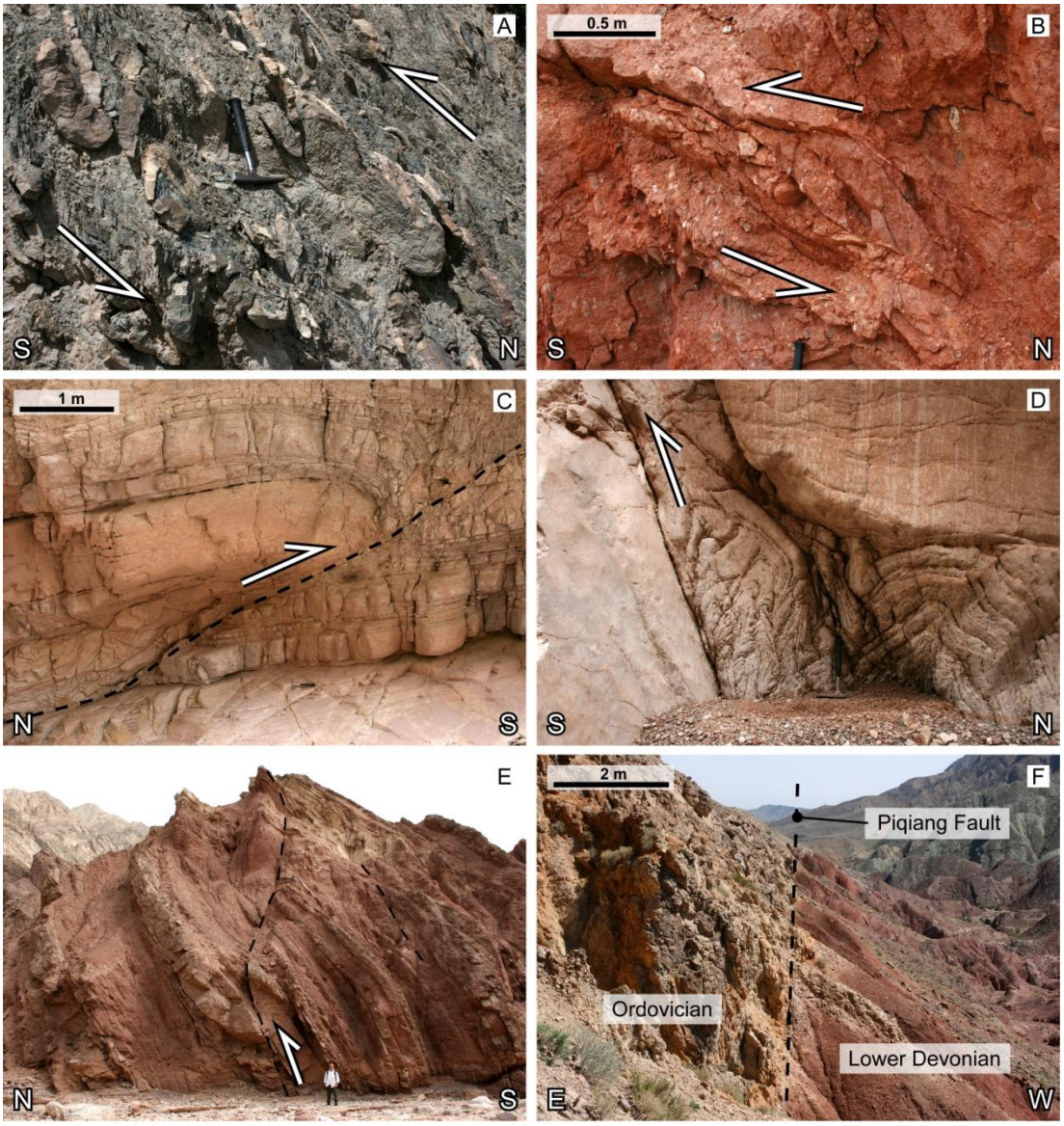

Fig. 6.4. Field photographs illustrating aspects of structural deformation in the Keping Shan: (a) Minor folding of interbedded quartzites and schists within the shear zone of the South Tien Shan Fault, (b) South-verging thrust duplex in Paleogene conglomerate immediately south of the South Tien Shan Fault; (c, d) Deformation within Ordovician limestones in the Mystery Canyon, in the hanging wall of the Keping Fault, showing a south-verging thrust and intense deformation above a minor thrust respectively; (e) North-verging back-thrust in the southern limb of a thrust-related anticline above the Keping Fault; (f) Middle Devonian red sandstones juxtaposed against Middle Ordovician limestones along the northern segment of the Piqiang Fault, near Piqiang.

6.3.2 Belt-Oblique (Cross) Fault Zones

Major fault zones which are oblique (by >45º) or perpendicular to the general trend of the Keping Shan are termed 'belt-oblique' and comprise oblique-slip and strike-slip (transfer) faults. Several of these faults have a prominent surface expression, whilst others are more subtle. In either case, belt-oblique faults have an important role in partitioning the thrust belt into a series of structural domains which are characterised by variations in the spatial distribution of belt-parallel thrusts. The initial formation of these faults predates the Late Cenozoic evolution of the Keping Shan Thrust Belt. A 280 km stratigraphic correlation panel was constructed by measuring the thickness of the sedimentary pile at nine sections along the hanging wall of the Keping Fault (Fig. 6.5). When hung from the base Cenozoic unconformity, the correlation panel demonstrates the impact of the inherited faults on the thickness of the sediment pile during an earlier phase of tectonism in the Tarim Basin. Although the event responsible for the inherited faults remains the subject of debate, it is likely that they formed during a brief phase of extension that affected the NW Tarim Basin during the Early Permian. This period was characterised by substantial basaltic magmatism, resulting in the emplacement of NW-SE trending dykes and extrusive basalt flows within the Lower Permian stratigraphic succession. The basalts yield ages of 274 ± 2 Ma (Zhang *et al.* 2008). Analysis of borehole data from the interior of the Tarim Basin has revealed that the basalts cover a total area of around 250,000 km^2 and are thought to have been caused by a short-lived mantle plume in the Early Permian (Zhang *et al.* 2008; Jia *et al.* 2004; Jiang *et al.* 2004). Incidentally, the area in which the sediment pile is thinnest in the Keping Shan (Fig. 6.5) – across a structure known as the Bachu Uplift – correlates to an area proposed to represent the source region of the Early Permian basalts which flooded much of the Tarim Basin (Zhang *et al.* 2008). Furthermore, Chen *et al.* (2006) identify this region as the central part of a much larger area affected by substantial crustal doming from the Late Cisuralian to the Guadalupian (~270-260 Ma). An alternative possibility is that the inherited faults relate to a later transtensional event which affected the NW Tarim Basin during the Jurassic (Sobel 1999; pers. comm., J. Suppe). Tectonism during this period was characterised by NW-SE trending strike-slip faults which formed deep and narrow transtensional basins in the western Tarim Basin (Sobel 1999).

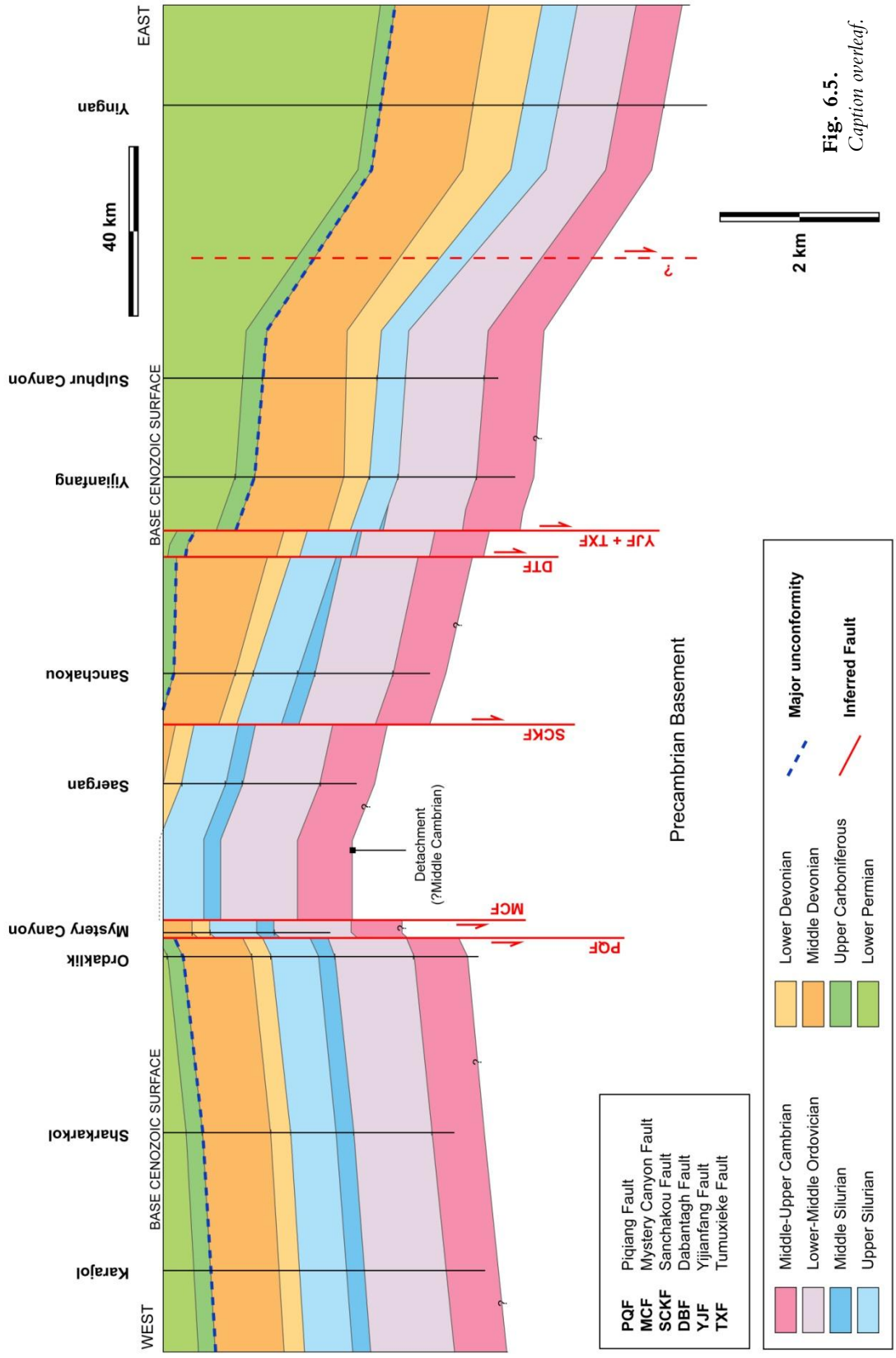

Fig. 6.5.
Caption overleaf.

A complete absence of Mesozoic sediments within the Keping Shan means that it remains speculative as to which event was responsible for the formation of the inherited faults, although we maintain that Early Permian extension was the most likely cause. In either case, given that the Keping Shan remained an intrabasinal high throughout the Mesozoic (Li *et al.* 1996) it is likely that a substantial amount of erosion occurred across individual fault blocks and the Bachu Uplift prior to the Early Cenozoic, accounting for the substantially reduced thickness of Palaeozoic strata over the central parts of the Keping Shan.

Piqiang Fault. This fault is expressed for more than 70 km as a prominent structural lineament that has a dramatic effect on the structural architecture of the Keping Shan Thrust Belt (Figs. 6.1, 6.2 & 6.6). The fault trends ~NNW–SSE (340–350º) and is defined by a series of segments which either offset or completely decouple the E–W trending belt-parallel thrusts to either side, thereby acting to partition the thrust belt. The trend of the fault is subparallel to the SSE-oriented thrust transport direction. Examination of the individual segments of the Piqiang Fault reveals that the faulting mechanism changes along strike at c. 20–25 km intervals, locally acting as either a strike-slip fault or as a lateral ramp. In plan view, the Piqiang Fault has an impact on the spatial organisation of the belt-parallel thrusts to either side of it, expressed as a change in the number and spacing of thrusts from west to east (Fig. 6.6). To the west, there are three major thrusts (with surface expression), one of which terminates against the Piqiang Fault as a lateral ramp. To the east, there are five major thrusts which are more closely spaced, creating narrower piggy-back basins. The greater abundance of thrusts to the east implies that the total horizontal shortening to the east of the Piqiang Fault is marginally greater than to the west.

Fig. 6.5. *(previous page)* Stratigraphic correlation panel across a series of measured sections taken from the hanging wall of the Keping Fault and restored to the base-Cenozoic unconformity. Major faults across which the sediment thickness changes abruptly were interpreted from the surface expression of structural lineaments (c.f. Fig. 6.1). There is a dramatic thinning of the Palaeozoic sediment pile across the central part of the Keping Shan, an area referred to as the Bachu Uplift. The depth to the Middle Cambrian detachment layer varies from more than 6 km to just over 2 km between the Piqiang and Sanchakou Faults. Much of the thickness change occurs in the Lower Permian succession, but further work is required to determine whether this is a syntectonic feature. An additional major fault is proposed for the west, between the Sulphur Canyon and Yingan sections, where sediment thickness increases substantially despite a lack of belt-oblique structures with surface expression in this area.

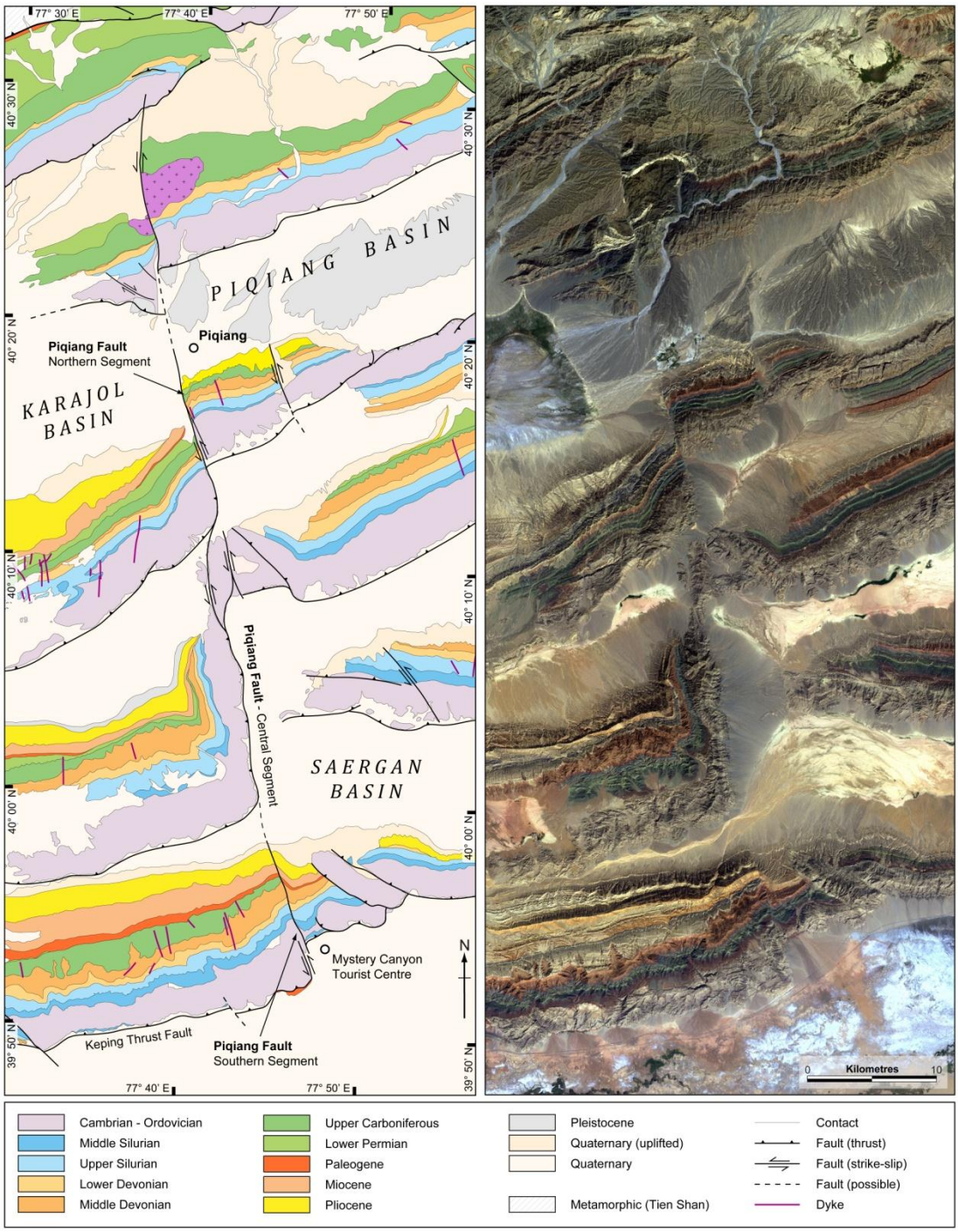

Fig. 6.6. Structure of the Piqiang Fault: (a) Geological map derived from the interpretation of (b), Landsat ETM+ (bands 321, 30 metre resolution) satellite image. Along strike, the faulting mechanism appears to change, acting either as a strike-slip fault (southern and northern segments) or as a lateral ramp (central segment).

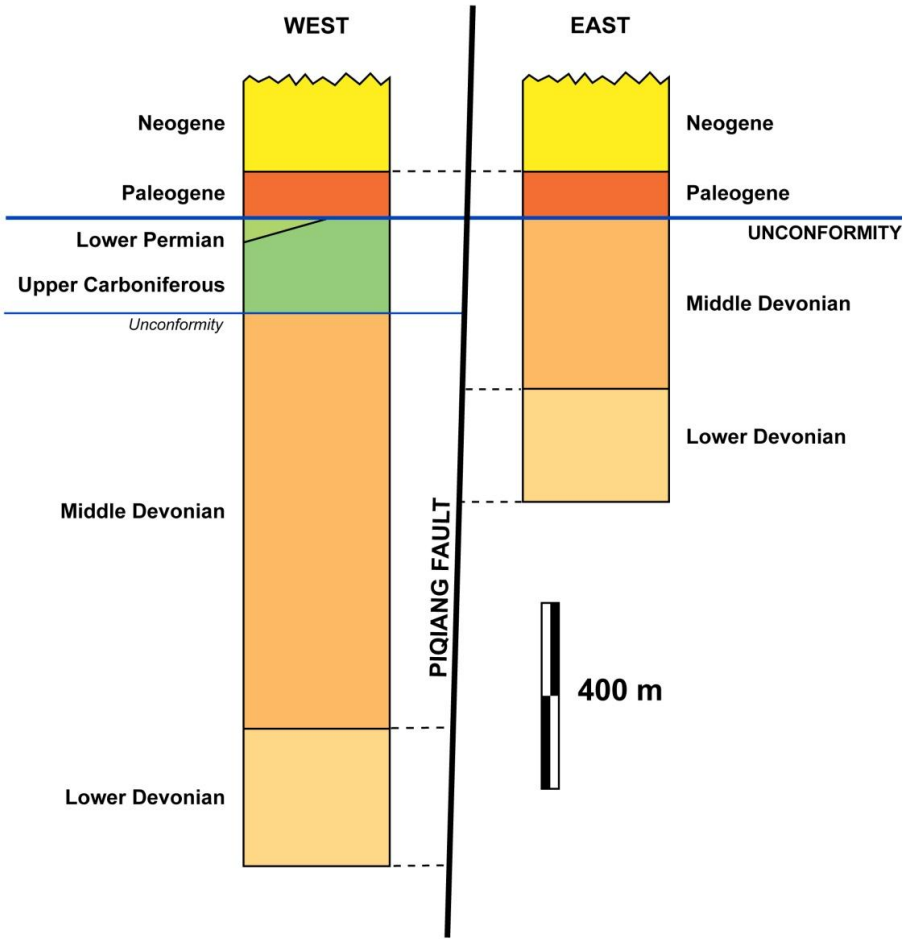

Fig. 6.7. Stratigraphic correlation across the Piqiang Fault, showing the net loss of nearly 800 metres of Middle Devonian, Upper Carboniferous and Lower Permian strata from west to east, and the unaffected Paleogene–Neogene strata above the base-Cenozoic unconformity.

Examination of the stratigraphy across the fault zone indicates that there is a net loss from west to east (Fig. 6.7). To both the east and west of the fault, the Palaeozoic megasequences are separated from the Cenozoic megasequence by a major unconformity which spans the Mesozoic. The anomaly lies in the age of the youngest Palaeozoic strata on the eastern and western sides of the Piqiang Fault. To the east, the unconformity separates the Middle Devonian from the Paleogene, while to the west, it separates the Lower Permian from the Paleogene (Fig. 6.7). The Upper Carboniferous and Lower Permian sediments that are absent from the eastern side of the fault are shallow marine to fluvial carbonates and sandstones which were deposited in the Late Carboniferous foreland basin that developed adjacent to the ancestral Tien

Shan (Carroll *et al.* 1995). On both sides of the fault, Paleogene sediments are interbedded fluvial sandstones and mudstones which maintain the same thickness across the fault suggesting they were deposited onto a flat, peneplain surface in the Early Cenozoic. In total, we estimate that ~800 metres of sediment is absent from the eastern side of the Piqiang Fault.

Saergan Fault. Similar to the Piqiang Fault, the Saergan Fault is a prominent structure which cross-cuts belt-parallel thrusts (Figs. 6.1 & 6.2). It can be traced for ~40 km across the belt, and acts as a major right-lateral strike-slip fault. Unlike the other faults described in this section, however, there appears to be little or no stratigraphic discontinuity across it. In addition, the orientation of the fault is notably different from other belt-oblique fault zones, which generally follow trends of NW-SE to N-S. This suggests that unlike many other belt-oblique faults, the Saergan Fault formed during the Late Cenozoic evolution of the Keping Shan and was not part of the Early Permian fault population. The fault may act to accommodate lateral changes in horizontal shortening which are not suitably attained through other reactivated belt-oblique structures, but this will require a further, detailed study of the structure.

Sanchakou Fault. This fault zone has little surface expression but correlates to an important change in sediment thickness and causes localised disruption to the Keping Fault. The surface expression of the fault crops out in the village of Sanchakou, to the south of the Keping Fault. Tracing the fault to the north, the fault interacts with the Keping Fault and causes it to branch into two faults to the west (Fig. 6.8). Based on the stratigraphic correlation across the fault (Fig. 6.5), the net loss of stratigraphy is 500-550 metres from east to west. Most of the stratigraphic loss occurs within the Middle Devonian, and only a few kilometres to the west a progressive thickening of Upper Carboniferous strata is observed in what would have been the original down-thrown block. The interaction of the Sanchakou and Keping Faults is characterised by a zone of structural complexity in which Upper Neoproterozoic to Lower Cambrian sediments are exposed (Fig. 6.8). These are the oldest sediments within the central part of the Keping Shan, and they have been exhumed from beneath the Middle Cambrian detachment layer.

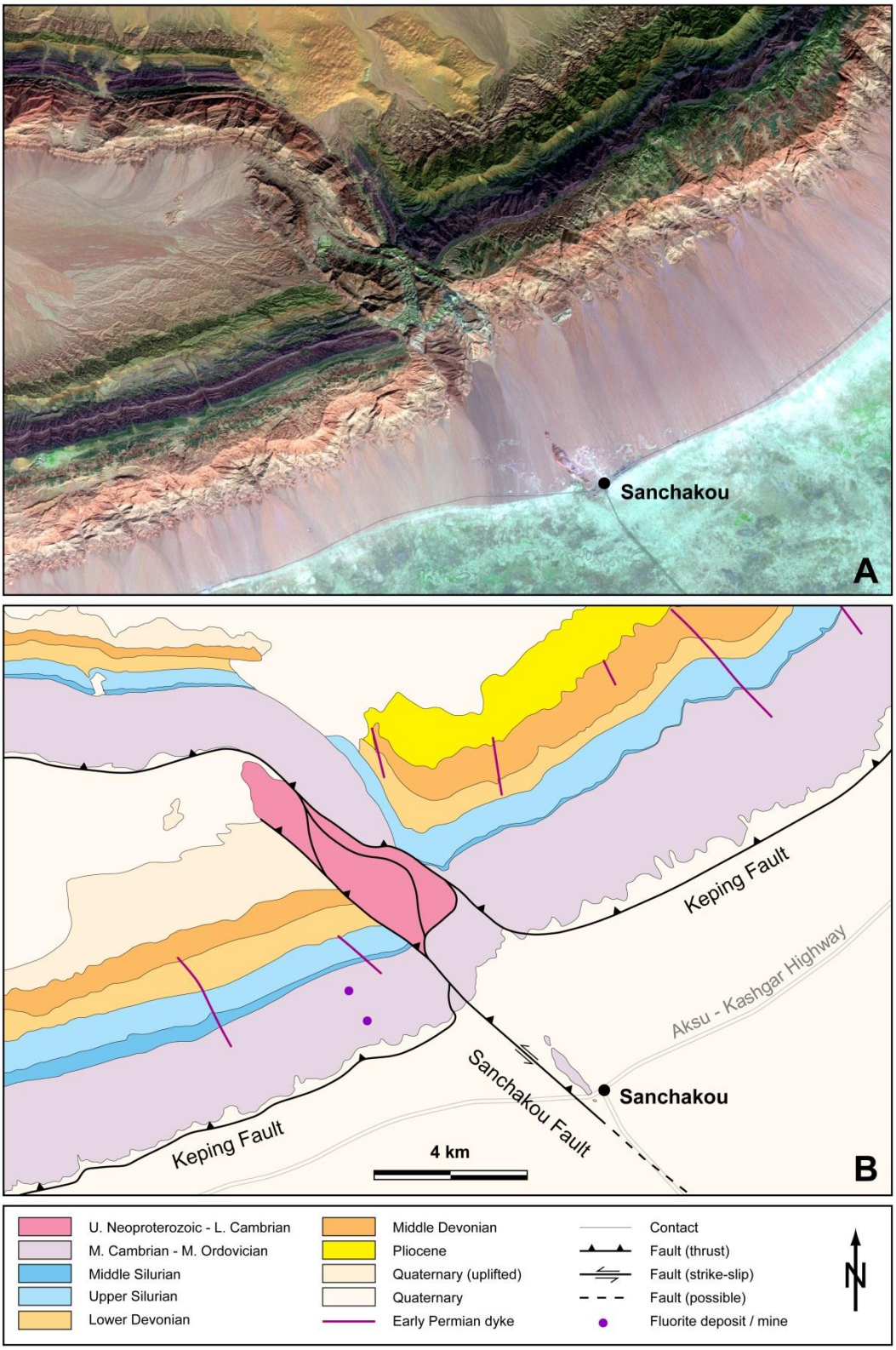

Fig. 6.8. Structure of the Sanchakou Fault: (a) SPOT-5 (bands 431, 5 metre resolution) false colour satellite image; (b) Geological map based on the interpretation of (a). The Middle Devonian thickens abruptly across the Sanchakou Fault. On interacting with the Sanchakou Fault, the Keping Fault branches across a zone of structural complexity in which Late Neoproterozoic sediments are exhumed from beneath the Middle Cambrian detachment layer.

Yijianfang Fault. The surface expression of the Yijianfang Fault is prominent within the Tarim Basin to the south of the Keping Shan, representing one of the few structural features that penetrate the present-day basin surface. The interaction with the Keping Shan is less obvious, but tracing the fault zone to the north it is apparent that it interacts with the Keping Fault and causes a kink in the NE-SW trend of it (Fig. 6.1). In addition, the structural dip of beds within the hanging walls of belt-parallel thrusts are substantially reduced for several kilometres eastward, from the average 35° dip values recorded across much of the Keping Shan to ~25°. Across the Yijianfang Fault, the change in stratigraphic thickness is ~500 metres and is most prominently demonstrated by the substantial increase in the thickness of Lower Permian sediments to the east (Fig. 6.5).

6.4 Discussion

Lateral variations in the structural architecture and partitioning of the Keping Shan Thrust Belt correlates with major lineaments and fault zones which are oblique or perpendicular to the general structural trend of the thrust belt. These fault zones predate the Late Cenozoic thrusting and previously acted as basin bounding faults which controlled the thickness of the sediment pile.

Partitioning of the belt correlates directly with changes in the total thickness of the sediment pile above the Middle Cambrian basalt detachment surface. These changes occur across major belt-oblique faults, which as noted above suggests they were active prior to thrusting. Plausibly, these faults were generated during an extensional phase associated with a mantle plume in the Early Permian (Zhang *et al.* 2008) or during a transtensional phase in the Jurassic (Sobel 1999).

Studies from other fold-thrust belts and analogue experiments have demonstrated the impact of sediment thickness on the structural architecture of superimposed compressional structures. Liu *et al.* (1992) show that in analogue sandbox experiments,

thicker sediment piles produce thrust systems in which major thrusts are widely spaced, creating wider piggy-back basins. Conversely, thinner sediment piles deform as a series of more closely spaced thrusts separated by narrower piggy-back basins (Fig. 6.9a). This arises because when a sediment pile is thick, fewer thrusts are required to attain the topography that satisfies the critical angle within the deforming wedge, than when the sediment pile is thin. When applied to the Keping Shan, this theory certainly seems to be applicable. The impact is best explored across the Piqiang Fault, the most prominent belt-oblique structure which causes substantial lateral discontinuity between the thrusts to either side and acts to partition two parts of the thrust belt. The sediment pile to the west of the Piqiang Fault is ~4 km thick, while to the east it is ~2 km thick. This is expressed in the deforming sediment pile as fewer thrusts to the west, and a greater number to the east (Fig. 6.9a). Furthermore, given that the Piqiang Fault was a pre-existing structure over which this stratigraphic discontinuity occurs, it provides an ideal plane of weakness that can be reactivated as a strike-slip (transfer) fault which effectively decouples the thrust belt to either side of it, accommodating the abrupt lateral change in horizontal shortening and spatial organisation of structures.

Where the change in sediment thickness appears to be less substantial, it follows that the lateral variation in the thrust belt will also be less substantial. Changes in sediment thickness in the order of several hundred metres, such as that observed across the Sanchakou Fault, still cause disruption to the belt-parallel thrusts. However, rather than creating major strike-slip fault systems that completely partition the thrust belt, the belt-parallel structures accommodate these changes by branching and splitting into two thrusts (Fig. 6.9b). Plausibly, this pattern continues to apply where the net loss of sediment thickness is smaller or the change is less abrupt, such as across the Yijianfang Fault. Such belt-oblique structures have only a minor impact on the superimposed thrust system, such as a minor kink in the trace of belt-parallel thrusts. There is no requirement to reactivate the fault to accommodate this lateral change and were it not for the surface expression of the structure to the south (Fig. 6.1), within the Tarim Basin interior, such structures would probably go unnoticed within the thrust belt.

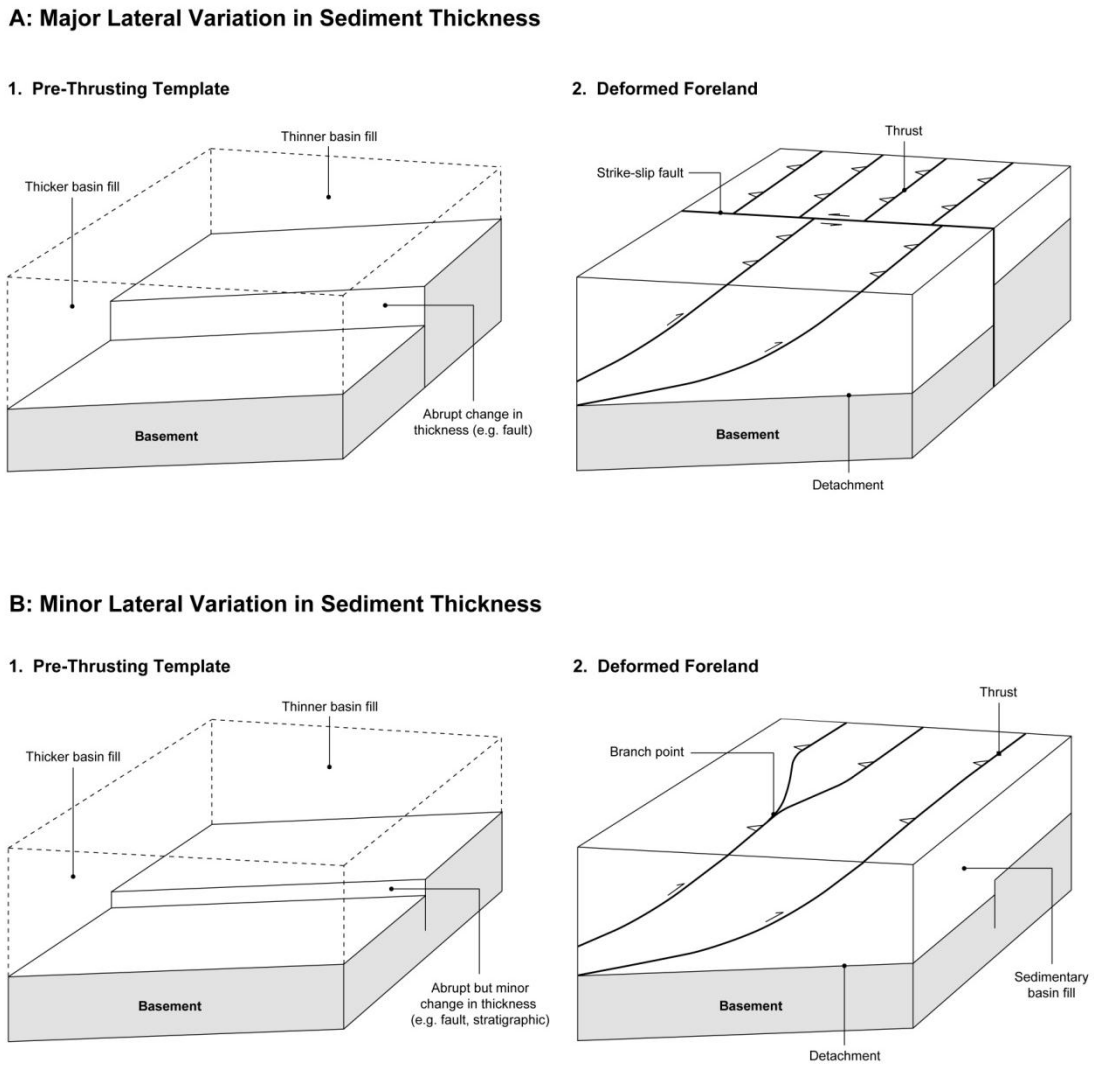

Fig. 6.9. Impact of sediment thickness on thrusting: (a) Abrupt and substantial lateral change across a major pre-existing fault zone, which results in the reactivation of the fault and lateral partitioning of the thrust belt; (b) Abrupt but small change across a pre-existing fault zone, causing a kink or branching of the superimposed thrusts but without the need to reactivate the fault. These models are based on direct observations from the Keping Shan and supported by theoretical models proposed by Liu *et al.* 1992.

Taking these observations into account, and applying the theoretical models (Fig. 6.9), we present a schematic model for the whole of the Keping Shan (Fig. 6.10). The model shows that lateral partitioning and structural variability is strongly affected by lateral variations in sediment thickness above the detachment horizon, which in turn are associated with the presence of major pre-existing structures that were potentially most active during the Early Permian.

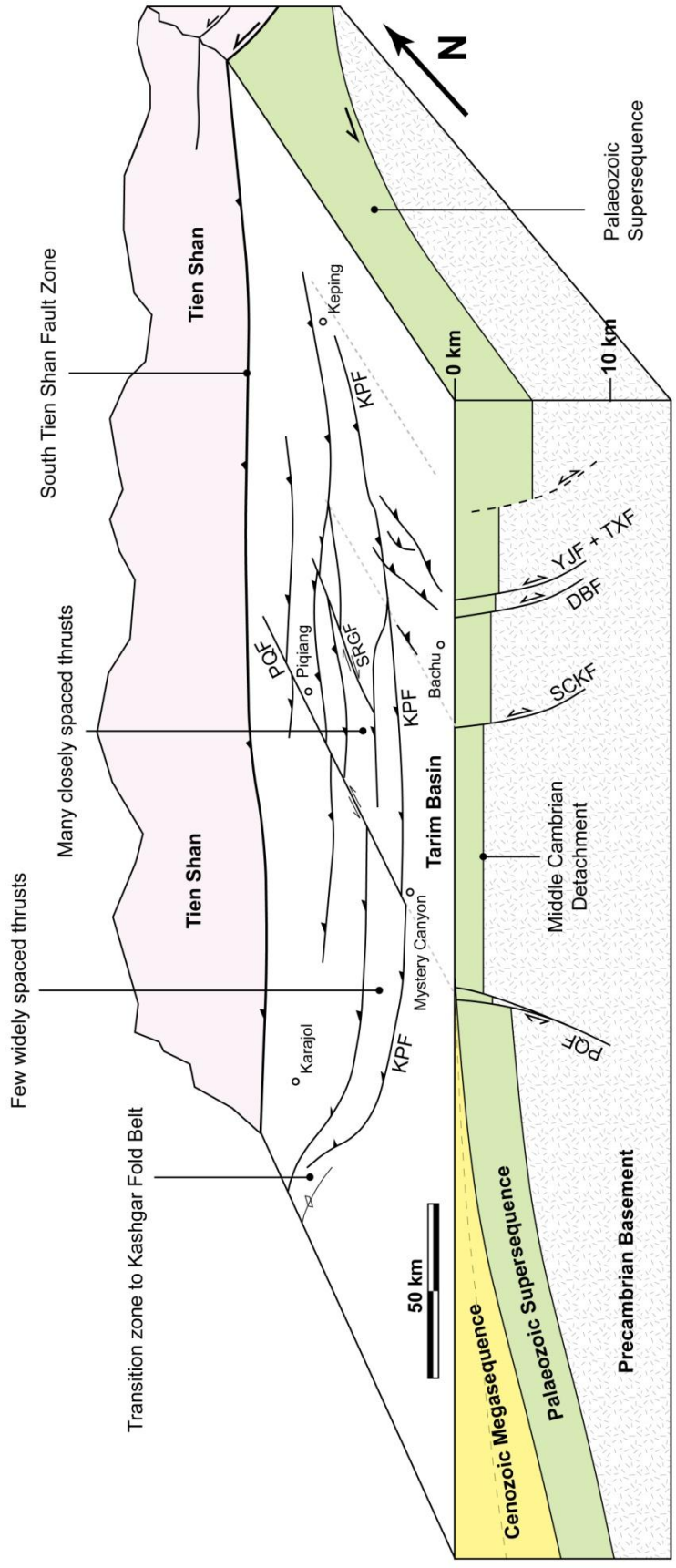

Fig. 6.10. Schematic model of the Keping Shan illustrating the impact of lateral variations in the thickness of the sediment pile, major pre-existing fault zones, and the structural architecture of the superimposed (Late Cenozoic) thrust belt.

Comparison with other studies demonstrates that the primary causes of lateral structural variability in the Keping Shan are well documented in other settings. Within the Cordilleran Fold-Thrust Belt, western United States, Lawton *et al.* (1994) show that abrupt discontinuities that form between segments (compartments) of the thrust belt arise because of rapid lateral changes in the thickness of the sedimentary section. Where the change in sedimentary thickness is less substantial, diffuse transition zones form without the requirement to generate major strike-slip fault zones. A similar case from the Apennines, Italy, is presented by Butler *et al.* (2006), where major belt-oblique lineaments which coincide with substantial changes in the thickness of Mesozoic to Lower Cenozoic strata have impacted on the plan-view architecture of the more recently imposed fold-thrust belt. In the Zagros Fold-Thrust Belt, Iran, major pre-existing structures such as the Kazerun Fault have long-lived histories and acted to control not just the sedimentary thickness but also the sedimentary facies. Early activity during the Cambrian controlled the distribution of the Hormuz salt, which has created a major lateral change in the detachment within the belt. Subsequent activity of these earlier structures during the Cretaceous impacted substantially on the thickness of the sediment pile, which has further enhanced lateral variability in the Cenozoic fold-thrust belt (Sepehr & Cosgrove 2004, 2007; Sepehr *et al.* 2006). These studies in other fold-thrust belts compare closely to the observations and interpretations we have drawn from the Keping Shan.

6.4.1 Implications for Hydrocarbon Exploration

Lateral structural variability within foreland fold-thrust belts has important implications for hydrocarbon exploration in similar settings, which as discussed throughout this volume are likely to become of increasing importance in the future. To date, there have been no discoveries of hydrocarbons in the Keping Shan, which reflects the lack of a suitable source rock within the stratigraphic succession. However, the Keping Shan provides an ideal analogue for similar settings which may be rich in hydrocarbons. Abrupt discontinuities within fold-thrust belts, such as those described in this chapter and in analogous settings such as the Cordilleran fold-thrust belt, the Apennines and the Zagros (Lawton *et al.* 1994; Butler *et al.* 2006; Sepehr *et*

al. 2006), act to partition the fold-thrust belt into a series of structural domains and may thereby compartmentalise structural reservoirs of hydrocarbons. In addition, lateral variations in the spatial organisation of structures between different compartments can enhance the reservoir potential of certain parts of the fold-thrust belt over others by enhancing the concentration of structural traps. An important consideration, and one which has formed the basis of much of this chapter, is the pre-existing basin template and the presence of major lateral variations in the pre-existing stratigraphic framework. This may have additional implications for hydrocarbon distribution, locally removing important reservoir or seal formations from certain parts of the fold-thrust belt. Thicker sediment piles may also be subjected to higher temperatures, thereby enhancing hydrocarbon generation relative to other parts of the fold-thrust belt.

6.5 Conclusions

Partitioning of belt-parallel thrusts within the E-W trending Keping Shan Thrust Belt occurs across major N-S to NW-SE belt-oblique fault zones and lineaments. Although these fault zones have developed coeval to thrusting during Late Cenozoic contraction, there is strong evidence of earlier activity linked to either a period of extension during the Early Permian or regional transtension in the Jurassic. This extension generated a series of major N-S to NW-SE trending faults across which there are substantial variations in the thickness of the sedimentary succession. Late Cenozoic contractional deformation, associated with foreland deformation adjacent to the Tien Shan orogenic belt, generated the Keping Shan Thrust Belt. The lateral structural variability and partitioning of the belt is strongly controlled by the pre-existing faults and associated variations in sedimentary thickness. In several examples, the inherited structures have been reactivated during thrusting either as oblique-slip or strike-slip (transfer) faults which cross the thrust belt and help to accommodate abrupt lateral changes in the structure. Understanding how inherited structures and their impact on the sediment pile combine to influence the partitioning of the fold-thrust belt has important implications for hydrocarbon exploration in foreland settings. The

Keping Shan serves not only to provide an insight into earlier phases of tectonism within the hydrocarbon-rich Tarim Basin, but can be applied as an analogue to fold-thrust belts worldwide.

CHAPTER SEVEN

Structural Controls on the Distribution of Seismicity

Abstract • Powerful earthquakes occur frequently in the NW Tarim Basin, China. Seismicity records spanning 36 years were obtained from global seismicity databases and have been combined with longer period historical records and field investigation in order to analyse the spatial and temporal clustering of earthquakes in relation to the regional structural geology. Our investigation has revealed a major structure within the interior of the Tarim Basin, the Jiashi Fault Zone (JFZ), which was the source of several devastating earthquakes in 1997 and 2003. The JFZ is a NW-SE trending strike-slip fault zone with no surface expression. Earthquakes are clustered in a zone where the structural trend of the fault changes, creating a large-scale releasing bend. The recurrence interval between the last two major episodes of intense seismic activity was ~40 years. Each episode lasted 6-8 years and was characterised by a series of earthquake swarms that last several months. A swarm initiates with movement on strike-slip faults, which triggers earthquakes generated predominantly on normal, but also on strike-slip and thrust faults.

Publication Details • Turner, S., Liu, J. G., Cosgrove, J. W. & Zhang, J. (in review). Structural controls on the spatial and temporal distribution of seismicity in the NW Tarim Basin, China: Towards an understanding of the regional seismic hazard. *Tectonophysics (Short Communication)*, submitted November 2009.

7.1 Introduction

Powerful seismic activity in the northwest Tarim Basin (Xinjiang Autonomous Region, China) shows an irregular spatial and temporal distribution. Earthquakes in the region are abundant, more so than anywhere else in the basin or indeed much of Central Asia (Fig. 7.1). Alarmingly, the region is also the most densely populated part of the Tarim Basin, and major population centres such as Kashgar and Aksu are growing at a phenomenal pace. In recent years, the region has experienced a number of powerful earthquakes that have resulted in substantial loss of life and damage to the infrastructure. These earthquakes are the result of rapid shortening across the region that occurs as a response to far-field stresses associated with the collision of India and Eurasia to the south. In this article, we examine the control of the regional geological structure on the spatial and temporal distribution of seismicity in the NW Tarim Basin, in order to reappraise the regional seismic hazard. The regional geological structure has been derived from satellite image interpretation and ground-based measurements obtained during fieldwork in the Tarim Basin, and examined in relation to earthquake and focal mechanism solution records obtained by several global seismicity networks (Figs. 7.1 and 7.2).

7.2 Structure of the NW Tarim Basin

The NW Tarim Basin is actively deformed by a series of foreland fold-thrust belts that have propagated outwards from the Tien Shan orogenic belt during the Late Cenozoic (Fig. 7.1). Shortening across the region occurs as a direct response to the collision of India and Eurasia (Yin *et al.* 1998; Chapter 6), that began 50-40 Myr ago (Yin & Harrison 2000). Published geodetic measurements indicate that current shortening rates across the foreland fold-thrust belts are rapid, i.e. 8 (± 3) mm yr^{-1} (Reigber *et al.* 2001). This shortening is accommodated by the development and growth of folds and faults which in turn are responsible for the abundant and powerful seismicity in the NW Tarim Basin.

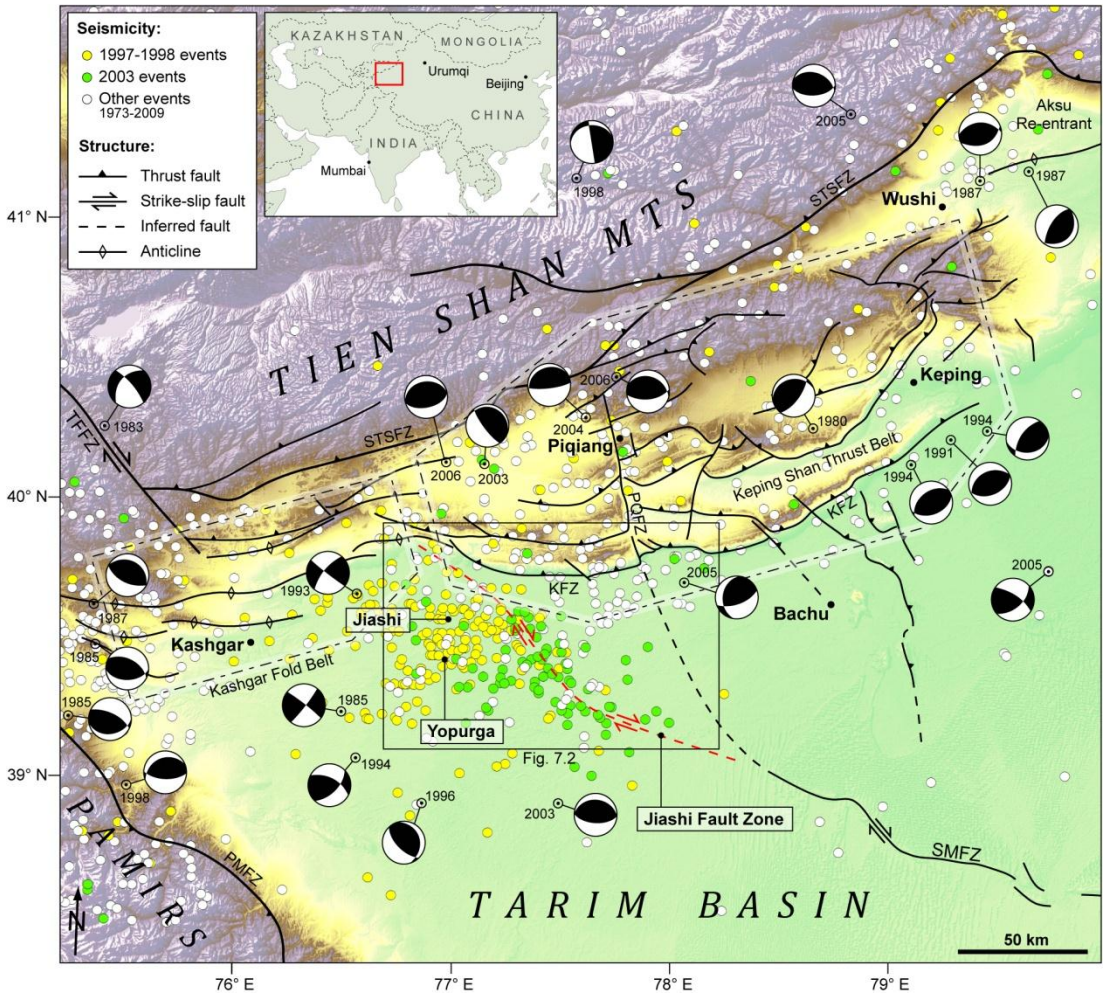

Fig. 7.1. Digital elevation model of the NW Tarim Basin with an overlay of the master structural elements. Recent seismicity is clustered predominantly in the Jiashi area and to a lesser extent in the foreland fold-thrust belts. The Tien Shan mountains and the basin interior are comparatively devoid of seismicity. SMFZ = Selibuya-Mazartagh Fault Zone; KFZ = Keping Fault Zone; PQFZ = Piqiang Fault Zone; STSFZ = South Tien Shan Fault Zone; PMFZ = Pamirs Fault Zone.

At the western end of the NW Tarim Basin, the foreland is characterised by the Kashgar Fold Belt, which comprises a series of detachment folds that deform a predominantly Cenozoic sedimentary succession (Fig. 7.1). The total shortening across this belt over the past 1.2 Myr is estimated to be 9.3 km, indicating a mean shortening rate of 7.8 mm yr^{-1} (Scharer *et al.* 2004). To the east, there is a gradual transition into the Keping Shan Thrust Belt. The Keping Shan is wider, forming an arcuate salient that propagates more than 100 km into the interior of the Tarim Basin (Fig. 7.1). The belt is characterised by a series of imbricate thrusts that deform a predominantly Palaeozoic sedimentary succession (Allen *et al.* 1999; Chapter 6). The

transition between the two belts probably reflects the dramatic thinning of the Cenozoic succession, from more than 10,000 m in the Kashgar area to less than 500 m at the centre of the Keping Shan.

Internally, the structural architecture of the WSW–ESE trending Keping Shan Thrust Belt is complicated by a series of inherited, oblique (NW–SE trending) fault zones which laterally partition the belt. It is thought that these faults evolved as transtensional structures during the Early Permian and that they were contemporaneous with widespread magmatism (Chapter 6). Another set of inherited NW–SE trending basement faults has been identified to the west of Kashgar and were generated during the Jurassic to Cretaceous and acted as major right-lateral strike-slip fault zones which created deep, narrow transtensional basins (Sobel 1999). These faults have been reactivated during the Cenozoic as the Talas-Ferghana (strike-slip) Fault and the Pamirs (thrust) Fault (Fig. 7.1). Throughout the Mesozoic, the NW–SE trending fault zones in the Keping Shan also remained active features, partitioning the Tarim Basin into two isolated depo-centres to the east and west of the Bachu Uplift, an intrabasinal high that cross-cuts the modern Keping Shan Thrust Belt (c.f. Fig. 7.3A).

7.3 Earthquake Distribution

A list of seismic events has been collated using data acquired from global seismicity networks including the USGS GSN and the Harvard CMT catalogue, which provide records of seismic events from 1973 onwards for earthquakes exceeding magnitudes of Mw 3.0. These data show that the distribution of seismicity across the NW Tarim Basin is both spatially and temporally irregular. The majority of recent earthquakes have occurred in the Jiashi area, and within the foreland fold-thrust belts (Figs. 7.1 and 7.2), while the interior of the Tarim Basin and the Tien Shan mountains are almost devoid of seismic activity.

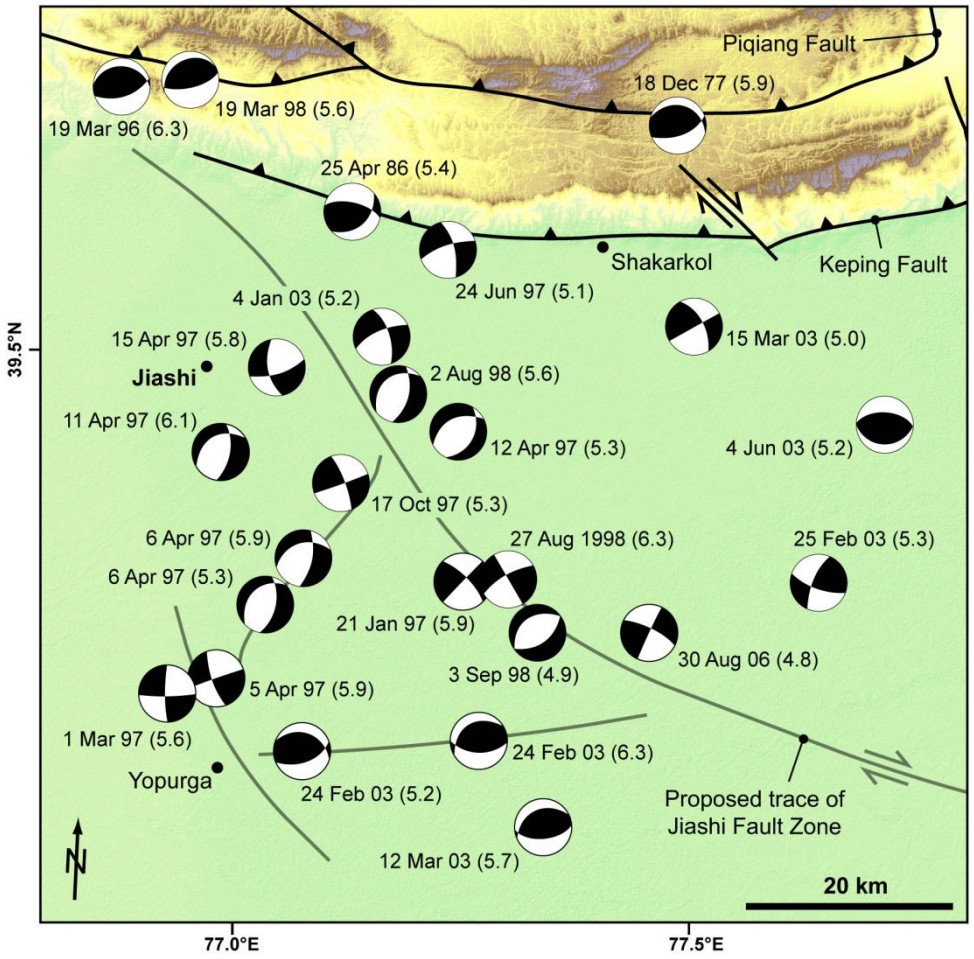

Fig. 7.2. Focal mechanism solutions (FMSs) for major (Mw > 5) earthquakes in the Jiashi region, showing the clustering of major earthquakes around the JFZ (Jiashi Fault Zone), which experienced two recent earthquake swarms in 1997–1998 and 2003. FMSs in this area indicate strike-slip, normal and reverse faulting mechanisms associated with a large-scale releasing bend (Fig. 7.3).

With the exception of a cluster of earthquakes in the far west, there has been relatively little recent seismic activity within the Kashgar Fold Belt, despite the rapid rates of shortening (7 mm yr^{-1}) proposed by Scharer *et al.* (2004). This may reflect the dominance of ductile, aseismic detachment folding rather than brittle, thrust faulting in this belt. The few recorded earthquakes that have occurred have focal mechanism solutions (FMSs) that indicate reverse faulting, implying that at least some of the shortening in this area is accommodated by thrusting. Seismic activity increases in intensity to the east, where it is relatively evenly distributed across the Keping Shan Thrust Belt. The majority of earthquakes have reverse fault FMSs, which is

compatible with the surface geology (Fig. 7.1) and indicate movement on N-dipping thrust faults with E-W to NE-SW trends.

Somewhat unexpectedly, the greatest abundance of recent seismicity has occurred in the area around Jiashi (Figs. 7.1 & 7.2), ~50 km into the interior of the Tarim Basin, rather than within the foreland fold-thrust belts. In this area, there are no structures expressed at the surface, implying that seismicity occurs on a series of blind faults. According to historical records provided by the China Earthquake Administration, several powerful earthquakes in 1953 and 1961 had their epicentres in the Jiashi area. During the latter swarm, a particularly powerful set of earthquakes with magnitudes of Mw 6.7, 6.4 and 6.8 occurred in April, 1961. These events were followed by a number of aftershocks that exceeded Mw 5.0. Unfortunately, FMSs are not available for these earthquakes. The Mw 6.8 event of the 14 April, 1961, was the largest earthquake recorded to date in the Jiashi region.

More recently, two particularly devastating earthquake swarms have occurred, one in 1997-1998 and the other in 2003 (Figs. 7.1 and 7.2). In the first instance, a Mw 5.9 earthquake occurred on 21 January, 1997 (Fig. 7.2) and was responsible for 50 fatalities. The FMS indicates the earthquake was caused by right-lateral movement on a NW-SE trending strike-slip fault. A series of smaller aftershocks continued throughout February, culminating with a Mw 5.6 earthquake on 1 March, 1997 (Fig. 7.2). The FMS is also interpreted as movement on NW-SE trending, right-lateral fault, but which lies ~30 km west of the fault associated with the primary earthquake on 21 January. In early April, 1997, a second wave of earthquakes occurred, this time with predominantly normal fault FMSs. The most powerful of these events was on 11 April, 1997, and measured Mw 6.1 (Fig 7.2). According to a Reuters report, the earthquake caused 9 fatalities. A number of powerful aftershocks linked to strike-slip movement on NW-SE trending faults occurred throughout the remainder of 1997 and into 1998.

Following several years of quiescence, the area was again subjected to intense seismic activity during 2003. An initial earthquake on 4 January, 2003, was linked to right-

lateral movement on a strike-slip fault that correlates with the source of the initial seismic activity in January 1997. This was followed by two powerful earthquakes (Mw 6.3 and 5.2) on 24 February, which occurred ~20 km apart and had reverse FMSs, indicating south-propagating movement on the same E-W trending thrust fault (Fig. 7.2). The town of Bachu, ~100 km east of the epicentral region, was utterly devastated by these earthquakes. International media reported at least 266 fatalities, 4,000 injuries and the destruction of more than 10,000 homes. A number of subsequent events occurred in the same area during March and April, 2003, and had similar reverse or strike-slip focal mechanism solutions.

7.4 Discussion

Contrary to expectation, seismicity in the NW Tarim Basin is concentrated predominantly in an area some distance into the interior of the Tarim Basin , in the Jiashi area, rather than in the foreland fold-thrust belts or the Tien Shan orogenic belt. We propose that seismicity in the Jiashi area relates to a particularly earthquake-prone section of a major NW-SE trending fault system, which we define as the Jiashi Fault Zone (JFZ) (Fig. 7.3A). This zone acts primarily as a system of interacting right-lateral strike-slip faults that have no surface expression (Fig. 7.3B). It may possibly represent the lateral continuation of the WNW-ESE trending Selibuya-Mazartagh Fault Zone (SMFZ), which has a surface expression ~100 km to the southeast (Fig. 7.1). The change in trend of the fault system from WNW-ESE to NW-SE in the Jiashi area creates a releasing bend that is characterised by an abundance of extensional structures and, possibly, an extensional pull-apart system (Fig. 7.3B). This would account for the observed intense seismicity in the region and for the seismically-devoid sections of the fault zone to the southeast. In 1997, an earthquake on a NW-SE trending strike-slip fault triggered a second wave of seismicity which, assuming that the error on the position of the epicentres is minimal, occurred on a sub-parallel strike-slip fault some 30 km to the west. A third wave of seismicity, which occurred in April, 1997, is of particular interest as the epicentres are all located in between the previous two strike-slip ruptures, and are characterised by movement on NW-SE trending extensional

faults. It is proposed that this third and most devastating wave of seismicity occurred as a result of extension between two interacting strike-slip faults, and that this represents the evolution of an extensional pull-apart characterised by a series of NE-SW trending normal faults. The second swarm of earthquakes which occurred in 2003 similarly began with movement on a NW-SE trending strike-slip fault, that subsequently triggered movement on an E-W trending reverse fault. This demonstrates the complexity of the releasing bend (c.f. Woodcock & Fischer 1986) which results in the development and interaction of strike-slip, normal and reverse faults under a N-S oriented principal stress (Fig. 7.3B)

Qualitative reports show that the number of casualties and damage to buildings and infrastructure were significantly lower during the 1997 earthquakes than they were during 2003, despite the magnitudes of the most powerful earthquakes being nearly the same (Mw 6.1 in 1997, and Mw 6.3 in 2003). Furthermore, the effects of the 2003 earthquakes were felt across a much wider area. These observations are compatible with the fact that the distortional elastic strain energy linked to the reactivation of a thrust is considerably greater than that associated with the reactivation of strike-slip faults (Sibson 1973).

The trace of the JFZ to the northwest of Jiashi coincides with the transition zone between the Kashgar Fold Belt and the Keping Shan Thrust Belt (Fig. 7.3A). The wider, Keping Shan salient has advanced further into the Tarim Basin than the Kashgar Fold Belt. This may be aided by the JFZ acting as a decoupling horizon, accounting further for the abundance of seismic activity in this area. In addition, like other NW-SE trending fault zones across the region, the JFZ is probably an inherited, basement fault that developed during an earlier phase of tectonism in either the Early Permian or Jurassic. The SMFZ (Figs. 7.1 & 7.3A), which we suspect is the lateral continuation of the JFZ to the southeast, has a prolonged history of activity and has acted as the western boundary fault of the Bachu Uplift (Chapter 6).

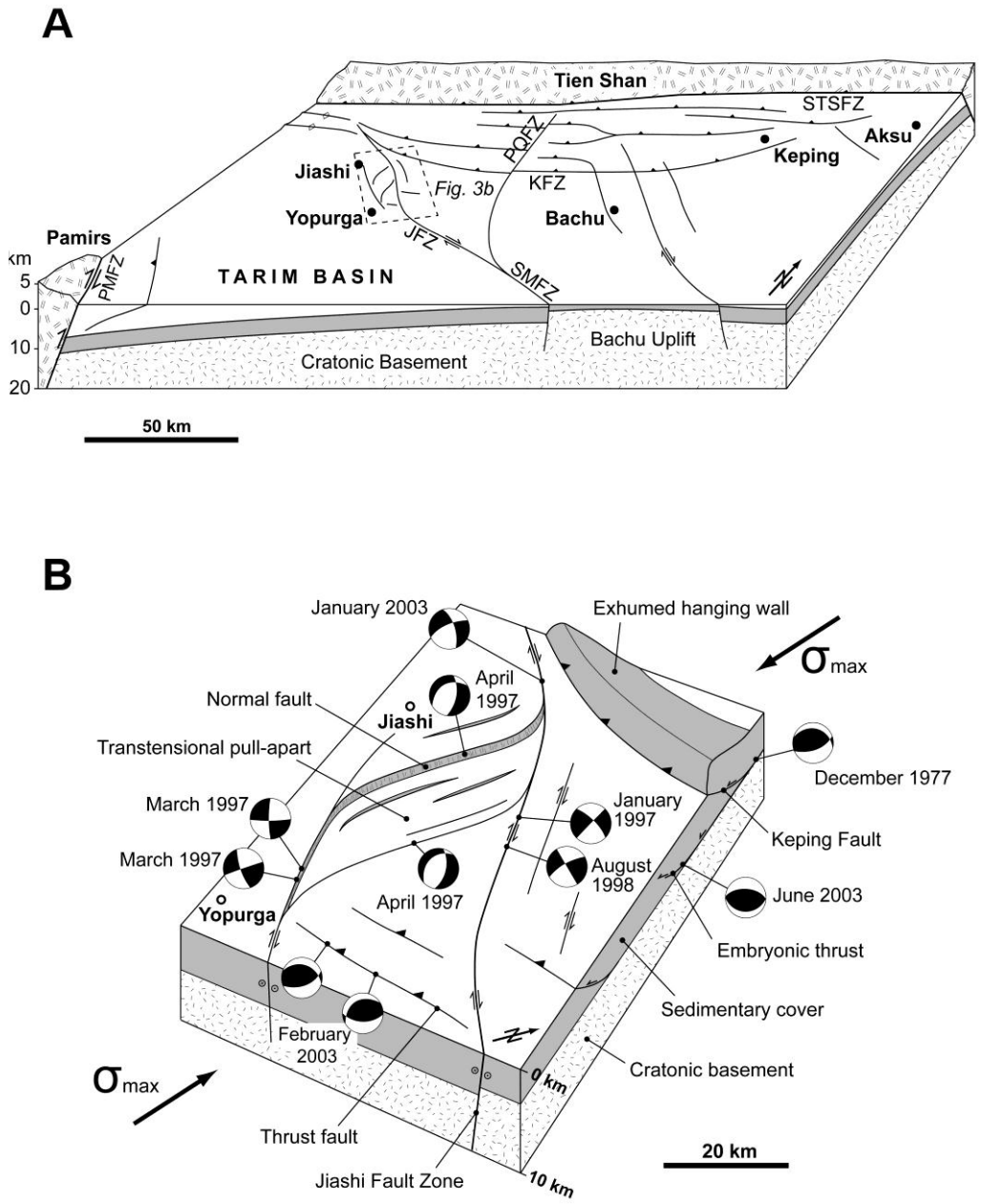

Fig. 7.3. (A) Schematic structural framework of the northwest Tarim Basin, showing the interaction of major fault zones and the relative position of the JFZ (Jiashi Fault Zone); (B) Schematic model of the JFZ in the area outlined in *(a)*, showing the distribution of major earthquakes in relation to a potential suite of structures that have no surface expression.

The pattern of seismicity linked to the 1997 and 2003 events provides an insight into the regional seismic hazard. Powerful earthquakes nucleate on a major releasing bend, along a section of the JFZ in the Jiashi area. Initial strike-slip motion on the JFZ triggers a swarm of earthquakes that lasts up to several months and can involve

movement on all types of fault. Several swarms appear to occur in succession, during an episode of earthquake activity that lasts for 6-8 years. Although no focal mechanism solutions are available for the seismicity of 1953 and 1961, it is possible that it represents a similarly coupled sequence of events and would imply a recurrence interval of ~40 years between major episodes of seismicity. Although the precise timing of the next period of intense seismicity is difficult to determine, when it does occur it is likely to begin with strike-slip movement on the JFZ. This will trigger a series of large magnitude events (Mw > 5.0) over the following 6-8 years, occurring on normal, strike-slip and reverse faults. It is suggested that this model be used as the first step in attempting to quantify the seismic hazard of the region.

7.5 Conclusions

The majority of recent earthquakes in the NW Tarim Basin have occurred as a result of movement along the Jiashi Fault Zone (JFZ). The zone forms part of a large NW-SE trending strike-slip fault system that may be a lateral continuation of the Selibuya-Mazartagh Fault Zone. Based on evidence from similar NW-SE trending fault zones in the region, the JFZ is likely to be an inherited fault zone that was generated either during the Early Permian or Jurassic. We propose that the change in the trend of the JFZ from WNW-ESE to NW-SE has resulted in the development of a large-scale releasing bend (Fig. 7.3). The releasing bend causes a localised build up of stress and thereby acts as a nucleation site for powerful seismicity. The recurrence interval of major episodes of earthquake activity on the JFZ is ~40 years. The most recent episode occurred in 1997-2003, prior to which there had been little seismic activity since a series of large magnitude earthquakes in 1953-1961. These episodes last 6-8 years, and comprise a series of earthquake swarms that occur in temporal clusters that last for several months. During recent swarms, the first earthquakes have been linked via their focal mechanism solutions to movement on strike-slip faults that directly reflect the position of the JFZ. This movement triggers further events on normal, strike-slip and thrust faults as stress is dissipated on and around the releasing bend and between interacting strike-slip fault segments (Fig. 7.3B).

PART THREE

Discussion and Conclusions

CHAPTER EIGHT

Synthesis and Discussion

The thesis set out to investigate the structural evolution of the NW Tarim Basin, by examining the tectonostratigraphic record and the structure of recent foreland fold-thrust belts that deform the basin margin. This was achieved by an integrated approach of satellite image interpretation and field-based investigation. These data were interpreted in the context of published literature on the study area and analogous settings in order to meet the thesis objectives. The research in this thesis has been presented in a series of six chapters that were written as stand-alone documents but which together form part of a coherent investigation. Chapters 2–5 are focused predominantly on examining the stratigraphic and structural evolution of the NW Tarim Basin and linking these observations with the crustal-scale events that governed the break-up of Gondwana and the amalgamation of Central Asia. Chapters 6–7 examine the structure of the Middle to Late Cenozoic foreland fold-thrust belt and discuss the role that pre-existing stratigraphy and structure had in controlling the structural geometry and architecture of the Keping Shan Thrust Belt, and the spatial and temporal distribution of powerful seismicity. The purpose of this chapter is to synthesise and summarise the main findings of this thesis, in terms of the tectonostratigraphic framework of the NW Tarim Basin and the structure of the foreland fold-thrust belt system. The interplay between these two aspects is then discussed with the aim of presenting a final, concluding model for the study area.

8.1 Tectonostratigraphic Framework

The NW Tarim Basin contains a thick (3–16 km) sedimentary succession that spans the Late Neoproterozoic to Recent. Sedimentary facies, thickness variations and interaction with ancestral fault zones provides an insight into the evolution of the basin and the adjacent orogenic belts, and can be considered in the context of the Early Palaeozoic break-up of Gondwana and the Phanerozoic amalgamation of Central Asia.

8.1.1 Late Neoproterozoic (Rift Basin)

In Chapter 2, it was shown that the NW Tarim Basin is underlain by a cratonic basement that comprises blueschists and greenschists that reached peak metamorphism in the Early Neoproterozoic (Chen *et al.* 2004) and once formed part of East Gondwana, connected to the Kimberley region of NW Australia. The basement is unconformably overlain by an 800 m Upper Neoproterozoic synrift sequence comprising a lower, non-marine and volcanic unit which passes upwards into shallow marine carbonates. This sequence is likely to correspond to a widespread rifting event which resulted in the separation of the Tarim Block from East Gondwana by the Early Palaeozoic.

8.1.2 Cambrian to Devonian (Intracratonic Basin)

An investigation of the sedimentary facies, stratigraphy and spatial distribution of the Palaeozoic succession was presented in Chapter 3. During the Cambrian to Ordovician, the Tarim Basin was situated in the equatorial latitudes and was covered by a relatively shallow epicontinental sea that was conducive to carbonate deposition. In total, 1,500-1,800 m of dolomite and limestone were accumulated. The predominantly dolomitic, upward-shallowing succession of the Cambrian relates to the post-rift phase of the Late Neoproterozoic–Early Palaeozoic rifting event, which

was followed by an upward-deepening succession in the Early to Middle Ordovician which may relate to the collision of the Yixieke arc along the southwest margin of the Tarim Block. Regional variations in the thickness of the Cambrian-Ordovician megasequence were primarily caused by erosion associated with subaerial exposure of the basin during the Late Ordovician to Early Silurian, forming a basin-wide unconformity. The cause of this unconformity was ascribed partly to a Hirnantian glaciation, which caused a decline of up to 100 m in relative sea levels in the Late Ordovician, and to long wavelength dynamic topography associated with a subduction zone along the southern margin of the Tarim Craton.

Deposition from the Early Silurian to Middle Devonian marked a new phase of tectonic subsidence across the NW Tarim Basin, and the accumulation of a 1,000–2,600 m thick marine to non-marine clastic sequence in an intracratonic setting. These sediments were largely sourced from a developing orogenic belt immediately to the south of the Tarim Basin, which was created by the accretion of the Kudi and Kunlun-Kongur terranes that presently constitute the Kunlun Shan and Pamirs orogenic belts.

8.1.3 Late Carboniferous to Early Permian (Foreland Basin)

By the Late Palaeozoic, Tarim had drifted north to latitudes of 30° N and was proximal to the southern margin of the Eurasian continent. The ensuing closure of the intervening Turkestan Ocean resulted in the formation of the South Tien Shan orogenic belt, and the development of a foreland basin along the northern margin of the Tarim Basin. The Upper Carboniferous to Lower Permian succession deposited in the basin is characterised by shallow marine (flysch) to fluvial (molasse) facies respectively, and thickens substantially to the north reflecting the asymmetry of the foreland basin.

8.1.4 Early Permian (Transtension and Volcanism)

In Chapter 4, the disputed cause of widespread Early Permian extension in the NW Tarim Basin was evaluated through an integrated analysis of the stratigraphy, structure and volcanism that occurred during this time. It was proposed that the interior of the Tarim Basin (and the underlying craton) were deformed by large-scale, anticlockwise block rotation, induced by left-lateral transpression in the South Tien Shan during the late stages of orogenesis. This resulted in the development of NW-striking transtensional fault zones and fractures, which had a strong influence on the thickness of the sedimentary succession. The development of the Bachu Uplift (Fig. 8.1), which has remained an important structural feature ever since, is likely to have been caused by activity on these NW-striking fault zones that were active in the Early Permian. Across the Bachu Uplift, the Lower Permian succession is completely absent, whilst to the east and west, the succession locally thickens to more than 3,000 m. In addition, the NW-striking fractures were exploited by mafic dykes, which were emplaced from 270–275 Ma (Zhang *et al.* 2008) and resulted in the extrusion of voluminous basalts across the NW Tarim Basin.

With the exception of the most western parts of the NW Tarim Basin, Mesozoic sediments are absent across the study area. It was suggested by Sobel (1999) that much of the NW Tarim Basin remained an intrabasinal high throughout this period. As a result, differential erosion across the uplifted and tilted Early Permian fault blocks, and particularly across the Bachu Uplift, further reduced the thickness of the underlying (pre-Permian) stratigraphic succession. The fault zones that were active during the Early Permian may have been periodically reactivated by a succession of collisions along the southern margin of Central Asia, which are recorded in a Mesozoic succession in the eastern Tarim Basin (Hendrix *et al.* 1992) and were responsible for activity on NW-striking fault zones in the western Tarim Basin (Sobel 1999).

8.1.5 Neogene to Recent (Foreland Basin)

It is shown in Chapter 5 that subsidence in the NW Tarim Basin during the Neogene was driven largely by flexural deflection of the Tarim Craton in response to loading by the Pamirs and Tien Shan orogenic belts. These belts were reactivated during widespread contraction in Central Asia, associated with the collision of India and the Himalayan Orogen to the south. A foreland basin that was generated adjacent to the Pamirs contains a 10 km thick Early Miocene to Recent sedimentary sequence that thins onto a forebulge which corresponds to the position of the Bachu Uplift. To the south of the Tien Shan, a foreland basin was generated that contains an 8 km thick Middle-Late Miocene to Recent sedimentary sequence, and implies that the Tien Shan began to uplift slightly later than the Pamirs. In both cases, sediments thin onto the Bachu Uplift, which corresponds to the position of a forebulge associated predominantly with deflection beneath the Pamirs. It is thought that tensile stress imposed during flexural deflection was sufficient to reactivate suitably oriented basement structures, and may have controlled the position of the forebulge.

8.2 Foreland Fold-Thrust Belts

The NW Tarim Basin is characterised by a foreland fold-thrust belt system that was generated by Late Cenozoic contraction of the basin margin in response to continued shortening in the South Tien Shan orogenic belt (Fig. 8.1). The fold-thrust belt system deforms the pre- and syntectonic sedimentary succession of the NW Tarim Basin that is summarised in §8.1. The northern boundary of the fold-thrust belt system is defined by the South Tien Shan Fault, a crustal-scale fault (Chapter 6) which separates metamorphic rocks of the South Tien Shan from the sedimentary rocks of the Tarim Basin. In plan view, the foreland fold-thrust belt system shows significant lateral (NE-SW) variations in structural geometry, architecture and style. Based on these variations, the system is divided into three discrete belts (Fig. 8.1), which from west to east comprise: (i) the Kashgar Fold Belt, (ii) the Keping Shan Thrust Belt, (iii) the Aksu Recess.

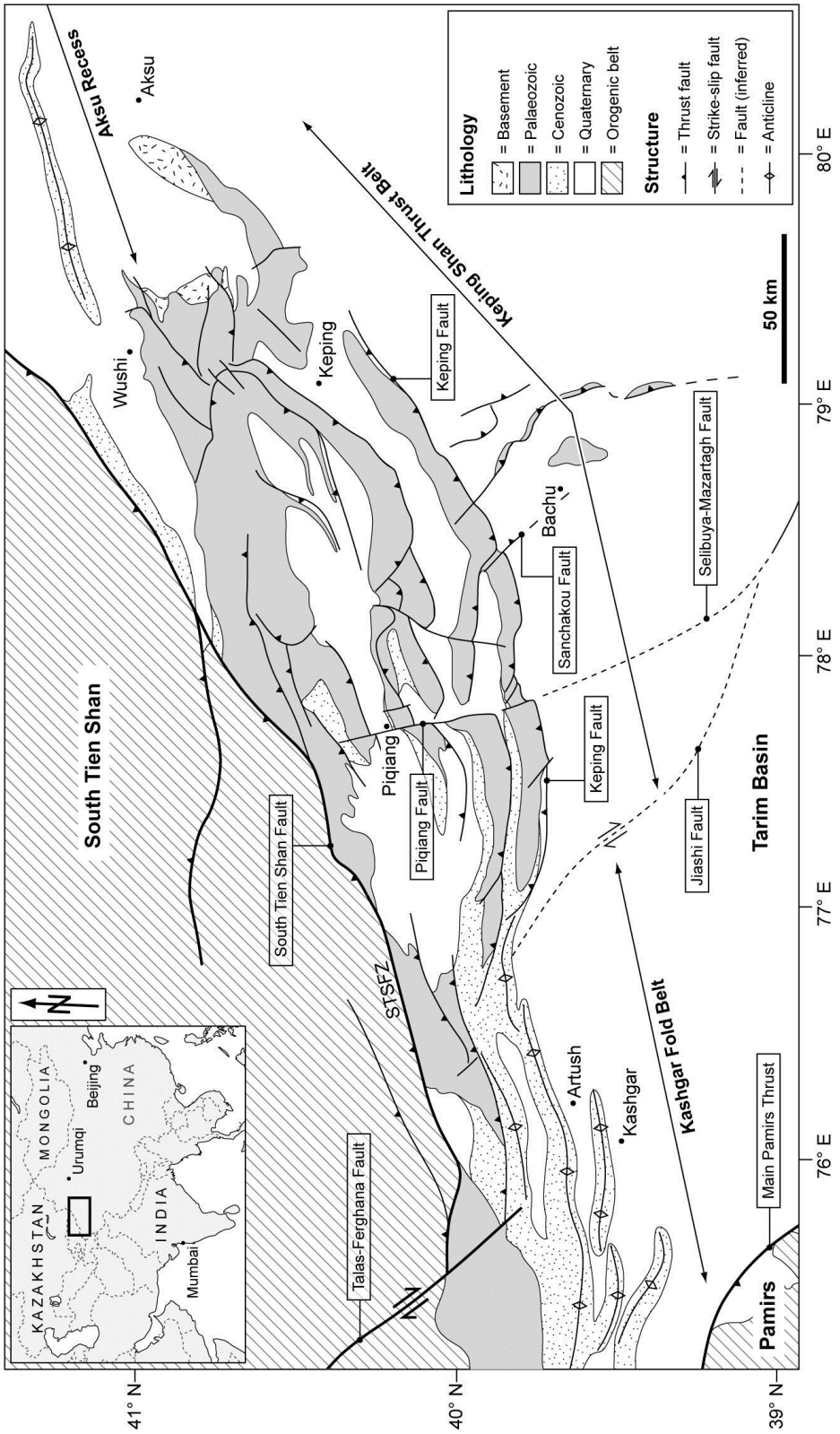

Fig. 8.1. Simplified geological map of the NW Tarim Basin, showing the distribution of Palaeozoic and Cenozoic sedimentary rocks and the structure of the foreland fold–thrust belt system.

8.2.1 Kashgar Fold Belt

The Kashgar Fold Belt was described in Chapters 5, 6 and 7. It forms a narrow belt in the northwest corner of the Tarim Basin, with a maximum N-S width of 55 km and an E-W length of 140 km (Fig. 8.1). The belt is characterised by a series of folds that deform a predominantly Cenozoic succession. In profile, the folds are asymmetric to the south (Scharer *et al.* 2004) and have particularly high length to width ratios which suggests they may be the surface expression of blind thrusts at depth (e.g. Cosgrove & Ameen 2001). This concurs with interpreted seismic sections (Heermance *et al.* 2008). The rate of shortening in the belt has been discussed by various authors, and ranges from 7.8 mm yr^{-1} (Scharer *et* al. 2004) to 2.2–2.7 mm yr^{-1} (Heermance *et al.* 2008). The evolution of structures in the Kashgar Fold Belt began in the Early Miocene, and accelerated in the Early Pliocene (Heermance *et al.* 2007).

8.2.2 Keping Shan Thrust Belt

The Keping Shan Thrust Belt was analysed in Chapter 6, and forms an arcuate salient with a maximum N-S width of 100 km and an E-W length of 300 km (Fig. 8.1). The structural transition from the Kashgar Fold Belt into the Keping Shan Thrust Belt is gradual, and is reflected in the progressive eastward emergence of imbricate thrusts at the surface. The master structural elements of the Keping Shan Thrust Belt have been divided into two categories based on their style and strike: (i) belt-parallel fault zones, (ii) belt-oblique fault zones.

Belt-parallel fault zones consist of persistently E to NE-striking imbricate thrusts that exploit an Upper Cambrian evaporite layer as a detachment (Allen *et al.* 1999; Chapters 3 and 6). The hanging walls of the thrusts exhume a predominantly Palaeozoic sedimentary succession, reflecting the thin nature of the Cenozoic succession across the Bachu Uplift. The belt-oblique faults strike predominantly NW or NNW, and comprise strike-slip and oblique-slip fault zones. These structures laterally partition the belt and act as tear faults that allow belt-parallel fault zones to be

decoupled across them. The most prominent belt-oblique structure is the Piqiang Fault, which is expressed at the surface for more than 70 km (Fig. 8.1, see Appendix B for a full structural analysis). To the west of the Piqiang Fault, there are three, major imbricate belt-parallel thrusts, while to the east, there are five, more closely-spaced thrusts. Onlapping of Middle to Late Miocene syntectonic strata onto thrusts in the Piqiang and Shorköl Hu areas (Fig. 8.1; Appendix C) constrains the timing of thrusting in the Keping Shan Thrust Belt. The total shortening across the central part of the belt is estimated to be 33% (Chapter 6), which therefore yields a shortening rate of 3.8–5 mm yr^{-1}.

8.2.3 Aksu Recess

A brief overview of the Aksu Recess was presented in Chapters 6 and 7 and is included in this chapter as it defines the eastern termination of the Keping Shan Thrust Belt. The Aksu Recess is 150 km wide and in comparison to the fold-thrust belt system to the west is characterised by very little internal deformation (Fig. 8.1). A solitary, asymmetric anticline with a high length-width ratio exposes the Cenozoic succession, and is therefore similar in nature to the structures in the Kashgar Fold Belt. To the north of the Aksu Recess, the South Tien Shan attains higher elevations than to the west.

8.3 Discussion

The structural geometry, architecture and style of the Late Cenozoic foreland fold-thrust belt system in the NW Tarim Basin is governed by the spatial and temporal distribution of the sedimentary cover succession. The regional-scale variations and transitions between the three belts described in §8.2 is controlled by variations in the thickness of the Cenozoic sequence, while internal structural variability in the Keping Shan Thrust Belt is ascribed to variations in the thickness of the Palaeozoic sequence, which in turn are controlled by a series of inherited, basement faults.

8.3.1 Impact of Syntectonic (Cenozoic) Sedimentation

The differences in the geometry and structural style of the Kashgar Fold Belt and the Keping Shan Thrust Belt is closely related to the spatial distribution of the Cenozoic sedimentary sequence. Critically, this sequence was deposited coeval to the development of the contractional structures which define the fold-thrust belt system. The impact of syntectonic sedimentation on the geometry and structural style of fold-thrust belts has been shown in both analogue and numerical models (e.g. Storti & McClay 1995; Simpson 2006) and in similar belts where syntectonic sedimentation was prevalent (e.g. the Apennines, Scarselli *et al.* 2006). By considering the fold-thrust belt as internally deforming Coulomb wedge (e.g. Dahlen 1990), the accumulation of syntectonic sediment onto the wedge increases the normal stress acting on the basal detachment surface, and depending on the distribution of these sediments would either increase or decrease the taper angle. Consequently, if the syntectonic sedimentation rate is high, the evolution of the fold-thrust belt is suppressed, generating a narrow belt that is characterised by asymmetric folds which form above blind thrusts at depth. On the contrary, if the syntectonic sedimentation rate is low, the a wide fold-thrust belt develops that is characterised by imbricate thrusting which achieves surface expression (Storti & McClay 1995; Simpson 2006).

This concept can be directly applied to the foreland fold-thrust belt system of the NW Tarim Basin (Fig. 8.2). Across the Kashgar Fold Belt, syntectonic sedimentation rates in the Cenozoic were relatively high (c. 0.6 mm yr^{-1}, Chapter 5). This has resulted in the development of a narrow fold-thrust belt, characterised by asymmetric folds that represent suppressed thrusts at depth and expose a predominantly Cenozoic sedimentary sequence. The eastward thinning of syntectonic sediment, associated with the asymmetry of the Cenozoic foreland basin adjacent to the Pamirs, corresponds to the transition from the Kashgar Fold Belt into the Keping Shan Thrust Belt. Across the Keping Shan Thrust Belt, syntectonic sedimentation rates in the Cenozoic were low (less than 0.04 mm yr^{-1}), and thus the effect of these sediments on the structural evolution of the thrust belt was minimal. Imbricate thrusts propagate further southwards into the Tarim Basin, and exhume a predominantly Palaeozoic succession.

Fig. 8.2. Schematic model of the NW Tarim Basin, integrating observations from this thesis to demonstrate how variations in sediment thickness and inherited fault zones impact the structural geometry, architecture and style of the foreland fold-thrust belt system.

The eastward tapering of the Keping Shan Thrust Belt into the Aksu Recess may also correspond to a progressive thickening of the Cenozoic sequence into the Aksu Depression, a foreland basin that relates to flexural deformation beneath the South Tien Shan (Chapter 5). However, in contrast to the Kashgar Fold Belt, the Aksu Recess is almost devoid of internal structure. Speculatively, the change in the character of the South Tien Shan orogenic belt to the north may also play a role in controlling the structure of the foreland in Aksu Recess. The anomalously high elevations could indicate that the South Tien Shan is accommodating shortening with greater efficiency, reducing the requirement for foreland contraction. Alternatively, the increased tectonic loading could induce a greater amount of flexural deflection in the foreland, thereby increasing the basal detachment angle and creating a zone less conducive to fold-thrust belt formation (e.g. Dahlen 1990; Boyer 1995).

8.3.2 Impact of Pre-tectonic (Palaeozoic) Sediment Thickness

As discussed in §8.2.2, the impact of syntectonic (Cenozoic) sedimentation across the Keping Shan Thrust Belt is minimal. Instead, lateral structural variability across the belt is caused by variations in the thickness of the Palaeozoic sequence. These thickness variations are controlled by a set of inherited basement faults that were active during the Early Permian (Chapter 4) (Fig. 8.2).

During the evolution of the Keping Shan Thrust Belt, areas across which the sediment is relatively thin have been deformed by closely spaced, imbricate thrusts (Fig. 8.2). In contrast, where the sediment is thicker, the belt is characterised by fewer, more widely spaced imbricate thrusts. These variations can be explained again by considering the fold-thrust belt as an imbricate Coulomb wedge. The thickness of the sediment determines the height of the deforming wedge and the depth of the detachment horizon. If the sediment is thin, many imbricate thrusts are required in order to generate sufficient topography in order to achieve the critical taper angle of the wedge. On the contrary, where the sediment is thick, the critical taper is attained

with fewer, more widely spaced thrusts. This concept was shown particularly well in a series of analogue sand models (Liu *et al.* 1991).

Furthermore, the lateral variations in Palaeozoic stratigraphic thickness, and consequently the spacing of the belt-parallel thrusts during Late Cenozoic contraction correspond to inherited, NW-striking fault zones. These fault zones are therefore reactivated in order to accommodate the lateral variations in the thrust belt architecture and act as strike-slip (tear) faults. These reactivated faults permit decoupling of the belt-parallel thrusts, and thereby structurally partition the Keping Shan Thrust Belt. The Piqiang Fault is the most prominent example of an inherited fault that has been reactivated in this way, and probably represents the substantial impact that it had on the thickness of the sedimentary succession prior to thrusting (see Chapter 6 and Appendix B for details). Other examples of these faults include the Dabantagh, Sanchakou and Tumuxieke Faults (Fig. 8.2), which have all impacted on the structural architecture of the Keping Shan Thrust Belt to varying degrees.

The response of a fold-thrust belt to lateral (belt-parallel) variations in stratigraphic thickness has been shown in a number of analogous settings. In the Zagros, Iran, thickness variations that occur across the Kazerun Fault, a major belt-oblique structure, have strongly impacted on the width of the fold-thrust belt and the style of folding across it (Sepehr & Cosgrove 2004, 2005, 2007). Lateral variations in sediment thickness associated with Precambrian basement faults in the foreland of the Urals, Russia, has similarly resulted in partitioning of the fold-thrust belt and reactivation of the basement structures as tear faults (Péréz-Estaún *et al.* 1997). Similarly, inherited fault zones in the Apennines, Italy (Butler 2006), the Cordilleran Fold-Thrust Belt, USA (Lawton *et al.* 1992) and the Adelaide Fold-Thrust Belt in Australia (Marshak & Flöttmann 1996) have resulted in lateral structural variability and fold-thrust belt partitioning. In all these examples, the inherited fault zones are associated with abrupt variations in stratigraphic thickness. The Keping Shan Thrust Belt therefore provides an ideal analogue for other foreland fold-thrust belts, and an opportunity to examine the causes of lateral structural variability and the development of belt-oblique fault zones.

8.3.3 Implications for the Distribution of Seismic Activity

Variations in the structural geometry and style of the foreland fold-thrust belt system has been shown to influence the spatial distribution of seismic activity in the NW Tarim Basin. In Chapter 7 it was proposed that the most powerful and devastating earthquakes in the past 30 years were caused by movement on a blind, NW-striking right-lateral fault zone in the Jiashi area. This fault, which was termed the Jiashi Fault Zone, can be traced northwards where it intercepts the transition zone between the Kashgar Fold Belt and the Keping Shan Thrust Belt. It was therefore proposed that the Jiashi Fault Zone may be accommodating part of the relative displacement between the two belts, permitting outward propagation of structures in the Keping Shan Thrust Belt relative to the Kashgar Fold Belt (Fig. 8.2). Although the structure was shown to be more complex, and probably forms a large-scale releasing bend beneath the Jiashi area, it is plausible that much of the displacement along the fault zone arises because of the differential movement in the foreland fold-thrust belt system which in turn generates powerful seismic activity. Furthermore, it is likely that the Jiashi Fault Zone replicates the characteristics of other NW-striking fault zones in the region, and has an earlier history of activity that predates the Late Cenozoic deformation of the NW Tarim Basin.

CHAPTER NINE

Conclusions

The structural evolution of the NW Tarim Basin provides a remarkable insight into the amalgamation of Central Asia and the controls that govern the evolution of foreland fold-thrust belts. The research presented in this thesis is anticipated to provide a significant contribution of new data and interpretations to several inadequately constrained, poorly understood and disputed issues.

The main conclusions drawn from this thesis are that:

- The Tarim Craton was separated from East Gondwana by the Early Palaeozoic. This event is recorded in the Upper Neoproterozoic to Lower Cambrian sedimentary and volcanic succession in the NW Tarim Basin, and correlates with a similar succession in the Kimberley region of NW Australia. On the basis of published literature and analysis of the subsequent Palaeozoic stratigraphy, it is argued that the Tarim Craton could not have been separated any later than the Middle Ordovician.

- An investigation of the Palaeozoic sedimentary succession in the NW Tarim Basin provides new insights into the regional paleogeography. In conjunction with new estimates of tectonic subsidence rates, the characteristics of the sedimentary record are shown to correlate well with the successive accretion of terranes at the southern margin of the Tarim Craton.

- During the Early Permian, the NW Tarim Basin was affected by regional transtension and volcanism. A new model is proposed in which the Tarim Craton was deformed by large-scale block rotation as a result of transpression across the Tien Shan orogenic belt. This led to the development of NW-striking transtensional fractures and fault zones, which provided conduits for the emplacement of mafic dykes and the extrusion of voluminous basaltic lava. These fault zones also acted to control the distribution of Lower Permian sediments, accounting for lateral thickness variations of up to 3 km.

- The formation of the Bachu Uplift is ascribed to the Early Permian transtensional event. The Bachu Uplift remained an intrabasinal high throughout the Mesozoic, and differential erosion across uplifted and subaerially exposed fault blocks resulted in further, localised loss of the Middle to Upper Palaeozoic strata.

- Subsidence in the NW Tarim Basin during the Cenozoic was driven by flexural deflection beneath the Pamirs and Tien Shan orogenic belts. The Pamirs became a topographically prominent belt by the end of the Early Miocene, but the Tien Shan did not attain equivalent topographic prominence until at least the Late Miocene. In both cases, a rapid increase in uplift, which was coupled with an increase in flexural subsidence, occurs in the Late Miocene and correlates with accelerated uplift in the Tibetan Plateau.

- Numerical modelling of flexural deflection indicates that the Tarim Craton has a flexural rigidity of 4×10^{23} Nm, which is equivalent to an effective elastic thickness of c. 40 km.

- Flexural deflection during the Cenozoic is likely to have induced tensile stresses across the surface of the Tarim Craton that were sufficient to reactivate the inherited basement faults. Consequently, the Bachu Uplift has remained a prominent intrabasinal high during the Cenozoic and it is suggested that it controlled the position of the flexural forebulge during much of this period.

- The foreland fold-thrust belt system that has evolved in the NW Tarim Basin during the Middle to Late Cenozoic shows dramatic lateral variations in structural geometry, architecture and style. The lateral, west to east transition from the

narrow, Kashgar Fold Belt into the wide, arcuate Keping Shan Thrust Belt is governed by a gradual thinning of the blanket of the syntectonic (Early Miocene to Recent) sedimentary succession. The syntectonic succession acted to suppress the evolution of the fold-thrust belt system where it is thickest, i.e. in the west, resulting in a narrow belt dominated by asymmetric folds. In contrast, where the syntectonic succession is thin, imbricate thrusting is expressed at the surface and the fold-thrust belt system propagated further into the interior of the Tarim Basin, forming the Keping Shan Thrust Belt.

- The internal structural architecture of the Keping Shan Thrust Belt is governed by inherited, basement faults and the associated lateral variations in the thickness of the Palaeozoic sedimentary succession. These faults, which were shown to have been active in the Early Permian, have been reactivated as belt-oblique strike-slip (tear) faults. They accommodate lateral differences in the spacing and abundance of belt-parallel thrust faults, which arise as a direct response to variations in the thickness of the deforming sedimentary wedge.

- Powerful seismicity in the NW Tarim Basin is spatially and temporally irregular. It occurs predominantly on a blind, NW-striking right-lateral strike-slip fault zone that may accommodate differential movement between the southward-propagating Kashgar Fold Belt and the Keping Shan Thrust Belt. In addition, a major releasing bend on the fault zone beneath the Jiashi area, to the south of the fold-thrust belts, acts as a nucleation site for powerful earthquakes which occur in swarms that last for several years and have a recurrence interval of c. 40 years. Activity on this fault zone accounts for the majority of earthquake-related casualties in the NW Tarim Basin during the last 15 years.

This thesis demonstrates that an evaluation of the structural evolution of a foreland fold-thrust belt system requires a comprehensive knowledge of the tectono-stratigraphic framework of the deforming basin. The published literature and the data collected in this thesis have only begun to unravel the complex evolution of the Tarim Basin whose secrets, for the time being at least, remain largely hidden beneath the sands of the Taklimakan Desert.

References

ABDRAKHMATOV, K. Y., ALDAZHANOV, S. A., HAGER, B. H., HAMBURGER, M. W., HERRING, T. A., KALABAEV, J. B., MAKAROV, V. I., MOLNAR, P, PANASYUK, S. V., PRILEPIN, M. T., REILINGER, R. E., SADYBAKASOV, I. S., SOUTER, B. J., YTAPEZNIKOV, Y. A., TSURKOV, V. Y. & ZUBOVICH, A. V. 1996. Relatively recent construction of the Tien Shan inferred from GPS measurements of present-day crustal deformation rates. *Nature*, **384**, 450-453.

ALLEN, M. B., VINCENT, S. J. & WHEELER, P. J. 1999. Late Cenozoic tectonics of the Kepingtage thrust zone: Interactions of the Tien Shan and Tarim Basin, northwest China. *Tectonics*, **18** (4), 639-654.

ALLEN, P. A. & ALLEN, J. R. 2005. *Basin analysis: principles and applications (2nd ed.)*. Blackwell Publishing, 549 pp.

ATKINSON, W. J, HUGHES, F. E. & SITH, C. B. 1984. A review of the kimberlitic rocks of Western Australia. *In:* Kornprobst, J. (ed), *Kimberlites I: Kimberlites and Related Rocks*. Amsterdam, 195-224.

AVOUAC, J. P., TAPPONNIER, P., BAI, M., YOU, H. & WANG, G. 1993. Active Thrusting and Folding Along the Northern Tien Shan and Late Cenozoic Rotation of the Tarim Relative to Dzungaria and Kazakhstan. *Journal of Geophysical Research*, **98**, 6755-6804.

BALLY, A. W., CHOU I-M., CLAYTON, R., EUGSTER, H. P., KIDWELL, S., MECKEL, L. D., RYDER, R. T., WATTS, A. B. & WILSON, A. A. 1986. Notes on sedimentary basins in China: Report of the American Sedimentary Basins Delegation to the People's Republic of China. *U.S. Geological Survey*, Open File Report **86-327**, 108pp.

BISKE, G. 1995. Late Paleozoic collision of the Tarimskiy and Kirgiz-Kazakh paleocontinents. *Geotectonics*, **29** (1), 26-34 (in Russian).

BISKE, Y. S. & SELTMANN, R. (in press). Paleozoic Tian-Shan as a transitional region between the Rheic and Urals-Turkestan Oceans. *Gondwana Research*, available online.

BOND, G. C. & KOMINZ, M. A. 1984. Construction of tectonic subsidence curves for the early Palaeozoic miogeocline, southern Canadian Rocky Mountains: Implications for subsidence mechanisms, age of breakup, and crustal thinning. *Geological Society of America Bulletin,* **95**, 155-173.

BOYER, S. E. 1995. Sedimentary basin taper as a factor controlling the geometry and advance of thrust belts. *American Journal of Science*, **295**, 1220-1254.

BRADLEY, D. C. & KIDD, W. S. F. 1991. Flexural extension of the upper continental crust in collisional foredeeps. *Geological Society of America Bulletin*, **103**, 1416-1438.

BRENCHLEY, P. J., MARSHALL, J. D., CARDEN, G. A., ROBERTSON, D. B. R., LONG, D. G. F., MEIDLA, T., HINTS, L. & ANDERSON, T. F. 1994. Bathymetric and isotopic evidence for a short-lived Late Ordovician glaciation in a greenhouse period. *Geology*, **22** (4), 295–298.

BROOKFIELD, M. E. 1994. Problems in applying preservation facies and sequence models to Sinian (Neoproterozoic) glacial sequences in Australia and Asia. *Precambrian Research*, **70**, 143–147.

BURGESS, P. M., GURNIS, M. & MORESI, L. 1997. Formation of sequences in the cratonic interior of North America by interaction between mantle, eustatic and stratigraphic processes. *Geological Society of America Bulletin*, **108**, 1515–1535.

BURRETT, C. F. 1974. Plate tectonics and the fusion of Asia. *Earth and Planetary Science Letters*, **21**, 181–189.

BURTMAN, V. S. 1975. Structural geology of the Variscan Tien Shan, USSR. *American Journal of Science*, **275A**, 157–186.

BURTMAN, V. S. & MOLNAR, P. 1993. Geological aand geophysical evidence for deep subduction of continental crust beneath the Pamir. *Geological Society of America,* Special Paper **281**.

BUTLER, R. W. H. 1982. The terminology of structures in thrust belts. *Journal of Structural Geology*, **4**, 239–245

BUTLER, R. W. H., TAVARNELLI, E. & GRASSO, M. 2006. Structural inheritance in mountain belts: An Alpine–Apennine perspective. *Journal of Structural Geology*, **28**, 1893–1908.

CARDOZO, N. & JORDAN, T. 2001. Causes of spatially variable tectonic subsidence in the Miocene Bermejo Foreland Basin, Argentina. *Basin Research*, **13**, 335–357.

CARROLL, A. R., GRAHAM, S. A., HENDRIX, M. S., YING, D. & ZHOU, D. 1995. Late Palaeozoic tectonic amalgamation of northwestern China: Sedimentary record of the northern Tarim, northwestern Turpan and southern Junggar Basins. *Geological Society of America Bulletin*, **107** (5), 571–594.

CARROLL, A. R., GRAHAM, S. A., CHANG, E. Z. & MCKNIGHT, C. 2001. Sinian through Permian tectonostratigraphic evolution of the northwestern Tarim basin, China. *In:* HENDRIX, M.S. & DAVIS, G.A. (eds), *Paleozoic and Mesozoic tectonic evolution of central Asia: From continental assembly to intracontinental deformation,* Geological Society of America Memoir, **194**, 47–69.

CHEN, H. L., YANG, S. F., WANG, Q. H., LUO, J. C., JIA, C. Z., WEI, G. Q. & LI, Z. L. 2006. Sedimentary response to the Early–mid-Permian basaltic magmatism in the Tarim Craton. *Geology of China*, **33**, 545–552 (in Chinese).

CHEN, J., BURBANK, D. W., SCHARER, K. M., SOBEL, E., YIN, J., RUBIN, C. & ZHAO, R. 2002. Magnetochronology of the Upper Cenozoic strata in the Southwestern Chinese Tian Shan: rates of Pleistocene folding and thrusting. *Earth and Planetary Science Letters*, **195**, 113–130.

CHEN, Y., XU, B., ZHAN, S. & LI, Y. 2004. First mid-Neoproterozoic paleomagnetic results from the Tarim Basin (NW China) and their geodynamic implications. *Precambrian Research*, **133**, 271–281.

COATS, R. P. & PREISS, W. V. 1980. Stratigraphic and geochronological reinterpretation of Late Proterozoic glaciogenic sequences in the Kimberley region, Western Australia. *Precambrian Research*, **13**, 181-208.

COLEMAN, R. G. 1989. Continental growth of Northwest China. *Tectonics*, **8**, 621-635.

COPELAND, P., HARRISON, T. M., KIDD, W. S. F., RONGHUA, X. & ZHANG, Y. 1987. Rapid early Miocene acceleration of uplift in the Gangdese Belt, Xizang (southern Tibet), and its bearing on accommodation mechanisms of the India-Asia collision. *Earth and Planetary Science Letters*, **86**, 240-252.

CORKERON, M. L. & GEORGE, A. D. 2001. Glacial incursion on a Neoproterozoic carbonate platform in the Kimberley region, Australia. *Geological Society of America Bulletin*, **113** (9), 1121-1132.

CORKERON, M., GREY, J., LI, Z. X. & POWELL, C. M. 1996. Neoproterozoic glacial episodes in the Kimberley region, northwestern Australia. *Abstracts of the Geological Society of Australia*, **41**, 97.

COSGROVE, J. W. & AMEEN, M. S. 2001. A comparison of the geometry, spatial organization and fracture patterns associated with forced folds and buckle folds. *In:* COSGROVE, J. W. & AMEEN, M. S. (eds), *Forced Folds and Fractures*, Geological Society, London, Special Publications, **169**, 7-21.

DAHLEN, F. A. 1990. Critical taper model of fold-and-thrust belts and accretionary wedges. *Annual Review of Earth and Planetary Science*, **18**, 55-99.

DAHLSTROM, C. D. A. 1970. Structural geology in the eastern margin of the Canadian Rocky Moutnains. *Bulletin of Canadian Petroleum Geology*, **18**, 332-406.

DAVIES, S. J., DAWERS, N. H., MCLEOD, A. E. & UNDERHILL, J. R. 2000. The structural and sedimentological evolution of early synrift successions: the Middle Jurassic Tarbert Formation, North Sea. *Basin Research*, **12**, 343-365.

DECELLES, P. G., GEHRELS, G. E., QUADE, J. & OJHA, T. P. 1998. Eocene-early Miocene foreland basin development and the history of Himalayan thrusting, western and central Nepal. *Tectonics*, **17** (5), 741-765.

DECELLES, P. G. & GILES, K. A. 1996. Foreland basin systems. *Basin Research,* **8** (2), 105-123.

DRURY, S.A. 1993. *Image Interpretation in Geology*. Chapman & Hall, London.

DUMITRU, T. A., ZHOU, D., CHANG, E. Z., GRAHAM, S. A., HENDRIX, M. S., SOBEL, E. R. & CARROLL, A. R. 2001. Uplift, exhumation, and deformation in the Chinese Tian Shan. *In:* HENDRIX, M. S. & DAVIS, G. A. (eds), *Paleozoic and Mesozoic tectonic evolution of central Asia: From continental assembly to intracontinental deformation*, Geological Society of America Memoir, **194**, 71-99.

ENGLAND, P. C. & HOUSEMAN, G. A. 1989. Extension during continental convergence, with application to the Tibetan Plateau. *Journal of Geophysical Research*, **94** (17), 561-579.

FAN, J. & MA, B. 1991. Oil-and-gas geology of Tarim. *In:* Biostratigraphy and geological evolution of Tarim, Vol. 4, Beijing Science Press, 466 pp.

FINK, J. H. & FLETCHER, R. C. 1978. Ropy pahoehoe: surface folding of a viscous fluid. *Journal of Volcanology and Geothermal Research*, **4**, 151–170.

FORTEY, R. A. & COCKS, L. R. M. 2003. Palaeontological evidence bearing on global Ordovician–Silurian continental reconstructions. *Earth-Science Reviews*, **61**, 245–307.

GAWTHORPE, R. L., FRASER, A. J. & COLLIER, R. E. L. 1994. Sequence stratigraphy in active extensional basins: implications for the interpretation of ancient basin fills. *Marine and Petroleum Geology,* **11**, 642–658.

GAWTHORPE, R. L. & LEEDER, M. R. 2000. Tectono-sedimentary evolution of active extensional basins. *Basin Research*, **12**, 195–218.

GILDER, S., ZHAO, X., COE, R., MENG, Z., COURTILLOT, V. & BESSE, J. 1996. Paleomagnetism and tectonics of the southern Tarim basin, northwestern China. *Journal of Geophysical Research*, **101** (B10), 22015–22031.

GLASS, L. M. & PHILLIPS, D. 2006. The Kalkarindji continental flood basalt province: A new Cambrian large igneous province in Australia with possible links to faunal extinctions. *Geology*, **34**, 461–646.

GREY, K. & CORKERON, M. 1998. Late Neoproterozoic stromatolites in glacigenic successions of the Kimberley region, Western Australia: evidence for a younger Marinoan glaciation. *Precambrian Research*, **92**, 65–87.

GUPTA, S., COWIE, P. A., DAWERS, N. H. & UNDERHILL, J. R. 1998. A mechanism to explain rift-basin subsidence and stratigraphic patterns through fault array evolution. *Geology*, **26**, 595–598.

GUPTA, S., UNDERHILL, J. R., SHARP, I. R. & GAWTHORPE, R. L. 1999. Role of fault interaction in controlling synrift dispersal patterns: Miocene, Abu Alaqa Group, Suez Rift, Sinai, Egypt. *Basin Research*, **11**, 167–189.

HANCOCK, P. L. & BEVAN, T. G. 1987. Brittle modes of foreland extension. *From*: COWARD, M. P., DEWEY, J. F. & HANCOCK, P. L. (eds), *Continental Extensional Tectonics,* Geological Society Special Publication No. 28, 127–137.

HANLEY, L. M. & WINGATE, M. T. D. 2000. SHRIMP zircon age for an Early Cambrian dolerite dyke: an intrusive phase of the Antrim Plateau Volcanics of northern Australia. *Australian Journal of Earth Sciences*, **47**, 1029–1040.

HAQ, B. U. & SCHUTTER, S. R. 2008. A chronology of Paleozoic sea-level change. *Science*, 322, 64–68.

HARRISON, T. M., COPELAND, P., KIDD, W. S. F. & YIN, A. 1992. Raising Tibet. *Science*, **255**, 1663–1670.

HARVARD GLOBAL CMT (Centroid Moment Tensor) Catalog, 2009. Accessed online: *<http://www.globalcmt.org/CMTsearch.html>*.

HEERMANCE, R. V., CHEN, J., BURBANK, D. W. & WANG, C. 2007. Chronology and tectonic controls of Late Tertiary deposition in the southwestern Tian Shan foreland, NW China. *Basin Research*, **19**, 599–632.

HEERMANCE, R. V., CHEN, J., BURBANK, D. W. & MIAO, J. 2008. Temporal constraints and pulsed Late Cenozoic deformation during the structural disruption of the active Kashi foreland, northwest China. *Tectonics*, **27**.

HENDRIX, M. S. 2000. Evolution of Mesozoic sandstone compositions, southern Junggar, northern Tarim, and western Turpan basins, northwest China: a detrital record of the ancestral Tian Shan. *Journal of Sedimentary Research*, **70** (3), 520-532.

HENDRIX, M. S., GRAHAM, S. A., CARROLL, A. R., SOBEL, E. R., MCKNIGHT, C. L., SCHULEIN, B. J. & ZUOXUN, W. 1992. Sedimentary record and climatic implications of recurrent deformation in the Tian Shan: Evidence from Mesozoic strata of the north Tarim, south Junggar, and Turpan basins, northwest China. *Geological Society of America Bulletin*, **104**, 53-79.

HETÉNYI, M. 1979. *Beams on Elastic Foundations*. Ann Arbor, Michigan, University of Michigan Press.

HEUBECK, C. 2001. Assembly of central Asia during the middle and late Paleozoic. *In:* HENDRIX, M. S. & DAVIS, G. A. (eds), *Paleozoic and Mesozoic tectonic evolution of central Asia: From continental assembly to intracontinental deformation*. Geological Society of America, Memoir, **194**, 1-22.

HUANG, B., XU, B., ZHANG, C., LI, Y. & ZHU, R. 2005. Paleomagnetism of the Baiyisi volcanic rocks (ca. 740 Ma) of Tarim, Northwest China: A continental fragment of Neoproterozoic Western Australia? *Precambrian Research*, **142**, 83-92.

JACKSON, J. 1994. Active tectonics of the Aegean region. *Annual Reviews of Earth and Planetary Science,* **22**, 239-271.

JIA, C. 1997. *Structural Geology and Petroleum Potential in the Tarim Basin, China*. Petroleum Industry Press House, Beijing, 438 pp.

JIA, C. Z. 1997. *Tectonic characteristics and oil-gas in the Tarim Basin, China*. Beijing, Petroleum Industry Press.

JIANG, C. Y., ZHANG, P. B., LU, D. R., BAI, K. Y., WANG, Y. P., TANG, S. H., WANG, J. H. & YANG, C. 2004. Petrology, geochemistry and petrogenesis of the Kalpin basalts and their Nd, Sr and Pb isotopic compositions. *Geology Review*, **50**, 492-500.

JORDAN, T. E. 1981. Thrust loads and foreland basin evolution, Cretaceous, western United States. *Bulletin of the American Association of Petroleum Geologists*, **65**, 2506-2520.

JUN, G., MAOSONG, L., XUCHUANG, X., YAOQING, T. & GUOQI, H. 1998. Paleozoic tectonic evolution of the Tianshan Orogen, northwestern China. *Tectonophysics*, **287**, 213-231.

KONOPELKO, D., BISKE, G., SELTMANN, R., EKLUND, O. & BELYATSKY, B. 2007. Hercynian post-collisional A-type granites of the Kokshaal Range, Southern Tien Shan, Kyrgyzstan. *Lithos*, **97**, 140-160.

KROON, D., STEENS, T. & TROELSTRA, S. R. 1991. Onset of monsoonal related upwelling in the western Arabian Sea as revealed by planktonic foramifers. *Proceedings of the Oceanic Drilling Program Scientific Results,* **117**, 257-263.

LAWTON, T.F., BOYER, S.E. & SCHMITT, J.G. 1994. Influence of inherited taper on structural variability and conglomerate distribution, Cordilleran fold and thrust belt, western United States. *Geology*, **22**, 339-342.

LE MAÎTRE, R. W. (ed.) 2002. Igneous Rocks: A Classification and Glossary of Terms. *Cambridge University Press*.

LEEDER, M. R. & GAWTHORPE, R. L. 1987. Sedimentary models for extensional tilt-block/half-graben basins. *In:* COWARD, M. P., DEWEY, J. F. & HANCOCK, P. L. (eds), *Continental Extensional Tectonics*, Geological Society Special Publications, **28**, 139-152.

LI, D., LIANG, D., CHENGZAO, J. GANG, W., QIZHI, W. & DENGFA, H. 1996. Hydrocarbon accumulations in the Tarim basin, China. *AAPG Bulletin*, **80**, 1587–1603.

LI, P., ZHOU, Z., LI, J., ZHANG, C., HE, W. & SHU, M. 2003. Structural framework and its formation of the Kalpin thrust belt, Tarim Basin, north-west China, from Landsat TM data. *International Journal of Remote Sensing*, **24**, 18, 3535-3546.

LI, X. H., LI, Z. X., WINGATE, M. T. D., CHUNG, S. L., LIU, Y., LIN, G. C. & LI, W. X. 2006. Geochemistry of the 755 Ma Mundine Well dyke swarm, northwestern Australia: Part of a Neoproterozoic mantle superplume beneath Rodinia? *Precambrian Research*, **146**, 1-15.

LI, Y. 1990. An apparent polar wander path from the Tarim Block, China. *Tectonophysics*, **181**, 31-41.

LI, Y., MCWILLIAMS, M., COX, A., SHARPS, R., LI, Y., GAO, Z., ZHANG, Z. & ZHAI, Y. 1988. Late Permian paleomagnetic poles from dikes of the Tarim craton, China. *Geology*, **16**, 275-278.

LI, Z. X. & POWELL, C. MCA. 2001. An outline of the paleogeographic evolution of the Australasian region since the beginning of the Neoproterozoic. *Earth Science Reviews*, **53**, 237-277.

LI, Z. X., ZHANG, L., POWELL, C. MCA. 1996. Positions of the East Asian cratons in the Neoproterozoic supercontinent Rodinia. *Australian Journal of Earth Sciences*, **43**, 593-604.

LINDSAY, J. F., KORSCH, R. J. & WILFORD, J. R. 1987. Timing and breakup of a Proterozoic supercontinent: Evidence from Australian intracractonic basins. *Geology*, **15**, 1061-1064.

LIOU, J. G., GRAHAM, S. A., MARUYAMA, S., WANG, X., XIAO, X., CARROLL, A. R., CHU, J., FENG, Y., HENDRIX, M. S., LIANG, Y. H., MCKNIGHT, C. L., TANG, Y., WANG, Z. X., ZHAO, M. & ZHU, B. 1989. Proterozoic blueschist belt in western China: Best documented Precambrian blueschists in the world. *Geology*, **17**, 1127-1131.

LIU, H., MCCLAY, K.R. & POWELL, D. 1992. Physical models of thrust wedges. *From:* MCCLAY, K.R. (ed.) 1992. *Thrust Tectonics*, Chapman & Hall.

LIU, J.G. 1991. Balance contrast enhancement technique and its application in image colour composition. *International Journal of Remote Sensing*, **12** (10), 2133-2151.

LIU, J.G. & MCMOORE, J. 1996. Direct decorrelation stretch technique for RGB colour composition. *International Journal of Remote Sensing*, **17** (5), 1005-1018.

MACEDO, J. & MARSHAK, S. 1999. Controls on the geometry of fold-thrust belt salients. *GSA Bulletin,* **111** (12), 1808-1822.

MARSHAK, S. & FLÖTTMANN, T. 1996. Structure and origin of the Fleurieu and Nackara Arcs in the Adelaide fold-thrust belt, South Australia: salient and recess development in the Delamerian Orogen. *Journal of Structural Geology*, **18** (7), 891-908.

MARSHAK, S., WILKERSON, M. S. & HSUI, A. T. 1992. Generation of curved fold-thrust belts: Insight from simple physical and analytical models. *From:* McClay, K. R. (ed.) 1992. *Thrust Tectonics*, Chapman & Hall.

MATTE, PH., TAPPONNIER, P., ARNAUD, N., BOURJOT, L., AVOUAC, J. P., VIDAL, PH., LIU, Q., PAN, Y., YI, W. 1996. Tectonics of Western Tibet, between the Tarim and the Indus. *Earth and Planetary Science Letters*, **142**, 311-330.

MCCLAY, K.R. 1992. Glossary of thrust tectonic terms. *From:* McClay, K.R. (ed.) 1992. *Thrust Tectonics*, Chapman & Hall.

MCKENZIE, D. & JACKSON, J. 1986. A block model of distributed deformation by faulting. *Journal of the Geological Society, London,* **143**, 349-353.

MCKERROW, W. S., SCOTESE, C. R. & BRASIER, M. D. 1992. Early Cambrian continental reconstructions. *Journal of the Geological Society, London*, **149**, 599-606.

MCKNIGHT, C.L. 1993. *Structural styles and tectonic significance of Tian Shan foothill fold and thrust belts, northwest China*. Ph.D. thesis, 207 pp, Stanford University, California.

METCALFE, I. 1996. Gondwanaland dispersion, Asian accretion and evolution of Eastern Tethys. *Australian Journal of Earth Sciences*, **43**, 605-623.

METCALFE, I. 2009. Late Palaeozoic and Mesozoic tectonic and palaeogeographical evolution of SE Asia. *In:* BUFFETAUT, E., CUNY, G., LE LOEUFF, J. & SUTEETHORN, V. (eds), *Late Palaeozoic and Mesozoic Ecosystems in SE Asia*, The Geological Society, London, Special Publications, **315**, 7-23.

MILLER, K. C., KOMINZ, M. A., BROWNING, J. V., WRIGHT, J. D., MOUNTAIN, G. S., KATZ, M. E., SUGARMAN, P. J., CRAMER, B. S., CHRISTIE-BLICK, N. & PEKAR, S. F. 2005. The Phanerozoic Record of Global Sea-Level Change. *Science*, **310**, 1293-1298.

MOLNAR, P., ENGLAND, P. & MARTINOD, J. 1993. Mantle Dynamics, Uplift of the Tibetan Plateau, and the Indian Monsoon. *Reviews of Geophysics*, **31** (4), 357-396.

NAKAJIMA, T., MARUYAMA, S., UCHIUMI, S., LIOU, J. G., WANG, X., XIAO, X. & GRAHAM, S. A. 1990. Evidence for late Proterozoic subduction from 700-Myr-old blueschists in China. *Nature*, **346**, 263-265.

PAN, Y. S. 1996. *Geological evolution of the Karakorum and Kunlun Mountains*. Seismological Press, Beijing.

PÉRÉZ-ESTAÚN A., ALVAREZ-MARRÓN, J., BROWN, D., PUCHKOV, V., GOROZHANINA, Y. & BARYHEV, V. 1997. Along-strike structural variations in the foreland thrust and fold belt of the southern Urals. *Tectonophysics*, **276**, 265-280.

PRELL, W. L. & KUTZBACH, J. E. 1992. Sensitivity of the Indian monsoon to forcing parameters and implications for its evolution. *Nature*, **360**, 647-652.

REIGBER, CH., MICHEL, G. W., GALAS, R., ANGERMANN, D., KLOTZ, J., CHEN, J. Y., PAPSCHEV, A., ARSLANOV, R., TZURKOV, V. E. & ISHANOV, M. C. 2001. New space geodetic constraints on the distribution of deformation in Central Asia. *Earth and Planetary Science Letters,* **191**, 157-165.

ROBINSON, A. C., YIN, A., MANNING, C. E., HARRISON, T. M., ZHANG, S-H. & WANG, X-F. 2004. Tectonic evolution of the northeastern Pamir: Constrains from the northern portion of the Cenozoic Kongur Shan extensional system, western China. *Geological Society of America Bulletin*, **116** (7/8), 953-973.

RODDAZ, M., BRUSSET, S., SOULA, J-C., BÉZIAT, D., ABBOU, M. B., DEBAT, P., DRIOUCH, Y., CHRISOPHOUL, F., NTARMOUCHANT, A. & DÉRAMOND, J. 2002. Foreland basin magmatism in the Western Moroccan Meseta and geodynamic inferences. *Tectonics*, **21** (5), 1043.

SABINS, F.F. 1996. *Remote Sensing Principles and Interpretation*. Freeman & Co., New York.

SCARSELLI, S., SIMPSON, G. D. H., ALLEN, P. A., MINELLI, G. & GAUDENZI, L. 2006. Association between Messinian drainage network formation and major tectonic activity in the Marche Apennines (Italy). *Terra Nova*, **19**, 74-81.

SCHARER, K. M., BURBANK, D. W., CHEN, J., WELDON, R. J., RUBIN, C., ZHAO, R. & SHEN, J. 2004. Detachment folding in the Southwestern Tian Shan-Tarim foreland, China: shortening estimates and rates. *Journal of Structural Geology*, **26**, 2119-2137.

SCHLISCHE, R. 1991. Half-graben basin filling models: new constraints on continental extensional basin development. *Basin Research*, **3**, 123-141.

SCLATER, J. G. & CHRISTIE, P. A. F. 1980. Continental stretching: an explanation of the post Mid-Cretaceous subsidence of the central North Sea basin. *Journal of Geophysical Research*, **85**, 3711-3739.

SELF, S., KESZTHELYI, L. & THORDARSON, T. 1998. The importance of pahoehoe. *Annual Reviews of Earth and Planetary Science*, **26**, 81-110.

SENGÖR, A. M. C. 1976. Collision of irregular continental margins: Implications for foreland deformation of Alpine-type orogens. *Geology*, **4**, 779-782.

SEPEHR, M. & COSGROVE, J.W. 2004. Structural framework of the Zagros Fold-Thrust Belt, Iran. *Marine and Petroleum Geology,* **21**, 829-843.

SEPEHR, M. & COSGROVE, J. W. 2007. The role of major fault zones in controlling the geometry and spatial organization of structures in the Zagros Fold-Thrust Belt. *From:* Ries, A. C., Butler, R. W. H. & Graham, R. H. (eds.) 2007.

Deformation of the Continental Crust: The Legacy of Mike Coward. Geological Society, London, Special Publications, **272**, 419–436.

SEPEHR, M., COSGROVE, J. W. & MOIENI, M. 2006. Role of the Kazerun Fault Zone in the formation and deformation of the Zagros Fold–Thrust Belt, Iran. *Tectonics*, **24**, TC5005.

SHEEHAN, P. M. 2001. The Late Ordovician Mass Extinction. *Annual Review of Earth and Planetary Science*, **29**, 331–364.

SHI, Y., LU, H., JIA, D., CAI, D., WU, S., CHEN, C., HOWELL, D. G. & VALIN, Z. C. 1995. Paleozoic plate-tectonic evolution of the Tarim and western Tianshan regions, western China. *International Geology Review*, **36**, 1058–1066.

SIBSON, R. H. 1973. Interactions between temperature and pore-fluid pressure during earthquake faulting and a mechanism for partial or total stress relief. *Nature*, **243** (126), 66–68.

SIMPSON, G. D. H. 2006. Interactions between fold-thrust belt deformation, foreland flexure and surface mass transport. *Basin Research*, **18**, 125–143.

SOBEL, E. & ARNAUD, N. 1999. A possible middle Paleozoic suture in the Altyn Tagh, NW China. *Tectonics*, **18**, 64–74.

SOBEL, E. R. & DUMITRU, T. A. 1997. Thrusting and exhumation around the margins of the western Tarim basin during the India–Asia collision. *Journal of Geophysical Research*, **102**, 5043–5063.

SOBEL, E. R. 1999. Basin analysis of the Jurassic–Lower Cretaceous southwest Tarim basin, northwest China. *Geological Society of America Bulletin*, **111** (5), 709–724.

SOLOMOVICH, L. I. & TRIFONOV, B. A. 2002. Postcollisional granites in the South Tien Shan Variscan Collisional Belts, Kyrgyzstan. *Journal of Asian Earth Sciences*, **21** (1), 7–21.

STORTI, F. & MCCLAY, K. 1995. Influence of syntectonic sedimentation on thrust wedges in analogue models. *Geology*, **23** (11), 999–1002.

SUN, J., ZHU, R. & BOWLER, J. 2004. Timing of the Tianshan Mountains uplift constrained by magnetostratigraphic analysis of molasse deposits. *Earth and Planetary Science Letters*, **219**, 239–253.

TAPPONNIER, P. & MOLNAR, P. 1979. Active faulting and Cenozoic tectonics of the Tien Shan, Mongolia, and Baykal regions. *Journal of Geophysical Research*, **84** (B7), 3425–3456.

TIAN, W., CAMPBELL, I. H. & ALLEN, C. M. 2009. The Tarim picrite–basalt–rhyolite suite of northwest China, a Permian flood basalt with contrasting, coeval rhyolites produced by fractional crystallization and anatexis. *Geological Society of America Annual Meeting Abstracts*, **106–15**, Portland, USA.

TURNER, S., COSGROVE, J.W. & LIU, J.G. 2009. Causes of along-strike structural segmentation in the Southwest Tien foreland, NW China. *Geophysical Research Abstracts*, **11**, EGU2009-0.

TURNER, S., COSGROVE, J. W. & LIU, J. G. 2010. Controls on lateral structural variability in the Keping Shan Thrust Belt, SW Tien Shan Foreland, China. *In:* GOFFEY, G. P., CRAIG, J., NEEDHAM, T. & SCOTT, R. (eds) *Hydrocarbons in Contractional Belts*. Geological Society, London, Special Publications, **348**, 71-85.

USGS GSN (Global Seismicity Network), 2009. Accessed online: <*http://earthquake.usgs.gov/regional/neic*>.

VEEVERS, J. J. 1984. Morphotectonics of the divergent or rifted margins. *In:* VEEVERS, J. J. (ed), *Phanerozoic Earth History of Australia*, Clarendon Press, Oxford, pp. 168-210.

VEEVERS, J. J., WALTER, M. R. & SCHEIBNER, E. 1997. Neoproterozoic tectonics of Australia-Antarctica and Laurentia and the 560 Ma birth of the Pacific ocean reflect the 400 Ma Pangean supercycle. *Journal of Geology*, **105**, 225-242.

WANG, Z-H., QI, Y-P. & BERGSTRÖM, S. M. 2007. Ordovician conodonts of the Tarim Region, Xinjiang, China: Occurrence and use as paleoenvironment indicatiors. *Journal of Asian Earth Sciences*, **5-6**, 832-843.

WATSON, M. P., HAYWARD, A. B., PARKINSON, D. N. & ZHANG, Z. M. 1987. Plate tectonic history, basin development, and petroleum source rock deposition, onshore China. *Marine and Petroleum Geology*, **4**, 205-225.

WATTS, A. B. 2001. *Isostasy and flexure of the lithosphere*. Cambridge University Press, 478 pp.

WEI, G., JIA, C., LI, B. & CHEN, H. 2002. Silurian to Devonian foreland basin in the south edge of Tarim Basin. *Chinese Science Bulletin,* **47***,* 42-46.

WHITE, R. & MCKENZIE, D. 1989. Magmatism at rift zones: The generation of volcanic continental margins and flood basalts. *Journal of Geophysical Research*, **94** (B6), 7685-7729.

WINDLEY, B. F., ALEXEIEV, D., XIAO, W., KRÖNER, A. & BADARCH, G. 2007. Tectonic models for the accretion of the Central Asian Orogenic Belt. *Journal of the Geological Society, London,* **164**, 31-47.

WINDLEY, B. F., ALLEN, M. B., ZHANG, C., ZHAO, Z-Y., WANG, G-R. 1990. Paleozoic accretion and Cenozoic redeformation of the Chinese Tien Shan Range, central Asia. *Geology*, **18**, 128-131.

WOODCOCK, N. H. & FISCHER, M. 1986. Strike-slip duplexes. *Journal of Structural Geology*, **8** (7), 725-735.

XIAO, W., WINDLEY, B. F., HAO, J. & LI, J. 2002. Arc-ophiolite obduction in the Western Kunlun Range (China): implications for the Palaeozoic evolution of central Asia. *Journal of the Geological Society, London*, **159**, 517-528.

XINJIANG STRATIGRAPHIC TABLE COMPILING GROUP 1981. *Xinjiang stratigraphic tables*. Beijing, Geological Publishing House, 496 pp.

XU, B., JIAN, P., ZHENG, H., ZOU, H., ZHANG, L. & LIU, D. 2005. U-Pb zircon geochronology and geochemistry of Neoproterozoic volcanic rocks in the Tarim Block of northwest China: implications for the breakup of Rodinia

supercontinent and Neoproterozoic glaciations. *Precambrian Research*, **136**, 107–123.

YANG, S. F., LI, Z., CHEN, H., SANTOSH, M., DONG, C. W. & YU, X. 2007. Permian bimodal dyke of Tarim Basin, NW China: geochemical characteristics and tectonic implications. *Gondwana Research*, **12**, 113–120.

YANG, Y. & LIU, M. 2002. Cenozoic deformation of the Tarim plate and the implications for mountain building in the Tibetan Plateau and the Tian Shan. *Tectonics*, **21** (6).

YIN, A. & HARRISON, T. M. 2000. Geologic evolution of the Himalayan–Tibetan orogen. *Annual Review of Earth and Planetary Sciences*, **28**, 211–280.

YIN, A., NIE, S., CRAIG, P., HARRISON, T. M., RYERSON, F. J., XIANGLIN, Q. & GENG, Y. 1998. Late Cenozoic tectonic evolution of the southern Chinese Tian Shan. *Tectonics*, **17** (1), 1–27.

YONG, L., ALLEN, P. A., DENSMORE, A. L. & QIANG, X. 2003. Evolution of the Longmen Shan Foreland Basin (Western Sichuan, China) during the Late Triassic Indosinian Orogeny. *Basin Research*, **15**, 117–138.

YU, B., CHEN, J., LI, X. & LIN, C. 2003. Geochemistry of black shale at the bottom of the Lower Cambrian in Tarim Basin and its significance for lithosphere evolution. *Science in China (Series D)*, **46** (5), 498–507.

ZHAN, S., CHEN, Y., XU, B., WANG, B. & FAURE, M. 2007. Late Neoproterozoic paleomagnetic results from the Sugetbrak Formation of the Aksu area, Tarim basin (NW China) and their implications to paleogeographic reconstructions and the snowball Earth hypothesis. *Precambrian Research*, **154**, 143–158.

ZHANG, C. L., LI, X. H., LI, Z. X., LU, S. N., YE, H. M. & LI, H. M. 2007. Neoproterozoic ultramafic–mafic–carbonatite complex and granitoids in Quruqtagh of northeastern Tarim Block, western China: Geochronology, geochemistry and tectonic implications. *Precambrian Research*, **152**, 149–169.

ZHANG, C. L., LI, X. H., LI, Z. X., YE, H. M. & LI, C. N. 2008. A Permian layered intrusive complex in the western Tarim block, northwestern China: Product of a ca. 275-Ma mantle plume? *The Journal of Geology*, **116**, 269–287.

ZHANG, C. L., LI, Z. X., LI, X. H. & YE, H. M. 2009. Neoproterozoic mafic dyke swarms at the northern margin of the Tarim Block, NW China: Age, geochemistry, petrogenesis and tectonic implications. *Journal of Asian Earth Sciences*, **35**, 167–179.

ZHANG, S. C., HANSON, A. D., MOLDOWAN, J. M., GRAHAM, S. A., LIANG, D. G., CHANG, E. & FAGO, F. 2000. Paleozoic oil-source rock correlations in the Tarim basin, NW China. *Organic Geochemistry*, **31**, 273–286.

ZHANG, Z. M., LIOU, J. G. & COLEMAN, R. G. 1984. An outline of the plate tectonics of China. *Geological Society of America Bulletin,* **95**, 295–312.

ZHOU, D. W., LIU, Y. Q., XIN, X. J., HAO, J. R., DONG, Y. P. & OUYANG, Z. J. 2006. Formation of the Permian basalts and implications of geochemical tracing for paleo-tectonic setting and regional tectonic background in the Turpan–Hami and Santaghu basins, Xinjiang. *Science of China Series D*, **49**, 584–596.

ZHOU, H., LI, J. L., HOU, Q. L., XIAO, W. J. & CHEN, H. H. 1999. The large-scaqle ductile shear zone in Kudi, West Kunlun. *Chinese Science Bulletin*, **44**, 2080-2082.

ZHOU, M. F., LESHER, C. M., YANG, Z. X., LI, J. W. & SUN M. 2004. Geochemistry and petrogenesis of 270 Ma Ni-Cu-(PGE) sulfide-bearing mafic intrusions in the Huangshan district, eastern Xinjiang, northwest China: implications for the tectonic evolution of the Central Asian orogenic belt. *Chemical Geology,* **209**, 233-257.

ZHU, Y., GUO, X., SONG, B., ZHANG, L. & GU, L. 2009. Petrology, Sr-Nd-Hf isotopic geochemistry and zircon chronology of the Late Palaeozoic volcanic rocks in the southwester Tianshan Mountains, Xinjiang, NW China. *Journal of the Geological Society, London,* **166**, 1085-1099.

Appendices

APPENDIX A

Application of Satellite Images for Geological Mapping

Satellite remote sensing has long been recognised as a powerful tool for the investigation of structures, stratigraphy and geomorphology in well exposed, remote and inaccessible regions. In addition, it also facilitates targeted and efficient fieldwork. This appendix provides a summary of the satellite image data, processing and interpretation techniques that were used in this study to examine the structure and stratigraphy of the NW Tarim Basin and to generate the geological map that is provided as Appendix C and was used and referred to throughout this thesis.

Satellite image data acquired from two different satellite sensors are used in this study (Table A.1). Landsat ETM+ images comprise wide coverage and suitable spatial resolution (30 × 30 m pixel size) for regional-scale analysis of the Kepingtagh. SPOT images have a higher spatial resolution (10 × 10 m pixel size) but a smaller area of coverage, and are useful for detailed analysis of complex or key areas. Both Landsat ETM+ and SPOT have multispectral scanners, which acquire image data in a number of spectral bands. Each band corresponds to a specific wavelength range (Tables A.2 and A.3).

Table A.1. Datasets used in this study

Sensor	Bands	Resolution	Acquisition Date	Path / Row
Landsat ETM+	7	30 m	18-09-1999	148 / 031
Landsat ETM+	7	30 m	13-09-2000	147 / 031
Landsat ETM+	7	30 m	09-09-1999	149 / 032
Landsat ETM+	7	30 m	18-09-1999	148 / 032
Landsat ETM+	7	30 m	02-10-2001	147 / 032
Landsat ETM+	7	30 m	25-09-1999	149 / 033
SPOT-5	4	10 m	10-07-2004	203 / 269
SPOT-5	4	10 m	31-07-2004	204 / 268
SPOT-5	4	10 m	21-08-2004	201 / 269
SPOT-5	4	10 m	21-08-2004	201 / 270
SPOT-5	4	10 m	11-09-04	201 / 269
SPOT-5	4	10 m	06-07-2005	202 / 269
SPOT-5	4	10 m	25-08-2005	201 / 269
SPOT-5	4	10 m	19-11-2005	199 / 270
SPOT-5	4	10 m	21-11-2005	203 / 269
SPOT-5	4	10 m	11-10-2005	200 / 269
SRTM	1	90 m	2000	148 / 031
SRTM	1	90 m	2000	147 / 031
SRTM	1	90 m	2000	149 / 032
SRTM	1	90 m	2000	148 / 032
SRTM	1	90 m	2000	147 / 032
SRTM	1	90 m	2000	149 / 033

Table A.2. Spectral bands of the Landsat ETM+ sensor

Band	Spectral range (μm)	Nominal spectral location
1	0.45-0.52	Blue
2	0.52-0.60	Green
3	0.63-0.69	Red
4	0.76-0.90	Near infrared
5	1.55-1.75	Mid infrared
7	2.08-2.35	Mid infrared
Pan	0.52-0.90	

Table A.3. Spectral bands of the SPOT-5 sensor

Band	Spectral range (μm)	Nominal spectral location
1	0.50-0.59	Green
2	0.61-0.68	Red
3	0.78-0.89	Near infrared
4	1.58-1.75	Mid infrared

In order to generate a dataset suitable for interpretation, three spectral bands are selected and displayed as the colours red, green and blue ('RGB') to create a colour composite image using ER Mapper software. A true colour composite (Landsat bands 321 as RGB respectively) displays the image as it would be seen by the human eye. The use of other band combinations to create false colour composites enables specific features to be targeted. For example, the RGB combination of Landsat bands 541 is useful for distinguishing variations in lithology, and bands 432 for vegetation. SPOT data does not have a band combination equivalent to 'true colour' because there is no band equivalent to blue. Various processing techniques are applied to the colour composites prior to interpretation. The images can be contrast enhanced, such that distribution of the image histogram is manually adjusted in order to display the data in the full value range. This is best achieved using the BCET (Balanced Contrast Enhancement) algorithm (Liu 1991), which eliminates colour bias (a major cause of poor colour in composite images) by stretching or compressing the histogram of the image to a given value range and mean for all bands. Thereafter, application of the DDS technique (Direct Decorrelation Stretch) enhances the saturation of the colour in the images (Fig. A.1) (Liu & McMoore 1996).

The enhanced colour composite images are imported into a GIS database, where vector layers are created for manual interpretation and picking of lithological boundaries and structural lineaments. Lithological boundaries are determined by variations in the colour of the surface because different rock types have different spectral reflectance properties (Sabins 1996). Structural lineaments (faults) appear as sharply defined linear features, often associated with changes in topography or scarps,

drag of the surrounding lithologies, stream and river offsets, drainage control and fault breccias or mylonites (Drury 1993).

The geological maps generated by image interpretation were validated during fieldwork to the NW Tarim Basin in 2007 and 2008. Measured stratigraphic sections provided further constraint on the lithostratigraphy and the map was modified accordingly.

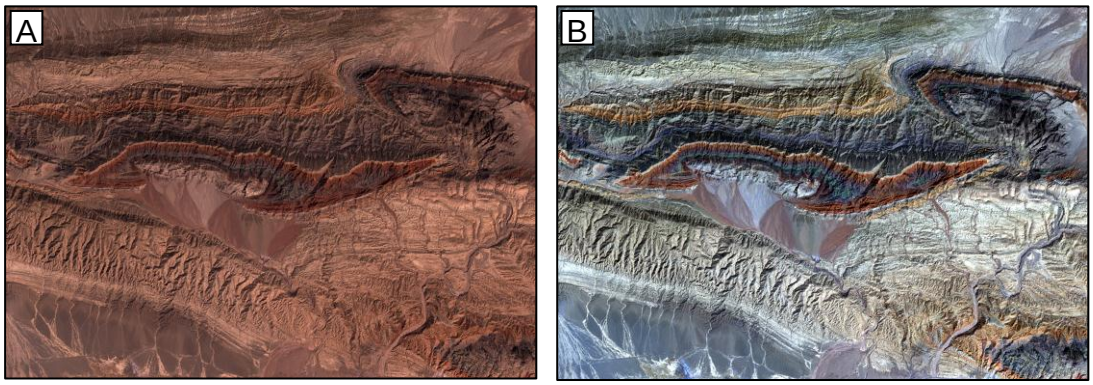

Fig. A.1. Dramatic improvements can be made to the colour of a raw satellite image, aiding structural, stratigraphic and geomorphologic interpretation: (A) Raw Landsat ETM+ true colour composite (bands 3, 2 and 1) from the NW Tarim Basin, prior to processing. (B) Processed version of *(A)* which have been contrast enhanced and to which the BCET and DDS algorithms have been applied. The vivid colours of the stratigraphy have been substantially enhanced.

References

See Reference list in main body of thesis.

APPENDIX B

Structural Evolution of the Piqiang Fault Zone

Abstract • The Piqiang Fault is a prominent strike-slip (tear) fault that laterally partitions the Keping Shan Thrust Belt in the NW Tarim Basin, China. In satellite images, the Piqiang Fault appears as a sharp, NW-trending lineament that can be traced for more than 70 km. It is oblique to the general structural trend of the thrust belt and subparallel to the thrust transport direction. This chapter presents a structural analysis of the Piqiang Fault, based on satellite image interpretation and field data. A net loss of Late Paleozoic sediment across the fault zone implies that it was initiated as a major normal fault during the Early Permian, and corresponds to widespread extension and magmatism during this period. Differential erosion across the fault resulted in the subsequent removal of sediment from the east relative to the west. During the Middle to Late Cenozoic, contraction of the NW Tarim Basin and the formation of the Keping Shan Thrust Belt resulted in reactivation of the Piqiang Fault as a strike-slip (tear) fault. The fault has accommodated lateral differences in thrust density and spacing which have arisen due to the abrupt, pre-existing change in stratigraphic thickness across it. The Piqiang Fault provides an insight into the formation of oblique, strike-slip (tear) faults in contractional belts and demonstrates the importance of inherited basement structures in such settings.

Publication Details • Turner, S. A., Liu, J. G. & Cosgrove, J. W. 2011. Structural evolution of the Piqiang Fault Zone, NW Tarim Basin, China. *Journal of Asian Earth Sciences*, **40**, 394-402.

B.1 Introduction

Strike-slip faults which develop oblique or perpendicular to the general structural trend of foreland fold-thrust belts commonly form in order to accommodate abrupt lateral changes in horizontal shortening or deformation style. Where such changes occur, these strike-slip (tear) faults allow folds and thrusts to decouple to either side (McClay 1992) and thereby act to partition the fold-thrust belt. As a result, such faults play an important role in controlling the spatial organisation of structures within the belt and may impact on the overall geometry of fold-thrust belt salients (e.g. Lawton *et al.* 1994; Sepehr & Cosgrove 2004, 2007; Butler *et al.* 2006). Abrupt lateral changes in horizontal shortening or deformation style within a fold-thrust belt may arise because of a change in the properties of the deforming foreland basin. This may include an abrupt change in the thickness of the sediment pile, the type or thickness of the detachment horizon, or interaction with pre-existing fault zones. It is not uncommon for two or more of these variations to be interrelated, as changes in the thickness or rheology of the sediment pile or variations in the detachment horizon may be related to activity on pre-existing faults.

The Piqiang Fault is an exceptional example of a strike-slip (tear) fault that has developed within the Keping Shan Thrust Belt, a foreland fold-thrust belt that has formed in the NW Tarim Basin, China (Fig. B.1). In satellite images, the Piqiang Fault appears as a sharply defined NW-trending lineament that can be traced for more than 70 km. It is oblique to the NE-SW trending thrusts of the Keping Shan and subparallel to the thrust transport direction. Previous work in the region (e.g. Allen *et al.* 1999; Li *et al.* 2003) has noted the structural importance of the Piqiang Fault, but there remains little detailed investigation into the structural evolution of the fault zone. The aim of this chapter is to establish a model for the evolution of the Piqiang Fault and to evaluate the impact that it has on the structural architecture of the Keping Shan Thrust Belt. The fault was examined in outcrop at a number of sites near to Piqiang village and the Mystery Canyon tourist centre (Fig. B.2). The field observations were supported by interpretation of Landsat ETM+ and SPOT-5 satellite images, which proved particularly useful where field access to the fault was not possible, and provided the foundation for large-scale geological mapping (Fig. B.2).

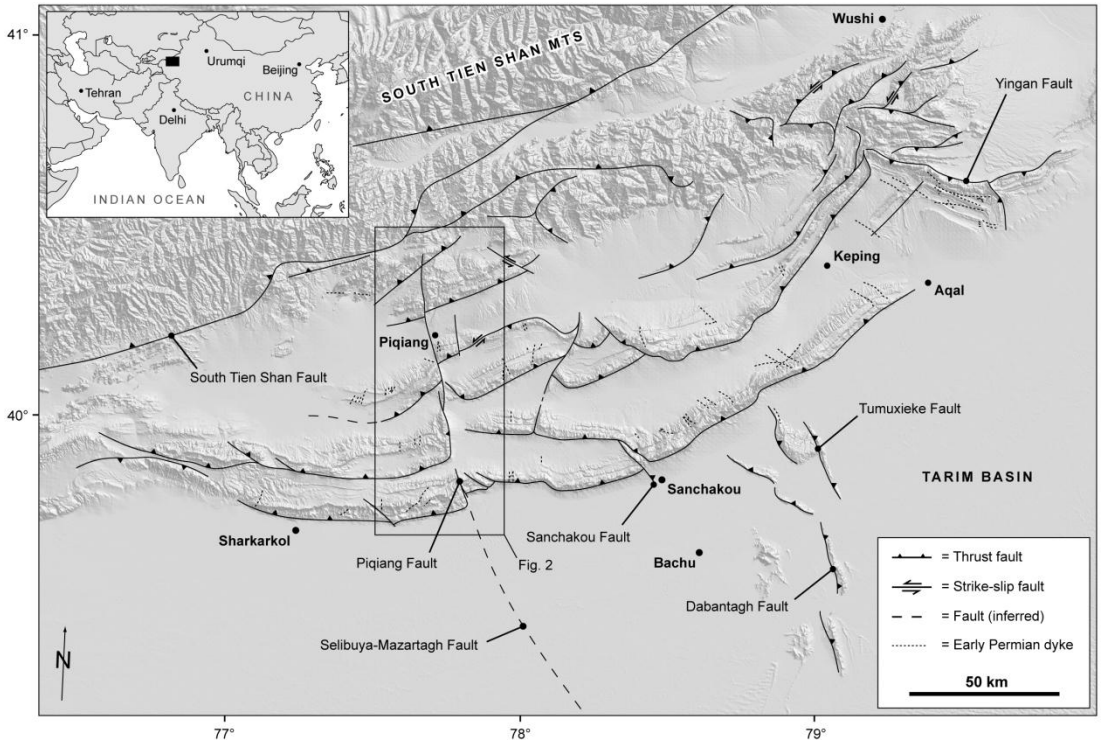

Fig. B.1. Structural map of the Keping Shan Thrust Belt in the NW Tarim Basin overlain on shaded topography, showing the location of the Piqiang Fault.

B.2 Geological Setting

The Keping Shan Thrust Belt, in which the Piqiang Fault is an important structural element, is one of several fold–thrust belt salients that have developed during the Middle to Late Cenozoic in the foreland of the South Tien Shan (Yin *et al.* 1998; Allen *et al.* 1999; Chen *et al.* 2002; Heermance *et al.* 2007), an area equating to the northern Tarim Basin. The South Tien Shan is a Paleozoic orogenic belt that formed in the Late Carboniferous to Early Permian, as a result of closure of the Turkestan Ocean and the collision of the Tarim Block with the southern margin of the growing Eurasian continent (Burtman 1975; Li 1990; Windley *et al.* 1990; Charvet *et al.* 2007). Throughout the Mesozoic, the South Tien Shan remained a topographically prominent feature, sustained by a series of terrane collisions to the south of the Tarim Block that are today preserved in the northern Tibetan Plateau (Hendrix *et al.* 1992; Hendrix 2000; Yin & Harrison 2001). Subsequent contraction during the Cenozoic,

associated with the collision of India and Eurasia (Tapponier & Molnar 1979), has resulted in the rejuvenation of the South Tien Shan since c. 20 Ma (Windley *et al.* 1990; Abdrakhmatov *et al.* 1996; Sun *et al.* 2004). Associated deformation of the adjacent foreland region (the northern Tarim Basin) has produced a series of fold-thrust belt salients and intermittent recesses (Yin *et al.* 1998). These belts, which include the Keping Shan Thrust Belt, actively deform the thick Phanerozoic sedimentary succession of the Tarim Basin.

The Keping Shan Thrust Belt forms an arcuate salient ~250 km in length between the cities of Kashgar and Aksu (Fig. B.1). The northern boundary of the belt is defined by the South Tien Shan Fault Zone, which in outcrop separates metamorphic, orogenic rocks of the South Tien Shan from the sedimentary succession of the Keping Shan Thrust Belt and the Tarim Basin. Unlike the intensely deformed and sheared orogenic rocks, the Keping Shan Thrust Belt is dominated by a series of widely spaced (10–15 km) imbricate thrusts that trend NE–SW to E–W. The thrusts verge predominantly to the south and detach onto a Middle Cambrian evaporite layer (McKnight 1993; Allen *et al.* 1999). The majority of belt-parallel thrusts are laterally continuous over long distances of up to several hundred kilometres. The hanging walls of these thrusts form topographically prominent ridges at the surface that rise up to 1,200 m relative to the surrounding basin. Erosion of the hanging walls fills the series of narrow (<15 km wide) piggy-back basins between the imbricate thrusts with Quaternary alluvial sediments. The thrust belt is partitioned by several prominent strike-slip faults which are oblique and perpendicular to the thrust belt (Fig. B.1). These faults, which include the Piqiang Fault, offset the belt-parallel thrusts and therefore have an important influence on the spatial organisation of structures within the thrust belt. The southern and frontal edge of the Keping Shan is defined by the Keping Fault, a thrust which can be traced for more than 260 km and separates the thrust belt from the presently alluvial Tarim Basin. The Keping Fault is associated with the most topographically prominent hanging wall ridge and the highest concentration of seismicity in the Keping Shan, indicating it is the most active and probably the youngest thrust in the thrust belt sequence.

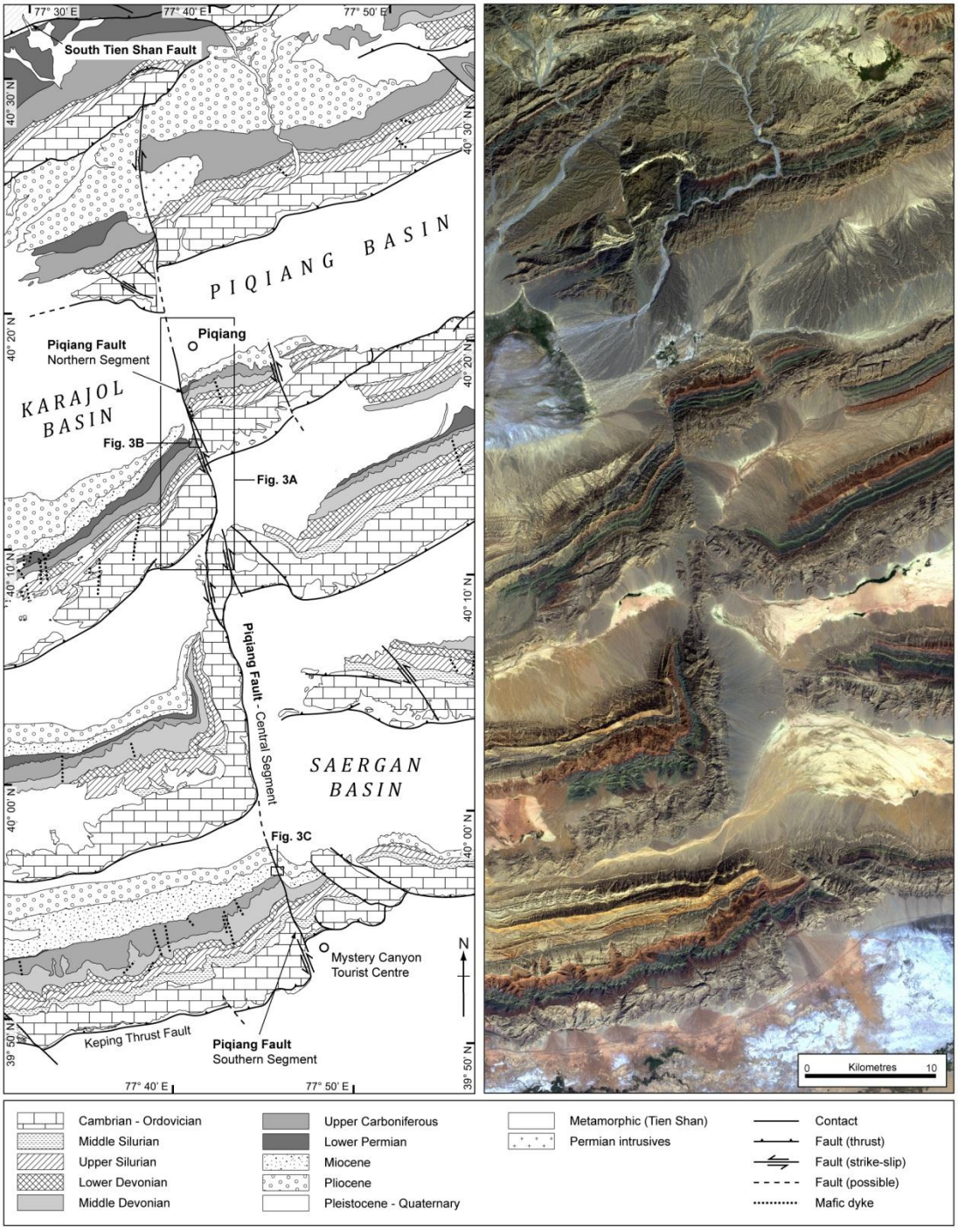

Fig. B.2. Geological map of the Piqiang Fault and adjacent areas derived from interpretation of Landsat ETM+ (true colour composite) image (see Appendix A). Stratigraphic discrimination and age constraints were obtained from Carroll *et al.* (2001) (and references therein) and combined with our own field observations.

B.3 Structure of the Piqiang Fault Zone

The Piqiang Fault is expressed for more than 70 km as a prominent structural lineament and trends broadly NW-SE (Figs. B.1, B.2). The fault zone can be examined as a series of segments, which either offset or completely decouple the E-W trending thrusts to either side. The trend of the fault is subparallel, if not very near parallel, to the thrust transport direction. Examination of the individual segments of the Piqiang Fault reveals that the faulting mechanism changes along strike, locally acting as either a strike-slip fault or as a lateral ramp.

In the north, the Piqiang Fault acts as a strike-slip fault and is dominated by horizontal displacement with little to no vertical offset. In satellite images (Fig. B.3A), the fault appears as a sharp lineament with an average trend of 340° that offsets the hanging wall of the belt-parallel Shorköl thrust fault (see Fig. B.2) in which the fault is exposed. The fault terminates ~18 km north of Piqiang village, ~15 km south of the South Tien Shan Fault Zone (Fig. B.2). The fault was examined in outcrop in the hanging wall of the Shorköl thrust, immediately south of Piqiang village (Figs. B.3A, B). The fault is defined by a vertical plane that juxtaposes Paleozoic strata of different ages from different parts of the thrust hanging wall. A brecciated zone (5-10 m width) surrounds the fault contact, with a 0.5 m core of very fine fault gouge (Fig. B.3B). The offset of the strata across the Piqiang Fault and large-scale drag of the bedding indicates a sinistral sense of displacement. Measurement from satellite images yields a horizontal offset of ~3.8 km immediately south of Piqiang, and ~2.9 km in the mountains to the north of Piqiang. The northern termination of the fault is only 4-5 km from the position where the latter measurement is taken, indicating that displacement reduces quickly towards the fault tip. Immediately west of Piqiang village, the surface of the Piqiang Fault can be traced through the piggy-back basin that has formed between the two thrust sheets to the north and south of Piqiang village (Fig. B.3A – position X). Given that the basin is filled with Quaternary alluvial clastics, the presence of this scarp is an indication that the fault has been active in recent time.

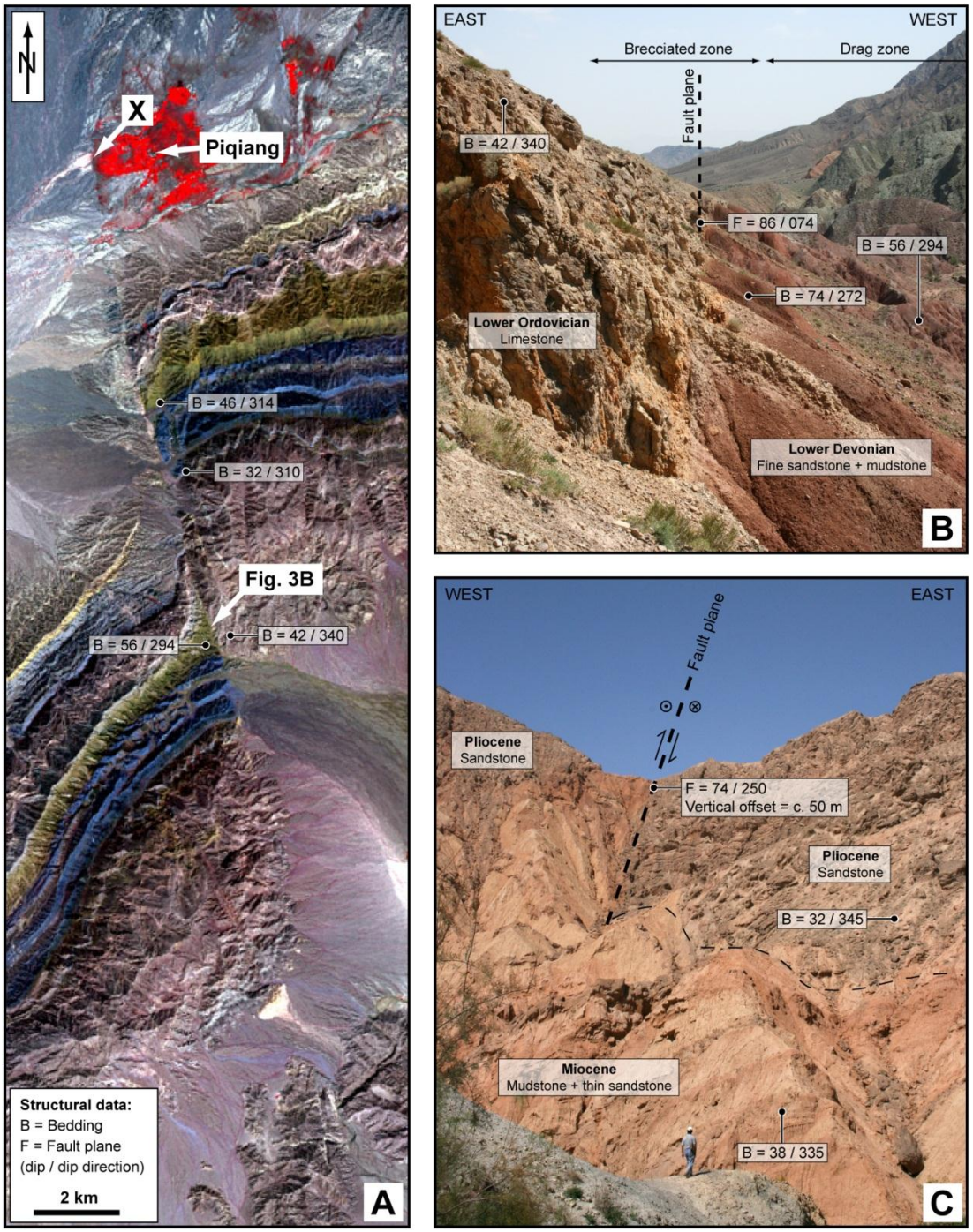

Fig. B.3. Satellite and field photographs of the Piqiang Fault Zone. (A) SPOT-5 satellite image (10 m resolution, false colour composite) of the northern segment of the Piqiang Fault. (B) Outcrop photograph of the northern segment of the Piqiang Fault, showing Lower Ordovician limestones (east) juxtaposed against Lower Devonian red mudstones and sandstones (west). Structural (bedding) readings emphasise the drag associated with the fault within the Lower Devonian on the western side of the fault. The Piqiang Fault is almost vertically dipping and strikes 164°. (C) Outcrop photograph from the southern segment of the Piqiang Fault showing Miocene mudstones and thin interbedded sandstones (west) juxtaposed against Pliocene sandstones (east). The fault dips 74° and strikes 160°. In addition to a horizontal offset of c. 0.8 km, there is a vertical offset of c. 50 m, verging to the east.

In contrast to the northern segment, the central segment of the Piqiang Fault acts as a lateral ramp. This is evident from the presence of a 16 km long lateral culmination wall (Fig. B.2). Furthermore, it is difficult to correlate thrust sheets across this segment of the fault. To the west, there is only one major belt-parallel thrust fault, which also forms the lateral ramp, while to the east there are two major belt-parallel thrusts. This suggests that this part of the Piqiang Fault acts not simply to offset the thrusts to either side of the fault, but to completely decouple and partition the thrust system.

The southern segment of the Piqiang Fault is exposed in the hanging wall of the Keping Thrust Fault, immediately northwest of the Mystery Canyon tourist centre (Figs. B.2, B.3C). This segment acts as an oblique-slip fault with a predominantly horizontal offset. In satellite images the fault appears as a well defined linear feature with a trend of 340º (160°) (Fig. B.2). In outcrop, the fault dips steeply (74º) to the west and is characterised by a narrow (0.5–1.0 m) zone of fault breccia (Fig. B.3C), which in the very south has been exploited by a river to form a linear valley almost 2 km in length. Along the southern segment, the horizontal component of offset measured from satellite images is c. 0.8 km, while the vertical component of offset measured at outcrop is c. 50 m. Although this is the most southerly surface expression of the Piqiang Fault, subsurface data confirms that that the fault continues for a considerable distance (~70 km) into the interior of the Tarim Basin (Allen *et al.* 1999).

In plan view (Fig. B.2), the Piqiang Fault has an impact on the geometry and spatial organisation of the belt-parallel thrusts to either side of it. Perhaps the most significant difference is that there are fewer thrusts to the west than to the east, and that this anomaly occurs predominantly across the central segment of the fault. Overall, thrusts in the east are more closely spaced, creating narrower piggy-back basins. The greater abundance of thrusts implies that there is a greater horizontal shortening across the thrust belt to the east of the Piqiang Fault than to the west.

B.4 Pre-Cenozoic activity on the Piqiang Fault

The present surface expression of the Piqiang Fault is primarily associated with recent (Late Cenozoic) activity on the fault and is related to the development of the Keping Shan Thrust Belt. However, examination and correlation of the stratigraphy across the southern segment of the Piqiang Fault reveals that the structure was active prior to the Middle to Late Cenozoic evolution of the thrust belt. From west to east, there is an abrupt net loss of Late Paleozoic stratigraphy immediately beneath the base-Cenozoic unconformity (Fig. B.4, see Fig. B.1 for location).

On both sides of the fault, the base of the Cenozoic is defined by an angular unconformity which is overlain by a c. 50–100 m thick succession of Upper Miocene mudstones and fine-grained sandstones and a c. 400 m thick succession of Pliocene medium to coarse-grained sandstones. These are interpreted as lacustrine and braided fluvial facies respectively, and can be correlated across much of the NW Tarim Basin (Heermance *et al.* 2007). Although there is up to 50 m of vertical offset across the Piqiang Fault, there is no apparent change in facies or stratigraphic thickness of the Miocene–Pliocene clastic sequence. On the western side of the Piqiang Fault, the base-Cenozoic unconformity is underlain by a thick Paleozoic succession. The upper part of this succession comprises a c. 900 m sequence of Lower to Middle Devonian red sandstones and mudstones, which are interpreted as braided fluvial to alluvial floodplain facies. The Devonian is unconformably overlain by a c. 250 m thick sequence of Upper Carboniferous shallow marine limestones and Lower Permian fluvial sandstones, which reflect deposition in a Late Paleozoic foreland basin during the development of the ancestral South Tien Shan (Carroll *et al.* 1995). Immediately adjacent to the fault, the Lower Permian succession is absent but is present and thickens c. 15 km to the west (Fig. B.1). Conversely, on the eastern side of the Piqiang Fault, much of the Late Paleozoic stratigraphy is absent beneath the base-Cenozoic unconformity. This includes all of the Upper Carboniferous and Early Permian sequence, and up to 400 m of the Middle Devonian (Fig. B.4), totalling more than 650 m of sediment. The sedimentary facies and stratigraphic thicknesses of the preceding Paleozoic sequences can be directly correlated across the fault. This

implies that the Piqiang Fault must have been active during the Late Paleozoic, and without taking compaction into account, suggests that the fault had a vertical throw of at least 650 m along its southern segment. Further examination of the geological map (Fig. B.2) shows that this pattern of stratigraphic discontinuity across the fault is also observed across the northern segment of the Piqiang Fault, where the Lower Permian and Upper Carboniferous thins across the fault but the older (Early to Middle Paleozoic) and younger (Cenozoic) strata are unaffected.

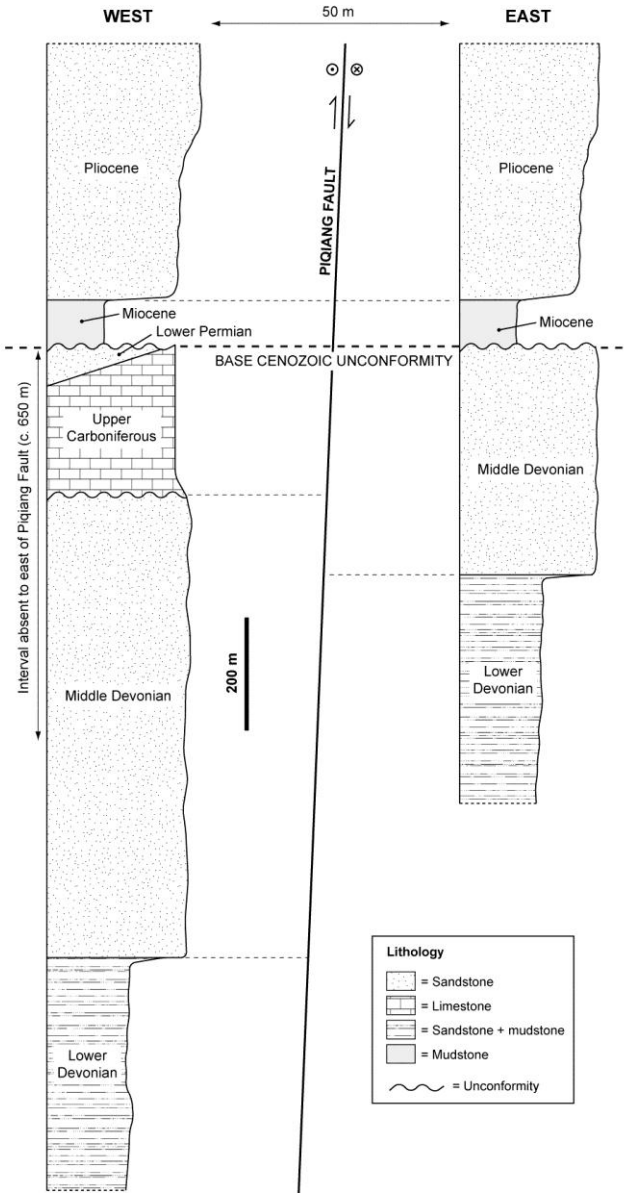

Fig. B.4. Stratigraphic correlation across the southern segment of the Piqiang Fault, near the Mystery Canyon Tourist Centre (see Fig. B.2. for location), showing the net loss of c. 650 m Late Paleozoic stratigraphy from west to east, beneath the base-Cenozoic unconformity.

B.5 Discussion

Drawing on the structural analysis of the Piqiang Fault presented in this chapter, we propose a model for the evolution of the fault zone (Fig. B.5). The fault is likely to have initially evolved as an extensional (or transtensional) normal fault prior to the Middle Cenozoic, and was subsequently reactivated as a strike-slip (tear) fault during the evolution of the Keping Shan Thrust Belt.

The abrupt loss of Late Paleozoic stratigraphy across the Piqiang Fault implies that the fault must predate deposition of the unconformable and equally distributed Miocene-Pliocene clastic sequence and therefore also predates the Late Cenozoic evolution of the Keping Shan Thrust Belt. It is conceived that the Piqiang Fault initiated as an extensional or transtensional fault which had a throw of at least 650 m (Fig. B.5A). The exact timing of fault activity is difficult to constrain from the stratigraphic discontinuity alone. The fault may have been active as early as the Middle Devonian, down-throwing to the west and permitting deposition of shallow marine facies carbonates during the Late Carboniferous. At this time, the uplifted fault block to the east may not have received any sediment at all. However, Upper Carboniferous sediments present to the west of the fault are characteristic of shallow marine deposition (Carroll *et al.* 1995, 2001) and therefore the lack of marginal basin facies seems inappropriate for the margins of an extensional or transtensional basin. This also contradicts previous work that has suggested the Late Carboniferous to Early Permian sequence is associated with sedimentation in a foreland basin (Carroll *et al.* 1995; Allen *et al.* 1999).

Instead, we perceive that the Piqiang Fault was active in the late stages of, or after, deposition of the Late Carboniferous to Early Permian sequence. It is therefore plausible that elements of syntectonic sedimentation and post-tectonic differential erosion across the fault were both causes of the abrupt decrease in stratigraphic thickness from east to west (Fig. B.5B). It is likely that the fault remained an important topographic feature for some time during the Late Paleozoic and Mesozoic. A lack of Mesozoic strata in the vicinity of the Piqiang Fault means it is difficult to

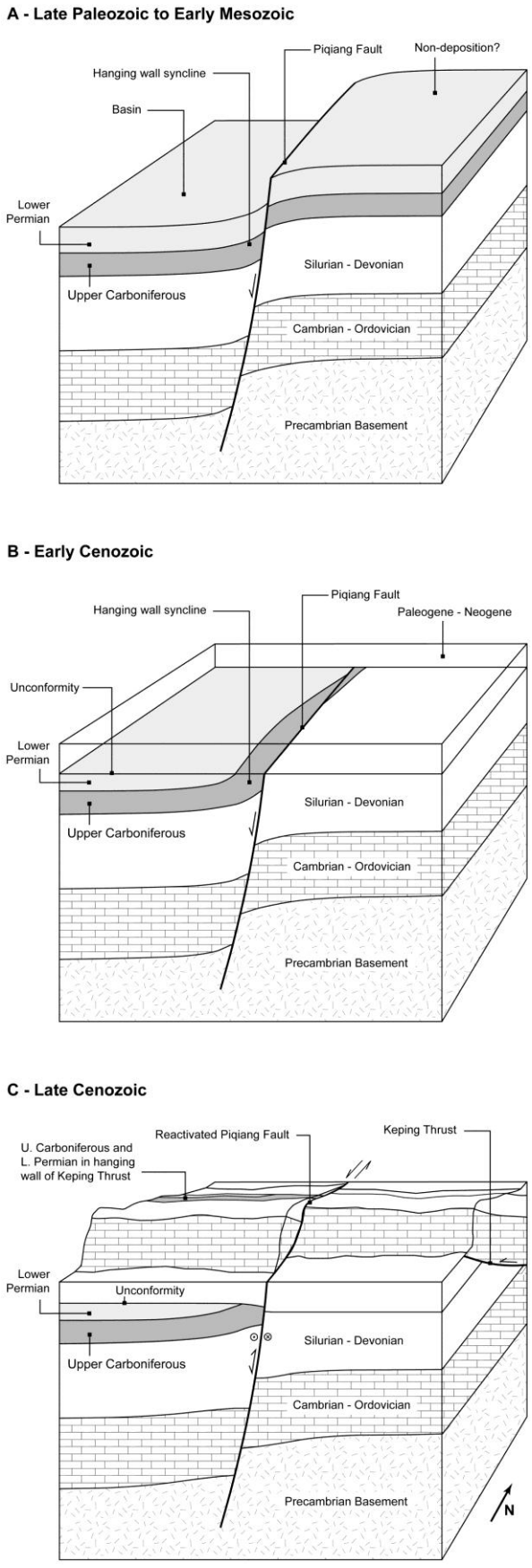

Fig. B.5. Schematic model showing the structural evolution of the Piqiang Fault Zone. (A) Late Paleozoic to Early Mesozoic development of a major normal fault, with a throw to the west. (B) Early Cenozoic deposition of sediment above an eroded, peneplain surface. (C) Late Cenozoic evolution of the Keping Thrust

constrain whether the fault remained active during this period. Isopach maps of the Tarim Basin (e.g. Bally *et al.* 1986) indicate that a major intrabasinal high, known as the Bachu Uplift, partitioned the Tarim Basin into two isolated depocentres throughout the Jurassic and Early Cretaceous. The Bachu Uplift was bounded to the west by a major structure which most likely correlates to the Piqiang Fault Zone (Li *et al.* 1996; Allen *et al.* 1999; Sobel 1999).

The initiation of the Piqiang Fault may correspond to a brief but significant period of regional extension or transtension in the Early Permian which was associated with widespread volcanism. This period was characterised by the emplacement

of a NW-SE trending dyke swarm and the extrusion of voluminous basaltic lava (Carroll *et al.* 1995, 2001; Chen *et al.* 2006; Zhang *et al.* 2008;), which yield ages of 280 to 270 Ma (Zhang *et al.* 2008; Jia 2004; Jiang *et al.* 2004; Zhou *et al.* 2006; Tian *et al.* 2009). The cause of the extension and volcanism has been widely disputed, with recent work proposing that it may be the result of a short-lived mantle plume (Zhang *et al.* 2008) or orogen-parallel extension associated with an irregular collision (Carroll *et al.* 2001). Alternatively, the structural and volcanic activity in the Tarim Basin may relate to major strike-slip shear that has been reported to have occurred across the Tien Shan during the Early Permian (Laurent-Charvet *et al.* 2002, 2003; Konopelko *et al.* 2007; Biske & Seltmann 2010), and could have resulted in transtension and large-scale block rotation within the Tarim interior.

Reactivation of the Piqiang Fault did not occur until the Late Cenozoic, and was coeval to the evolution of the Keping Shan Thrust Belt (Fig. B.5C). The presence of a major, inherited structural lineament provided an ideal plane of weakness which could be reactivated as a major strike-slip fault oriented parallel to the thrust transport direction. Reactivation of the Piqiang Fault occurred because of the abrupt change in the thickness of the sediment pile across the fault, which in turn affects the depth to the Middle Cambrian detachment. Analogue models (e.g. Liu *et al.* 1992) demonstrate that the spacing of thrusts is dependent on the thickness of the deforming wedge, whereby thicker sediment piles produce more widely spaced thrusts (Fig. B.6). This occurs because in a thicker sediment pile, fewer thrusts are required to achieve the necessary topography that satisfies the critical taper angle in the deforming wedge. Consequently, the Piqiang Fault accommodates an abrupt lateral change in the number and spacing of E-W trending thrusts, and acts both to locally offset the thrusts and to completely decouple them. The latter observation is demonstrated by the central segment of the Piqiang Fault, where a single thrust to the west is decoupled from two thrusts to the east (Fig. B.2).

Evidence for an inherited, NW-striking fault population gleaned from the structural analysis of the Piqiang Fault provides an insight into the potential origins of similar fault zones observed across the wider region of the NW Tarim Basin. A series of

NW-striking oblique- and strike-slip faults, including the Sanchakou, Dabantagh and Tumuxieke Faults (Fig. B.1), have varying degrees of impact on the structural architecture of the Keping Shan Thrust Belt. Similar to the Piqiang Fault, these fault zones correspond to abrupt lateral changes in the thickness of the pre-existing sediment pile (c.f. Chapter 6). In addition, these faults maintain subparallel trends to the Early Permian mafic dyke swarm and add to the growing body of evidence that implies the NW Tarim Basin experienced widespread extension or transtension during this period. Consequently, the somewhat simplified model of the area as a foreland basin during the Early Permian must be revised to account for these structures and the associated volcanism, forming the core of future work in the region.

Furthermore, the structure of the Piqiang Fault and its impact on the surrounding foreland fold-thrust belt provides an excellent analogue for similar structures and may have important implications for the distribution of hydrocarbons and seismic activity in such settings. The Piqiang Fault also compares well with other documented examples of tear faults. Lawton *et al.* (1994) describe a remarkably similar strike-slip fault that cross-cuts the Cordilleran Fold-Thrust Belt, western United States, while Butler *et al.* (2006) describe a series of major oblique lineaments that cross-cut the Apennines, Italy. In both examples, these fault zones correspond to abrupt lateral changes in sediment thickness and have impacted on the structural architecture of the respective fold-thrust belts. Sepehr & Cosgrove (2004, 2007) and Sepehr *et al.* (2006) report that the Kazerun Fault, a major oblique lineament that intersects the Zagros Fold-Thrust Belt, Iran, not only affected sediment thickness but also controlled the distribution of the Hormuz Salt, an important detachment horizon that was exploited during contraction. Consequently, the lateral change in the structural architecture of the Zagros across the Kazerun Fault is particularly pronounced.

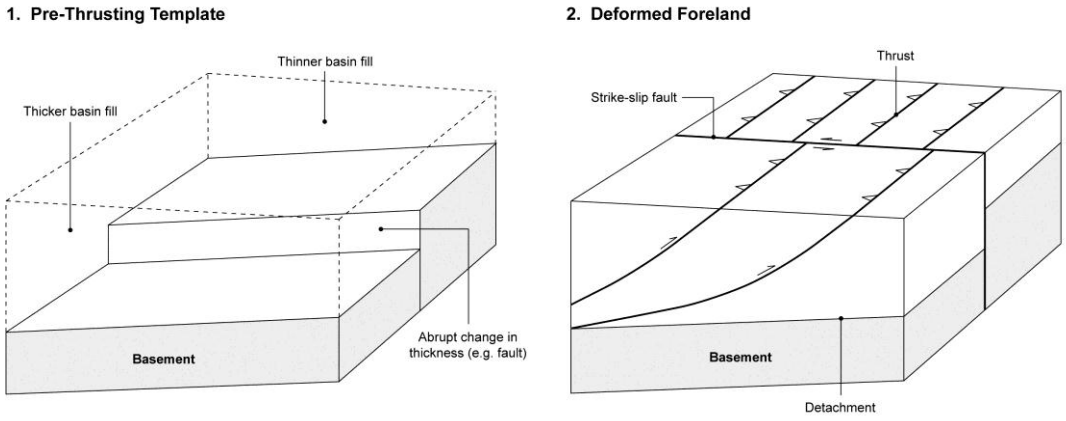

Fig. B.6. Schematic model showing the impact of lateral variation in sediment thickness, associated with a major pre-existing fault zone, on the spatial distribution of thrusts in a superimposed fold-thrust belt. This model is partly derived from analogue models by Liu *et al.* (1992) and observations from the Cordilleran Fold-Thrust Belt by Lawton *et al.* (1994). Because the lateral variation in stratigraphic thickness is abrupt, the pre-existing fault is reactivated as a strike-slip (tear) fault which acts to partition the thrust belt by allowing the thrusts to either side to be decoupled.

B.6 Conclusions

The Piqiang Fault is a major strike-slip fault which partitions the E-W to NE-SW trending contractional structures of the Keping Shan Thrust Belt. The first phase of fault evolution occurred prior to the Late Cenozoic, probably in the Early Permian during a period of E-W oriented extension in the Tarim Basin. The early Piqiang Fault was probably a major extensional fault with a throw to the west of up to 650 m. The formation of the fault is coeval to the emplacement of similarly orientated basic dykes which are prevalent across the Keping Shan, and associated basalt flows within Lower Permian strata. From the Early Permian onwards, the uplifted fault block to the east remained a topographic high and the Piqiang Fault represents the major boundary fault for the Bachu Uplift, a long-lived intrabasinal high which partitioned the Tarim Basin throughout the Mesozoic. Differential erosion across the fault resulted in a substantial reduction in the thickness of the sediment pile to the east relative to the west. The initiation of thrusting during the Late Cenozoic occurred as a response to continued compression associated with the collision of India and Asia and outward propagation of the Tien Shan into the adjacent foreland (the Tarim

Basin). The Piqiang Fault was reactivated in order to accommodate lateral variations in the spacing of structures, which occurred as a result of the abrupt lateral variation in the thickness of the sediment pile. Along its length, the faulting mechanism varies, acting locally either to offset the belt-parallel thrusts or to completely decouple them. A prominent scarp within Quaternary sediments near Piqiang village suggests that the fault has been recently active. This chapter demonstrates the impact of pre-existing structures, which in turn are associated with abrupt lateral variations in the thickness or rheology of the sediment pile, on the structural architecture of a superimposed fold-thrust belt in a foreland setting. This has important implications for hydrocarbon exploration in foreland fold-thrust belts and also provides an insight into earlier phases of structural evolution within the Tarim Basin.

References

See Reference list in main body of thesis.

Imperial College London

NATURAL ENVIRONMENT RESEARCH COUNCIL

Geological Map of the Southwest Tien Shan and Northwest Tarim Basin

Xinjiang Autonomous Region, China / Southeast Kyrgyzstan 1:500 000

CENOZOIC

Quaternary

Holocene

- Q3 — **Quaternary** Alluvial conglomerates and sandstones
- Q2 — **Quaternary** Uplifted alluvial conglomerates and sandstones

Pleistocene

- Q1 — **Xiyu Formation** Alluvial conglomerate

Neogene

Pliocene

- N3 — **Atushi Formation** Alluvial conglomerate

Miocene

- N2 — **Pakabulake Formation** Fluvial sandstones and overbank siltstones
- N1 — **Keziluoyi - Anjuan Formations** Lacustrine siltstones and fluvial sandstones

MESOZOIC

Cretaceous

- M1 — Fluvial sandstones

PALEOZOIC

Permian

Lower Permian

- P3 — **Kaipaizileke Formation** Basaltic lava flows and fluvial sandstones
- P2 — **Kaipaizileke Formation** Fluvial sandstones and overbank siltstones
- P1 — **Kupukuziuman Formation** Basaltic lava flows and fluvial sandstones

Carboniferous

Upper Carboniferous

- C1 — **Sishichang - Kangkelin Formations** Shallow marine sandstones and limestones

Devonian

Middle Devonian

- D2 — **Keziertage Formation** Fluvial sandstones

Upper Silurian to Lower Devonian

- D1 — **Tataaiertage + Yimungantawu Formations** Fluvial sandstones and overbank siltstones

Silurian

Middle to Upper Silurian

- S2 — **Kepingtage Formation** Marine sandstones and siltstones

Lower Silurian

- S1 — **Kepingtage Formation** Fluvial sandstones and overbank siltstones

Cambrian - Ordovician

Lower Cambrian - Middle Ordovician

- CO — **Yurtusi - Xiaoerbulake - Awatage - Qiulitage - Qilang - Yingan Formations** Shallow marine micritic limestones and dolomites

PROTEROZOIC

Neoproterozoic

Ediacaran

- NP1 — **Sugaitebulake - Qegebulake Formations** Fluvial sandstones, basaltic lava flows and marine dolomites

IGNEOUS & METAMORPHIC

Plutonic rocks

Lower Permian

- GR — Granite

Metamorphic rocks

- TS — **Tien Shan (Carboniferous)** Mica schists and quartzites
- TM — **Aksu Group (Middle Neoproterozoic)** Blueschist- and greenschist- facies basement

Structure

- Lithological contact
- Major (crustal-scale) thrust fault
- Thrust fault
- Strike-slip fault
- Fault (inferred)
- Dyke
- Bedding
- Schistosity

0 10 20 30 40 50

Kilometres

Geography

- Major road
- Minor road
- Railway
- Village
- Small town
- Large town
- Airport
- International border

General Information

The geological map was generated by interpretation of satellite images acquired by the Landsat ETM+ and SPOT sensors, in conjunction with ground-based mapping undertaken in 2007 and 2008. The background geographical map is derived jointly from satellite image interpretation and from the GiziMap (China Northwest), ISBN 9630080516, 2007. The background Digital Elevation Model was acquired by the Shuttle Radar Topography Mission (SRTM).

Scale 1:500 000.

Supported by

cnes

The Geological Society

中国地震局 China Earthquake Administration